Development of Improved Methods to Establish Toughness Requirements for North American Steel Highway Bridges

by

Michelle Yong Xin Chien

A thesis
presented to the University of Waterloo
in fulfilment of the
thesis requirement for the degree of
Doctor of Philosophy
in
Civil Engineering

Waterloo, Ontario, Canada, 2024

© Michelle Yong Xin Chien

Examining Committee Membership

The following served on the Examining Committee for this thesis. The decision of the Examining Committee is by majority vote.

External Examiner	Dr. Kyle Tousignant Associate Professor Department of Civil & Resource Engineering Dalhousie University
Supervisor	Dr. Scott Walbridge Professor Civil and Environmental Engineering
Internal Members	Dr. Lei Xu Professor Civil and Environmental Engineering
	Dr. Mahesh Pandey Professor Civil and Environmental Engineering
Internal-External Member	Dr. Hamid Jahed Professor Mechanical and Mechatronics Engineering

Author's Declaration

This thesis consists of material all of which I authored or co-authored: see Statement of Contributions included in the thesis. This is a true copy of the thesis, including any required final revisions, as accepted by my examiners.

I understand that my thesis may be made electronically available to the public.

Statement of Contributions

This project was undertaken in collaboration with Dr. Mohammad Javad Tolou Kian, Dr. Ali Chehrazi, and Prof. Scott Walbridge. This work builds on a collaborative project with Prof. Bertram Kühn from Technische Hochschule Mittelhessen (Gießen, Germany), who provided technical advice on implementation of the Eurocode provisions for design against brittle fracture.

The first Visual Basic code implementing the Eurocode in a time independent probabilistic model was developed by the author, under the supervision of Prof. Walbridge, and is presented in Section 3.2 and Chapter 5. Dr. Tolou Kian assisted the author with improving and implementing this code in MATLAB. The resulting code is presented and applied in Sections 3.5 and Chapter 7. Dr. Tolou Kian also assisted with developing the first iteration of a time-dependent version of the code in MATLAB, which is presented and applied in Sections 3.3 and 5.6. These tasks were completed while Dr. Tolou Kian was working as a post-doctoral fellow in Prof. Walbridge's research group. In completing these tasks, the model development was collaborative, with Dr. Tolou Kian taking the lead on the MATLAB coding effort.

Dr. Chehrazi assisted the author with implementing modifications to the time-dependent MATLAB code, to further improve its efficiency, so that manageable run times could be achieved. This work was completed while Dr. Chehrazi was working as a post-doctoral fellow in Prof. Walbridge's research group. The resulting code is presented and used in Section 3.4 and Chapter 6.

Abstract

Brittle fracture is a major concern to structural engineers as it can have significant consequences in terms of safety and cost. Although modern day occurrences are rare, it is well known that they can occur without warning and may lead to the sudden closure of a bridge, loss of service, expensive repairs, and/or loss of property or life. In Canada, steel bridge fracture is a more significant concern due to the harsh climate present through much of the country, which, if the toughness properties are improperly specified, is sufficient to put many steels on the lower shelf of the toughness-temperature curve.

The provisions for avoidance of brittle fracture in various bridge design codes vary in complexity. The existing Canadian CSA standards take a fairly simplistic approach for design against brittle fracture, using design tables that have two temperature zones. Depending on the minimum mean daily temperature of the location of interest, one can determine the Charpy V-Notch testing requirements for the grade of steel. However, it is known that temperature is not the only factor that plays a role in the fracture behaviour of steels. Other factors influencing fracture, such as plate thickness, crack size, demand-to-capacity ratio, and considerations related to traffic, are currently neglected. It is generally known, for example, that thin plates (e.g., less than 12.5-19.0 mm in bridge applications) are less susceptible to brittle fracture, due to the rolling reduction ratio at the mill. However, for the same steel grade (with a small distinction between base and weld metal), the same CVN requirements are applicable to a wide range of plate thicknesses (i.e., from the minimum allowed for corrosion considerations up to 100 mm). The existing CSA standards also assign responsibility for identifying fracture-critical members (FCMs) to the design engineer, though regulations on how to identify them are limited and vague, leaving much to engineering judgement.

A comparison of brittle fracture design provisions around the world reveals that more sophisticated approaches have been developed in terms of modelling and understanding brittle fracture in existing and new bridges than the ones currently in use in North America. One of these more involved methods is the fracture mechanics method in the European EN 1993-1-10 standard, which allows factors such as plate thickness, crack size, and strain rate to be considered. This standard also gives designers the option of using a simplified method or a much more involved, fracture mechanics-based approach.

While the current Canadian brittle fracture provisions generally appear to be meeting the needs of the code users, two issues are noteworthy. The first, which has already been alluded to, is that the North American provisions offer less flexibility and guidance for handling unusual situations than the Eurocode methods. The ‘one size fits all’ approach in the Canadian design standards may not be optimal and may result in structures being overdesigned or under-designed, leading to inefficiencies in safety and cost. This highlights the need for answering questions regarding the feasibility of allowing reduced toughness requirements for bridges fabricated with thinner plates or experiencing lower traffic volumes or demand-to-capacity ratios.

The second issue is that few studies can be found in the literature around the world attempting to assess the level of reliability against brittle fracture provided by any of the existing design provisions. The lack of a probabilistic assessment of brittle fracture risk in Canada and the few studies globally highlights a gap in the current understanding and implementation of these design standards.

This thesis includes a literature review on: 1) factors affecting material toughness, 2) common methods of evaluating toughness, 3) North American and European brittle fracture provisions, and 4) previous work on design code calibration and reliability analysis for steel structures subject to various failure modes, including brittle fracture. A comparison of the North American and European design provisions using the example of a typical steel-concrete composite highway bridge is then presented. For this case study, it was found that North American codes are typically more conservative than the Eurocode for bridge elements made with thinner plates and less conservative for elements made with thicker plates.

Following this, the fracture mechanics-based European brittle fracture limit state is then evaluated in a probabilistic framework using Monte Carlo Simulation (MCS). In order to do this, statistical distributions are established for the various input parameters, and – in particular – statistical models for the live traffic load and temperature are established. Prior to application of the model, a calibration step is performed to establish a design crack depth. Sensitivity studies are then performed where key input parameters are varied to examine how the failure probability is affected by variations in each parameter.

The work is then cast in a time-dependent reliability framework, using historical temperature and traffic data, to determine the failure probability with temperature and traffic loading fluctuating on a time scale throughout the year. This time-dependent model is then used to assess the reliability level provided by the current Canadian brittle fracture provisions. Given certain plate thickness, crack size, load levels and geographical temperature data, the annual probability of failure and annual reliability index, β, are obtained. The obtained reliability indices are compared with a target reliability index to assess the extent to which the Canadian provisions provide consistent and adequate levels of reliability against brittle fracture.

On the basis of the results, the North American brittle fracture design provisions are critically assessed, and new design tools from these probabilistic studies are presented. Opportunities for improvement in the existing Canadian standards and areas warranting further study are lastly highlighted.

Acknowledgements

This thesis could not have been done without the support of my funding organizations, the members of University of Waterloo, Technische Hochschule Mittelhessen, my family, friends, and colleagues.

First and foremost, I would like to thank my supervisor, Dr. Scott Walbridge, for encouraging me to leave all my career doors open. If it were not for your advice, I might never have pursued graduate studies and would not be where I am today. Thank you for encouraging me to apply for scholarships that I did not feel qualified for, and supporting me when I felt like an imposter in academia. I will always be grateful for your guidance and technical expertise for nearly a decade throughout my undergraduate and graduate degrees. Most importantly as a mentor, thank you for being understanding and patient when I made mistakes. When it comes time for me to mentor the next generation of engineers, I'll strive to treat them with the same level of patience and understanding as you have treated me.

To Prof. Dr.-Ing. Bertram Kühn, my "unofficial" co-supervisor, thank you for all your help understanding the Eurocode brittle fracture provisions, and all the collaboration and emails in person, and remotely, over the last five years. Most importantly, thank you for welcoming me at THM for several months, and for all your work in corresponding with the International Office and translating important information to ensure the smoothest transition for my visit. I will always be grateful for the kindness from you and all your team.

I would like to thank my thesis committee, Dr. Lei Xu, Dr. Mahesh Pandey, Dr. Hamid Jahed, and Dr. Kyle Tousignant for taking the time to review my thesis and the valuable insight and feedback provided from each of your areas of expertise.

To my fellow colleagues in Giessen, Noah, Natalie, Lisa, Kristina, Felix, Till, Philipp, thank you for welcoming me warmly on my first trip to Germany, for helping me get settled in, giving me a tour of the city and campus, for recommending places to visit, and recommending amazing food! Thank you all for your warm hospitality. The exchange was an opportunity of a lifetime, I hope we all keep in touch, and I cannot wait to be back in Germany again.

To my fellow colleagues in Waterloo, Ali Chehrazi, Laurent Gerin, Melanie Perreault, Carol Liang, Rakesh Ranjan, Mohammad Barkhori Mehni, Spencer Arbuckle, Eduardo Fontes, Abdullah Abdelbadie, Jason Lee, Mi Zhou, Mahmoud Trimech, and Mohammad Tolou Kian: I thank you for the mutual support, inviting me to social events (dodgeball, skating), the friendly conversations in the office, and working together in our TAships / teaching endeavours. It has been wonderful to work with and learn from all of you. A special thanks is extended to Ali and Mohammad Tolou for the collaboration over the years.

I am incredibly grateful for all the people in my life who encouraged me to transfer from a MASc to a PhD, and told me I could do it even though I doubted my intelligence. There are so many of you to name, though

I would like to particularly acknowledge Mansour Esnaashary Esfahani as one of these kind people, who was aboard Flight 752.

I owe a great debt of gratitude to my fiancé, Watkin Tang, for being my rock. Thank you for always being a listening ear, for providing advice when I needed it, and always celebrating my successes with me. You constantly inspire me to be a better person.

I am grateful to my grandparents, two retired Materials Engineers, and my great-uncle, a retired bridge engineer, who shared their knowledge of steel manufacturing with me to help me prepare for graduate school. A special thanks goes to my grandfather, who gave me my first basic German language lessons to prepare me for my academic exchange, and for supporting me by reading all my publications, despite the language barrier.

I would like to thank the counsellors, doctors, and staff at UW Counselling Services and UW Health Services for keeping me alive during my graduate studies.

I thank the Canadian Institute of Steel Construction (CISC), the National Sciences and Engineering Research Council of Canada (NSERC), the Ontario Graduate Scholarship (OGS), and Waterloo Engineering Fellowship for their financial support of this project, and the DAAD German Academic Exchange Service and Technische Hochschule Mittelhessen for supporting my academic visit to Germany. Lastly, I would like to thank the Digital Research Alliance of Canada for the use of the SHARCNET consortium of supercomputer systems.

Dedication

I dedicate this to my great-uncle, Fu Feng Liang, a retired bridge engineer who cheers me on from the other side of the globe. Thank you for being so proud of me.

Table of Contents

Examining Committee Membership ii
Author's Declaration iii
Statement of Contributions iv
Abstract v
Acknowledgements vii
Dedication ix
List of Figures xiv
List of Tables xvii
List of Abbreviations xviii
List of Symbols xx
Quote xxiii
1 Introduction 1
1.1 Background and Motivation 2
1.2 Objectives and Key Tasks 5
1.3 Thesis Outline 6
2 Literature Review 8
2.1 Factors Affecting Material Toughness 8
2.2 Methods of Toughness Evaluation 9
2.2.1 Charpy V-Notch Method for Impact Toughness 9
2.2.2 Critical Stress Intensity Factor, K_{Ic}, for Fracture Toughness 9
2.2.3 J-Integral Method 11
2.3 Existing International Brittle Fracture Design Provisions 11
2.3.1 Canadian Highway Bridge Design Code (CSA S6-19) 11
2.3.2 AASHTO LRFD Part 6 – Steel Structures 13
2.3.3 Wallin Master Curve 14
2.3.4 Eurocode (EN 1993-1-10) 14
2.3.5 Further Contributions to European Brittle Fracture Standards 28
2.4 Previous Work on Code Calibration and Reliability Analysis 28
2.5 Previous US Study on Brittle Fracture using MCS and Probabilistic Analysis 31
2.6 Suggested Revisions to CVN Requirements in Literature 33
2.7 Initial and Design Crack Size from Literature 35
2.8 Crack Detection Probability Studies 38
2.9 Hourly Temperature Modelling Methods 38

2.10 Effect of Heat Affected Zones (HAZ) on Brittle Fracture 41
2.11 Fundamentals on Probability Theory and Probabilistic Analysis 42
2.11.1 Knowledge and Uncertainty 42
2.11.2 Risk Assessment 42
2.11.3 Philosophy of Reliability Analysis and Probabilistic Design 44
2.11.5 Turkstra's Rule 45
2.11.6 Monte Carlo Simulation 45
3 Methodology 47
3.1 Comparison of International Design Provisions 47
3.1.1 Extreme Air Temperature Calculation 49
3.1.2 Use of Eurocode Design Tables 50
3.1.3 Deterministic Application of Fracture Mechanics Method 50
3.2 Development of Preliminary Time-Independent Probabilistic Model 52
3.2.1 Distribution Types and Statistical Parameters 53
3.3 Development of Preliminary Time-Dependent Probabilistic Model 57
3.3.1 Preliminary MATLAB Code Procedure 58
3.3.2 Distribution Types and Statistical Parameters 60
3.4 Time-Dependent Probabilistic Assessment of Reliability Levels in CSA S6 61
3.4.1 Limit State Function and Probabilistic Framework 62
3.4.2 Climate and Load Models 62
3.4.3 Statistical Parameters 65
3.4.4 Conversion CVN Test Temperature into Equivalent 27J Temperature 67
3.4.5 Design Crack Depth 68
3.4.6 Time-Dependent Reliability Analysis 70
3.5 Sensitivity Studies with Time Independent Model and Development of Design Tools 73
3.5.1 Limit State Function and Probabilistic Framework 73
3.5.2 Climate and Load Models 73
3.5.3 Statistical Parameters 74
3.5.4 Design Crack Depth 75
3.5.5 Time-Independent Reliability Analysis and T_{27J} Calibration 76
4 Comparison of Design Provisions for a Typical Bridge 79
4.1 Part 1 – Single Point Analysis 79
4.2 Part 2 – Entire Girder Analysis 82
5 Probabilistic Fracture Mechanics Analysis 84

5.1 Results: Base Case Analysis 84
5.2 Variation of Crack Size 85
5.3 Variation of Load 86
5.4 Variation of Weld Size 87
5.5 Variation of Plate Thickness 88
5.6 Preliminary Time-Dependent Probabilistic Model 89
6 Time-Dependent Probabilistic Assessment of Current CSA S6 Design Tables 92
6.1 Reliability Index Provided by CSA S6-19 for Various Cases 93
6.1.1 Effect of Steel Strength 93
6.1.2 Effect of Plate Thickness 94
6.2 T_{27J} Required to Achieve Consistent Reliability Level 95
6.2.1 Effect of Steel Strength 96
6.2.2 Effect of Plate Thickness 97
6.3 Sensitivity Studies 99
6.3.1 COV of *Z17* (δ_2) Parameter 99
6.3.2 Strain Rate 100
6.3.3 *L/D* Ratio 101
6.3.4 Design Crack Size 102
6.3.5 Fracture Critical / Non-Redundant Tension Members 102
7 Sensitivity Studies and Design Tool Development 104
7.1 Comparison of Time-Dependent and -Independent Analysis Results 104
7.2 Sensitivity Studies 105
7.2.1 Climate Study 105
7.2.2 Bridge Span and Influence Line Study 106
7.2.3 Traffic Volume Study 107
7.2.4 Multiple Vehicle Crossing Study 108
7.3 Design Tool Development 109
7.3.1 Primary Tension Members 110
7.3.2 Fracture Critical Members 114
7.3.3 Consideration of Other Parameters and Situations 117
8 Conclusions and Recommendations for Future Work 118
8.1 Conclusions 118
8.1.1 Ch. 4 – Comparison of Design Provisions for a Typical Bridge 118
8.1.2 Ch. 5 –Probabilistic Fracture Mechanics Analysis 119

8.1.3 Ch. 6 – Time-Dependent Probabilistic Assessment of Current CSA S6 Design Tables... 119
8.1.4 Ch. 7 – Sensitivity Studies and Design Tool Development 121
8.2 Recommendations for Future Work 121
8.2.1 European Code Verification 122
8.2.2 Rapid Assessment Tools for Bridge Inspection 122
8.2.3 Plastically Deformed Structures 122
8.2.4 Pedestrian Bridges 122
8.2.5 Aluminum Structures 123
8.2.6 Design Crack Depth Definition 123
8.2.7 Effects of Routine Inspection 123
8.2.8 Continued Refinement 123
References 125
Appendix A – Time-Dependent MATLAB Code 132
Appendix B – Time-Independent MATLAB Code 147

List of Figures

Figure 1-1 Toughness-Temperature Curve (NDT Education Resource Center, 2020) 1
Figure 1-2 Example of a Pin and Hanger Assembly (Graybeal et al., 2000) 2
Figure 1-3 Detail Exhibiting Tri-axial Stress State (Connor et al., 2007) 4
Figure 2-1 Effects of cold forming on material S-curve (Sedlacek et al., 2008) 8
Figure 2-2 Different fracture crack modes (Zamiri et al., 2018) 9
Figure 2-3 CT specimen shape and proportions (ASTM International, 2020) 10
Figure 2-4 Minimum mean daily temperature, Figure A3.1.2 from CSA-S6 12
Figure 2-5 Excerpt of Brittle Fracture Design Provisions (Table 10.12) in CSA S6 12
Figure 2-6 Excerpt of Brittle Fracture Design Provisions (Table 10.13) in CSA S6 13
Figure 2-7 Excerpt of Brittle Fracture Design Provisions (Table C6.6.2.1-1) in AASHTO 13
Figure 2-8 Excerpt of Table 2-3 SIFs for various crack configurations (Sedlacek et al., 2008) 19
Figure 2-9 Excerpt of Table 2-4 M_k for semi-elliptical surface cracks at different welded attachments (Sedlacek et al., 2008) 20
Figure 2-10 R6 Failure Assessment Diagram (Sedlacek et al., 2008) 21
Figure 2-11 Definition of ρ (Sedlacek et al., 2008) 22
Figure 2-12 Definition of b_{eff} (Sedlacek et al., 2008) 23
Figure 2-13 Thick plate inhomogeneity temperature shift curve (Sedlacek et al., 2008) 24
Figure 2-14 Temperature dependence of K_0 for 25 mm specimens (Wallin, 1992) 27
Figure 2-15 Initial and design crack sizes from EUR 23510 EN and EN 10163-3 37
Figure 2-16 Example of sub-surface length limitations, partial capture of Fig 12.5 from W59-18 38
Figure 2-17 Risk indicators for a bridge scenario (Joint Committee on Structural Safety, 2008) 43
Figure 2-18 Probability density function of the safety index, Z (Pandey & Jyrkama, 2019) 44
Figure 3-1 Straight plate girder bridge design (Canadian Institute of Steel Construction, 2002) 47
Figure 3-2 Assumed girder detail for analysis 48
Figure 3-3 Characteristic weld detail from (Sedlacek et al., 2008) 54
Figure 3-4 Sample schematic of determining K_{mat} 58
Figure 3-5 Sample schematic of determining K_{appld} 59
Figure 3-6 Hourly temperature envelopes and means for Climate 1, 2003-2021 (top) and Climate 2, 1953-2021 (bottom) 64
Figure 3-7 MTO 1995 truck database GVW histogram 65
Figure 3-8 Master curve scatter considered by δ_1 parameter (left) and raw data from (Sedlacek et al., 2008), including trendlines for +/-2σ, used to establish δ_2 parameter (right) 67
Figure 3-9 Calibration of a_d (left) and β vs. T_{27J} curves for various steel strengths (right) 70

Figure 3-10 Flow chart for time-dependent model 72
Figure 3-11 MTO 2012 truck database GVW histogram 74
Figure 3-12 Calibration of a_d (left) and β vs. T_{27J} curves (right) 75
Figure 3-13 Flow chart of time-independent model 77
Figure 4-1 Required CVN test temperature for Waterloo ($\sigma_{ed} / f_y(t) = 0.46$) 80
Figure 4-2 Required CVN test temperature for Vancouver ($\sigma_{ed} / f_y(t) = 0.46$) 80
Figure 4-3 Required CVN test temperature for Fort McMurray ($\sigma_{ed} / f_y(t) = 0.46$) 80
Figure 4-4 Required CVN test temperature for different stress levels for Waterloo 81
Figure 4-5 Required CVN test temperature for different stress levels for Vancouver 81
Figure 4-6 Required CVN test temperature for different stress levels for Fort McMurray 82
Figure 4-7 Comparison of Eurocode simplified and fracture mechanics models for three locations 83
Figure 5-1 Sample output for base case (Ft. McMurray, 50-year service period, T_{27J} = -30°C) 85
Figure 5-2 P_f vs. Crack Size (T_{27J} = -20°C) 86
Figure 5-3: β vs. Crack Size (T_{27J} = -20°C) 86
Figure 5-4: P_f vs. Maximum Nominal Applied Stress (T_{27J} = -20°C) 87
Figure 5-5 P_f vs. Weld Size (8 mm crack case) 87
Figure 5-6: P_f vs. plate thickness (8 mm mean initial crack size, T_{27J} = -20°C) 88
Figure 5-7: P_f vs. plate thickness (12 mm mean initial crack size, T_{27J} = -20°C) 89
Figure 5-8 Probability and cumulative distributions for K_{mat} 89
Figure 5-9 Probability and cumulative distributions for K^*_{appld} 90
Figure 5-10 Sample temperature and live load stress fluctuations over one year 90
Figure 5-11 Annual probability of failure over number of iterations (100 years) 91
Figure 6-1 Typical K_{mat} and K^*_{appld} fluctuation over time 92
Figure 6-2 Annual reliability index for t = 38 mm, a = 0.53 mm 93
Figure 6-3 Annual reliability index for t = 25 mm, a = 0.53 mm 94
Figure 6-4 Annual reliability index for t = 25 mm, a = 0.35 mm 94
Figure 6-5 Annual reliability index for t = 75 mm, a = 0.53 mm 95
Figure 6-6 Annual reliability index for t = 75 mm, a = 1.06 mm 95
Figure 6-7 β vs. T_{27J} for t = 38 mm, a = 0.53 mm, CSA Grades, Climate 1 96
Figure 6-8 β vs. T_{27J} for t = 38 mm, a = 0.53 mm, ASTM Grades, Climate 1 96
Figure 6-9 T_{27J} before and after calibration for t = 38 mm, a = 0.53 mm 97
Figure 6-10 T_{27J} before and after calibration for t = 25 mm, a = 0.53 mm 98
Figure 6-11 T_{27J} before and after calibration for t = 25 mm, a = 0.35 mm 98
Figure 6-12 T_{27J} before and after calibration for t = 75 mm, a = 0.53 mm 98

Figure 6-13 T_{27J} before and after calibration for t = 75 mm, a = 1.06 mm 99
Figure 6-14 T_{27J} for CVN to Fracture Toughness Conversion COVs of 13 and 34.2 for t = 38 mm 100
Figure 6-15 T_{27J} for different strain rate adjustments 101
Figure 6-16 T_{27J} for L/D of 0.5, 1.0, and 4.0 101
Figure 6-17 T_{27J} for crack sizes of 0.53 and 9.5 mm 102
Figure 6-18 T_{27J} for β = 3.25, 3.5, 3.75, and 4.0 in Climate 1 103
Figure 7-1 Comparison of time-dependent and -independent models 105
Figure 7-2 Effects of Location within each Climate Zone 106
Figure 7-3 Effect of Bridge Span and Influence Line 107
Figure 7-4 Required T_{27J} for various highway classes in Climate 1 and Climate 2 107
Figure 7-5 Simultaneous crossing effects on required T_{27J} in Climate 1 and Climate 2 109
Figure 7-6 Contour plot for t = 38 mm, Climate 1, ADTT = 4000, primary tension member 110
Figure 7-7 T_{27J} Contours for Primary Tension Members in Climate 1 112
Figure 7-8 T_{27J} Contours for Primary Tension Members in Climate 2 113
Figure 7-9 T_{27J} Contours for Fracture Critical Members in Climate 1 115
Figure 7-10 T_{27J} Contours for Fracture Critical Members in Climate 2 116

List of Tables

Table 2-1 Eurocode Simplified Method Design Table Excerpt (reproduced from EN 1993-1-10)..... 17
Table 2-2 YS/K_c Ratios for Static and Dynamic Loading (Altstadt, Wright, & Connor, 2014)..... 34
Table 2-3 Calibrated CVN Requirements (Altstadt, Wright, & Connor, 2014) 34
Table 2-4 Maximum Permissible Depth of Discontinuities for Class C (European Standard, 2004)..... 36
Table 2-5 T_{max} and T_{min} Times Suggested by CIBSE Guide A2 (Chow & Levermore, 2007)..... 40
Table 3-1 Sub-Grades of S355 Structural Steel..... 48
Table 3-2 Deterministic Model Parameters 54
Table 3-3 Statistical Variables for Base Case Analysis (Ft. McMurray)..... 57
Table 3-4 Statistical Variables and Distribution Types 60
Table 3-5 Statistical Parameters and Distribution Types..... 66
Table 3-6 Conversion of Table 10.13 from CSA S6 into Equivalent T_{27J} 68
Table 3-7 Design Crack Depth Cases 70

List of Abbreviations

AASHTO	American Association of State Highway and Transportation Officials
AB	Alberta
ADTT	Average daily truck traffic
ASCE	American Society of Civil Engineers
ASTM	American Society for Testing and Materials
AWS	American Welding Society
BC	British Columbia
BM	Base metal
BS	British Standard
CDF	Cumulative distribution function
CIBSE	Chartered Institution of Building Services Engineers
CIF	Constraint-induced fracture
CISC	Canadian Institute of Steel Construction
COV	Coefficient of variation
CSA	Canadian Standards Association
CSCE	Canadian Society for Civil Engineering
CT	Compact tension
CVN	Charpy V-notch
DAAD	Deutscher Akademischer Austauschdienst (German Academic Exchange Service)
DAF	Dynamic allowance factor
DCR	Demand to capacity ratio
DL	Day length
EN / EUR	European Standard or “Euronorm”
ESW-NG	Electroslag welding – narrow gap
FAD	Failure assessment diagram
FCM	Fracture-critical member
FHWA	Federal Highway Administration
GVW	Gross vehicle weight
HAZ	Heat affected zones
HPS	High performance steel
HSC	Handbook of Steel Construction (Canada)
HSS	Hollow structural sections
JCCBI	Jacques Cartier and Champlain Bridges Incorporated
JRC	European Commission Joint Research Centre
LAST	Lowest anticipated service temperature
LRFD	Load and Resistance Factor Design

MCS	Monte Carlo Simulation
MTO	Ministry of Transportation of Ontario
NBIS	National Bridge Inspection Standards
NCHRP	National Cooperative Highway Research Program
NDI	Non-destructive inspection
NDT	Non-destructive testing
NSERC	National Sciences and Engineering Research Council of Canada
OGS	Ontario Graduate Scholarship
ON	Ontario
PB	Bulk permit according to CSA S6
PDF	Probability density function
RMSE	Root mean square of errors
SCF	Stress concentration factor
SI	International System (of units)
SIF	Stress intensity factor
SLS	Serviceability limit state
THM	Technische Hochschule Mittelhessen
TRB	Transportation Research Board
ULS	Ultimate limit state
US/USA	United States / United States of America
UW	University of Waterloo
WM	Weld metal
WWF	Welded wide flange
YS	Yield strength
YT	Yukon Territory

List of Symbols

a	Crack size
a/c	Depth-to-width ratio for cracks
a_0	Initial size of the crack
a_d	Critical design size of the crack
B	Width of flange
B_0, B_1	Reference thickness of 25 mm, in the derivation of the master curve (Chapter 2)
B_2, B	Thickness as a variable in the derivation of the master curve (Chapter 2)
b_{eff}	Length of the critical crack front
E	Modulus of elasticity
E_d	Action side effects
f_y, F_y	Yield strength of steel
$f_y(t)$	Thickness-adjusted yield strength in the Eurocode
g	Limit state function
H_w	Weld height
J, J_{Ic}	J-integral for Mode I cracking
K^*_{appld}	Adjusted stress intensity factor for applied load effects
K_{0B}	A specimen thickness- and temperature-dependent normalization parameter
K_{0B1}, K_0	Stress intensity factor associated with test specimens of size B_1
K_{0B2}	Stress intensity factor associated with specimens of size B_2
K_{appld}	Stress intensity factor for applied load effects
K_{Ic}	Critical stress intensity factor for Mode I cracking
K_{IIc}	Critical stress intensity factor for Mode II cracking
K_{IIIc}	Critical stress intensity factor for Mode III cracking
K_{Jc}	Elastic-plastic equivalent fracture toughness obtained from a J-integral
K_{mat}	Fracture toughness of the material
K_{min}	Lower bound fracture toughness, 20 MPa·√m for steel materials
k_{R6}	Correction factor to account for local plasticity at the crack tip
L	Longitudinal length of the weld
L/D	Live to dead load ratio
L_r	Ligament yielding parameter
M_k	Correction factor for attachments with semi-elliptical cracks at a weld toe
P_f	Probability of failure
Q	Factor for calculating the shape parameter Y for semi-elliptical cracks
R_d	Resistance side effects
t	Plate thickness
T	Temperature

t_0	Reference plate thickness, taken as 1 mm
T_{27J}	Temperature associated with an absorbed energy of 27 J
T_{ave}	Average temperature of the day
t_{cover}	Cover plate thickness
T_{Ed}	Temperature representing action side effects
$T_{K100,}\ T_0$	Temperature associated with a fracture toughness of 100 MPa·√m
T_{KV}	Temperature associated with an absorbed energy of *KV*
T_{max}	Maximum temperature of the day
t_{max}	Time at which the maximum temperature occurs in the day
T_{md}	Lowest daily air temperature of the location of interest, with a 50-year return period
T_{min}	Minimum temperature of the day
t_{min}	Time at which the minimum temperature occurs in the day
T_{Rd}	Temperature representing resistance side effects
T_s	Sunset temperature
V	Coefficient of variation
W_w	Weld width
Y	Correction factor for various crack positions and shapes
YS/K_c	Yield strength to fracture toughness ratio
α	Material constant, 31, in master curve derivation
β	Material constant, 77, in master curve derivation
β	Reliability index
γ	Material constant, 0.019, in master curve derivation
δ_1	Factor to model uncertainty in the master curve
δ_2	Additive factor to model the scatter in test data correlating T_{100} to T_{27J}.
Δa_{FCG}	Amount of fatigue crack growth over a service period
ΔT_r	Adjustment for radiation loss
ΔT_R	Adjustment for safety allowance
ΔT_t	Adjustment for material toughness in the through-thickness direction
$\Delta T_{\dot{\varepsilon}}$	Adjustment for a strain rate
$\Delta T_{\varepsilon cf}$	Adjustment for the degree of cold forming
ΔT_σ	Adjustment for stress and yield strength, crack imperfection and member shape, and dimensions
$\Delta\sigma_{ref}$	Reference stress range, 100 N/mm$^{1/2}$
ε	Strain
ε_0	Reference strain rate, 10^{-4} s^{-1}
ε_{cf}	Degree of cold forming
ζ	Shape parameter for lognormal distribution
θ	Angle of the fillet weld

λ	Scale parameter for lognormal distribution
ρ	Correction factor for local residual stresses caused by welding
ρ_G	Geometric ratio
ρ_M	Material ratio
ρ_P	Professional ratio
ρ_R	Overall resistance ratio
σ	Stress
σ_{D1}	Combined dead load stresses
σ_{DLac}	Dead load stresses, after composite action
σ_{DLbc}	Dead load stresses, before composite action
σ_{Ed}	Maximum stress due to external loads, plus 100 MPa to account for residual stresses
σ_{gy}	Stress applied to the gross section to obtain net section yielding
σ_{LL}	Live load stresses
σ_p	Stress due to external applied loads at that location of the span
ϕ	Performance factor
Φ	CDF of the standard normal distribution

"There is no limit as to what we, as women, can accomplish." – Michelle Obama

1 Introduction

Structural steel has been used in bridge construction since the 1800s and its use has become more widespread for bridge construction ever since. The very first in North America was the Eads Bridge (built 1874), a steel arch bridge in St. Louis, Missouri, which still remains in service (Kline, 2008). Truss bridges started to become more widely used in bridge design as they enabled longer spans to be built using shorter elements. Numerous truss configurations such as the Pratt and Howe models were patented in this era. Early steel trusses used pin connections, whereas riveted connections became later implemented with connection developments in the 20th century (Jarosz & Sorgenfrei, 2005).

While structural steel has many benefits including its high strength-to-weight ratio, ductility, and speed of construction, it also presents disadvantages such as the need for corrosion protection, as well as the need for bolted or welded connections which, if poorly designed or poorly welded, become areas of weakness susceptible to fatigue failure. Common modes of failure for steel bridges include brittle fracture, ductile fracture, plastic collapse, fatigue, creep, and buckling (Gordon, 1993). Among these, brittle fracture remains a concern to structural engineers, as it has significant consequences in terms of safety and cost. Although occurrences are rare in the present day, it is well known that they occur without warning and may lead to the sudden closure of a bridge, loss of service and the need for traffic diversion, expensive repairs, loss of property, and in the most tragic cases, loss of life.

The phenomenon of brittle fracture occurs on the lower shelf region of the toughness-temperature S-curve, illustrated in Figure 1-1, making it a concern in Canadian climates due to the long winter and extremely low temperatures that most communities experience. Methods of prevention involve proper detailing, regular inspections, and selecting the appropriate grade to ensure the material behaves in the upper shelf region for the given geographic location and climatic conditions.

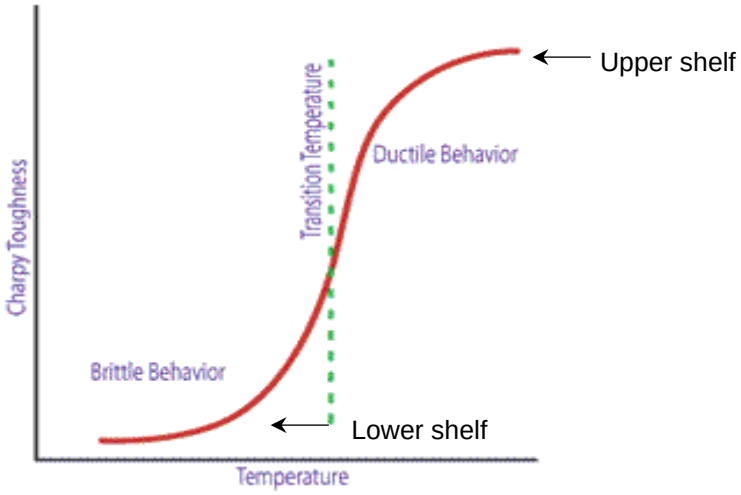


Figure 1-1 Toughness-Temperature Curve (NDT Education Resource Center, 2020)

1.1 Background and Motivation

Collapses of the Duplessis Bridge in Trois-Rivières, Québec (failed in 1951, 4 fatalities) and Silver Bridge in Point Pleasant, West Virginia (failed in 1967, 46 fatalities) are a few historical examples of brittle fracture-related bridge failures in North America (Hopwood & Deen, 1984). Prior to the early 1970s, Charpy V-Notch (CVN) toughness requirements were not part of any North American specifications. The tragedy of the Point Pleasant Bridge was a major initiating factor for research programs in the United States, leading to the American Association of State Highway and Transportation Officials (AASHTO) developing fracture toughness requirements for welds and base metals in 1974 (Altstadt et al., 2014).

Another notable collapse is the Mianus River Bridge on I-95 in Cos Cob, Connecticut (failed 1983), where a fracture occurred in the pin and hanger assembly and caused the bridge to collapse, resulting in three fatalities (Connor et al., 2005). In the present day, pin and hanger assemblies, shown in Figure 1-2, are rarely (if ever) used in new designs due to their lack of redundancy.

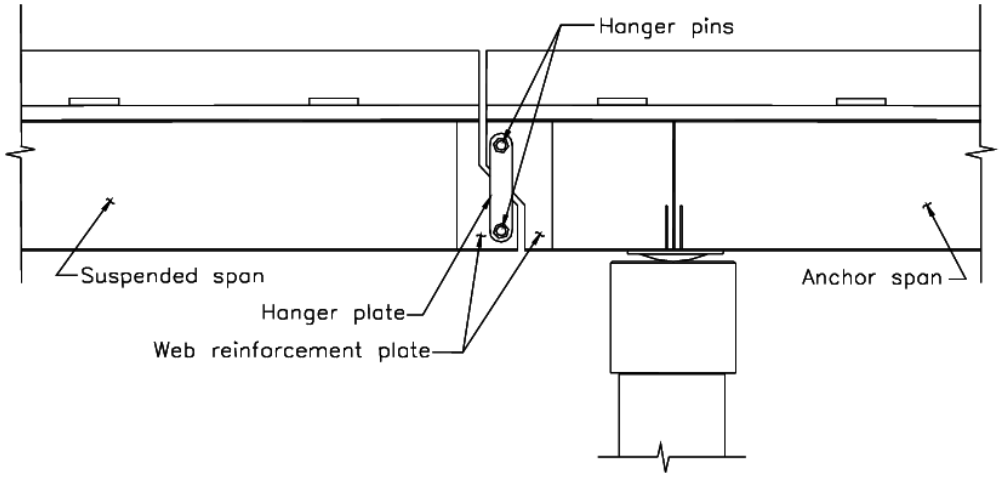


Figure 1-2 Example of a Pin and Hanger Assembly (Graybeal et al., 2000)

Following the Mianus River Bridge failure, provisions were added to the North American bridge design codes, AASHTO LRFD Part 6 and CSA S6, requiring that "fracture-critical members" (FCMs or "non-redundant tension members") be identified by the design engineer and be treated with particular attention in the design of new bridges (Connor et al., 2007), (Wright, 2002). The CSA definition of fracture-critical members are "members, including attachments, in a single load path structure that are subject to tensile stress and the failure of which can lead to collapse of the structure" (CSA, 2019), and AASHTO has a similar definition, "a steel primary member or portion thereof subject to tension whose failure would probably cause a portion of or the entire bridge to collapse" (AASHTO, 2017). Additionally, the Federal Highway Administration's (FHWA) National Bridge Inspection Standards (NBIS) were revised to include new requirements on hands-on inspection for any identified fracture-critical members. This is a

distinguishing point between North American codes and the Eurocode, the latter of which does not have specific wording on FCMs. Additionally, in America, as per the AWS D1.5 Bridge Welding Code, Clause 12 (known as the Fracture Control Plan) requires that the toughness and fabrication standards are more stringent for FCMs than for non-FCMs (Federal Highway Administration, 2019).

CSA and AASHTO assign the responsibility of identifying FCMs to the design engineer. However, in both codes, regulations on how to identify them are very limited and vague, leaving much of the classification of these members to engineering judgement. Some jurisdictions, such as North Dakota (North Dakota Department of Transportation Bridge Division, 2000), provide a guideline document on the types of members or details that could potentially be fracture-susceptible, and to which an inspector should pay more attention, but these guidelines are still relatively broad.

Over the last 45 years, while the North American provisions for design of steel bridges against brittle fracture appear to be meeting the needs of designers and the general public in the sense that they are easy to use, and the number of brittle fracture bridge failures in North America has remained relatively small, they still occasionally occur in the 21st century. Modern day examples include the Sgt. Aubrey Cosens VC Memorial Bridge in Latchford, Ontario (failed in 2003), the US 422 Bridge (failed 2003), and Hoan Bridge (failed 2000) to name a few. The latter two examples both showed little signs of fatigue cracking and were both caused by a phenomenon called constraint-induced fracture or CIF (Connor et al., 2007).

Constraint-induced fracture (CIF) is a special case of brittle fracture, which is caused by a tri-axial state of stress. This may occur when there are multiple intersecting welds, such as a web-flange-stiffener connection without a sufficiently wide web gap, illustrated in Figure 1-3. Three conditions must exist for a detail to be susceptible to CIF, and removing one of them will decrease the susceptibility of occurrence: 1) a high local stress concentration; 2) the stress concentration is at a location of high constraint, which prevents local yielding; 3) there are sufficiently high tensile stresses. With proper detailing (e.g. sufficiently large web gap), the use of thinner plates, higher material toughness, or typically a combination thereof, a designer can reduce the risk of CIF (Connor et al., 2007).

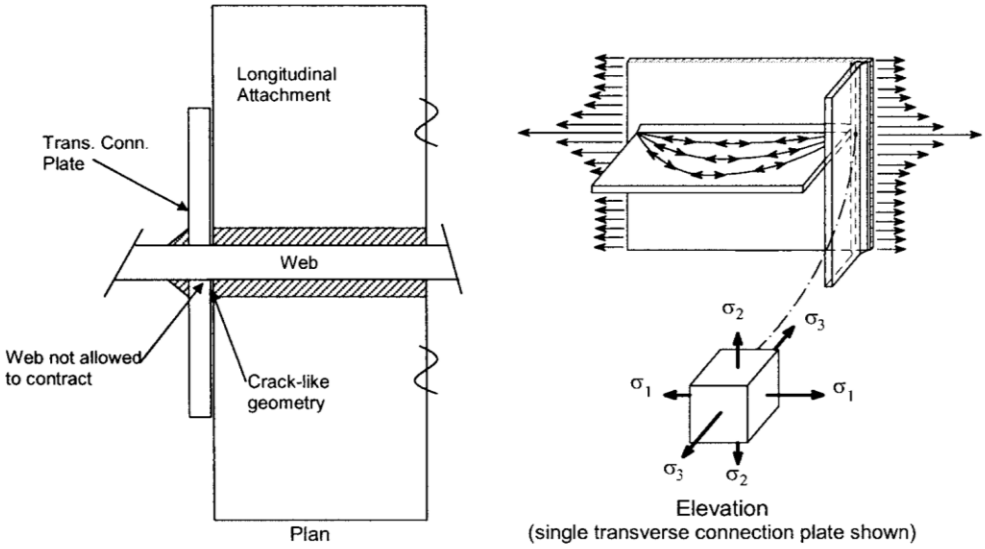


Figure 1-3 Detail Exhibiting Tri-axial Stress State (Connor et al., 2007)

However, CIF can occur in bridges even when the steels used on the structure meet CVN and AASHTO requirements. In the case of the Hoan Bridge failure in 2000, the brittle fracture cracks found in all three bridge girders were a result of intersecting and overlapping welds between shelf plates, gusset plates, and transverse connection plates, causing high levels of triaxial constraint. Both the web and flange plate metals were tested to meet the CVN and AASHTO requirements at the time the structure was built in 1972, and furthermore, met the CVN requirements at the year of failure.

In the latest revision cycle of the CSA S6 Canadian Highway Bridge Design Code, the code writers have identified the following issues surrounding the issue of brittle fracture:

- new, less conservative, design rules are needed for very thin plate structures, and structures that are plastically deformed (i.e. bent) either from vehicle impact or intentionally in fabrication (such as large culverts and orthotropic bridge deck ribs) resulting in local loss of toughness,
- the definition of "fracture critical", which is currently highly open to interpretation, needs to be better clarified for certain structure types, to prevent expensive overdesign,
- new design rules may be needed for pedestrian bridge structures, with lower impact velocities, and
- the design rules need to be critically assessed for aluminum structures, recognizing that aluminum does not exhibit a ductile-to-brittle transition at low temperatures in the same way as steel.

The basis for the North American provisions has largely been experience, common sense, and engineering judgement (Altstadt et al., 2014). As there is very little "in-house expertise" in Canada on brittle fracture or CIF of civil infrastructure such as steel bridge structures, international experts are generally relied upon when these cases arise. In Europe, significant advances have been made in recent decades in the

sophistication of the tools available for modelling and understanding brittle fracture in new and existing structures. While adoption of similar approaches in North America to assess these special situations may be of interest, it is worth noting that only a few preliminary attempts have been made to establish reliability levels provided by any existing design provisions (Artmont & Murphy, 2018), whereas significant work has been done to calibrate probabilistically provisions for other limit states (Kennedy & Gad Aly, 1980) (Zhao et al., 1994) and construction materials (MacGregor, 1976).

1.2 Objectives and Key Tasks

To address the gaps in the current Canadian state-of-knowledge regarding brittle fracture assessment, the following project objectives were defined:

1) to investigate alternative approached for evaluating the notional reliability level against brittle fracture for elements in steel highway bridge structures, including time dependent and independent formulations for assessing an appropriate limit state function,

2) to assess and quantify the reliability level against brittle fracture implied by the current toughness provisions for structural steel in the Canadian bridge code (CSA S6), and

3) to develop an improved practical tool for assessing brittle fracture risk in bridges, based on the results of the reliability analyses performed to address Objectives 1) and 2).

The major tasks to complete the project objectives are as follows:

Task 1 – Literature review and data gathering

A primary goal of this task was to review existing methodologies and input models for performing brittle fracture reliability analysis, in order to better understand the current state-of-knowledge on the subject of brittle fracture in steel bridges. In addition, the general state-of-knowledge related to brittle fracture as well as code calibration and structural reliability theory was investigated within this task.

Task 2 – Reliability-based assessment of current brittle fracture provisions

In this step, an analysis was performed to assess the reliability level associated with the current toughness requirements of the Canadian design standards (e.g. CSA S6). It was found that the existing Canadian standard is less conservative than the Eurocode for designing against brittle fracture in thick plate structures and fails to consider many factors such as member shape and dimensions, strain rate, cold forming, etc., which the Eurocode considers as key input parameters in their model. This is an area of concern, as steel fracture behaviour is known to depend considerably on a number of these factors.

One novel aspect of this research project is that it includes first attempt at assessing brittle fracture risk of steel bridges in a probabilistic framework. For this task, an algorithm was developed to automate the

calculation processes of the European brittle fracture provisions. Using this program, MCS was applied on the current bridge model and various application examples. The application examples aim at providing Canadian code writers with answers to their brittle fracture questions concerning topics including, but not limited to: consideration of thickness effects and treatment of "fracture critical members".

Task 3 – Consideration of time-dependent effects

The reliability analysis was then refined with a focus on a more sophisticated treatment of the time-dependent parameters. This required a different framework for modelling of the loading, where the service temperature fluctuated on a time scale and extreme value statistics were used to sample extreme live loads for a given analysis increment. Failures occur when a random combination of an exceptionally low temperature and exceptionally high truck load happen simultaneously. For this task, traffic survey data was provided by various highway authorities (e.g., the Ontario Ministry of Transportation).

Task 4 – Development of assessment tools

For this last task, the developed models were run for a wide range of cases, to produce user-friendly design aids and/or procedures for rapid assessment of new and existing structures in Canada. It is hoped that these tools will also help the bridge engineer to better understand what they are effectively doing when they specify a certain level of fracture toughness in the design of a new steel bridge.

1.3 Thesis Outline

Chapter 2 of the thesis includes the literature review on related topics including factors affecting material toughness, existing codes and methodologies for evaluating brittle fracture risk, and background studies on how these design standards were developed. Literature on new recommendations for CVN requirements, crack detection probabilities, and how heat affected zones affect brittle fracture, is also reviewed.

Chapter 3 describes the methodologies, key assumptions, equations, and input parameters used in each of the studies conducted within the overall project scope. This covers the comparison between three different codes and the initial probabilistic model developed in Excel Visual Basic. The process of developing models in MATLAB for the later studies, including a preliminary time-dependent model (which was later abandoned), a refined time-dependent model, and a time-independent model are then presented. The statistical parameters and distribution types assumed are presented in tabular form. Throughout the chapter, it is shown how the models were continuously refined in each phase of the project.

Chapter 4 describes the results of the first study of comparing international codes on brittle fracture design, highlighting the simplicity of current Canadian codes. It is found that the Canadian code is highly conservative for thin plates, whereas it is arguably unconservative for thick plates.

Chapter 5 presents the results of a preliminary probabilistic investigation using Excel Visual Basic. Several sensitivity studies performed with the developed model are presented, where initial crack size, load, and plate thickness were varied, and the resulting failure probabilities were calculated. Following this, histograms and cumulative density functions are defined for a preliminary time-dependent probabilistic MATLAB code. These are shown for K_{mat} at different temperature increments and K^*_{appld} for different live load increments. The hourly modeled temperature and live load graphs are illustrated, along with a sample case for 100 trials. The computational demand of this code version is also discussed.

Chapter 6 details the results of analyses conducted with a refined version of the time-dependent MATLAB code, which proved to result in significantly reduced analysis times with no loss in accuracy. These analyses highlight inconsistencies in current reliability levels in CSA S6, expressed by comparing current impact energy requirements vs. suggested impact energy requirements to achieve consistent reliabilities across different steel grades. Several sensitivity studies are then presented using this new model, where parameters varied include the assumed relationship between Charpy toughness to fracture toughness, the assumed strain rate, the ratio of live-to-dead load acting on the critical detail, and the design crack size.

Chapter 7 presents results obtained using a refined time-independent MATLAB code with a new calibrated design crack size, for time saving purposes. Several sensitivity studies are presented, which illustrate the effects of geographical location, span, influence line, traffic volume, and presence of multiple vehicles on the recommended impact energy requirements. Design tools in the form of contour plots are then developed, for different steel strengths, climates, thicknesses, and demand-to-capacity ratios.

Finally, Chapter 8 summarizes the conclusions from each study of the project and recommends areas of continued work.

2 Literature Review

The following literature review summarizes the factors that affect material toughness, methods of toughness evaluation, and existing code provisions for design against brittle fracture in Canada, USA, and Europe. Additionally, the topics of previous work on the master curve development, code calibration and reliability analysis for brittle fracture and other failure modes for steel structures in North America, which form the foundations of European and North American brittle fracture design standards, are discussed. Lastly, further studies on new recommendations for CVN requirements, crack detection probabilities, and how heat affected zones affect brittle fracture are reviewed.

2.1 Factors Affecting Material Toughness

The fracture behaviour of ferritic steels is strongly dependent on the temperature of the material at the time of failure. Fracture is considered brittle if it occurs before net section yielding (occurring in the lower shelf of the temperature vs. impact energy S-curve), otherwise it is considered ductile (occurring in the upper shelf) (Sedlacek et al., 2008). The temperature a which the failure mode type changes is termed the transition temperature. The transition temperature for steels is also an indicator of toughness: generally, a higher transition temperature correlates to a lower toughness steel and a lower transition temperature is associated with higher toughness.

Factors affecting the fracture toughness in a steel element include thickness, temperature, and loading rate. In general, steel toughness increases with increasing temperature and decreasing loading rate (Barsom, 1975). Thick plates are associated with an increased likelihood of a triaxial state of stress and variations in metallurgy through the thickness, due to the cooling process in fabrication. Thus, thinner plates typically have a higher fracture toughness, everything else being equal. Additionally, high degrees of cold forming reduce toughness (Sedlacek et al., 2008), as shown in Figure 2-1.

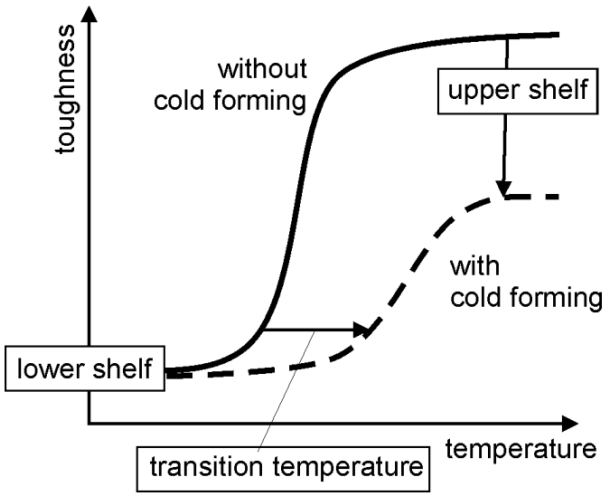


Figure 2-1 Effects of cold forming on material S-curve (Sedlacek et al., 2008)

2.2 Methods of Toughness Evaluation

2.2.1 Charpy V-Notch Method for Impact Toughness

The most commonly used method in specifications for measuring impact toughness is through the Charpy V-Notch (CVN) impact test method, due to its low cost, simplicity, and speed at which the test can be conducted (Barsom, 1975).

The CVN test is performed according to ASTM E23 (ASTM International, 2013). A standard specimen of 55 mm x 10 mm x 10 mm with a machined V-shaped notch at the middle is placed in the test apparatus and is impacted by a swinging pendulum. The initial and final heights of the pendulum are measured and the difference in height is used to calculate the energy absorbed by the specimen prior to fracture, in Joules (J). A typical procedure consists of testing three specimens at a specific temperature and repeating the test for varying temperatures. Heating or cooling of specimens may be conducted in a liquid bath or gas medium, and the specimens must be transferred to the testing apparatus and tested within 5 seconds of removal from the temperature-controlled medium. When a series of specimens are tested at different test temperatures, the results are plotted as energy vs. temperature and can be used to characterize the temperature vs. toughness S-curve showing the upper shelf, lower shelf, and transition region.

2.2.2 Critical Stress Intensity Factor, K_{Ic}, for Fracture Toughness

The critical plane-strain stress intensity factor (SIF), denoted by K_{Ic}, corresponds the stress at which unstable crack propagation will occur in a specimen (Barsom, 1975). K_{Ic} refers to Mode I cracking, the opening mode, which is depicted in Figure 2-2. Other modes of fracture are Mode II, sliding mode, and Mode III, tearing mode, which each have their own corresponding critical SIFs, K_{IIc} and K_{IIIc}, respectively. It is also noted that K-values for different crack modes cannot be added together, though they can be added for the same fracture mode by the principle of superposition. Cracks tend to propagate most easily under Mode I loading. In many design problems, the other loading modes are therefore often ignored.

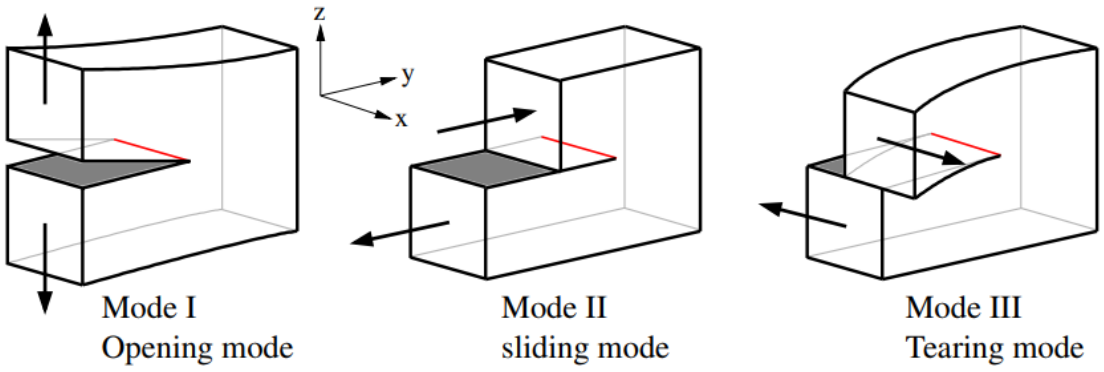


Figure 2-2 Different fracture crack modes (Zamiri et al., 2018)

K_{Ic} is commonly determined through either: 1) the bend test, using single-edge-notched pre-cracked beam specimens, loaded in 3-point bending, or 2) the compact test (CT), using single-edge-notched and fatigue pre-cracked plates loaded in tension. Other common shapes for the compact test are disk-shaped and arc-shaped specimens. Although the size of specimens may vary, they must conform to the dimensional proportions specified in ASTM E399 (ASTM International, 2020). An example of the dimensional and shape tolerances of a typical CT specimen is shown in Figure 2-3.

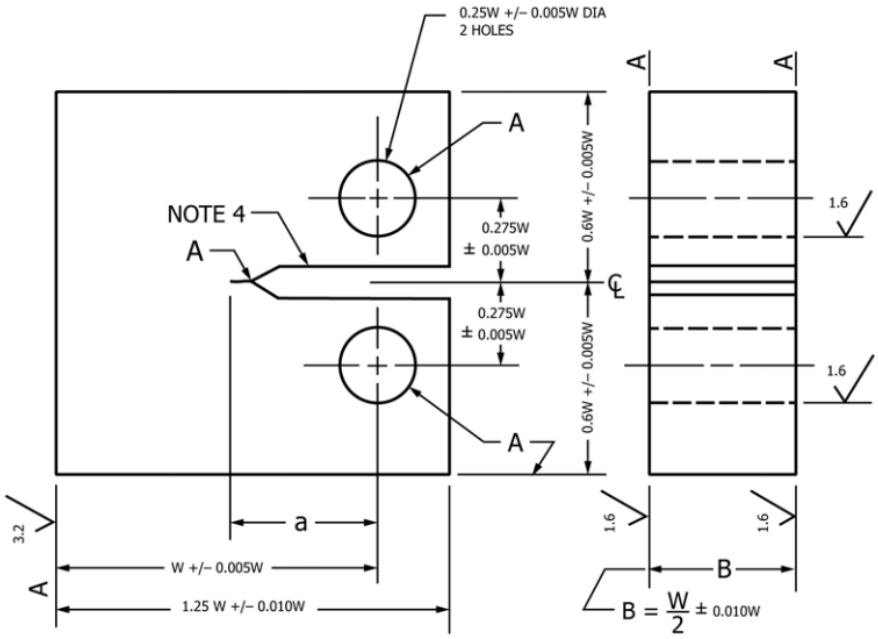


Figure 2-3 CT specimen shape and proportions (ASTM International, 2020)

The output of CT tests consist of force vs. displacement plots, where the crack mouth displacement is measured using a suitable displacement gauge or extensometer. Specimens are loaded until P_{max} is reached and they cannot sustain any more applied load. The calculation of the stress intensity factor, K, is done using equations presented in ASTM E399, which are dependent on the specimen shape. It is recommended that at least three tests are performed for each material condition.

K_{Ic} tests are performed relatively rarely as a means of quality control as the costs associated with fabricating and preparing the K_{Ic} specimens, and performing the test, are high. For this reason, different relationships have been developed to correlate CVN energy and K_{Ic}, as Charpy impact tests are quick, easy, and cheap. In (Collins et al., 2016), numerous relationships are described, and their equations presented. These include the Barsom and Rolfe original correlation (Barsom & Rolfe, 1970), Barsom and Rolfe two-stage correlation, BS 7910 Correlation, Corten and Sailors Correlation, Marandet and Sanz Correlation, Roberts and Newton Lower Bound Correlation, Rolfe-Novak-Barsom Upper Shelf Correlation, and Wallin Correlation.

2.2.3 J-Integral Method

The J-integral is a common method used to determine the stress intensity factor, as a simple conversion exists between *J* and *K* for linear-elastic materials, as shown in Equation 2-1 (Langford, 1980), where *E* is the modulus of elasticity of the material. The tests are performed according to ASTM E1820 (ASTM International, 2020). A major benefit to performing J_{Ic} tests is that the specimen dimensions can be much smaller than the ones required for a typical K_{Ic} test. The J-integral can also be determined by finite element analysis for complex specimen geometries, which is another reason for its popularity.

$$J_{Ic} = \frac{K_{Ic}^2}{E} \qquad \text{Equation 2-1}$$

2.3 Existing International Brittle Fracture Design Provisions

Design codes for preventing brittle fracture vary around the world. Key highlights of the development of practical design provisions to prevent brittle fracture in bridges in North America can be found, e.g., in Barsom (1975), Wright (2002), and Altstadt et al. (2014). As stated in Wright (2002), *"The current approach for avoiding brittle fracture in bridges in general normally involves specifying a level of toughness sufficient to prevent lower-shelf, brittle fracture at service temperatures and loading rates experienced by bridges"*. In the North American design codes, this is generally done with relatively simple lookup tables. In this section, a comparison is made between the existing toughness provisions in the Canadian code CSA S6-19, AASHTO, and the Eurocode.

2.3.1 Canadian Highway Bridge Design Code (CSA S6-19)

The existing CSA brittle fracture provisions are relatively simplified and consist of a design table to select the appropriate CVN energy requirements based on the steel grade, using the following steps. It is worth noting that the Canadian provisions are independent of plate thickness.

Step 1 – Identify fracture-critical and primary tension members on the structure.

Recall that Clause 10.23.1 in CSA S6 states that fracture-critical members are "*those tension components of a single load path bridge structure whose failure would be expected to result in the collapse of the bridge… A fracture-critical member may be either a complete bridge member, or a part thereof*". The key difference between fracture-critical and primary tension members is the level of redundancy. The CSA definition for primary tension members is "*members or member components whose failure would not cause the bridge to collapse*" (Canadian Standards Association, 2019).

Step 2 – Determine the minimum service temperature using Figure A3.1.2 in CSA-S6.

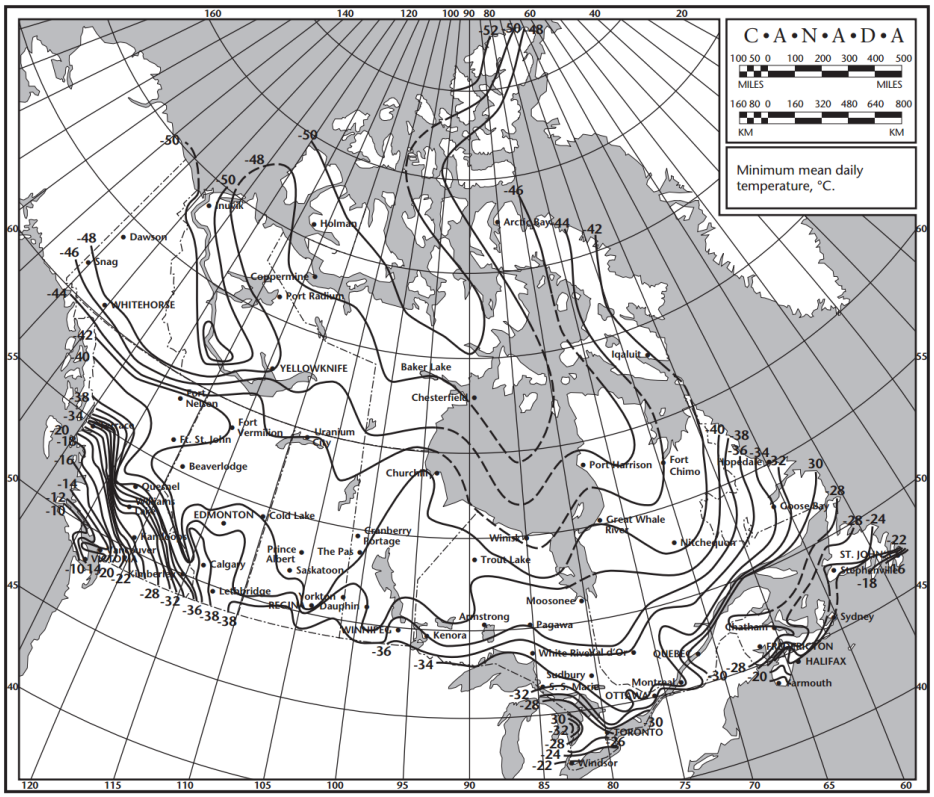


Figure A3.1.2
Minimum mean daily temperature
(See Clauses 3.9.4.1 and 10.23.3.4.)

Figure 2-4 Minimum mean daily temperature, Figure A3.1.2 from CSA-S6

Step 3 – Based on the minimum service temperature and steel grade, determine the appropriate CVN requirements: the minimum energy [Joules] tested at specified temperature [°C]. In CSA S6-19, Table 10.12 and Table 10.13 divide the minimum service temperature into two zones, excerpts shown in Figure 2-5 and Figure 2-6 (full tables not shown).

	Base metal test temperature T_t for minimum service temperature T_s,°C			Weld metal test temperature T_t for minimum service temperature T_s,°C		
Minimum service temperature	Minimum average energy (J)	$T_s \geq$ –30 °C	–30 °C > T_s > –52 °C	Minimum average energy (J)	$T_s \geq$ –40 °C	–40 °C > T_s > –52 °C
CSA G40.21 grades						
260WT	20	0	–20	20	–30	–30
300WT	20	0	–20	20	–30	–30
350WT and AT	27	0	–20	27	–30	–30
400WT and AT	27	0	–20	27	–30	–30
Steels requiring approval						
480WT and AT	27	–10	–30	27	–30	–40
700QT	48	–20	–35	48	–30	–40

Figure 2-5 Excerpt of Brittle Fracture Design Provisions (Table 10.12) in CSA S6

	Base metal test temperature T_t for minimum service temperature T_s,°C			Weld metal test temperature T_t for minimum service temperature T_s,°C		
Minimum service temperature	Minimum average energy (J)	$T_s \geq$ –30 °C	–30 °C > T_s > –52 °C	Minimum average energy (J)	$T_s \geq$ –40 °C	–40 °C > T_s > –52 °C
CSA G40.21 grades						
260WT	20	–20	–30	20	–30	–30
300WT	20	–20	–30	20	–30	–30
350WT and AT	27	–20	–30	27	–30	–30
400WT and AT	27	–20	–30	27	–30	–40
Steels requiring approval						
480WT and AT	27	–20	-40	27	–40	–50
700QT	Not permitted					

Figure 2-6 Excerpt of Brittle Fracture Design Provisions (Table 10.13) in CSA S6

It should be noted that CSA-S6 Table 10.12 corresponds to Table L.1 in the Canadian Handbook of Steel Construction (HSC) "*Recommended test temperatures and CVN impact test values for primary tension members under dynamic loading*", and that CSA-S6 Table 10.13 corresponds to Table L.3 in the Canadian HSC "*Recommended test temperatures and CVN impact test values for fracture critical members under dynamic loading*" (Canadian Institute of Steel Construction, 2021).

It should also be noted that the tables in CSA S6 correspond to the "dynamic loading" tables in the Canadian HSC. The Canadian HSC Commentary page 1-222 has two additional tables for impact loading. However, only the dynamic loading tables applicable to bridges are presented here.

2.3.2 AASHTO LRFD Part 6 – Steel Structures

It is well known that temperature is not the only factor that plays a role in the fracture behaviour of steels. The American code, AASHTO LRFD Part 6, provides a slightly more sophisticated table, which has three temperature zones and takes into account the steel plate thickness (AASHTO, 2017).

Grade (Y.P./Y.S.)	Thickness (in.)	Fracture-Critical				Nonfracture-Critical		
		Min. Test Value Energy (ft-lbs.)	Zone 1 (ft-lbs. @ °F)	Zone 2 (ft-lbs. @ °F)	Zone 3 (ft-lbs. @ °F)	Zone 1 (ft-lbs. @ °F)	Zone 2 (ft-lbs. @ °F)	Zone 3 (ft-lbs. @ °F)
36	$t \leq 4$	20	25 @ 70	25 @ 40	25 @ 10	15 @ 70	15 @ 40	15 @ 10
50/50S/ 50W	$t \leq 2$	20	25 @ 70	25 @ 40	25 @ 10	15 @ 70	15 @ 40	15 @ 10
	$2 < t \leq 4$	24	30 @ 70	30 @ 40	30 @ 10	20 @ 70	20 @ 40	20 @ 10
HPS 50W	$t \leq 4$	24	30 @ 10	30 @ 10	30 @ 10	20 @ 10	20 @ 10	20 @ 10
HPS 70W	$t \leq 4$	28	35 @ −10	35 @ −10	35 @ −10	25 @ −10	25 @ −10	25 @ −10
HPS 100W	$t \leq 2½$	28	35 @ –30	35 @ –30	35 @ −30	25 @ –30	25 @ –30	25 @ −30
	$2½ < t \leq 4$	36	not permitted	not permitted	not permitted	35 @ –30	35 @ –30	35 @ −30

Figure 2-7 Excerpt of Brittle Fracture Design Provisions (Table C6.6.2.1-1) in AASHTO

2.3.3 Wallin Master Curve

Wallin (1992) developed a correlation for calculating fracture toughness using a Master Curve approach. Fracture toughness tests (K_{1C}) are difficult and expensive. Although Charpy V-Notch (CVN) tests offer a faster and more economical alternative to fracture toughness tests, it is important to note that empirical correlations between Charpy and *K* values cannot be universally applied to all materials.

Wallin presents a fracture probability cleavage model (Wallin, 1992), and describes the process and assumptions, such as reference thickness and lower bound of fracture toughness, leading to the derivation of the Master Curve, which is applicable to ferritic structural steels. This curve, which is a function of temperature, Charpy test temperature, and effective length of the flaw, forms the basis of the Fracture Mechanics Method in the Eurocode presented in the subsequent section.

2.3.4 Eurocode (EN 1993-1-10)

Key research in Europe on toughness requirements for structural steel is discussed in Wallin (2002) and Sedlacek et al. (2008). As can be seen in Sedlacek et al. (2008), the European design provisions for avoiding brittle fracture are relatively sophisticated, compared with the North American ones. They include a simplified approach, with adjustment factors allowing a number of parameters (e.g., plate thickness, demand to capacity ratio, degree of cold work, etc.) to be explicitly considered, and a fracture mechanics-based approach for use situations such as assessing structures with existing cracks.

2.3.4.1 Eurocode Simplified Method

The following work presented in Section 2.3.4.1 has been published to CSCE 2020 Annual Conference and TRB 2021 Annual Meeting, with edits and modifications made for this thesis.

The brittle fracture provisions within Eurocode 3: Design of steel structures (also referred to as EN 1993-1-10) (European Commission, 2006) consist of two methods of analysis: a simplified method using design tables, and a more complex fracture-mechanics-based method. Both the Eurocode simplified method and CSA S6-19 Section 10.23 (Canadian Standards Association, 2019), and AASHTO LRFD 2017 Part 6 (AASHTO, 2017) procedures for brittle fracture use the minimum service temperature of the location of interest to determine the appropriate steel grade, subgrade, and CVN test requirements, i.e.: test temperature [°C or °F] and energy absorbed [J or ft-lbs]. However, aside from the use of the minimum service temperature as a primary input, the similarities end there. The design Table C6.6.2.1-1 in AASHTO Part 6 additionally considers plate thickness for specifying grade and toughness and has three different temperature zones as opposed to the two specified in the CSA S6 code. EN 1993-1-10 also takes into account numerous other factors such as plate thickness, yield strength of the material, stresses on the

component, radiation losses, member shape and dimensions, safety allowances, strain rate, and cold forming (if applicable). The five steps required for the EN 1993-1-10 simplified method are:

Step 1 – A thickness-adjusted yield strength $f_y(t)$ is calculated from the nominal strength.

$$f_y(t) = f_{y,nom} - 0.25 \cdot \frac{t}{t_0} \text{ [N/mm]} \quad \text{Equation 2-2}$$

where t is the thickness of the plate in mm and t_0 = 1 mm.

Step 2 – The maximum stress due to external loads, $\sigma_{Ed,max}$ [MPa], is calculated using a serviceability limit state (SLS) load combination.

Step 3 – Three theoretical stress levels are prepared for the lookup table, representing stress from external loads, are calculated using Equation 2-3 through Equation 2-5.

$$\sigma_{Ed} = 0.75 \cdot f_y(t) \text{ [N/mm}^2\text{]} \quad \text{Equation 2-3}$$

$$\sigma_{Ed} = 0.50 \cdot f_y(t) \text{ [N/mm}^2\text{]} \quad \text{Equation 2-4}$$

$$\sigma_{Ed} = 0.25 \cdot f_y(t) \text{ [N/mm}^2\text{]} \quad \text{Equation 2-5}$$

where σ_{Ed} is the maximum stress level, expressed as a proportion of $f_y(t)$.

Step 4 – The reference temperature is determined from the minimum extreme temperature with a 50-year return period, with temperature adjustments applied to consider radiation losses, member shape and dimension, safety allowance, strain rate, and degree of cold forming. This is shown in Equation 2-6. It is noted that T_{md} and ΔT_r have units of temperature, whereas the remaining adjustments account for other effects, originally in non-temperature units, which are then converted into an "equivalent temperature" for calculating T_{Ed}.

$$T_{Ed} = T_{md} + \Delta T_r + \Delta T_\sigma + \Delta T_R + T_{\dot{\varepsilon}} + \Delta T_{\epsilon_{cf}} \quad \text{Equation 2-6}$$

where T_{md} is the lowest daily air temperature of the location of interest, with a 50-year return period.

ΔT_r is an adjustment for radiation loss, which depends on the topography, latitude, albedo, etc., of the location of interest. Currently, research has been done in Germany to establish an average value of -5 °K radiation loss for the entire country. Other European countries often adopt the -5 °K radiation loss from Germany. However, this parameter has not yet been established in Canada.

ΔT_σ is the adjustment for stress and yield strength of the material, crack imperfection and member shape, and dimensions. If the detail fits within one of the welded details from the fatigue section of Eurocode 3 (EN 1993-1-9), this term is zero and no calculations are needed.

ΔT_R is a safety allowance, if required, to reflect different reliability levels for different applications.

- When the input values for strength and toughness (f_y and T_{27J}) are based on test measured data, there is a level of uncertainty associated with laboratory test data. An adjustment of -38 °K is used as a conservative adjustment to account for the uncertainties in the input values.
- Most European steels manufactured to the standard, EN 10025 - Hot rolled products of structural steels (European Commission 2005), are generally manufactured to a higher standard, so their nominal values of T_{27J} and f_y represent a lower bound for the material's actual strength and toughness. An adjustment of +7 °K can be used to account for the fact that most materials manufactured to the standard are, in reality, much stronger than specified.
- Note that the difference between the measured and specified toughness in EN 10025 is 45 °K.
- Since +7 °K is close to 0 °K, it is acceptable to use an adjustment of 0 °K when steels manufactured to EN 10025 are used, since it is conservative. 0 °K is used in the EN 1993-1-10 design table.

$\Delta T_{\dot{\varepsilon}}$ is the adjustment for a strain rate other than the reference strain rate.

- The design table assumes reference strain rate of $\dot{\varepsilon}_0 = 10^{-4}$/sec, which is suitable for dynamic action effects for most transient and persistent design situations.
- For other strain rates (e.g., impact loads), Equation 2-7 should be used.

$$\Delta T_{\dot{\varepsilon}} = -\left(1440 - f_y(t)/550\right) \cdot (\ln \dot{\varepsilon}/\dot{\varepsilon}_0)^{1.5} \text{ [°C]} \qquad \text{Equation 2-7}$$

$\Delta T_{\varepsilon cf}$ is the adjustment for the degree of cold forming ε_{cf}. The design table assumes non-cold-formed material with $\varepsilon_{cf} = 0\%$. For any non-zero ε_{cf}, an adjustment is calculated using Equation 2-8.

$$\Delta T_{\varepsilon_{cf}} = -3 \cdot \varepsilon_{cf} \text{ [°C]} \qquad \text{Equation 2-8}$$

Step 5 – A steel sub-grade is then selected from the design table – Table 2.1 in EN 1993-1-10. Based on the maximum stress of the component, σ_{Ed}, calculated in Step 4, expressed as a proportion of yield strength, the designer finds the stress level in Table 2.1 (0.75, 0.50, or $0.25 \cdot f_y(t)$). The designer then finds the column corresponding to the reference temperature calculated in Step 5. Based on the maximum plate thickness, the required grade and sub-grade of steel can be determined. Conversely, if the sub-grade is known, the maximum allowable plate thickness for the component can be determined. Linear interpolation can be used for values of $\sigma_{Ed} / f_y(t)$ between the three tabulated values, or the next highest value can be used.

Table 2-1 Eurocode Simplified Method Design Table Excerpt (reproduced from EN 1993-1-10)

		KV		Reference Temperature, T_{Ed} [°C]																					
				σ_{Ed}	0.75	fy(t)					σ_{Ed}	0.5	fy(t)					σ_{Ed}	0.25	fy(t)				
Steel Grade	Sub-grade	at T [°C]	J_{min}	10	0	-10	-20	-30	-40	-50	10	0	-10	-20	-30	-40	-50	10	0	-10	-20	-30	-40	-50
S235	JR	20	27	60	50	40	35	30	25	20	90	75	65	55	45	40	35	135	115	100	85	75	65	60
	J0	0	27	90	75	60	50	40	35	30	125	105	90	75	65	55	45	175	155	135	115	100	85	75
	J2	-20	27	125	105	90	75	60	50	40	170	145	125	105	90	75	65	200	200	175	155	135	115	100
S275	JR	20	27	55	45	35	30	25	20	15	80	70	55	50	40	35	30	125	110	95	80	70	60	55
	J0	0	27	75	65	55	45	35	30	25	115	95	80	70	55	50	40	165	145	125	110	95	80	70
	J2	-20	27	110	95	75	65	55	45	35	155	130	115	95	80	70	55	200	190	165	145	125	110	95
	M, N	-20	40	135	110	95	75	65	55	45	180	155	130	115	95	80	70	200	200	190	165	145	125	110
	ML, NL	-50	27	185	160	135	110	95	75	65	200	200	180	155	130	115	95	230	200	200	200	190	165	145
S355	JR	20	27	40	35	25	20	15	15	10	65	55	45	40	30	25	25	110	95	80	70	60	55	45
	J0	0	27	60	50	40	35	25	20	15	95	80	65	55	45	40	30	150	130	110	95	80	70	60
	J2	-20	27	90	75	60	50	40	35	25	135	110	95	80	65	55	45	200	175	150	130	110	95	80
	K2, M, N	-20	40	110	90	75	60	50	40	35	155	135	110	95	80	65	55	200	200	175	150	130	110	95
	ML, NL	-50	27	155	130	110	90	75	60	50	200	180	155	135	110	95	80	210	200	200	200	175	150	130

Based on Table 2-1, if the thickness of a steel exceeds the value in the table for a given reference temperature, then the material is at risk of brittle fracture. As this table only reaches temperatures of -50 °C, for colder temperatures reaching as low as -120 °C, there is an extended table in the European Commission Joint Research Centre (JRC) report titled "Choice of Steel Material to Avoid Brittle Fracture for Hollow Section Structures" (Feldmann et al., 2012). Additionally, it is noted that if a grade of steel is unknown, then a conservative assumption can be made by assuming the values of the first row of the table, S235JR steel, as it has a particularly low fracture resistance (Zamiri et al., 2018).

2.3.4.2 Eurocode Fracture Mechanics Method

Along with the simplified method, an alternate and more complex way of determining the toughness requirement is presented in the commentary to EN 1993-1-10, EUR 23510 EN (Sedlacek et al., 2008), using fracture mechanics. This method can be expressed in terms of stress intensity factor (*K*-value) or temperature. Each of these possibilities are described in the next sections. Regardless of the units, the basis of this analysis method is to ensure that the effects on the "action" side of the limit state function cannot exceed the effects of the material "resistance" side. This can generally be expressed as:

Load/Action Side		Material Resistance Side
K_{appld}	$\leq$	K_{Mat}
T_{Ed}	$\geq$	T_{Rd}

2.3.4.2.1 Stress Intensity Factor Format

The first format of the fracture mechanics method involves verifying that the toughness of the material (K_{Mat}, which is a function of T_{Ed}) is greater than the corresponding applied load effect (expressed as the

stress intensity factor, K_{appld}). This is shown in Equation 2-9 (Sedlacek et al., 2008), and the input parameters are described in the following paragraphs. The original master curve, which forms the basis of this method was developed in Wallin (1998). It is noted that the master curve approach is only valid for the lower shelf of ferritic steels and cannot be used to make predictions on upper shelf behaviour. Equation 2-9 is presented in SI units (MPa, m, mm, °C).

$$K^*_{appld} = \frac{K_{appld}}{k_{R6}-\rho} \leq 20 + \left[70\left\{\exp\frac{T_{Ed}-T_{27J}+18℃+\Delta T_R}{52}\right\}+10\right]\cdot\left(\frac{25}{b_{eff}}\right)^{\frac{1}{4}} \quad \text{Equation 2-9}$$

The left hand of the inequality represents the load/action side of the limit state function, the adjusted stress intensity factor K^*_{appld} is expressed as Equation 2-10.

$$K^*_{appld} = \frac{K_{appld}}{k_{R6}-\rho} \quad \text{Equation 2-10}$$

In this equation, the applied stress intensity factor, K_{appld}, is calculated using Equation 2-11.

$$K_{appld} = \sigma_{Ed}\sqrt{\pi a_d}\cdot Y\cdot M_k \quad \left[MPa\sqrt{m}\right] \quad \text{Equation 2-11}$$

where σ_{Ed} is the design value of stress applied from external loads, plus 100 MPa to account for tensile residual stresses that may be present due to welding [MPa].

a_d is the critical design size of the crack, in other words, the final size at the end of the safe operating period [m]. This is not to be confused with a_0, which is the initial size of the crack, often measured through non-destructive testing (NDT) methods or assumed when it cannot be measured. Reasonable assumptions of initial crack size would be the smallest detectable size from NDT methods or estimated using equations provided by Sedlacek et al. (2008). Equation 2-12 shows how a_d would be calculated, where Δa_{FCG} is the amount of fatigue crack growth over a service period (Zamiri et al., 2018). Section 2.7 highlights more literature on the definition of a_d.

$$a_d = a_0 + \Delta a_{FCG} \quad \text{Equation 2-12}$$

Y is the correction function for various crack positions and shapes [-]. The determination of *Y* depends on whether the crack is semi-elliptical, double edge, through-thickness, or single-edge. Table 2-3 in Sedlacek et al. (2008) shows equations for *Y* based on different literature sources from Raju-Newman and Murakami for different crack configurations. An excerpt of this table is shown in Figure 2-8.

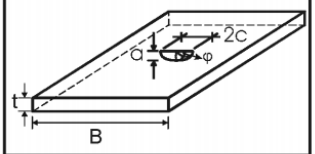
Case	Function Y	Source
Surface crack 	$Y = \frac{F_s}{\sqrt{Q}}$ $Q = 1 + 1.464\left(\frac{a}{c}\right)^{1.65}$ $F_s = \left[M_1 + M_2 \cdot \left(\frac{a}{t}\right)^2 + M_3 \cdot \left(\frac{a}{t}\right)^4\right] \cdot g \cdot f_\varphi \cdot f_w$	Raju - Newman
range of validity $0 \le \frac{a}{c} \le 1$ $\frac{2c}{B} \le 0.5$ $0 \le \varphi \le \pi$ $0 \le \frac{a}{t} \le 1$	$M_1 = 1.13 - 0.09 \cdot \left(\frac{a}{c}\right)$ $M_3 = 0.5 - \frac{1}{0.65 + \frac{a}{c}} + 14 \cdot \left(1 - \frac{a}{c}\right)^{24}$ $f_\varphi = \left[\left(\frac{a}{c}\right)^2 \cdot \cos^2\varphi + \sin^2\varphi\right]^{\frac{1}{4}}$	$M_2 = -0.54 + \frac{0.89}{0.2 + \frac{a}{c}}$ $g = 1 + \left[0.1 + 0.35\left(\frac{a}{t}\right)^2\right] \cdot (1 - \sin\varphi)^2$ $f_w = \left[\frac{1}{\cos\left(\frac{\pi \cdot c}{B}\sqrt{\frac{a}{t}}\right)}\right]^{1/2}$

Figure 2-8 Excerpt of Table 2-3 SIFs for various crack configurations (Sedlacek et al., 2008)

M_k is a stress intensity correction factor for attachments with semi-elliptical cracks at a weld toe [-]. The factor is taken as unity if the crack is non-semi-elliptical. The factor is retrieved from Table 2-4 in EUR 23510 EN (Sedlacek et al., 2008). An excerpt of the table is shown in Figure 2-9.

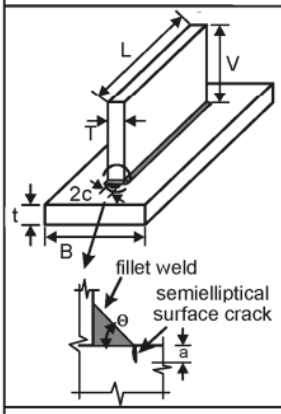
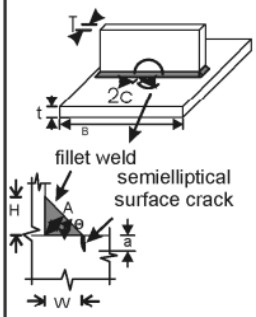
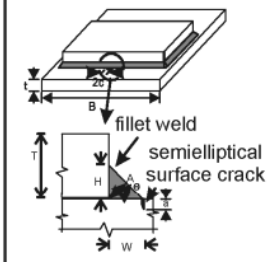
Case	Function	Source
	$M_k = C \cdot \left(\frac{a}{t}\right)^k$ and $M_k \geq 1$ $C = 0.9089 - 0.2357 \cdot \frac{T}{t} + 0.0249 \cdot \left(\frac{L}{t}\right)$ $-0.00038 \cdot \left(\frac{L}{t}\right)^2 + 0.0186 \cdot \frac{B}{t} - 0.1414 \cdot \frac{\Theta}{45°}$ $k = -0.02285 + 0.0167 \cdot \frac{T}{t}$ $-0.3863 \cdot \frac{\Theta}{45°} + 0.1230 \cdot \left(\frac{\Theta}{45°}\right)^2$	Hobbacher
range of validity $0.5 \leq \frac{L}{t} \leq 40$ $0.15 \leq \frac{T}{t} \leq 2$ $2.5 \leq \frac{B}{t} \leq 40$ $30° \leq \Theta \leq 60°$		
	$M_k = C \cdot \left(\frac{a}{t}\right)^k$ and $M_k \geq 1.0$ $C = 0.8068 - 0.1554 \cdot \frac{H}{t} + 0.0429 \cdot \left(\frac{H}{t}\right)^2 + 0.0794 \cdot \frac{W}{t}$ $k = -0.1993 - 0.1839 \cdot \frac{H}{t} + 0.0495 \left(\frac{H}{t}\right)^2 + 0.0815 \cdot \frac{W}{t}$	Hobbacher
range of validity $0.2 \leq \frac{H}{t} \leq 1.0$ $0.125 \leq \frac{T}{t} \leq 4.0$ $0.2 \leq \frac{W}{t} \leq 1.0$ $0.175 \leq \frac{A}{t} \leq 0.72$ $15° \leq \Theta \leq 60°$		
	$M_k = \frac{SCF}{1 + \frac{1}{0.1473} \cdot \left(\frac{a}{t}\right)^{0.4348}}$ and $M_k \geq 1.0$ $SCF = -3.539 \cdot \log\left(\frac{H}{t}\right) + 1.981 \cdot \log\left(\frac{T}{t}\right) + 5.798$	Fischer and Zettelmoyer
range of validity $0.32 \leq \frac{H}{t} \leq 0.96$ $0.64 \leq \frac{T}{t} \leq 2.0$		

Figure 2-9 Excerpt of Table 2-4 M_k for semi-elliptical surface cracks at different welded attachments (Sedlacek et al., 2008)

The action side stress intensity factor, K_{appld}, needs to be adjusted by two factors to account for local plasticity and residual stresses. These are the parameters in the denominator of Equation 2-10.

k_{R6} is a plasticity correction factor to account for local plasticity at the crack tip, ranging from 0.816 to 1, based on the R6 Failure Assessment Diagram (FAD). This is calculated using Equation 2-13, but as a conservative measure, it may also be taken as 0.816 (Zamiri et al., 2018).

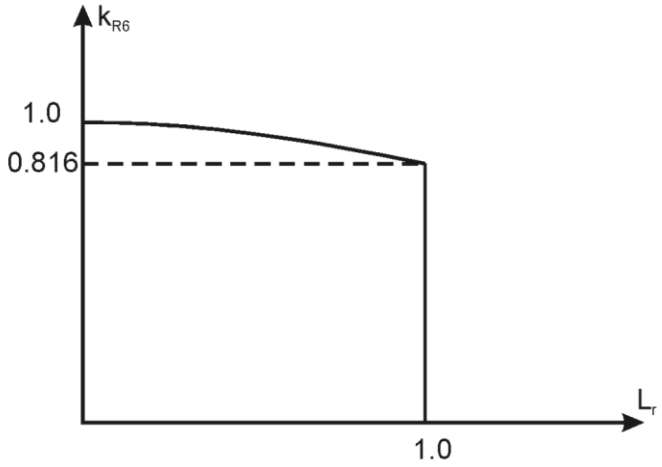


Figure 2-10 R6 Failure Assessment Diagram (Sedlacek et al., 2008)

$$k_{R6} = \frac{1}{\sqrt{1 + 0.5L_r^2}} \qquad \text{Equation 2-13}$$

In this equation, L_r is the ligament yielding parameter, defined as

$$L_r = \frac{\sigma_{Ed}}{\sigma_{gy}} \qquad \text{Equation 2-14}$$

where σ_{Ed} is the externally applied stress to the gross section [MPa], plus 100 MPa to account for residual stresses from welding. σ_{gy} is the stress applied to the gross section to obtain net section yielding [MPa], which is dependent on the crack type: surface, through-thickness, double edge, etc.

ρ is a correction factor for local residual stresses caused by welding and is taken as zero for non-welded details. For welded details, the value of ρ is dependent on the value of L_r. A more detailed breakdown of the determination of ρ is found in Table 2-6 of Sedlacek et al. (2008) (see Figure 2-11).

Definition of ρ	
$L_r \leq 0{,}8$	$\rho = \rho_1$
$0{,}8 \leq L_r \leq 1{,}05$	$\rho = 4\,\rho_1\,(1{,}05 - L_r)$
$1{,}05 \leq L_r$	$\rho = 0$
Definition of ρ_1	
$\psi = \frac{\sigma_S\, L_r}{\sigma_P} \leq 0$	$\rho_1 = 0$
$\psi = \frac{\sigma_S\, L_r}{\sigma_P} \leq 5{,}2$	$\rho_1 = 0{,}1\,\psi^{0{,}714} - 0{,}007\,\psi^2 + 0{,}00003\,\psi^5$
$\psi = \frac{\sigma_S\, L_r}{\sigma_P} > 5{,}2$	$\rho_1 = 0{,}25$

Figure 2-11 Definition of ρ (Sedlacek et al., 2008)

Equation 2-15 expresses the material resistance, which is derived using a base material *K* from the Wallin Master Curve (Wallin, 1998), modified for T_{K100} (the temperature associated with a fracture toughness of 100 MPa·√m) using the Sanz correlation, with the addition of the safety modification ΔT_R.

$$K_{mat}(T_{Ed}) = 20 + \left[70\left\{\exp\frac{T_{Ed} - T_{27J} + 18℃ + \Delta T_R}{52}\right\} + 10\right] \cdot \left(\frac{25}{b_{eff}}\right)^{\frac{1}{4}} \qquad \text{Equation 2-15}$$

b_{eff} represents the length of the critical crack front. Similar to σ_{gy}, it is also dependent on the crack type. The equations are given in Table 2-7 in the EUR 23510 EN and are functions of either the depth of the flaw or plate thickness, depending on the various crack types (Sedlacek et al., 2008) (see Figure 2-12).

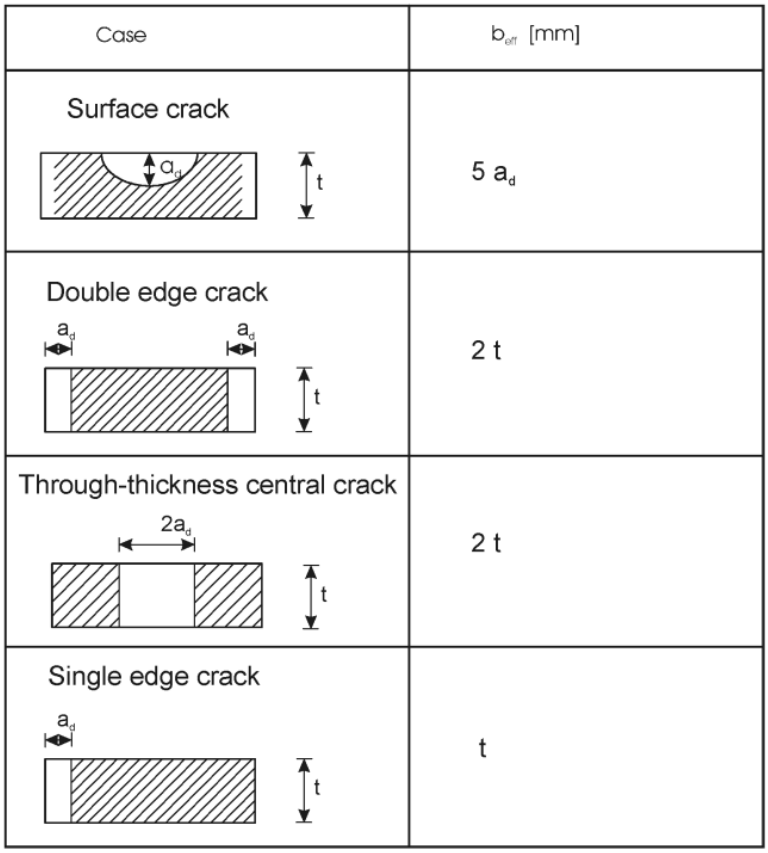


Figure 2-12 Definition of b_{eff} (Sedlacek et al., 2008)

2.3.4.2.2 Temperature Format

The fracture mechanics method may also be expressed in terms of equivalent temperature. Since the equation is on the temperature scale, the effects on the action side E_d, are required to be greater than the resistance side, R_d, in other words, $T_{Ed} \geq T_{Rd}$.

On the action side, the sum of the applied action effects is shown in Equation 2-16.

$$T_{Ed} = T_{md} + \Delta T_r + \Delta T_\sigma + \Delta T_R + \Delta T_{\dot{\varepsilon}} + \Delta T_{\varepsilon cf} \quad [°C] \qquad \text{Equation 2-16}$$

where T_{md}, ΔT_r, ΔT_R, $\Delta T_{\dot{\varepsilon}}$, and $\Delta T_{\varepsilon cf}$ are the same as the parameters of the same name in the simplified method presented in Section 2.3.4.1. The major difference in fracture mechanics is the determination of ΔT_σ, the adjustment for the influence of member shape, size and dimension, shown in Equation 2-17.

$$\Delta T_\sigma = -52 \ln \left[\frac{\left(\frac{K_{appld}}{k_{R6}-\rho} - 20\right)\left(\frac{b_{eff}}{25}\right)^{\frac{1}{4}}}{70} \right] \leq 120 \ [K] \qquad \text{Equation 2-17}$$

where K_{appld}, k_{R6}, ρ and b_{eff} are the same as defined in Section 2.3.4.2.1. On the resistance side, the effective "strength" of the material converted into temperature units is determined by Equation 2-18.

$$T_{Rd} = T_{K100} + \Delta T_t \ \ [°C] \qquad \text{Equation 2-18}$$

In this equation, the influence of material toughness, T_{K100}, is obtained using the Sanz Correlation shown in Equation 2-19, which relates the temperature corresponding with a fracture toughness of 100 MPa·√m to the temperature at which a Charpy sample absorbs 27 J of energy, T_{27J}.

$$T_{K100} = T_{27J} - 18 \ \ [°C] \qquad \text{Equation 2-19}$$

In a steel plate, the toughness varies between the surface area and core area of a plate due to inhomogeneity of the material. In general, when a thick plate cools it solidifies from the outer surface towards the core area, causing a decrease in toughness from the surface to the core of thick plates (Sedlacek et al., 2008). Due to this cooling phenomena, Zamiri et al. (2018) summarizes that the lower solubility of impurities and gases means that they will concentrate more in the regions that cool the latest; in other words, the outer regions are more pure and thus have higher quality of mechanical properties. The variation of material toughness in the through-thickness direction is represented by the new term ΔT_t and the relation shown in Equation 2-20, where t is the plate thickness in mm, and this is also illustrated in Figure 2-13 (Sedlacek et al., 2008).

$$\Delta T_t = 12.9 \tanh(1.9 \cdot \ln(t) - 7.6) + 12.8 \ \ [K] \qquad \text{Equation 2-20}$$

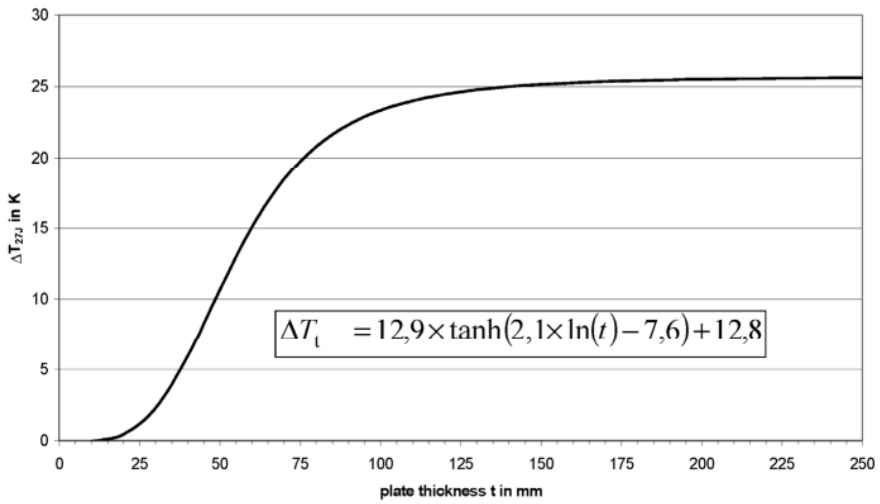


Figure 2-13 Thick plate inhomogeneity temperature shift curve (Sedlacek et al., 2008)

2.3.4.2.3 Basis of the Master Curve approach and Derivation of Stress Intensity Factor Equation in the Eurocode Background Document EUR 23510 EN

A cumulative probability density (CDF) function for cleavage fracture has been fitted to brittle fracture toughness test data (Wallin, 1992) and takes the form shown in Equation 2-21. This may also be called the "fracture probability cleavage model" (Viehrig et al., 2010).

$$P_f = 1 - \exp\left[-\left(\frac{K_{Ic} - K_{min}}{K_{0B} - K_{min}}\right)^4\right]$$ Equation 2-21

In this equation, K_{0B} is a specimen thickness- and temperature-dependent normalization parameter. This parameter allows the original CDF to be corrected based on different test temperature and specimen thicknesses. At a constant temperature, the relationship between K_{0B} and thickness dependence can be defined by the following equation, which is later used to make a thickness adjustment in the CDF:

$$K_{0B_1} = K_{min} + \left(K_{0B_2} - K_{min}\right)\left(\frac{B_2}{B_1}\right)^{\frac{1}{4}}$$ Equation 2-22

where B_1 is the reference thickness and K_{0B1} is the stress intensity factor associated with test specimens of size B_1, and B_2 is the new thickness of interest, and K_{0B2} is the stress intensity factor associated with specimens of size B_2. K_{min} represents a lower bound fracture toughness of the material of interest, which in the case of steel materials, is approximately $20\ \text{MPa}\sqrt{\text{m}}$. Wallin (1992) states that Equation 2-22 has been validated with test data for a large number of structural steels, ranging between low and high strength and 10 mm to 200 mm thicknesses. The previous equation is rearranged to solve for K_{0B2}:

$$K_{0B2} = (K_{0B1} - K_{min})\left(\frac{B_1}{B_2}\right)^{\frac{1}{4}} + K_{min}$$ Equation 2-23

K_{0B2} is then substituted in place of K_{0B} in the original CDF equation, to achieve a thickness-adjusted CDF:

$$P_f = 1 - \exp\left[-\left(\frac{K_{Ic} - K_{min}}{(K_{0B1} - K_{min})\left(\frac{B_1}{B_2}\right)^{\frac{1}{4}} + K_{min} - K_{min}}\right)^4\right]$$

$$P_f = 1 - \exp\left[-\left(\frac{K_{Ic} - K_{min}}{(K_{0B1} - K_{min})\left(\frac{B_1}{B_2}\right)^{\frac{1}{4}}}\right)^4\right]$$ Equation 2-24

$$P_f = 1 - \exp\left[-\left(\frac{B_2}{B_1}\right)\left(\frac{K_{Ic} - K_{min}}{K_{0B1} - K_{min}}\right)^4\right]$$

In this equation, B_1 is the reference thickness of 25 mm, which is the thickness of the typical compact tension (CT) specimens tested in the process of generating the master curve. As B_1 is now assigned to the "reference thickness" and is constant, and B_2 is variable, the parameters can be re-defined as B_0 and B, respectively. The parameter K_{0B1} can also be re-defined as simply K_0.

The thickness-adjusted CDF function becomes:

$$P_f = 1 - \exp\left[-\left(\frac{B}{B_0}\right)\left(\frac{K_{Ic} - K_{min}}{K_0 - K_{min}}\right)^4\right] \quad \text{Equation 2-25}$$

This equation is then rearranged to solve for K_{Ic}:

$$\exp\left[-\left(\frac{B}{B_0}\right)\left(\frac{K_{Ic} - K_{min}}{K_0 - K_{min}}\right)^4\right] = 1 - P_f$$

$$-\left(\frac{B}{B_0}\right)\left(\frac{K_{Ic} - K_{min}}{K_0 - K_{min}}\right)^4 = \ln 1 - P_f$$

$$\left(\frac{B}{B_0}\right)\left(\frac{K_{Ic} - K_{min}}{K_0 - K_{min}}\right)^4 = -\ln 1 - P_f$$

$$\frac{K_{Ic} - K_{min}}{K_0 - K_{min}}\left(\frac{B}{B_0}\right)^{1/4} = \left(-\ln 1 - P_f\right)^{\frac{1}{4}} \quad \text{Equation 2-26}$$

$$\frac{K_{Ic} - K_{min}}{K_0 - K_{min}} = \left(\frac{B_0}{B}\right)^{1/4}\left(\ln\frac{1}{1 - P_f}\right)^{\frac{1}{4}}$$

$$K_{Ic} = K_{min} + (K_0 - K_{min})\left(\frac{B_0}{B}\right)^{1/4}\left(\ln\frac{1}{1 - P_f}\right)^{\frac{1}{4}}$$

Previously in the original CDF, K_{0B} was defined as a thickness and temperature-dependent normalization parameter. After applying the thickness adjustment to the CDF function, K_{0B} is replaced with K_0, now a temperature dependent parameter. In Equation 2-26, K_0 is a function following the form:

$$K_0 = \alpha + \beta \cdot \exp[\gamma \cdot (T - T_0)] \quad \text{Equation 2-27}$$

In this equation, $\alpha + \beta = 108\ \text{MPa}\sqrt{\text{m}}$, γ is a material constant, and T_0 is defined as the temperature at which the mean fracture toughness is $100\ \text{MPa}\sqrt{\text{m}}$ (Wallin, 1992). Based on experimental data, the values of α, β, and γ do not vary significantly between different types of materials, and accordingly, different yield strengths. This can be observed in the toughness-temperature transition curve for 25 mm thick specimens (see Figure 2-14 (Wallin, 1992)), where the fitted curve using the same α, β, and γ values fits well for the various materials tested. Considering these parameters to be material independent and constants, they are found to be $\alpha = 31$, $\beta = 77$, and $\gamma = 0.019$. The K_0 equation takes the following form.

$$K_0 = 31 + 77 \cdot \exp[0.019 \cdot (T - T_0)] \quad \text{Equation 2-28}$$

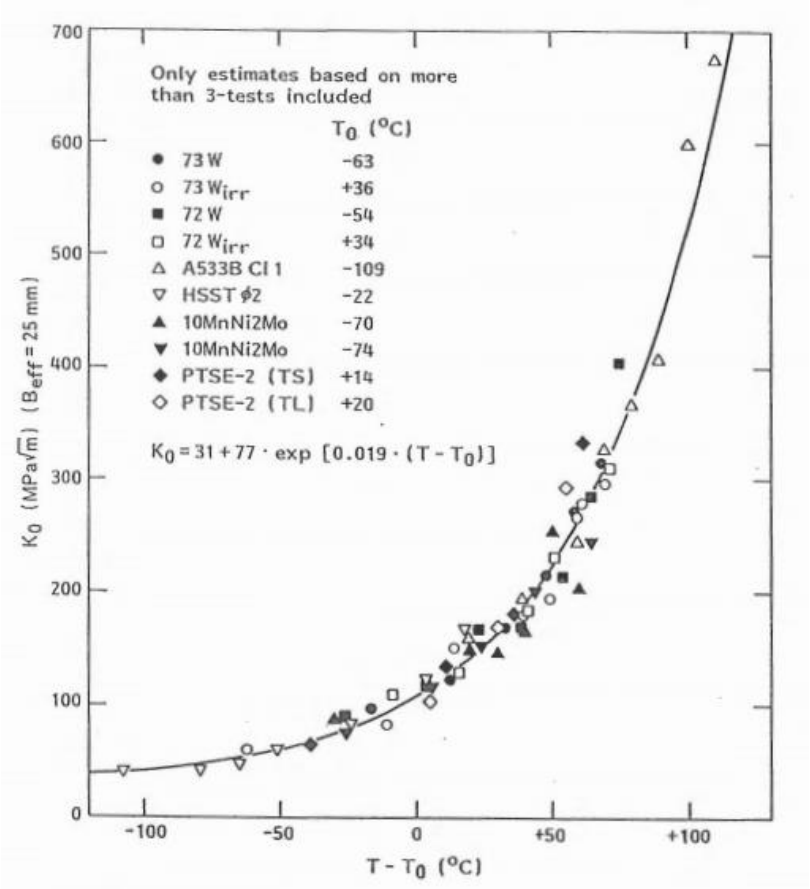


Figure 2-14 Temperature dependence of K_0 for 25 mm specimens (Wallin, 1992)

Substituting K_0 into the K_{Ic} equation:

$$K_{Ic} = K_{min} + (31 + 77 \cdot \exp[0.019 \cdot (T - T_0)] - K_{min}) \left(\frac{B_0}{B}\right)^{1/4} \left(\ln \frac{1}{1 - P_f}\right)^{\frac{1}{4}} \quad \text{Equation 2-29}$$

The Eurocode uses the median cumulative fracture probability (Viehrig, Zurbuchen, Schindler, & Kalkhof, 2010). Substituting the 50th percentile as P_f, the equation becomes:

$$K_{Ic} = K_{min} + (31 + 77 \cdot \exp[0.019 \cdot (T - T_0)] - K_{min}) \left(\frac{B_0}{B}\right)^{1/4} \left(\ln \frac{1}{1 - 0.5}\right)^{\frac{1}{4}}$$

$$K_{Ic} = K_{min} + (31 + 77 \cdot \exp[0.019 \cdot (T - T_0)] - K_{min}) \left(\frac{B_0}{B}\right)^{\frac{1}{4}} (0.9124) \quad \text{Equation 2-30}$$

$$K_{Ic} = K_{min} + (28.28 + 70.25 \cdot \exp[0.019 \cdot (T - T_0)] - K_{min}) \left(\frac{B_0}{B}\right)^{\frac{1}{4}}$$

Finally, substituting $K_{min} = 20$ MPa$\sqrt{\text{m}}$ and B_0 = 25 mm, the K_{Ic} equation becomes:

$$K_{Ic} = 20 + (28.28 + 70.25 \cdot \exp[0.019 \cdot (T - T_0)] - 20)\left(\frac{25}{B}\right)^{\frac{1}{4}}$$

Equation 2-31

$$K_{Ic} = 20 + [70.25 \cdot \exp 0.019 \cdot (T - T_0) + 8.28]\left(\frac{25}{B}\right)^{\frac{1}{4}}$$

The final format of the derived K_{Ic} equation is very close to the stress intensity inequality presented in the Eurocode fracture mechanics section for the material resistance side:

$$K_{mat} = 20 + \left[70 \cdot \exp\frac{T_{Ed} - T_{K100}}{52} + 10\right]\left(\frac{25}{B}\right)^{\frac{1}{4}}$$

Equation 2-32

where $0.019 \approx 1/52$, $T_0 = T_{K100}$, and it is suspected 70.25 was rounded to 70, and 8.28 was rounded to 10.

2.3.5 Further Contributions to European Brittle Fracture Standards

2.3.5.1 Strain Rate Effects on Brittle Fracture

Kühn (2005) provides information on the impact of strain rate on toughness. Typical strains range from $1x10^{-4}$ and $5x10^{3}$ for steels with a yield strength between 178 MPa and 890 MPa. Notably, traffic loads (vehicle crossings) fall into the category of quasi-static loading, thus, in most cases, one can neglect the strain rate effect for bridge structures. While there is a dynamic effect when a truck crosses over a bridge, Kühn (2005) shows that the maximum strain rate never occurs at the same time that the maximum stress occurs. To illustrate, if one were to assume the influence line due to a moving truck follows a sinusoidal curve, the maximum strain rate occurs when the stress level is zero. Further investigation was done on the effect when both stress and strain (σ and ε) are non-zero but not at their absolute maxima, and it was shown that the resulting largest strain effect (ΔT_{σ}, found to be 7 °K) is overall negligible.

2.3.5.2 Conversion CVN Test Temperature into Equivalent 27J Temperature

Kühn (2005) also derived an important equation which can be used to convert Charpy test data at different temperatures and impact energies to an equivalent T_{27J}, or vice versa.

$$T_{27J} = T_{KV} + 41.33 - 8.16 \cdot \sqrt{KV - 1.373}$$

Equation 2-33

where KV is the fracture toughness of a particular steel grade [J] at test temperature T_{KV}. Equation 2-33 is used in this project to enable comparisons between the Eurocode, AASHTO and CSA S6 tables.

2.4 Previous Work on Code Calibration and Reliability Analysis

A study done by Kennedy and Gad Aly in 1980 laid the foundation for making recommendations to the limit states design provisions in CSA S16 (Canadian Standards Association, 2019). Geometric and material

properties for W shapes, including their mean and coefficient of variation (COV) for steel columns and beams, were established based on measurements and coupon tests from Canadian mills (Kennedy & Gad Aly, 1980). Geometrical properties were measured and compared to the nominal dimensions through a geometric ratio, ρ_G (measured dimension / nominal dimension). Material properties (i.e. yield stress) was tested and compared to the nominal yield stress through a material ratio, ρ_M (tested yield stress / nominal yield stress). The study then related the tested capacity to the theoretical capacity (flexure and compression) to establish a professional ratio, ρ_P. These three ratios were multiplied together into an overall resistance ratio ρ_R, used along with the coefficient of variation, V, in an exponential model to determine a performance factor, ϕ, for various limit states, which captures the uncertainty in the prediction of structural resistance. The target reliability index, β, used to establish ϕ was 3.0, which was representative of simple beams and axially loaded columns at the time. The modes of failure investigated were flexure (laterally supported and unsupported) and compression. It was found in this study that the performance factor of 0.9 previously established for various limit states in S16 was conservative except for the cases of buckling for W and HSS shapes (Kennedy & Gad Aly, 1980).

In a comprehensive four-part paper series on fatigue reliability, the Committee on Fatigue and Fracture Reliability of the Committee on Structural Safety and Reliability of the Structural Division (American Society of Civil Engineers, 1982) presented an exploration into various aspects of fatigue analysis and structural integrity. Part 1 served as a foundational introduction, detailing the general process of fatigue crack growth and introducing key methodologies for modeling S-N relationships, such as the Basquin Equation and Lagner Model. Additionally, the authors provided typical fatigue data from literature, such as the COV of the number of cycles to failure. Part 2 covered quality control and maintenance techniques for bridges. Visual inspection can be performed at a rate of 0.8 ft^2 (750 cm^2) per minute, though the speed would be slower with a magnifier. Visual inspection is often dependent on the surface condition, and cleaning the surface may also take additional time. The paper discussed the sensitivity of non-destructive inspection (NDI) methods, including dye-penetrant, ultrasonics, x-ray, and magnetic particle inspection. highlighting the challenges of translating lab-controlled testing conditions to real-world field inspections. There are limited data on the sensitivity of these results under field conditions, though the general consensus is that field inspections may be less effective compared to lab-controlled conditions of testing. Part 3 of the series delves into variable amplitude loading, practical fatigue loads encountered in practice, and considerations for crack propagation. The authors presented Miner's rule, Wide Band Stresses (also known as Rainflow Method), and Paris' Law for cumulative damage calculation, cycle counting, and understanding fatigue crack propagation over time. Building upon these foundational principles, Part 4 of the series focused on the integration of methods presented in the preceding papers. It explored the application of reliability-based design principles and criteria for assessing structural fatigue.

Kennedy & Baker (1984) further studied resistance factors for the Ontario Highway Bridge Design Code, building upon prior work by Kennedy & Gad Aly (1980) and Nowak & Lind (1979). This work considered factors such as truncated distribution curves, fitting appropriate curves to experimental data, and accounting for skewness, in addition to addressing errors in measurement that could inflate coefficients of variation. The authors noted that continuous bridges may be assigned a lower safety index compared to single-span bridges, recognizing differences in collapse mechanisms. Monte Carlo simulation (MCS) was used to construct statistical distribution curves for resistance functions, considering geometric properties, material properties, and test/predicted ratios. Mean values and coefficients of variation were derived assuming lognormal distribution curves, which were very close to those obtained from the MCS distributions. Using a target reliability index of 3.5, resistance factors were then developed for various failure modes, including fully plastic moment resistance, yield moment resistance, inelastic buckling moment resistance, elastic buckling moment resistance, composite moment resistance, and column resistances, considering different slenderness parameter values. The authors recommended a general resistance factor of 0.93 for both welded and rolled sections, applicable to both single-span and multi-span bridges. Specifically for laterally supported steel bridges, the authors recommended resistance factors of 0.95 for welded sections and 0.98 for rolled sections. They also note that their original target reliability index of 3.5 may be lowered to 3.0 for some cases.

Two decades later in 2002, Schmidt & Bartlett (2002) reassessed the resistance factors from the Kennedy & Gad Aly (1980) study. One of the key driving factors for this reassessment was that the manufacturer that supplied materials for the previous study had ceased to produce W shapes in Canada, and it was beneficial to perform a reassessment from steels manufactured in Canada and imported from the United States to obtain a more comprehensive data set. Additionally, the resistance factors from CSA S16 needed to be reviewed, as over the decades, there had been changes in the industry and how steels were manufactured and underwent quality control procedures. New material tests were performed, and data was gathered based on steel from numerous major steel suppliers across North America. A similar procedure to Kennedy & Gad Aly (1980) was followed, using δ instead of ρ as notation for the ratio between the measured to nominal parameter. Yield strength, ultimate strength, and modulus of elasticity were investigated. In this study, it was found that the ratio of actual to nominal dimensions had improved (i.e. a reduction in the scatter was observed), likely due to reduced tolerances in CSA G40.20, and the yield strength bias factor increased and COV decreased for HSS and WWF shapes compared to the Kennedy & Gad Aly study. However, the statistical parameters were found to be slightly worse for W shapes (Schmidt & Bartlett, 2002).

The fundamental principles developed in these seminal works continue to be employed to establish safety levels for failure modes and structural elements not included in previous calibration efforts. For example, a fatigue reliability analysis was performed on steel-concrete composite shear connectors in one study, where MCS was used along with an iterative structural analysis (employing a structural model developed in the software SAP 2000, along with a Python script that "turns off" elements to simulate connector failures) to model the progressive sequence of shear connector failures under cyclic fatigue loading (Sjaarda et al., 2021). In another study, MCS was used to study the effects of slenderness, eccentricity, concrete strength on the reliability index of concrete-filled HSS beam-columns, comparing the new and previous design rules against target reliability indices (Rahbarimanesh & Tousignant, 2024). It is noteworthy that brittle fracture was not assessed as a mode of failure in any of these aforementioned studies.

Despite significant work on reliability analyses with respect to other failure modes (e.g., yielding, buckling, fatigue), similar studies on brittle fracture are extremely scarce. This highlights the ongoing need for a comprehensive probabilistic assessment of brittle fracture risk in steel bridges.

2.5 Previous US Study on Brittle Fracture using MCS and Probabilistic Analysis

One more recent development on the subject of probabilistic brittle fracture analysis is a study from US Department of Transportation in 2018 (Artmont et al., 2018). In this study, the methods used generally followed the same fracture mechanics principles and equations presented in the Eurocode, EN 1993-1-10, where a limit state function was set such that failure occurred if the applied K is greater than the material resistance K. Two different types of cracks were assessed: a single edge crack and semi-elliptical crack. Both cases assumed to occur on the tension flange of a girder. The minor differences between this study and the Eurocode methodology were observed in the equations for correction factors M_k and Q, and a slightly different a/c ratio for a semi-elliptical crack shape case.

MCS was employed in this probabilistic study. Crack sizes were assumed to be deterministic because there was no sufficient database on flaw sizes in steel bridges to use for generating realistic statistical parameters. The applied dead and live load were assumed to follow normal distributions. Statistical parameters for loads were obtained from NCHRP Report 386 (Nowak, 1999), used to represent a typical highway bridge.

This study used a time-invariant approach, where the live load and temperature were assumed to be a single point in time. The bias factor and COV for live load were selected as a 1-month maximum for a 100 ft span. The service temperature was assumed as -30 °F, for AASHTO Zone 2 conditions.

Some of the steels investigated in this study were “legacy steels” and some were modern:

- Legacy ASTM A242
- Legacy ASTM A572 Grade 50
- Modern ASTM A709 Grade 50
- Modern ASTM A709 Grade 50W
- Modern ASTM A709 HPS50W

Two plate thicknesses were assessed in the study: 1 in (25.4 mm) and 2.5 in (63.5 mm). Crack sizes were varied from 0.1 in (2.5 mm) to 0.65 in (16.5 mm), with increments of 0.05 in (1.27 mm). Each material was simulated for the different combinations between each of the plate thicknesses, crack types, and crack sizes. Preliminary simulations used 50 000 trials in an Excel spreadsheet. Later, 5 million trials were tested but it was found that the reliability indices did not change much with the larger number of samples.

The reliability index, β, is a numerical measure of the level of reliability in a system. A higher reliability index is associated with a lower probability of failure, and vice versa. In this study, each simulation produced a probability of failure (number of failed trials divided by 50 000 total trials) which was then converted into a corresponding β value. It was found that the reliability index decreased as crack size increased, as expected. The reliability index also decreased for thicker components, which was also expected as it is well known that thicker plate behaviour is more brittle. It was also found that the reliability index was higher for the semi-elliptical crack than the edge crack, for the same flaw size. The authors explain that the single edge crack has a higher stress intensity due to the crack shape parameter Y.

Further in the study, the maximum crack sizes corresponding with a target reliability index of 3.5 were presented for each material. This target index value corresponds to the AASHTO specification for a target failure rate of 1/5000 within the 75-year design life span of a bridge (AASHTO, 2017). Not unexpectedly, the maximum allowable crack size decreased as the plate thickness increased for each material. The allowable crack size was smaller for the edge crack, again because of the higher stress intensity. Additionally, the modern steels generally had a higher allowable crack size compared to the legacy steels. For example, for a semi-elliptical crack in a 1 in (25.4 mm) plate, the maximum crack sizes were in the range of 0.16 in (4.1 mm) to 0.2 in (5.1 mm) for the legacy steels compared to the range of 0.2 in (5.1 mm) to 0.52 in (13.2 mm) for the modern steels.

Overall, for the same plate thickness, the modern steels generally had improved performance. However, this increase in performance is more prominent for larger crack sizes than smaller crack sizes for the modern steels. For example, the reliability index was more than doubled at a = 0.65 in (16.5 mm) for Modern A709 vs. Legacy A572, and was only 15% better at a = 0.1 in (2.5 mm) for Modern A709 vs Legacy A572. This

can be attributed to the stress intensity factor equation, where the square root of the crack size is taken, so the influence of *a* is more prominent in the stress intensity factor *K* at smaller crack sizes. In other words, at smaller crack sizes, reliability is more influenced by demand rather than material resistance.

These results demonstrate extra benefit in using modern steels: if there are manufactured defects, corrosion effects, damage and fatigue which can cause larger cracks to be present in the material over its lifetime, the improvement in reliability associated with modern steels means that these structures would likely be safer than those fabricated with legacy steels. The main objective of this US study was to quantify the relationship between material toughness and fracture reliability in steel bridges in a probabilistic framework using MCS, though there are several limitations on the scope of the work. Only two plate thicknesses were assessed: 1 in (25.4 mm) and 2.5 in (63.5 mm), which certainly shows the effect of plate thickness on brittle fracture resistance but does not extend further to illustrate the results from a wider range of thicknesses. Only one temperature zone was assessed: AASHTO Zone 2, -30 °F, which corresponds to approximately -34 °C. The omission of other temperature zones, such as AASHTO Zone 3 (-60 °F, -51 °C), limited the study's applicability to regions with severe climates, similar to those in Canada. Additionally, this study did not consider time-dependency, and assumed that an extreme temperature and extreme load occurs at the same time. Nonetheless, the findings highlighted the benefits of using modern steels in improving structural reliability, particularly in mitigating the effects of manufactured defects, corrosion damage, and fatigue, which can cause larger cracks to be present over the course of the bridge lifespan.

2.6 Suggested Revisions to CVN Requirements in Literature

A study done by Altstadt et al. (2014) examined the current base metal CVN requirements for ASTM A709 grades. In the study, a quantitative comparison between grades was done by finding the ratio between yield strength and fracture toughness (YS/K_c). The fracture toughness was estimated using the master curve method proposed by Wallin (1992) with an assumed probability of failure, P_f = 0.5, and plate thickness, β = 50.8 mm. It is noted that the master curve method is also the foundation of the Eurocode provisions for design against brittle fracture. The master curve takes the following form.

$$K_c = 20 + [11 + 77 \cdot \exp(0.019 \cdot (T - T_0))] \left(\frac{25mm}{B}\right)^{\frac{1}{4}} \left[\ln\left(\frac{1}{1 - P_f}\right)\right]^{1/4} \qquad \text{Equation 2-34}$$

In this equation, T is the actual temperature and T_0 is defined as the temperature at which the median fracture toughness is $100\ \text{MPa}\sqrt{\text{m}}$. In Altstadt et al. (2014), yield stress is considered to be the demand, and K_c the resistance. A high YS/K_c ratio is taken to represent a low fracture resistance and vice versa. The study presents two tables of YS/K_c ratios, for static loading and dynamic loading. It was observed that there were large variations in the YS/K_c ratios, ranging between 3.1 to 7.2 for static loading, and ranging between 4.4

to 9.0 for dynamic loading. This indicated a significant variation in brittle fracture risk between the steel grades, where the authors suggest that the CVN test temperatures and minimum impact energies should be adjusted such that there is less variation between the brittle fracture risks. Notably, the lowest YS/K_c ratio was observed for the 250 MPa (36 ksi) grade in most cases – the only exception being the 50 ksi (HPS350W) in Zone 1 having slightly better fracture resistance, as shown in Table 2-2.

Table 2-2 YS/K_c Ratios for Static and Dynamic Loading (Altstadt, Wright, & Connor, 2014)

	Static Loading			**1/10-s Loading Rate to Failure**		
Grade	Zone 1 $1/m^{1/2}$ ($1/in.^{1/2}$)	Zone 2 $1/m^{1/2}$ ($1/in.^{1/2}$)	Zone 3 $1/m^{1/2}$ ($1/in.^{1/2}$)	Zone 1 $1/m^{1/2}$ ($1/in.^{1/2}$)	Zone 2 $1/m^{1/2}$ ($1/in.^{1/2}$)	Zone 3 $1/m^{1/2}$ ($1/in.^{1/2}$)
250 MPa (36 ksi)	3.6 (0.6)	3.5 (0.6)	3.6 (0.6)	4.6(0.7)	4.7 (0.7)	4.9 (0.8)
250 MPa (50 ksi)	5.0 (0.8)	4.9 (0.8)	5.0 (0.8)	6.4 (1.0)	6.5 (1.0)	6.8 (1.1)
50 ksi (HPS350W)	3.1 (0.5)	3.9 (0.6)	4.8 (0.8)	4.4 (0.7)	5.3 (0.8)	6.3 (1.0)
70 ksi (HPS485W)	3.7 (0.6)	4.7 (0.7)	5.8 (0.9)	5.1 (0.8)	6.2 (1.0)	7.5 (1.2)
690 MPa (100 ksi)	7.2 (1.1)	7.1 (1.1)	7.2 (1.1)	8.6 (1.4)	8.7 (1.4)	9.0 (1.4)
100 ksi (HPS690W)	4.5 (0.7)	5.7 (0.9)	7.2 (1.1)	5.8 (0.9)	7.2 (1.1)	9.0 (1.4)

It is observed that the 250 MPa (36 ksi) grade had the lowest YS/K_c ratio for most of the categories in Table 2-2, with the only exception being the 50 ksi (HPS350W) in Zone 1 being slightly better. The authors identified that it would be most appropriate to use a uniform crack tolerance that is consistent across all grades, but there was insufficient data within the U.S. bridge industry to define a suitable critical defect size or crack tolerance. Thus, the authors calibrated CVN requirements based on the 250 MPa (36 ksi) steel grade as a baseline, given its historically good performance. New CVN requirements were suggested to make the fracture resistance more consistent across the different steel grades and temperature zones, as summarized in Table 2-3.

Table 2-3 Calibrated CVN Requirements (Altstadt, Wright, & Connor, 2014)

Yield Strength	**CVN Energy**	**Zone 1 LAST = -18°C (0°F)**	**Zone 2 LAST = -34°C (-30°F)**	**Zone 3 LAST = -51°C (-60°F)**
MPa (ksi)	J	T (°C)	T (°C)	T (°C)
250 (36)	34	21	4	-12
350 (50)	41	-4	-20	-35
485 (70)	41	-29	-45	-61
690 (100)	41	-49	-65	-81

As of the latest iteration of AASHTO LRFD Part 6 (AASHTO, 2020), the suggestions made by Altstadt et al. (2014) have not yet been implemented.

2.7 Initial and Design Crack Size from Literature

One of the critical parameters required for application of the Eurocode fracture mechanics-based approach is a design crack size, a_d. This parameter is defined in the Eurocode as the sum of an initial flaw size a_0 and the fatigue crack growth over time. In Sedlacek et al. (2008), the fatigue crack growth is calculated over 500 000 cycles, which is suggested to represent approximately one quarter of the service life.

$$a_d = a_0 + \sum da_i \qquad \text{Equation 2-35}$$

The initial crack size, a_0, is assumed to depend on plate thickness and taken as:

$$a_0 = 0.5 \cdot \ln\left(1 + \frac{t}{t_0}\right) \text{for } t < 15 \text{ mm or } 0.5 \cdot \ln\left(\frac{t}{t_0}\right) \text{for } t \geq 15 \text{ mm} \qquad \text{Equation 2-36}$$

where t is the plate thickness [mm], and t_0 = 1 mm.

The basis for Equation 2-36 appears to be the European Standard EN 10163-3 (European Standard, 2004), wherein the maximum permissible depths of discontinuities for welds are tabulated in a step function and also depend on plate thickness. Smaller imperfections are considered to be inherent of the manufacturing process and are permissible. Additionally, there is no limit on the number of defects permissible under the threshold sizes. Surface defects exceeding these depths would need to be repaired before the structure is commissioned. Given the initial crack size, a_0, the resulting design crack size, a_d, after fatigue crack growth is modelled, can also empirically be represented as a function of plate thickness, and is taken as:

$$a_d = 2 \cdot 10^{-6}(t^3) + 6 \cdot 10^{-4}(t^2) + 0.1341 \cdot t + 0.6349 \qquad \text{Equation 2-37}$$

In the report by Zamiri et al. (2018), the authors also say that a_d may be approximated as half the thickness of the cracked plate for simplicity. The book by Nussbaumer et al. (2011) provide a similar equation for a_d that includes stress ranges, where $\Delta\sigma_{ref}$ = 100 N/ √ mm is the reference stress range. However, it is unclear how this equation was developed to include the stress ranges (and thus, was not used in the subsequent analyses for the current study).

$$a_d = (2 \times 10^{-6}(t^3) + 6 \times 10^{-4}(t^2) + 0.134t + 0.635)\left(\frac{\Delta\sigma_c}{\Delta\sigma_{ref}}\right)^3 \qquad \text{Equation 2-38}$$

In the European Standard EN 10163-3 (European Standard, 2004), the maximum permissible depths of discontinuities are listed in a table for Class C (general applications), shown in Table 2-4.

Table 2-4 Maximum Permissible Depth of Discontinuities for Class C (European Standard, 2004)

Nominal thickness of the product, *t* [mm]	**Maximum permissible depth of discontinuities [mm]**
$3 \leq t < 6$	20% of t
$6 \leq t < 20$	1.2
$20 \leq t < 40$	1.7
$40 \leq t < 80$	2.5
$80 \leq t < 160$	3.0

Imperfections smaller than the values in the table are considered to be inherent of the manufacturing process and are permissible. Additionally, there is no limit on the number of defects permissible under the threshold sizes, i.e. a plate containing one defect and another plate containing one hundred defects, all under the permissible depth of discontinuities, are acceptable plates. Surface defects exceeding these depths would need to be repaired before the structure is commissioned. These values in the table correspond loosely with the values calculated using the a_0 equation presented in Equation 2-36. For example, a plate of 25 mm thickness has a $a_0 = 1.61$ mm, which is close to the permissible depth in the table of $a_0 = 1.7$ mm.

Figure 2-15 illustrates these relationships of initial crack size, a_0, and design crack size, a_d, determined by the Eurocode (EN 10163-3 and EUR 23510 EN). The vertical difference between a_d and a_0 is the allowable crack growth for the corresponding plate thickness. In Kühn (2005), a similar figure exists with a lower bound on $a_d = 3$ mm for thinner plates below 16 mm.

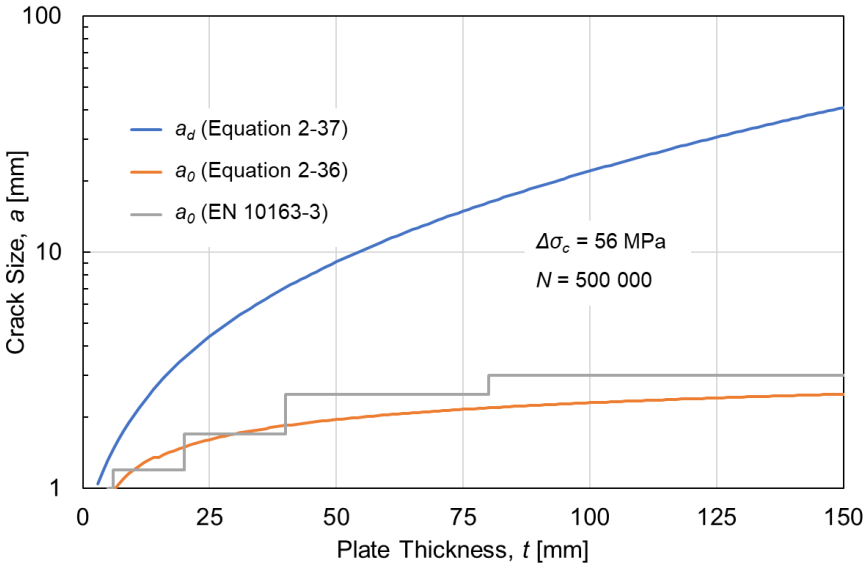


Figure 2-15 Initial and design crack sizes from EUR 23510 EN and EN 10163-3

Unlike the European standards, both Canadian and American standards do not tolerate initial defects from fabrication. The Canadian steel welding standard, W59-18, states in Clause 12.5.4.2 that "A weld subject to visual inspection shall be considered acceptable if visual inspection shows: a) no surface cracks; …" (Canadian Standards Association, 2018) and the American equivalent AWS D1.1 states in their visual inspection criteria table that "Any crack is unacceptable, regardless of size or location" (Section 6.9, Table 6.1) (American Welding Society, 2000)

Additionally, both codes have limitations on the length of sub-surface defects (porosity or fusion-type discontinuities), but not for defect depth. This is shown in Figure 2-16, a partial capture of Fig 12.5 from W59-18, and similar figures with different axes exist for AWS D1.1.

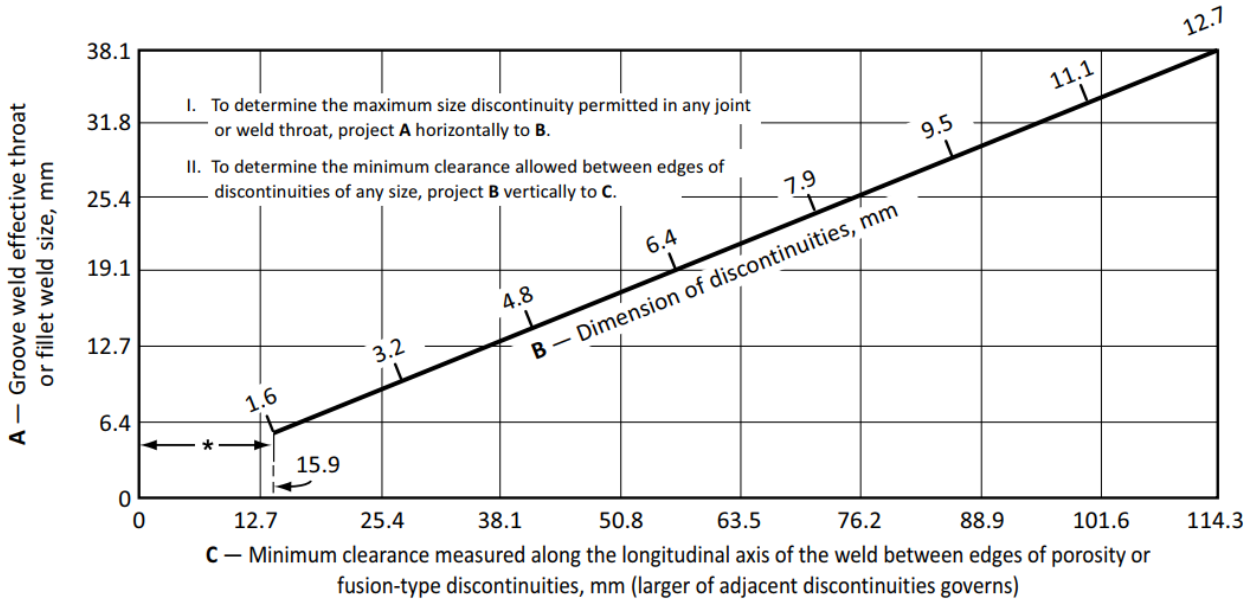


Figure 2-16 Example of sub-surface length limitations, partial capture of Fig 12.5 from W59-18

It is clear that there is a gap in the current North American welding codes for an allowable tolerance for crack-like defects at the surface from fabrication processes, as a zero-crack tolerance seems impractical. A defect tolerant design may be more practical for new steel structures in North America.

2.8 Crack Detection Probability Studies

In establishing a design crack size, the influence of inspection on the failure probability may be relevant. A challenge that arises when considering this aspect is the difficulty associated with detecting small cracks and the high scatter in detection rates associated with methods such as visual inspection. For example, a study done by Campbell et al. (2019) assessed 30 bridge inspectors and found that inspection of weathered specimens yielded an average crack detection rate of only 11%, and painted specimens yielded an average crack detection rate of only 65%. Longer cracks yielded somewhat higher detection rates. Using a log-odds model, the authors calculated an average detection rate of 50% for a 1 in (25.4 mm) crack and a 95% average detection rate for a 5.5 in (139.7 mm) crack. Probability detection curves can be found for other inspection methods (e.g., magnetic particle inspection) elsewhere in the literature (see for example, Lassen (1991)). Practical questions remain, however, in what the actual probability of detection is for cracks on real structures inspected under the difficult situations encountered in the field.

2.9 Hourly Temperature Modelling Methods

A probabilistic analysis of brittle fracture in steel bridges is necessarily going to require a rational approach for modelling the constantly varying ambient temperature during the service life.

One possible approach to model hourly temperature in a time-dependent analysis would be to use historical temperature data from multiple years, assume the temperature in a given hour of a given year can be obtained by fitting (for example) a normal distribution to the data for that hour over the multiple years, and then randomly sample a temperature for each hour using the hourly statistical distributions thus obtained. One issue with this approach is that independence of the temperatures in adjacent hours is assumed, which can result in highly unrealistic temperature jumps from one hour to the next.

Several sources discuss modelling temperature on an hourly basis by using historical data and applying a sinusoidal curve to model the daily temperature cycle and linking the last and first hours between days. A study done by Chow & Levermore (2007) suggests three methods based on known maximum and minimum temperatures, T_{max} and T_{min}, of each day and applying sinusoidal curves to obtain hourly temperatures between the extremes. The CIBSE method, shown in the following equations, relies on determining the times t_{max} and t_{min} at which the extreme temperatures occur in each day.

$$T(t) = f_1 \cdot T_{min} + f_2 \cdot T_{max} \ [℃] \qquad \text{Equation 2-39}$$

where: for $t < t_{min}$:

$$f_1 = \frac{\cos\left(\frac{\pi(t_{min} - t)}{24} + t_{min} - t_{max}\right) + 1}{2} \qquad \text{Equation 2-40}$$

for $t_{min} < t < t_{max}$:

$$f_1 = \frac{\cos\left(\frac{\pi(t - t_{min})}{t_{max}} - t_{min}\right) + 1}{2} \qquad \text{Equation 2-41}$$

for $t_{min} < t$

$$f_1 = \frac{\cos\left(\frac{\pi(24 + t_{min} - t)}{24} + t_{min} - t_{max}\right) + 1}{2} \qquad \text{Equation 2-42}$$

and

$$f_1 + f_2 = 1 \qquad \text{Equation 2-43}$$

The CIBSE Guide suggests the times t_{max} and t_{min} for each month (Chow & Levermore, 2007).

Table 2-5 T_{max} and T_{min} Times Suggested by CIBSE Guide A2 (Chow & Levermore, 2007)

Month	T_{max} time (t_{max})	T_{min} time (t_{min})
January	14	6
February	14	6
March	14	5
April	15	5
May	15	4
June	16	4
July	15	4
August	15	5
September	15	5
October	14	6
November	14	6
December	14	7

The Sin (14R-1) method is similar to the CIBSE method but assumes that T_{max} occurs in Hour 14 of each day and that T_{min} occurs one hour before sunrise (Chow & Levermore, 2007).

The previous two method link temperature between hours but fail to consider the continuity between the last hour of one day with the first hour of the next day, thus leaving the possibility for unrealistic temperature jumps between days. The Linking Days method provides an equation that addresses this concern (Chow & Levermore, 2007).

$$T(t) = \left(\frac{Temp_{next} + Temp_{prev}}{2}\right) - \left[\left(\frac{Temp_{next} - Temp_{prev}}{2}\right) \times \cos\left(\frac{\pi(t - t_{prev})}{(t_{next} - t_{prev})}\right)\right]$$

Equation 2-44

The Linking Days method equation may be used on its own, or with the t_{max} and t_{min} assumptions of the CIBSE method or Sin (14R-1) method. Chow & Levermore (2007) also describe the Q-Sin method which uses a combination of T_{max}, T_{min} and T_{ave} and quarter-sine waves.

The study compared the performance of each method by assessing three aspects: root mean square of errors (RMSE), comparing the average curves, and comparing averaged hourly data. The authors identified that the Q-sin method performed better than the Sin (14R-1) and CIBSE methods for the three aspects, and also

that when the Linking Days method was implemented, the results were better (smaller errors) than the same methods using individual days.

Other sources have developed equations to generate hourly temperatures based on historical data, along with the length of day using the latitude. Linvill (1990) describes a method for modelling hourly temperature for agricultural purposes. Equation 2-45 shows the equation for daytime warming where *t* is the time after sunrise and DL is the day length in hours. T_{max} and T_{min} are the maximum and minimum temperatures in the day.

$$T(t) = (T_{max} - T_{min}) \cdot \sin\left[\frac{\pi \cdot t}{DL + 4}\right] + \mathrm{T_{min}} \qquad \text{Equation 2-45}$$

Equation 2-46 shows the equation for nighttime cooling where *t* is the time after sunset and T_s is the sunset temperature.

$$T(t) = T_s - \left[\frac{(T_s - T_{min})}{\ln(24 - DL)}\right] \cdot \ln(t) \qquad \text{Equation 2-46}$$

2.10 Effect of Heat Affected Zones (HAZ) on Brittle Fracture

NCHRP Report 1056 addresses the heat-affected zone (HAZ) for welded structural steels, as current specifications only focus on weld metals and base metals. High temperatures in welding processes create microstructural changes in the steel, which in turn affect the mechanical properties of the material – fracture toughness included (National Academies of Sciences, Engineering, and Medicine, 2023).

The toughness requirements for steel used in highway bridges are governed by standards such as AASHTO M 270 and the AASHTO/AWS D1.5 Bridge Welding Code. These standards ensure the structural steel meets the necessary chemical, mechanical, and toughness properties through Charpy V-Notch (CVN) impact energy testing. However, correlations between CVN impact energy and fracture toughness were not developed for HAZs, and the current specifications do not adequately address the toughness requirements for HAZs.

A pilot study and full fracture characterization study involving CVN tests and K_{Jc} tests were conducted. These studies indicated that the toughness of HAZ may meet current requirements, though for some grades can be significantly lower than that of the base metal, which can reduce the critical flaw size and increase the susceptibility to brittle fracture under service conditions. This is apparent in the reduction in allowable critical flaw length compared to the historically accepted levels, particularly for AASHTO Zone 2 and Zone 3 service temperatures. It is also more apparent for fracture critical members compared to non-fracture critical members. Additionally, it was observed that some cracks in HAZ regions are unable to propagate into base metal before reaching the critical flaw size.

This report emphasized the need for HAZ-specific toughness requirements and the authors proposed changes to the AASHTO/AWS D1.5 Bridge Welding Code to fill the gaps in current specifications and improve the overall safety and reliability of welded steel highway bridges. These included the prohibition of electroslag welding (ESW-NG) for use in members subject to tensile stresses, updated commentary for Clause 7 discussing HAZ impact testing, and additional commentary to Clause 12 remarking the trend of decreasing fracture toughness with increasing heat input.

2.11 Fundamentals on Probability Theory and Probabilistic Analysis

2.11.1 Knowledge and Uncertainty

The Joint Committee on Structural Safety (JCSS) provides insight on the fundamentals of risk assessment in engineering (Joint Committee on Structural Safety, 2008).

Uncertainty in systems can be classified into two main categories. The first category, aleatory (or Type 1) uncertainty, arises from the intrinsic natural variability of the system. Examples of this include weather conditions such as temperature, wind speed, and precipitation.

Epistemic (or Type 2) uncertainties are caused by a lack of knowledge, typically as model uncertainties and statistical uncertainties. They generally have fixed but unknown values. For example, for safety, the yield strength of steel produced from the manufacturing plant will have a strength exceeding the specified yield strength. The actual yield strength of the steel would be unknown until it is tested to failure.

Both types of uncertainties need to be accounted for in probabilistic modelling, generally in the form of probability density functions with appropriate statistical parameters. Additionally, statistical dependency between two or more parameters should be appropriately accounted for in the model.

2.11.2 Risk Assessment

An important aspect of probabilistic design is risk assessment, which involves identifying, evaluating, and comparing potential hazards and their corresponding impacts on the structure.

The general equation for calculating risk is the probability of the event multiplied by the consequences resulting from that event, shown in Equation 2-47.

$$Risk = Probability \times Consequence \quad \text{Equation 2-47}$$

Effective risk assessment on structural systems requires accurate system representation, including:

- Exposures: Identifying elements at risk.
- Hazards: Recognizing potential sources of harm.
- Consequences: Estimating potential impacts.

Some modern examples of risk assessment tools include Bayesian Probabilistic Nets and Influence Diagrams.

Two key terms are commonly used when discussing risk: vulnerability and robustness. Vulnerability refers to the susceptibility of a system to harm, and is typically related to risk over time considering all possible events that could lead to such risk. Robustness measures a system's ability to respond to changes and recover from adverse events.

Quantifiable indicators can be used to measure and compare risks for different decisions alternatives. These indicators help in identifying the most critical risks and prioritizing mitigation efforts. In the example of a bridge, shown in Figure 2-17, indicators for exposure include the functionality, location, environment, and design life. Indicators for vulnerability include age of the structure, materials used, condition of the structure. Indicators for robustness include redundancy of the structural systems, emergency preparedness, ductility.

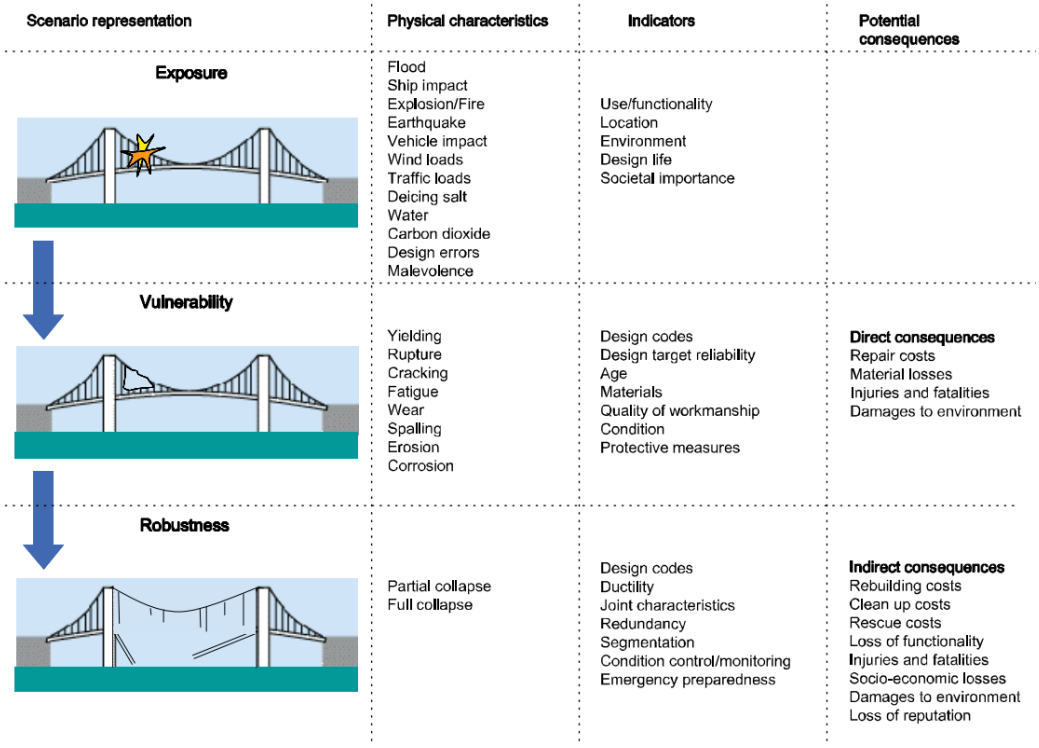


Figure 2-17 Risk indicators for a bridge scenario (Joint Committee on Structural Safety, 2008)

Decision trees for prior and posterior analyses are then outlined, illustrating the techniques for comparing the risks and benefits of different decision options.

Ultimately, risk can be mitigated but is generally impractical to eliminate completely in engineering design. Thus, there is some level of risk acceptance based on criteria such as life-cycle benefits, economic impacts, risks to people and safety, and environmental impacts. Tangible risks can be quantified in monetary terms,

whereas intangible risks cannot – common examples include loss of life, injuries, and sometimes environmental impacts.

2.11.3 Philosophy of Reliability Analysis and Probabilistic Design

Due to failures in structural systems being rare occurrences, unique to the extreme events that occur on a structure, and different structures being unique (i.e. not all bridges are identical), it is difficult to compile a comprehensive set of failure data. A probabilistic design problem involves obtaining the statistical information on each of the parameters involved, and using them to develop a probabilistic model for the load and resistance sides (commonly denoted as *S* and *R*, respectively) (Pandey & Jyrkama, 2019).

The safety margin, *Z*, can be denoted as $R - S$, where failure occurs if $Z \leq 0$.

2.11.4 Reliability Index

Reliability index (also known as the safety index) is the number of standard deviations above zero that mean of the safety margin (μ_Z) is, shown in Figure 2-18. A reliability index of zero indicates exactly a 50% probability of failure, and a negative reliability index indicates a failure probability of greater than 50%.

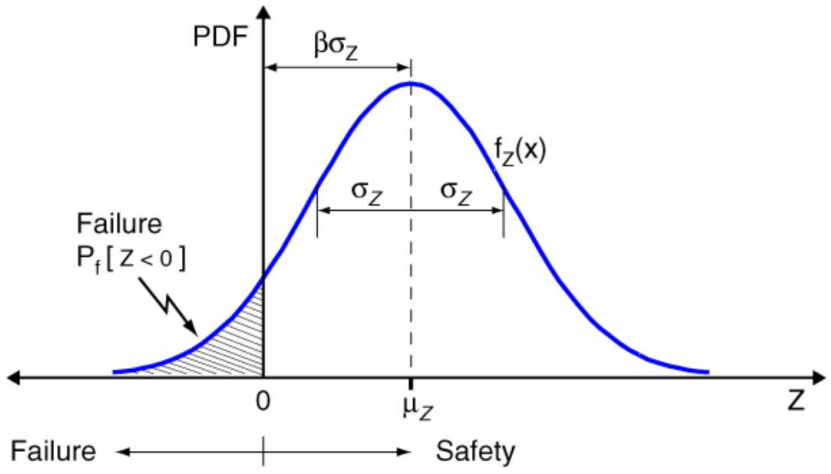


Figure 2-18 Probability density function of the safety index, *Z* (Pandey & Jyrkama, 2019)

Reliability index can be calculated using two different equations. Equation 2-49 can be used if *S* and *R* are assumed to have normal distributions, leading to *Z*, the linear combination of *S* and *R*, to also be normally distributed.

$$\beta = -\Phi^{-1}(P_f) = -NORMSINV(P_f) \qquad \text{Equation 2-48}$$

$$\beta = \frac{\mu_R - \mu_S}{\sqrt{\sigma_R^2 + \sigma_S^2}} = \frac{\mu_Z}{\sigma_Z} \qquad \text{Equation 2-49}$$

2.11.5 Turkstra's Rule

Turkstra's rule on load combinations states that the maximum value of a load from one source (or of one type) is reached during the design life of a bridge combined with an instantaneous or mean value of a load from another source or another load type. In simpler terms, because extreme loads generally occur in a short time, it is highly unlikely that the extreme values of two different load effects will occur at the same time (e.g. an earthquake occurrence plus an extremely heavy truck crossing a bridge) (Sun, Wang, & Sun, 2014).

If the load combination is assumed to have two load effects, Turkstra's rule can be expressed in the following form (Ghosn et al., 2003).

$$X_{max,T} = \max \begin{Bmatrix} [\max(x_1) + \bar{x}_2] \\ [\bar{x}_1 + \max(x_2)] \end{Bmatrix} \quad \text{Equation 2-50}$$

where $X_{max,T}$ is the maximum value of combined load effects in a time period of *T*.

$\max(x_1)$ is the maximum of all possible values x_1 of the load effect 1.

$\max(x_2)$ is the maximum of all possible values x_2 of the load effect 2.

$\bar{x}_1$ is the mean value of the load effect x_1.

$\bar{x}_2$ is the mean value of the load effect x_2.

Equation 2-50 can be summarized as follows: Evaluate the largest lifetime value of Load 1 plus the value of Load 2 that will occur when Load 1 is at its maximum. Evaluate the lifetime maximum of Load 2 plus the value of Load 1 that will occur when Load 2 is at its maximum. Select the larger of the two for design.

It is worth noting that Turkstra's rule is restricted to linear load combinations and loads that are statistically independent (Naess & Røyset, 2000).

2.11.6 Monte Carlo Simulation

Monte Carlo Simulation (MCS) is now a common tool for scientific research, which uses random sampling and statistical evaluation where individual trials are independent of each other. One of the major benefits is that it can be used for circumstances in which sampling would be too time consuming or impractical. However, it also has downsides which include requiring a significant amount of computing energy, and the model used can have imperfections or the code may have bugs (Harrison, 2010). Thus, spending much effort in correctly setting up the models, input parameters, and debugging is crucial.

A common use of this is random sampling from a PDF function, or alternately, using the inverse CDF method. The basis of the process is summarized in the following:

1. Sample a value between 0 and 1 to represent a probability, which can then be correlated back to the value of the parameter based on the distribution type and it's mean & COV (statistical parameters).
2. Evaluate the model.
3. Tally the simulation results.
4. Re-evaluate n times.
5. Construct histogram and determine probability of failure.

It is noted that the larger number of trials, the more accurate the simulation is.

3 Methodology

3.1 Comparison of International Design Provisions

The following work presented in Section 3.1 has been published in CSCE 2020 Annual Conference (Fan et al., 2020), TRB 2021 Annual Meeting (Fan et al., 2021), and the Transportation Research Record (Chien et al., 2021) with edits and modifications made for this thesis. The results of the design code comparison are presented in Chapter 4.

Although the Eurocode takes more factors into consideration for design against brittle fracture than the North American standards, it is uncertain how the results compare with the North American provisions, and whether this increased complexity is justified. As a first step in investigating these uncertainties, an analysis was performed to compare the brittle fracture provisions in EN 1993-1-10 with those in CSA S6-19 and AASHTO LRFD 2017 using a typical steel-concrete composite bridge based on a design example developed by the Canadian Institute of Steel Construction (CISC) for teaching purposes, shown in Figure 3-1 (Canadian Institute of Steel Construction, 2002). This bridge has four three-span continuous girders (43 m / 53 m / 43 m) with flange and web plate thicknesses varying along the span.

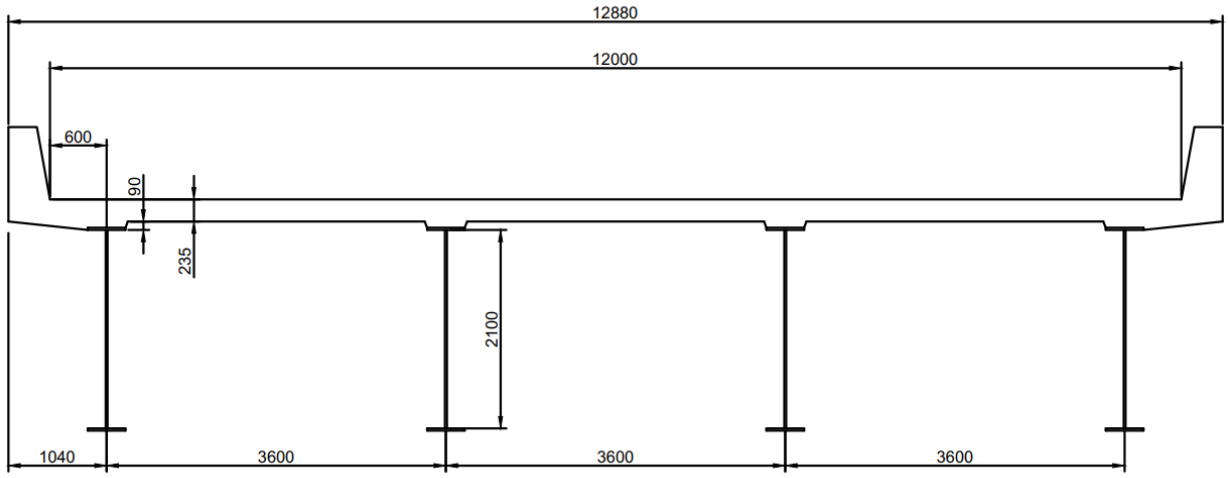


Figure 3-1 Straight plate girder bridge design (Canadian Institute of Steel Construction, 2002)

The assumed detail on the girder is a welded I-beam with a web stiffener and a semi-elliptical crack occurring in the bottom flange, as illustrated in Figure 3-2.

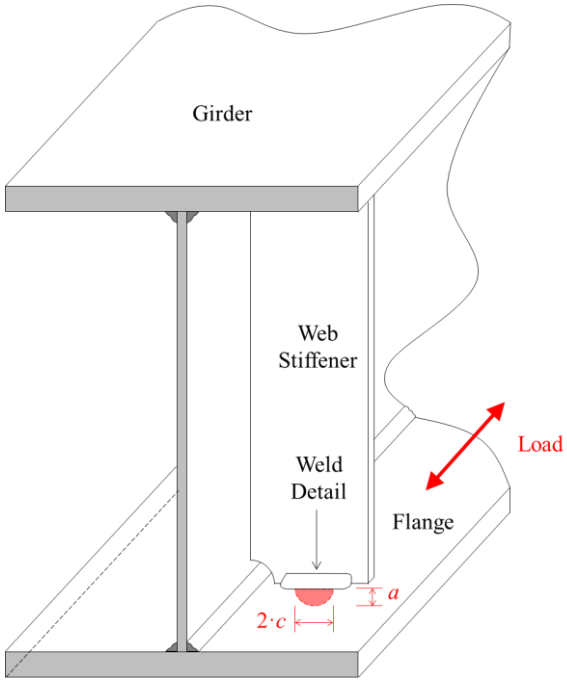


Figure 3-2 Assumed girder detail for analysis

For comparison purposes, the structural steel grades chosen are Canadian 350W (nominal yield strength of 350 MPa), which is roughly equivalent in yield strength to European S355 (nominal yield strength of 355 MPa) and American 50W (nominal yield strength of 50 ksi) steels. Note that, as in North America, the European steels are available in several sub-grades or toughness levels, corresponding with minimum CVN impact energies for different test temperatures. For the S355, the subgrades are summarized in Table 3-1.

Table 3-1 Sub-Grades of S355 Structural Steel

Sub-grade	Test Temperature [°C]	Impact Energy [J]
JR	20	27
J0	0	27
J2	-20	27
K2, M, N	-20	40
ML, NL	-50	27

The first step of the comparative analysis involved varying plate thickness at a single reference point on the girder while holding all other parameters constant, to study the effects of different thickness on the toughness requirements between the three codes. The point selected was the location of maximum positive bending stress along the girder span. A second comparison was then done for the entire bridge span, which

looked at the changes in steel subgrade requirements using EN 1993-1-10 where the stress level and plate thickness were both varying along the bridge length.

The CISC design example provided useful information on the typical dimensions and loads of straight girder bridges, but the example is set in "a Canadian town" whose name is unspecified. As climatic data was needed to determine brittle fracture requirements, three Canadian cities of interest were chosen for comparison: Waterloo, ON, Vancouver, BC, and Fort McMurray, AB. Each of these were selected to represent moderate, mild, and severe climates in Canada, respectively.

3.1.1 Extreme Air Temperature Calculation

While CSA S6 bases brittle fracture design on two temperature zones depending on minimum mean daily temperature and AASHTO uses three temperature zones depending on minimum service temperature, EN 1993-1-10 requires that the extreme temperature with a 50-year return period be specified. To determine this parameter, historical daily temperature data was collected from Environment Canada, and the lowest daily temperature was determined for each year. An Extreme Value Type 1 (Gumbel) distribution was then fitted to the data, following the procedure in the Calibration Report for CAN/CSA-S6 for obtaining extreme wind velocities from similar datasets (Agarwal et al., 2007). It should be noted that the sign on the temperature data was reversed, to obtain the probability of exceeding a negative temperature. The cumulative distribution function (CDF) of the Gumbel distribution follows Equation 3-1:

$$F_V(T) = \mathrm{EXP}\{-\mathrm{EXP}[-\alpha \cdot (\mathrm{T} - \mu)]\} \quad \text{Equation 3-1}$$

where

$$\bar{T} = \mu + 0.577/\alpha, \text{ and} \quad \text{Equation 3-2}$$

$$\sigma = 1.282/\alpha \quad \text{Equation 3-3}$$

In this case, *T* is extreme (i.e., minimum) daily temperature. The extreme daily temperature corresponding with an *N* year reference period has a CDF, which is expressed in Equation 3-4.

$$F_{T_N}(T_N) = \mathrm{EXP}\{-\mathrm{EXP}[-\alpha_N \cdot (T_N - \mu_N)]\} \quad \text{Equation 3-4}$$

where

$$\alpha_N = \alpha_1, \text{ and} \quad \text{Equation 3-5}$$

$$\mu_N = \mu_1 + \mathrm{LN}\left(N^{1/\alpha_1}\right) \quad \text{Equation 3-6}$$

Equation 3-1 through Equation 3-6 were applied with the *N* = 50 years. Using the CDFs of the extreme 50-year temperature event, 95th percentile values for this parameter were established (i.e. values associated with a 5% probability of exceedance). The resulting design extreme temperature values obtained for

Vancouver, BC, Waterloo, ON, and Fort McMurray, AB, were -26 °C (-14.8 °F), -45 °C (-49 °F), and -57 °C (-70.6 °F), respectively. If these were considered "minimum service temperatures", then they would correspond to AASHTO Temperature Zones 2, 3, and 3, respectively (AASHTO, 2017).

3.1.2 Use of Eurocode Design Tables

Table 2.1 in EN 1993-1-10 is the brittle fracture design table, which sets limitations on the maximum allowable plate thicknesses for a given steel, stress level, and reference temperature. As described in Section 2.3.4.1, either interpolation, or a more simplified "round up" method for the stress level and temperatures, can be applied when using the Table 2.1.

In the single-point comparison, interpolation was utilized: first interpolating the plate thicknesses at each stress level (0.75, 0.5, and $0.25 \cdot f_y(t)$) corresponding to the reference temperature of each city, and then interpolating the plate thickness for the appropriate stress level ($0.46 \cdot f_y(t)$). The rounding method was used for the entire bridge span analysis, where the stress level ($0.46 \cdot f_y(t)$) was rounded to $0.5 \cdot f_y(t)$ and the reference temperature was rounded down to the nearest 10 °C.

The reference temperature for the severe climate, in Fort McMurray, fell below the lowest temperature permissible in Table 2.1 in the current edition of EN 1993-1-10. For this analysis, as mentioned in Section 2.3.4.1, the European Commission Joint Research Centre (JRC) report "Choice of Steel Material to Avoid Brittle Fracture for Hollow Section Structures" (Feldmann et al., 2012) can be used for temperatures below -50 °C. Table 12-1 in this report covers plate thicknesses for temperatures down to -120 °C, but the table values above -50 °C are slightly different than prescribed in EN 1993-1-10. This is because the input parameters in the report vary slightly from those used in the original development of EN 1993-1-10. However, the differences are minor. The extended Table 12-1 has been recommended to replace Table 2.1 in future versions of EN 1993-1-10, so the use of the Table 12-1 in this study was reasonable.

It is worth noting that the CVN test temperatures for subgrades of the European S355 steel are not all specified for a 27 J notch toughness. The European subgrades are converted to "equivalent 27 J" subgrades, with an adjustment made to their test temperature using Equation 2-33 (see Chapter 2 of this thesis) from Kühn (2005), to make direct comparison possible.

3.1.3 Deterministic Application of Fracture Mechanics Method

Analyses were also performed using the temperature-based Eurocode fracture mechanics method. To compare the effects of CVN test temperature vs. plate thickness using this method, first, as the independent variable to be plotted, different CVN test temperatures were set between -50 °C and 60 °C at 10-degree increments. T_{Rd} (the temperature on the resistance side of the design equation) was calculated for each designated temperature using Equation 2-18. T_{Ed} (on the action side of the design equation) was calculated

using Equation 2-16. Note that for the adjustment of ΔT_σ, values for K_{appld}, k_{R6} and ρ are calculated using several nested equations, based on the information and tables from the Eurocode 3 background document, EUR 23510 EN (Sedlacek et al., 2008). Several assumptions had to be made in order to apply the correct equations: an assumed fillet weld size of 10 mm, semi-elliptical surface crack, crack depth to width (a/c) ratio of 0.4, and design crack size a_d determined using Equation 3-7.

$$a_d = 2 \times 10^{-6}(t^3) + 6 \times 10^{-4}(t^2) + 0.1341t + 0.6349 \quad \text{Equation 3-7}$$

The effective width, b_{eff}, for a surface crack is taken as $5 \cdot a_d$. The stresses due to external loads is calculated from Equation 3-8.

$$\sigma_{Ed} = \sigma_p + 100 \text{ MPa} \quad \text{Equation 3-8}$$

where σ_p is the stress due to external applied loads at that location of the span, and the additional 100 MPa accounts for residual stresses due to welding. The stress applied to the gross section to achieve yielding of the net section is calculated using Equation 3-9 for a semi-elliptical crack.

$$\sigma_{gy}(t) = f_y(t)\left(1 - \frac{\pi \cdot 2.5 \cdot a_d^2}{2t(5a_d + t)}\right) \quad \text{Equation 3-9}$$

The value of L_r is then calculated using the Equation 3-10.

$$L_r = \sigma_{Ed}/\sigma_{gr} \leq 1 \quad \text{Equation 3-10}$$

The plasticity correction factor, k_{R6} is then calculated using Equation 3-11.

$$k_{R6} = \frac{1}{\sqrt{1 + 0.5L_r^2}} \text{ for } L_r \leq 1 \text{ or } 0.816 \text{ for } L_r = 1 \quad \text{Equation 3-11}$$

The value of ρ is calculated using the equations in Table 2-6 from EUR 23510 EN (Sedlacek et al., 2008).

The applied K on the action side is calculated using Equation 3-12.

$$K_{appld} = \sigma_{Ed}\sqrt{\pi \cdot a_d} \cdot Y \cdot M_k \quad \text{Equation 3-12}$$

In this equation, the parameter Y is dependent on the crack shape and configuration and based on *Table 2-7* of EUR 23510 EN (Sedlacek et al., 2008). For a semi-elliptical surface crack, Y is calculated as:

$$Y = \frac{F_s}{\sqrt{Q}} \quad \text{Equation 3-13}$$

where:

$$Q = 1 + 1.464\left(\frac{a}{c}\right)^{1.65} \quad \text{Equation 3-14}$$

$$F_s = \left[M_1 + M_2\left(\frac{a}{t}\right)^2 + M_3\left(\frac{a}{t}\right)^4\right] \cdot g \cdot f_\varphi \cdot f_w \qquad \text{Equation 3-15}$$

The parameters of in Equation 3-15 are functions of defect size, defect width, and plate thickness. The calculation of parameter M_k is also dependent on the crack shape and configuration, based on Table 2-4 of EUR 23510 EN (Sedlacek et al., 2008). For a semi-elliptical crack, the equations used are as follows:

$$M_k = C\left(\frac{a}{t}\right)^k \geq 1 \qquad \text{Equation 3-16}$$

where:

$$C = 0.9089 - 0.2357\frac{T}{t} + 0.0249\left(\frac{L}{t}\right) - 0.00038\left(\frac{L}{t}\right)^2 + 0.0186\frac{B}{t} - 0.1414\frac{\theta}{45°} \qquad \text{Equation 3-17}$$

$$k = -0.02285 + 0.167\frac{T}{t} - 0.3863\frac{\theta}{45°} + 0.1230\left(\frac{\theta}{45°}\right)^2 \qquad \text{Equation 3-18}$$

where T is the web thickness in these equations (not to be confused with temperature), t is the flange plate thickness, B is the width of the flange, θ is the angle of the fillet weld (assumed to be 45°) and L is the longitudinal length of the weld. After calculating the values of K_{appld}, k_{R6}, and ρ, ΔT_σ is calculated from Equation 2-17. Excel's SOLVER function was used to solve for the plate thickness, t, such that $T_{Ed} = T_{Rd}$ for each CVN test temperature increment from -50 °C and 60 °C. These were plotted alongside the curves for the AASHTO and Eurocode simplified method.

The process was repeated by varying the design crack size by +20% and -20% to assess the sensitivity of the results to defect size, and again repeated for weld sizes of 25 mm and 50 mm. For each of these cases, the Microsoft Excel SOLVER was used to obtain the plate thickness.

At the location of maximum positive bending stress along the span, the ratio of $\sigma_{real}/f_y(t)$ was 0.46, which is close to 0.5. Further graphs were plotted at stress ratios of 0.25 and 0.75 to study the effect of stress level. Analyses at each location along the span were then performed to generate curves of CVN temperature vs. location, which could be compared with similar values using the other code provisions.

Chapter 4 presents the results of the code comparison described in this section.

3.2 Development of Preliminary Time-Independent Probabilistic Model

The work presented in this section has been published in the CSCE 2021 Annual Conference – Structures Specialty (Chien et al., 2021), with edits and modifications made for this thesis.

Following the preliminary comparison of codes, a probabilistic analysis was performed to compare the sensitivity of changes in each of the input parameters of the Eurocode fracture mechanics limit state equation to the annual probability of failure, P_f. The Eurocode equations and tables were first automated

using Visual Basic. Monte Carlo simulation (MCS) (Ang & Tang, 2006) was then used to obtain P_f. By simulating a large number of trials, the sensitivity of the P_f to changes in each input parameter can be determined.

P_f can then be used to calculate an annual reliability index, β, (and vice versa) using Equation 3-19, where Φ is the CDF of the standard normal distribution.

$$P_f = \Phi(-\beta) \qquad \text{Equation 3-19}$$

It is worth noting that every reliability analysis has some degree of time-dependency associated with it. However, for the purposes of this thesis, "time-independent" refers to an annual analysis without hour-to-hour fluctuations in parameters, whereas a time-dependent analysis involved hourly treatment of parameters later on.

3.2.1 Distribution Types and Statistical Parameters

In the probabilistic implementation of the Eurocode fracture mechanics method, bias factors are applied to the deterministic model parameters, typically in the form of "multipliers", which are defined to account for the various sources of uncertainty associated with each parameter. Table 3-2 summarizes the deterministic values assumed for each input parameter, with sources given where appropriate. These parameters are previously introduced in the Eurocode methods in Section 2.3.4. In this table, t and B are the girder flange thickness and width, flange stresses at the location of interest are denoted with a σ, and H_w and W_w are the weld height and width associated with the critical detail. The weld parameters are used to calculate the local stress intensity factor using equations not shown here for reasons of brevity. To apply these equations, a weld detail geometry must be assumed. In the calibration of the Eurocode simplified method, a longitudinal plate attachment detail was assumed, due to its relative severity, illustrated in Figure 3-3. Thus, a similar detail is conservatively assumed in the current analysis.

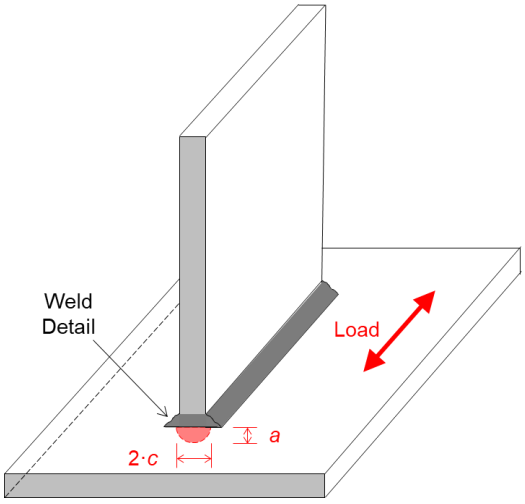


Figure 3-3 Characteristic weld detail from (Sedlacek et al., 2008)

Table 3-2 Deterministic Model Parameters

Parameter	Units	Value	Source
F_y	MPa	350	(Canadian Standards Association, 2019)
t	mm	25	(Canadian Institute of Steel Construction, 2002)
B	mm	375	(Canadian Institute of Steel Construction, 2002)
T_{md}	°C	location-dependent	-
ΔT_r	°C	-5.0	(Sedlacek et al., 2008)
ΔT_σ	°C	0.0	-
ΔT_R	°C	0.0	-
ΔT_ε	°C	0.0	-
ΔT_{ecf}	°C	0.0	-
T_{27J}	°C	-20 or -30	(Canadian Standards Association, 2019)
a	m	0.0022	(Sedlacek et al., 2008)
σ_{DLbc}	MPa	102.99	(Canadian Institute of Steel Construction, 2002)
σ_{DLac}	MPa	21.43	(Canadian Institute of Steel Construction, 2002)
σ_{LL}	MPa	64.78	(Canadian Institute of Steel Construction, 2002)
H_w	mm	10	-
W_w	mm	10	-

Table 3-3 summarizes the bias factors assumed in the probabilistic analysis. A normal distribution was assumed for the air temperature, T_{md}, as it can take both positive and negative values. The distributions for

f_y, t, B, a, σ_i, H, W, and t_{cover} were assumed to be lognormal as they cannot have negative values. The Eurocode temperature adjustments, ΔT_i, along with the 27 J notch toughness test temperature, were assumed to be constant.

The statistical parameters for the non-constant variables were found in literature. For lognormal distributions, the scale and shape parameters, λ and ζ, were then calculated using Equation 3-20 and Equation 3-21, respectively.

$$\lambda = \ln(\mu) - \frac{1}{2}\zeta^2 \qquad \text{Equation 3-20}$$

$$\zeta = \sqrt{\ln\left(1 + \frac{\sigma^2}{\mu^2}\right)} \qquad \text{Equation 3-21}$$

Sources used to establish the distribution type, mean, and COV for each bias factor are given in this table where appropriate. Concerning parameters in Table 3-3, the following additional information is noteworthy:

- The COV of the extreme minimum temperature was calculated following a procedure described in the CAN/CSA-S6 Calibration Report (Agarwal et al., 2007).
- The COV of the crack size was taken as 0.2 from Vojdani et al. (2018). For the base case, a 2.2 mm crack size constant is assumed, as was done for the Eurocode simplified method calibration (Feldmann et al., 2012). This parameter is varied subsequently in a parametric study. (Note: later on, this parameter is calibrated using a process that will be described later.)
- The bias factor for the dead load stress was obtained from Canadian Standards Association (2019) with type D1 (factory-produced components) assumed for the entire dead load. In reality, if the concrete deck were cast-in-place and covered with an asphalt wearing surface, a larger COV would be appropriate, or separate bias factors should be used for each dead load source. Uncertainties in the brittle fracture resistance can be captured using bias factors, *Z9* and *Z10*, to consider uncertainties associated with the brittle fracture "master curve" formula and the notch to fracture toughness conversion, based on raw test data in EUR 23510 EN (Sedlacek et al., 2008). Steel grades S355, S460, S690, and S890 were tested (and are reported in this reference) and the lower shelf of the master curve was fitted. Since the master curve was fitted to the average of the data, *Z9* is a multiplicative factor to model the scatter of test data for the fitting, which has been assigned a mean of 1.0 and standard deviation of 25%. Using this value, a close replication of the 50%, 95%, and 5% failure probability curves for the raw test data from *Fig. 2-7* in EUR 23510 EN (Sedlacek et al., 2008) could be produced. Note that the 20 MPa$\sqrt{\text{m}}$ term is not multiplied by *Z9* because K = 20 MPa$\sqrt{\text{m}}$ represents the lower bound for cleavage fracture in steels, and therefore the stress intensity factor cannot be lower than that

value (Wallin, 1992). Also note that in later iterations of the probabilistic model, an improved approach for modelling this statistical variable was employed, which will be described later.

- *Z10* is an additive factor to model the scatter in test data correlating the fracture mechanics transition temperature, T_{100}, to the Charpy test temperature, T_{27J}. which has been assigned a mean of 0 and standard deviation of 0.13 (the transition temperature standard deviation is 13 °C), based on the raw data from *Fig. 2-8* in EUR 23510 EN (Sedlacek et al., 2008). Further elaboration on how this was done will be discussed where the time dependent reliability model is described.

Table 3-3 Statistical Variables for Base Case Analysis (Ft. McMurray)

Z	Modifies	$\bar{Z}$	V_Z (σ_Z)	Distribution	Source
Z1	F_y	1.101	0.0915	Lognormal	(Kennedy & Baker, 1984)
Z2	t	1.02	0.012	Lognormal	(Kennedy & Gad Aly, 1980)
Z3	T_{md}	1.0	0.0569	Normal	50-year service period, calculated based on (Agarwal et al., 2007)
Z4	a	1.0	0.20	Lognormal	(Vojdani et al., 2018)
Z5	σ_{D1}	1.03	0.08	Lognormal	(Agarwal et al., 2007)
Z6	σ_{LL}	1.5228	0.0304	Lognormal	50-year service period, calculated based on (Agarwal et al., 2007)
Z7	H_w	1.0	0.16	Lognormal	(Kala et al., 2009)
Z8	W_w	1.0	0.16	Lognormal	(Kala et al., 2009)
Z9	Master Curve	1.0	0.25	Lognormal	(Sedlacek et al., 2008)
Z10	CVN to SIF Conversion	0.0	(13°C)	Normal	(Sedlacek et al., 2008)

The modified limit state function is presented as Equation 3-22 to Equation 3-24.

$$K^*_{appld} = \frac{K_{appld}}{k_{R6}-\rho} \leq 20 + Z_9\left[70\left\{\mathrm{EXP}\left(\frac{T_{Ed}-T_{27J}+18℃+Z_{10}+\Delta T_R}{52}\right)\right\}+10\right]\cdot\left(\frac{25}{b_{eff}}\right)^{1/4} \quad \text{Equation 3-22}$$

$$K^*_{appld} = \frac{K_{appld}}{k_{R6}-\rho} = \frac{(\sigma_{D1}\cdot Z_5 + \sigma_L \cdot Z_6)\cdot\sqrt{\pi\cdot a\cdot Z_4}\cdot Y\cdot M_k}{k_{R6}-\rho} \quad \left[\mathrm{MPa}\sqrt{\mathrm{m}}\right] \quad \text{Equation 3-23}$$

$$T_{Ed} = T_{md}\cdot Z_3 + \Delta T_r + \Delta T_\sigma + \Delta T_{\dot{\varepsilon}} + \Delta T_{cf} \quad [°\mathrm{C}] \quad \text{Equation 3-24}$$

The results of analyses conducted using the described methodology are presented in Chapter 5.

3.3 Development of Preliminary Time-Dependent Probabilistic Model

Following the preliminary time-independent probabilistic analysis conducted using Excel Visual Basic, it was concluded that the treatment of the traffic load and extreme cold temperature was highly simplistic (i.e., to conservatively assume the worst loading and lowest temperature during the analysis period will occur at the same time) and that it was necessary to cast the problem as a time-dependent reliability problem, to capture the extreme traffic and temperature fluctuating realistically over time.

This section presents a first attempt to develop automated code to perform reliability analysis in a time-dependent framework, which involved transferring the Visual Basic code into MATLAB and then looping the code iteratively to perform essentially an hour-by-hour analysis over the course of an entire year.

The work presented in this section has been presented previously at the CSCE 2022 Annual Conference (Chien et al., 2022), with edits and modifications made for this thesis.

3.3.1 Preliminary MATLAB Code Procedure

After the code was transferred into MATLAB, it was verified by generating an equivalent procedure in Excel, which was not as rapid to implement, but allowed the calculation steps to be understood and checked. The iterative analysis procedure employed in both implementations is as follows:

1. Generate K_{mat} cumulative distribution functions (CDFs) for different deterministic temperatures in Waterloo, ON (range between -55 °C and +55 °C, using 10 °C increments).
2. Generate K_{appld} CDFs for different deterministic stress levels for highway bridge traffic in Waterloo, ON (ranging between 1 MPa and 400 MPa, with 50 MPa increments).
3. Using historical temperature data between 2003-2021 for Waterloo, Ontario, a random number *X0* is generated between 0 and 1. A probabilistic temperature model with a normal distribution is assumed and *X0* is used to sample a temperature for the time step of interest.
4. For each time step (hour) in a 1-year simulation:
   a. Pick random number *X1* to get trial value for resistance uncertainty associated with the bridge detail of interest. Obtain the temperature for the time step from the annual temperature history that was randomly selected in Step 3. and determine K_{mat} for that time step by linearly interpolating between the two K_{mat} CDFs generated in Step 1 bounding the actual temperature at the time step with ordinate = *X1*. This is illustrated in Figure 3-4.

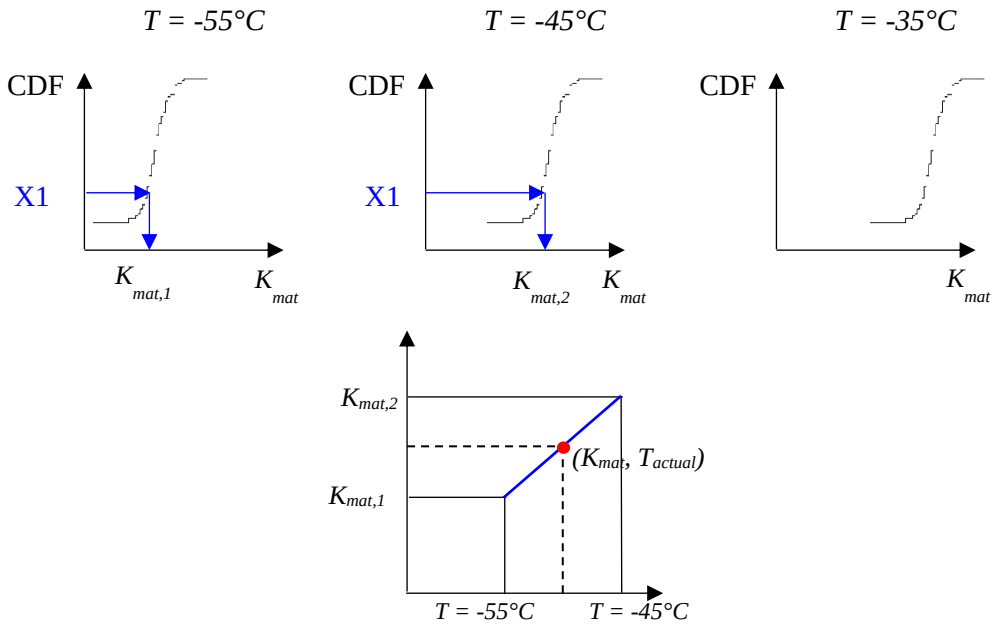


Figure 3-4 Sample schematic of determining K_{mat}

b. Pick random number *X2* to get trial value for the "solicitation" uncertainty associated with the bridge detail of interest**. (**Note: *X2* accounts for the bridge detail parameters such as the actual weld geometry, crack size, etc., which affect K_{appld} but do not vary from one hour to the next over the year.) Using historical traffic data for Ontario, obtain the stress level for the time step*** and determine K_{appld} by interpolating between the two K_{appld} CDFs generated in Step 2 bounding the actual stress level at the time step with ordinate = *X2*. This is illustrated in Figure 3-5. (***Note: there are several ways this can be done: 1) a similar approach to the one use for temperature can be used for a site where hourly peak stress or load levels are available for an entire year, or 2) peak hourly stress or load level due to traffic can be simulated using a truck weight or load effect histogram, fitted to a continuous distribution, which can then be sampled using extreme value statistics theory in a manner similar to the one used to calibrate the live load factors in CSA S6 (see Agarwal, 2007) and MCS sampling with an additional parameter (*X3*) which accounts for hourly fluctuation in the live load. For the current study, the latter approach was employed.)

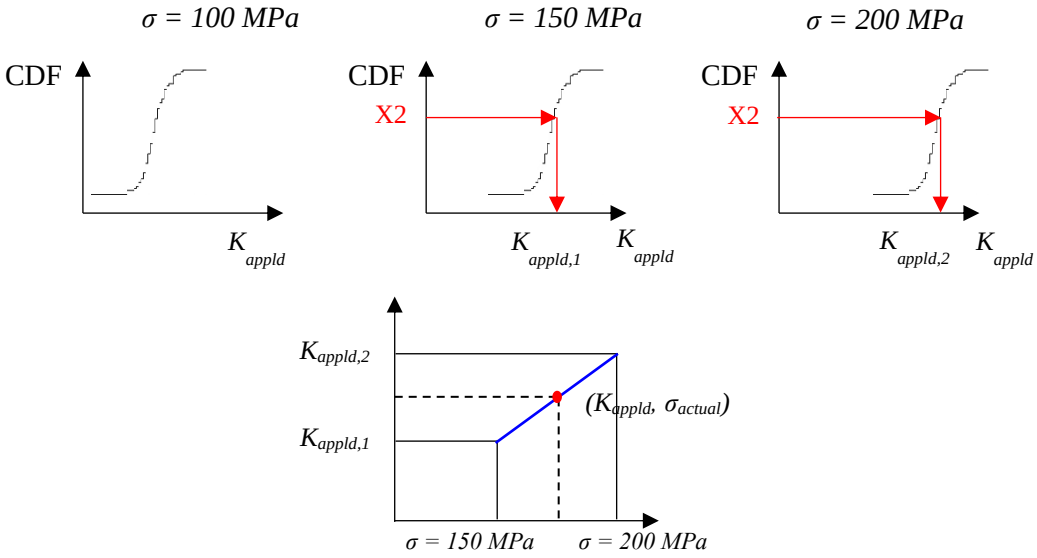


Figure 3-5 Sample schematic of determining K_{appld}

c. Determine whether failure occurs by checking if $K_{appld} > K_{mat}$ for that time step. If yes, record failure, and if not, go to the next time step.

5. This process is repeated for each time step (hour) throughout the year to determine if the detail will fail within the year or not for the 1-year simulation or "trial".

Repeat for many 1-year simulations to determine the annual probability of failure of the detail.

It is worth mentioning that the MATLAB model was verified against the VBA model described in Section 3.2 to ensure consistency.

3.3.2 Distribution Types and Statistical Parameters

In the previous probabilistic implementation of the Eurocode fracture mechanics method in Section 3.2, bias factors were applied to the deterministic input parameters, typically in the form of "multipliers", which are defined to account for the various sources of uncertainty associated with each parameter. It was identified that further investigation was needed to capture the uncertainties in the other parameters embedded in the Eurocode fracture mechanics method, including some theoretical functions for parameters such as the correction factors on the action side of the limit states function.

Table 3-4 summarizes the updated bias factors and their distribution type, mean and COV, with sources given where appropriate. The new parameters that are being treated probabilistically from the previous study are indicated by *Z11* through *Z15* in Table 3-4.

Table 3-4 Statistical Variables and Distribution Types

Z	Modifies	$\overline{Z}$	V_Z (σ_Z)	Distribution	Source
Z1	F_y	1.101	0.0915	Lognormal	(Kennedy & Baker, 1984)
Z2	t	1.02	0.0120	Lognormal	(Kennedy & Gad Aly, 1980)
Z3	T_{md}	1	0.1509	Normal	1 hour service period, calculated based on (Agarwal et al., 2007)
Z4	a	1	0.2000	Lognormal	(Vojdaniet al., 2018)
Z5	σ_{D1}	1.03	0.0800	Lognormal	(Agarwal et al., 2007)
Z6	σ_{LL}	0.8524	0.1144	Lognormal	1 hour service period, calculated based on (Agarwal et al., 2007) for Waterloo, ON
Z7	H_w	1	0.1600	Lognormal	(Kala et al. 2009)
Z8	W_w	1	0.1600	Lognormal	(Kala et al. 2009)
Z9	master curve	1	0.2500	Lognormal	(Sedlacek et al., 2008)
Z10	CVN to SIF conversion	0	(13°C)	Normal	(Sedlacek et al., 2008)
Z11	σ_s	1	0.25	Lognormal	(Walbridge, 2005)
Z12	σ_{Ed}	0.93	0.12	Lognormal	(Agarwal et al., 2007)
Z13	a/c ratio (crack shape)	1	0.32	Lognormal	(Walbridge & Nussbaumer, 2007)
Z14	M_k	1	0.05	Lognormal	(Walbridge, 2005)
Z15	SCF	1	0.04	Lognormal	(Walbridge, 2005)

Concerning parameters in Table 3-4, the following additional information is noteworthy:

- In this table, *t* is the girder flange thickness, flange stresses at the location of interest are denoted with σ, and H_w and W_w are the weld height and width associated with the critical detail. The *a/c* ratio is the ratio between the crack depth to width, M_k is a weld toe correction factor, and *SCF* is the stress concentration factor relating the local stress to the far field (nominal) stress.
- The weld parameters are used to calculate the local stress intensity factor using equations not shown here for reasons of brevity. To apply these equations, a weld detail geometry must be assumed. In the calibration of the Eurocode simplified method, a longitudinal plate attachment detail was assumed, due to its relative severity. Thus, a similar detail is assumed in the current analysis.
- Uncertainties in the brittle fracture resistance can be captured using bias factors *Z9* and *Z10*, to consider uncertainties associated with the brittle fracture "master curve" formula and the notch to fracture toughness conversion, based on raw test data in EUR 23510 EN (Sedlacek et al., 2008). Steel grades S355, S460, S690, and S890 were tested (and are reported in this reference) and the lower shelf of the master curve was fitted. Since the master curve was fitted to the average of the data, *Z9* is a multiplicative factor to model the scatter of test data for the fitting, which has been assigned a mean of 1.0 and standard deviation of 25%. Using this value, a close replication of the 50%, 95%, and 5% failure probability curves for the raw test data from Fig. 2-7 in EUR 23510 EN (Sedlacek et al., 2008) could be produced. Note that the 20 MPa$\sqrt{\text{m}}$ term is not multiplied by *Z9* because K = 20 MPa$\sqrt{\text{m}}$ represents the lower bound for cleavage fracture in steels, and therefore the stress intensity factor cannot be lower than that value (Wallin, 1992). Again, note that in later iterations of this model, an improved approach for modelling this statistical variable was employed, which will be described later.
- *Z10* is an additive factor to model the scatter in test data correlating the fracture mechanics transition temperature, T_{100}, to the Charpy test temperature, T_{27J}. which has been assigned a mean of 0 and standard deviation of 0.13 (the transition temperature standard deviation is 13°C), based on the raw data from Fig. 2-8 in EUR 23510 EN (Sedlacek et al., 2008).

The results of analyses conducted using the described methodology are presented in Section 5.6.

3.4 Time-Dependent Probabilistic Assessment of Reliability Levels in CSA S6

This section is a continuation of the previous work in refining the time-dependent probabilistic MCS framework. Due to the computational demand of the preliminary time-dependent MATLAB code, the original code was largely rewritten to improve the processing speed, which involved using a matrix form for calculations at each time step instead of loops. In addition, parallel processing was leveraged, and the author used the SHARCNET consortium of supercomputer systems for additional computational resources.

This newer code version was able to run a case of 10 000 MCS trials within seconds, which allowed for larger studies involving 1 million, 3 million, or upwards of 5 million trials to improve accuracy for cases where the probability of failure was very low. Details of the methodology are presented in the following sections.

This work has been published in the ASCE Journal of Bridge Engineering (Chien et al., 2024), with edits and modifications made for this thesis.

3.4.1 Limit State Function and Probabilistic Framework

In Section 2.3.4.2.1, the basic brittle fracture verification from Sedlacek et al. (2008) is presented. This can be written as a limit state function, $g(\boldsymbol{x})$ (Equation 3-25) where $\boldsymbol{x}$ is the vector of statistical input parameters, and $g(\boldsymbol{x}) = 0$ is the failure surface. K_{mat} is the material resistance, and K^*_{appld} can be thought of as the solicitation or "load".

$$g(\boldsymbol{x}) = K_{mat} - K^*_{appld} \qquad \text{Equation 3-25}$$

where:

$$K^*_{appld} = \frac{K_{appld}}{k_{R6-\rho}} = \frac{\sigma_{Ed}\sqrt{\pi \cdot a_d} \cdot Y \cdot M_k}{k_{R6-\rho}} \qquad \text{Equation 3-26}$$

$$K_{mat} = 20 + \left[70\left\{\text{EXP}\left(\frac{T_{Ed} - T_{27J} + 18°\text{C} + \delta_2 + 13(0.5 - \delta_1)}{52}\right)\right\} + 11\right] \cdot \left(\frac{25\text{ mm}}{b_{eff}}\right)^{\frac{1}{4}} \cdot \left(\ln\left(\frac{1}{1-\delta_1}\right)\right)^{\frac{1}{4}} \qquad \text{Equation 3-27}$$

In Equation 3-26 for K^*_{appld}, the parameters σ_{Ed}, a_d, Y, M_k, k_{R6}, ρ all take the same definitions as described in Section 2.3.4.2.1. In Equation 3-27 for K_{mat}, T_{Ed} and b_{eff} also take the same definitions as described in Section 2.3.4.2.1. Two additional parameters are added to modify the original master curve, δ_1 and δ_2, which are detailed in Section 3.4.3. The reliability analysis was performed by identifying limit state function parameters to be treated probabilistically, assigning distributions to these parameters, and then sampling them in a series of MCS "trials". The number of trials resulting in failure ($g(\mathbf{x}) < 0$) is counted and divided by the total number of trials to obtain the annual probability of failure, P_f, and annual reliability index, β.

3.4.2 Climate and Load Models

For the current study, the "linking days" method proposed by Chow & Levermore (2007) is used to model hourly temperature. It is assumed as a simplification that the minimum temperature occurs at 5:00 each day and the maximum temperature occurs at 14:00 each day. This is generally representative of most months throughout the year, with some exceptions being the maximum temperature possibly occurring at 15:00 or 16:00 in summer months, and the minimum temperature ranging between 4:00 and 7:00 depending on the season (Chow & Levermore, 2007).

Two locations were selected to represent the two climate zones in the CSA S6-19 tables (Canadian Standards Association, 2019) and demonstrate the proposed methodology. Waterloo, ON, was selected as representing the "moderate" climate, with a minimum mean daily temperature of approximately -30 °C. Whitehorse, YT, was selected as representing the "severe" climate, with a minimum mean daily temperature of -52 °C, according to Figure A3.1.2 in CSA S6 (Canadian Standards Association, 2019). They are referred to as simply "Climate 1" and Climate 2" henceforth.

It is worth mentioning that Waterloo and Whitehorse roughly correspond to Temperature Zone 2 and Temperature Zone 3, respectively, as defined in AASHTO (AASHTO, 2020). However, this statement must be qualified by noting that AASHTO defines design temperature as "minimum service temperature" (note: it is understood that "with a 1% probability of exceedance" is often assumed by US bridge owners), whereas CSA S6 defines it as "minimum mean daily temperature".

Historical hourly temperature data was gathered from Environment Canada (Environment Canada, 2022) and used for the hourly temperature simulation. Figure 3-6 illustrates upper and lower envelopes of temperature data for Climate 1 and Climate 2, with the mean hourly temperatures highlighted in red and the mean daily temperatures in a typical year in black.

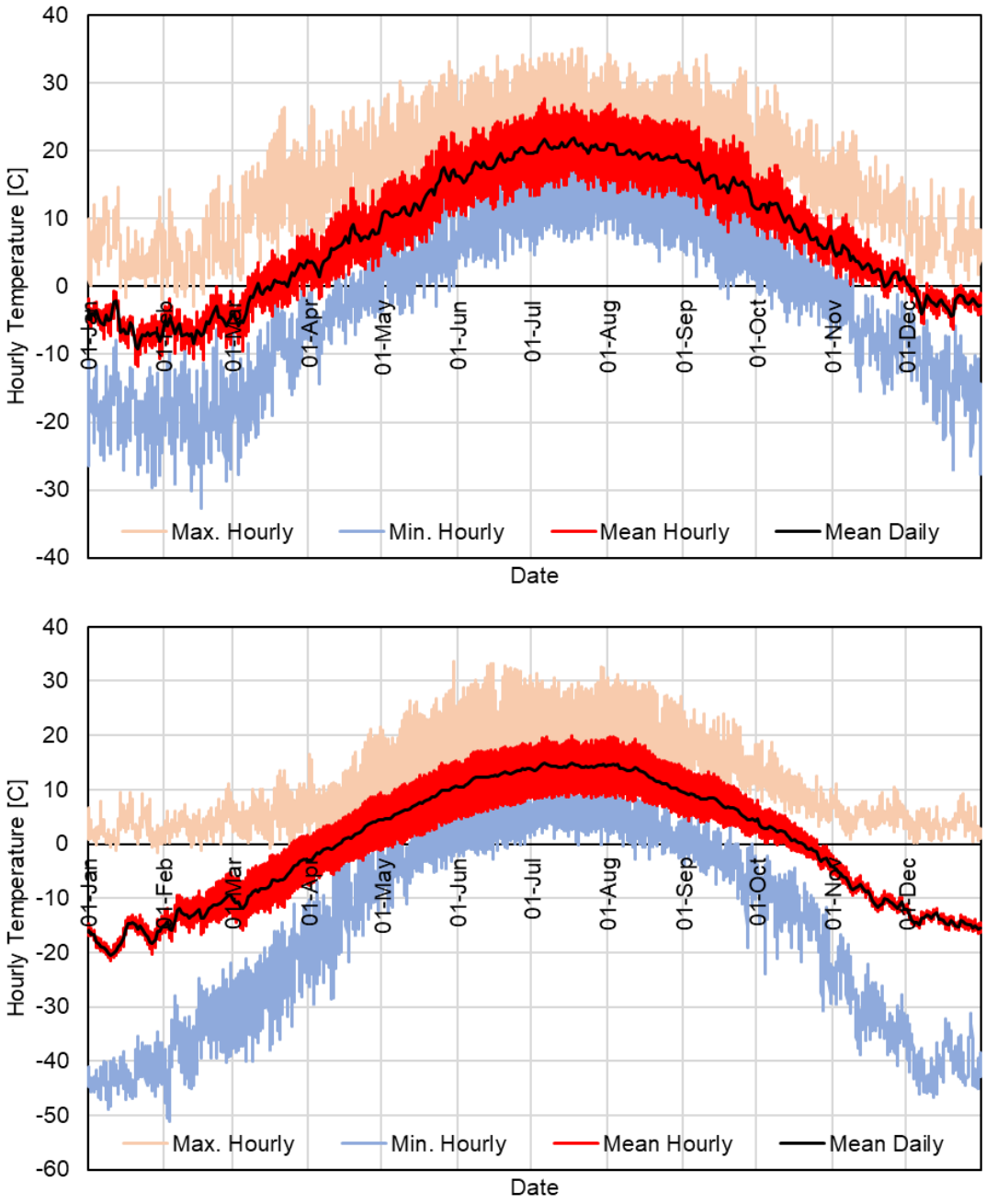


Figure 3-6 Hourly temperature envelopes and means for Climate 1, 2003-2021 (top) and Climate 2, 1953-2021 (bottom)

To establish realistic extreme loads for a weld detail on a steel highway bridge, the live-to-dead stress/load ratio was first selected as $L/D = 0.5$. It should be noted that the actual ratio can be much higher – in particular for long span bridges. To address this aspect, a sensitivity study was subsequently performed on this parameter. The load combination for ultimate strength design was taken as $1.1D + 1.7L = 0.9F_y$. The dead load factor (1.1) for factory-produced components, live load factor (1.7) for ULS Combination 1 were

obtained from Chapter 3 of CSA S6-19. The resistance factor for steel yielding (0.9) was obtained from Chapter 10 of CSA S6-19 (Canadian Standards Association, 2019). Nominal live and dead load stresses, *D* and *L*, were then calculated as a function of the yield strength input to represent a detail that just passes the ULS Combination 1 verification. After this, to model fluctuation in the live load and extreme live load events, a database of 10,000+ trucks measured using stationary scales by the MTO was used (see Figure 3-7), and for a given traffic volume (average daily truck traffic = 4000 trucks) extreme value statistics were employed to obtain a distribution for the peak hourly live load. A Gumbel distribution was then used with statistical parameters established following a procedure described in Soriano et al. (2017).

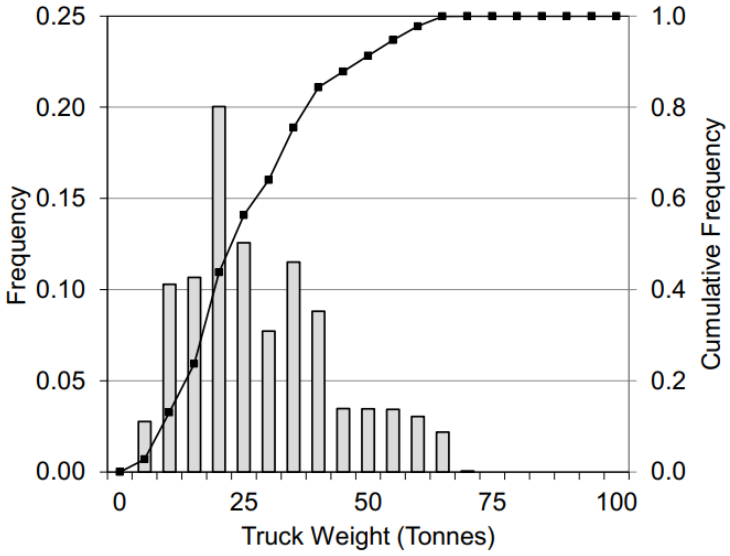


Figure 3-7 MTO 1995 truck database GVW histogram

It is noted that the histogram in Figure 3-7 is one of gross vehicle weight (GVW), whereas the ULS limit state function requires a load effect or stress. In using the GVW histogram directly, a load effect such as moment in a long span bridge is effectively being modelled, where the GVW and load effect histograms have the same form.

3.4.3 Statistical Parameters

In implementing the time-dependent analysis, most of the statistical parameters are sampled only once per bridge year, as the characteristics do not fluctuate from hour to hour. The only parameters sampled each hour are the temperature and live load. In simple terms, the scenario simulated is one where different identical bridges are (fictitiously) fabricated for each "trial" and observed to fail or not fail in a random year (with a different climate history). While noteworthy that bridges are typically designed for longer service lives (50, 75, or even 100 years), a simpler 1-year analysis is adopted for this study, as the effects of climate

history and traffic volume may change in the future. The assumed statistical parameters are shown in Table 3-5. It is worth noting that some of the *Z*-values in this table may be different from those presented previously in Table 3-4.

Table 3-5 Statistical Parameters and Distribution Types

Z	Variables	Units	Mean	Bias Factor *(Z)*	*Vz* (*σz*) *Bias COV*	Distribution	Source
Z1	F_y	MPa	Varied	1.101	0.0915	Lognormal	(Kennedy & Baker, 1984)
Z2	t	mm	Varied	1.02	0.012	Lognormal	(Kennedy & Gad Aly, 1980)
Z3	B	mm	375	-	-	Deterministic	-
Z4	T_{md}	°C	*Calculated hourly*				
Z5	ΔT_r	°C	-5	-	-	Deterministic	-
Z6	ΔT_σ	°C	0	-	-	Deterministic	-
Z7	ΔT_R	°C	0	-	-	Deterministic	-
Z8	ΔT_{ep}	°C	0	-	-	Deterministic	-
Z9	ΔT_{ecf}	°C	0	-	-	Deterministic	-
Z10	T_{27J}	°C	Varied	-	-	Deterministic	-
Z11	a_d	m	Varied	-	-	Deterministic	-
Z12	σ_{D1}	MPa	-	1.03	0.08	Lognormal	(Agarwal et al., 2007)
Z13	σ_{LL}	MPa	*Calculated hourly*				
Z14	H_w	mm	10	1.0	0.16	Lognormal	(Kala et al., 2009)
Z15	W_w	mm	10	1.0	0.16	Lognormal	(Kala et al., 2009)
Z16	δ_1	-	*Uniform distribution (min. = 0, max. = 1)*				
Z17	δ_2	°C	0	-	(13°C)	Normal	-
Z18	σ_s	MPa	100	1.0	0.25	Lognormal	(Walbridge, 2005)
Z19	σ_{Ed}	MPa	1.0	0.93	0.12	Lognormal	(Agarwal et al., 2007)
Z20	*a*/*c* (crack shape) ratio	-	0.4	1.0	0.32	Lognormal	(Walbridge & Nussbaumer, 2007)
Z21	M_k	-	1.0	1.0	0.05	Lognormal	(Walbridge, 2005)
Z22	*SCF*	-	1.0	1.0	0.04	Lognormal	(Walbridge, 2005)
Z23	*DAF*	-	1.0	1.15	0.104	Normal	-

The parameters in Table 3-5 were retrieved from the literature in most cases, with references as shown. Parameters were treated deterministically if they did not have significance or significant uncertainty

associated with them. Justification of these parameters can be found in the cited sources, and most are well established in studies describing code calibration of load and resistance factors for ultimate strength (ULS) design (e.g., F_y, t, σ_{d1}), or probabilistic fracture mechanics-based fatigue reliability analysis (e.g., σ_s, a/c ratio, M_k, SCF). The two most important statistical parameters established specifically for the current study were *Z16* and *Z17*, which account for the uncertainties associated with the use of the master curve and those associated with the conversion from CVN to fracture toughness respectively.

Z16 (δ_1) is a random variable with a uniform distribution and range of 0 to 1 used to model uncertainty in the master curve. This scatter in the resulting scatter associated with the master curve is shown in Figure 3-8 (left) with 5000 trial points. The bounds of these trial points can be compared with probabilistic envelopes in Sedlacek et al. (2008), which show a good match with the scatter in available test data. It is worth noting that this is slightly different that what was done in the previous sections (3.2 and 0) to model this source of scatter, but the difference is small and this approach is better aligned with the foundational principles on which the master curve concept is based.

Z17 (δ_2) is an additive factor to model the scatter in test data correlating the fracture mechanics transition temperature, T_{100}, to the Charpy test temperature, T_{27J}. which has been assigned a mean of 0 °C and standard deviation of 13 °C, based on Sedlacek et al. (2008), as shown in Figure 3-8 (right).

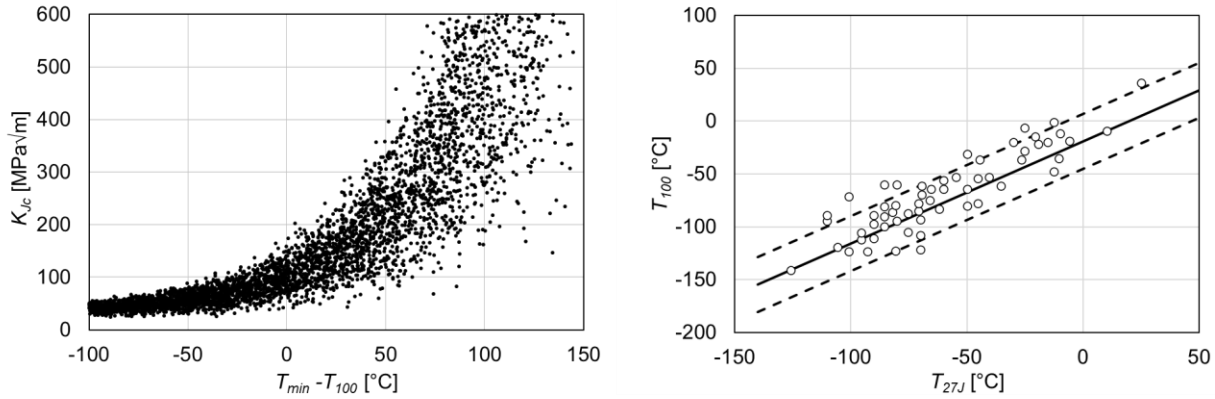


Figure 3-8 Master curve scatter considered by δ_1 parameter (left) and raw data from (Sedlacek et al., 2008), including trendlines for +/-2σ, used to establish δ_2 parameter (right)

3.4.4 Conversion CVN Test Temperature into Equivalent 27J Temperature

To make a direct comparison possible, CVN test temperatures in the AASHTO and CSA S6 tables were converted to an equivalent 27 J notch toughness, using Equation 2-33 from Kühn (2005).

The converted values are bold shown in Table 3-6. These values are later shown graphically in Chapters 6 and 7, and become relevant for suggesting new CVN requirements.

Table 3-6 Conversion of Table 10.13 from CSA S6 into Equivalent T_{27J}

	Base metal test temperature T_t for minimum service temperature T_s, °C			Weld metal test temperature T_t for minimum service temperature T_s, °C		
Min service temperature	Min avg energy (J)	$T_s \geq$ -30°C	-30°C > T_s > -52°C	Min avg energy (J)	$T_s \geq$ -40°C	-40°C > T_s > -52°C
CSA G40.21 Grades						
260WT	27	**-13.89**	**-23.89**	27	**-23.89**	**-23.89**
300WT	27	**-13.89**	**-23.89**	27	**-23.89**	**-23.89**
350WT and AT	27	-20	-30	27	-30	-30
400WT and AT	27	-20	-30	27	-30	-40
480WT and AT	27	-20	-40	27	-40	-50
700QT	Not permitted					
ASTM A709M Grades						
250F	27	**-1.28**	**-17.28**	27	**-23.89**	**-23.89**
345F <51mm	27	**-1.28**	**-17.28**	27	-30	-30
345SF and 345WF	27	**-6.04**	**-22.04**	27	-30	-30
HPS 345WF	27	**-22.04**	**-22.04**	27	-30	-30
HPS 485WF	27	**-37.39**	**-37.39**	27	-40	-50
HPS 690WF < 65mm	27	**-48.39**	**-48.39**	27	**-54.39**	**-64.39**
HPS 690WF > 65mm	Not permitted					

3.4.5 Design Crack Depth

While the defect or crack depth, a, in a weld is known to be highly variable and have a significant impact on brittle fracture risk, establishing a distribution for this parameter, considering both fabrication tolerances and the possibility of future fatigue crack growth, is an extremely difficult task without access to fabricated structures or broad knowledge of industry practices surround such things as inspection and repair/rejection structures with defects. Unlike the European standards for fabrication of steel structures, the corresponding North American standards do not clearly acknowledge toleration of initial surface crack-like defects from fabrication, and therefore provide little guidance on a suitable value for a_0. For example, CSA W59-18 states: *"A weld subject to visual inspection shall be considered acceptable if visual inspection shows: a) no surface cracks; …"* (Canadian Standards Association, 2018).

To circumvent this issue and to illustrate practical implementation of the proposed methodology, for the current study, it was decided to define a deterministic design crack depth, a_d, to model initial fabrication flaws that were missed during inspection "a_0" (and therefore did not lead to repair or rejection) combined with some amount of subsequent fatigue crack growth "Δa_{fcg}". The process employed to establish this crack depth followed the suggestion by Altstadt et al. (2014) that mild structural steel, with the current toughness requirements, has a long track record of good performance. On this basis, a mild (F_y = 350 MPa) steel plate with moderate thickness (t = 38 mm) was used to calibrate a design crack depth that resulted in an adequate reliability level. This crack depth was then used to assess reliability levels for other grades, plate thicknesses, etc. This process is summarized as having the following steps:

1. 350 MPa steel was chosen as the reference strength for calibration.
2. In contrast with what was assumed in the preliminary study, for this study the target annual reliability index was defined as β = 3.25, based on CSA S6-19 for assessment of structures with intermediate system behaviour S2 (redundancy), element behaviour E2 (ductility), and inspection possibility INSP2. This is deemed to be reasonable for illustrative purposes of a primary tension member, though a higher target reliability index may be appropriate for fracture critical members.
3. T_{27J} for the selected steel was determined. According to CSA S6-19, 350 MPa steel is required to achieve T_{27J} = 0 °C for a primary tension member in Climate Zone 1.
4. The deterministic crack depth a_d was then varied until the time-dependent reliability analysis yielded β = 3.25. On this basis, a_d = 0.53 mm was selected as the design crack depth.

Figure 3-9 (left) explains this calibration process. It is worth noting this value for a_d is generally lower than the values used in the deterministic Eurocode code calibration (see Figure 2-15), suggesting further reflection on the appropriate values for a_d and the target annual reliability index may be beneficial. It is also worth noting that a design crack size of this size, in reality, likely cannot be detected through visual inspection as discussed in Campbell et al. (2019). In the current study, these values are nevertheless retained, on the basis they serve the purpose of demonstrating the proposed methodology and commenting on the consistency of the reliability levels provided in the current code.

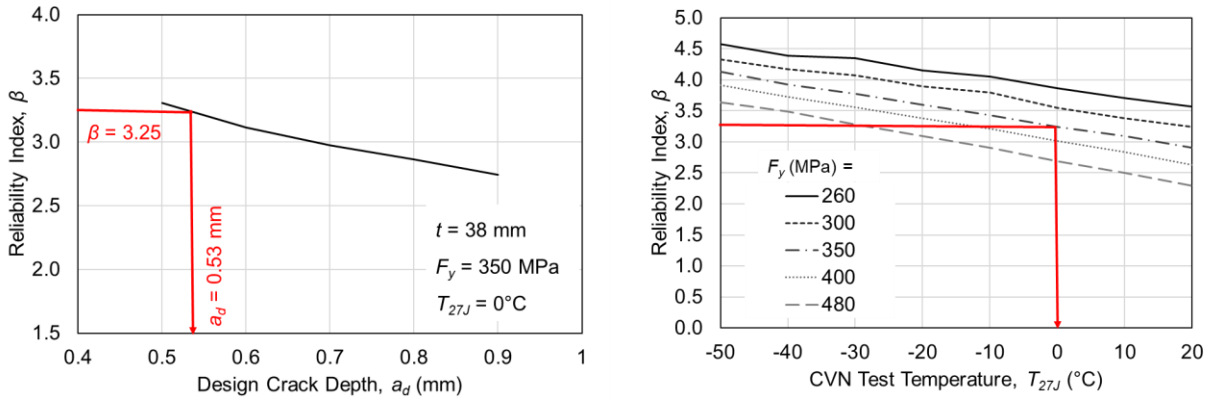


Figure 3-9 Calibration of a_d (left) and β vs. T_{27J} curves for various steel strengths (right)

With a_d established for t = 38 mm, and again for illustrative purposes and with limited guidance from the North American structural welding standards, subsequent reliability analyses for different plate thicknesses were performed with two assumptions: 1) that a_d is the same for all plate thicknesses, and 2) that a_d / t remains constant and equal to 0.53 mm / 38 mm = 0.014. This is summarized in Table 3-7.

Table 3-7 Design Crack Depth Cases

Plate Thickness [mm]	Case 1 (a_d [mm] based on calibration from t = 38 mm, constant)	Case 2 (a_d [mm] based on a_d/t ratio = 0.014)
25	0.53	0.35
38	0.53	-
75	0.53	1.06

3.4.6 Time-Dependent Reliability Analysis

A MATLAB code containing three segments was written to implement the time-dependent reliability analysis. This analysis can be broken down into the following primary steps:

1. Statistical parameters and deterministic input parameters are defined.
2. Parameters that need to be sampled once per bridge year are sampled.
3. The historical hourly temperature database is read, and daily maximum and minimum temperatures are identified from the hourly data for each year in the historical database.
4. For each day in the trial year, maximum and minimum temperature is sampled assuming the daily maxima and minima in the historical database follow a normal distribution.
5. The linking days method (Chow & Levermore, 2007) is used to calculate an hourly temperature for the 1-hour time step. K_{mat} is then calculated using that temperature.

6. The live load for the time step is sampled from the Gumbel distribution for hourly extreme live load obtained from the real traffic database. K^*_{appld} is then calculated using that live load.
7. A ductile fracture check is performed, to determine if the applied stress is sufficient to yield the cross section. If yielding occurs, a failure by ductile fracture is recorded.
8. Failure by brittle fracture is assumed if $g(\boldsymbol{x}) < 0$.
9. If failure has occurred, it is recorded, and the next bridge year is simulated (go to Step 2).
10. If failure has not occurred, the next time step is simulated (go to Step 5) until the end of the year.
11. This process repeats until the required number of bridge years (or "trials") has been simulated.
12. Results (P_f and β for ductile and brittle fracture, and number of trials) are written to an output file.

A flow chart illustrating the model procedure is shown in Figure 3-10.

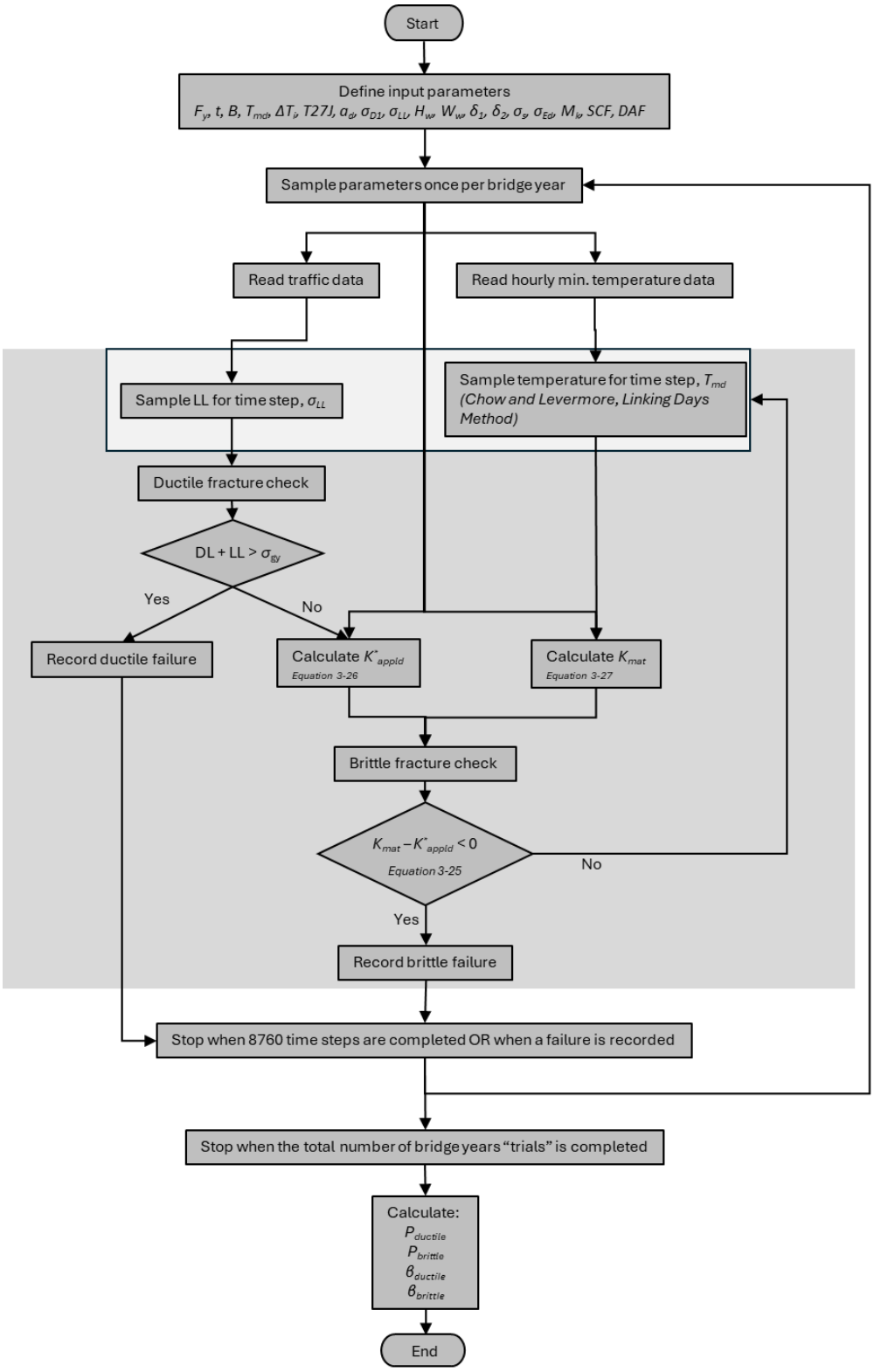


Figure 3-10 Flow chart for time-dependent model

The results of the studies using the new code are presented in Chapter 6.

3.5 Sensitivity Studies with Time Independent Model and Development of Design Tools

To accomplish Task 4 (from Section 1.2), the final goal of the project was to develop practical tools for bridge designers. This involved greatly increasing the number of analysis cases, including varying the demand-to-capacity ratio, and further sensitivity studies involving influence lines, inclusion of temperature data from different cities, varying traffic volume, and considering multiple vehicle presence.

To further save computational time, this part of the project involved an investigation on whether reverting back to a using a time-independent method would be a viable option to further increase analysis speed. Due to the conservatism in the time-independent method (i.e. assuming maximum load and minimum temperature occur at the same time), the design crack size was re-calibrated. Much of the overall methodology mirrors that in Section 3.4, with changes in the time-independent aspect.

The methodology is presented in the following sections.

This work has been submitted to the Canadian Journal of Civil Engineering, with edits and modifications made for this thesis. Parts of this work has been presented at the CSCE Annual Conference 2024 (Chien et al., 2024).

3.5.1 Limit State Function and Probabilistic Framework

The approach taken for this study closely mirrors that of the methodology presented in Section 3.4, with a few modifications for the time-independency, using MCS to see how often failure occurs (where $g(\mathbf{x}) < 0$). By counting these failures and comparing them to the total number of simulations, the annual probability of failure, P_f, and annual reliability index, β, can be calculated.

The limit state function used in this part of the project is the same as in the previous study, presented in Equation 3-25. Realistically, K^*_{appld} fluctuates over time as the traffic load changes, and K_{mat} fluctuates over time as the ambient temperature changes. However, in this section, a simplistic and conservative way to deal with this time dependence is adopted: to assume the coldest temperature and the highest traffic load happen at the same instant during the analysis period (in this case, one year, for annual probability of failure). This modelling approach is considered reasonable as K^*_{appld} fluctuations (which are minimal) are dwarfed by the much larger K_{mat} fluctuations (later shown in Chapter 6).

3.5.2 Climate and Load Models

Again, climate data from Waterloo and Whitehorse were used to represent Climate 1 “moderate” and Climate 2 “severe”, respectively. In the Section 7.2 Sensitivity Studies, however, a broader range of locations within each zone are assessed and compared. Historical yearly minimum temperature data was gathered from Environment Canada (Environment Canada, 2022) and used for the yearly temperature simulation, assuming an extreme value Gumbel distribution.

In the previous study, it was noted that the load ratio, $L/D = 0.5$ was relatively low, and perhaps not appropriate for longer span bridges. Therefore, a new live-to-dead stress/load ratio was selected and used in this last study of $L/D = 1.0$. This is close to the live-do-dead ratios observed in design examples such as in Canadian Institute of Steel Construction (2002) and Sedlacek et al. (2008), and hence assumed to be a typical *L/D*.

The same load combination for ultimate strength design was used: $1.1D + 1.7L = 0.9F_y$. Nominal live and dead load stresses, *D* and *L*, were then calculated correspondingly.

Statistical parameters for the live load were calculated using an updated truck database from 2012 from the MTO, with the histogram illustrated in Figure 3-11. These were slightly different from the ones calculated using the 1995 data in the previous study. A Gumbel distribution was used to obtain a distribution for the peak yearly live loads, for different traffic volumes (an average daily truck traffic, ADTT, ranging between 50 and 4000 trucks was assumed for the sensitivity studies).

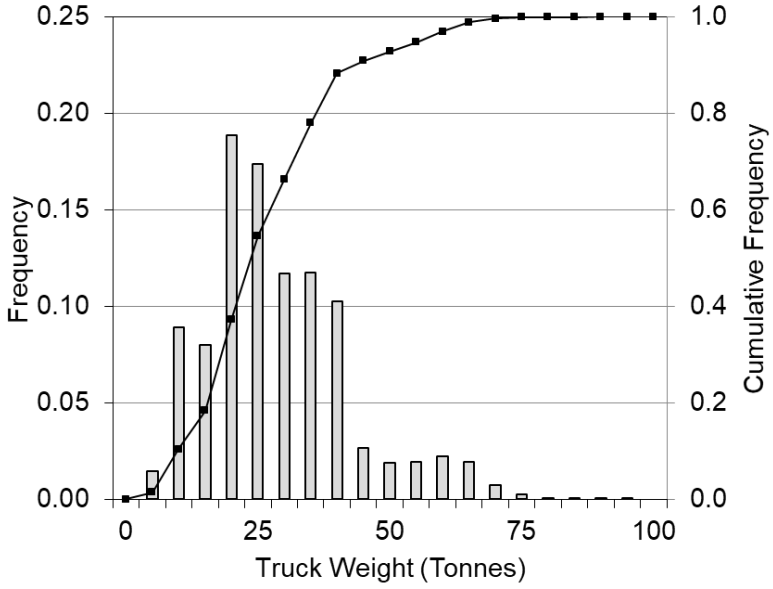


Figure 3-11 MTO 2012 truck database GVW histogram

3.5.3 Statistical Parameters

The assumed statistical parameters are mostly the same as the previous study, presented in Table 3-5, with a few minor differences:

- For the time independent analysis, all statistical parameters are sampled only once per bridge year, including T_{md} and σ_{LL} (which are no longer sampled hourly).
- *Z17* (δ_2) is an additive factor to model the scatter in test data correlating the fracture mechanics transition temperature, T_{100}, to the Charpy test temperature, T_{27J}. It has been assigned a mean of

0 °C. Different sources may suggest different standard deviations: Sedlacek et al. (2008) suggests a value of 13 °C, though other sources (Collins et al., 2016) suggest larger values based on different correlation methods. On this basis, a standard deviation of 34.2 °C was chosen for the Wallin correlation based on Collins et al. (2016).

All other parameters are assumed to be the same as those in Table 3-5.

3.5.4 Design Crack Depth

The process of calibrating a design crack depth followed the same steps as the previous study, outlined in Section 3.4.5, using a mild (F_y = 350 MPa) steel plate with moderate thickness (t = 38 mm) and annual reliability index of β = 3.25. Through linear interpolation, a_d = 0.13 mm was selected as the design crack depth, illustrated in Figure 3-12 (left). This crack depth is smaller than the previous value of 0.53 mm, due to the conservatism in the time-independent model in assuming the maximum load and minimum temperature occur at the same time. A crack this size would be even less likely to be found in inspection, though it is retained for illustrative purposes in the sensitivity studies and creation of new design tools.

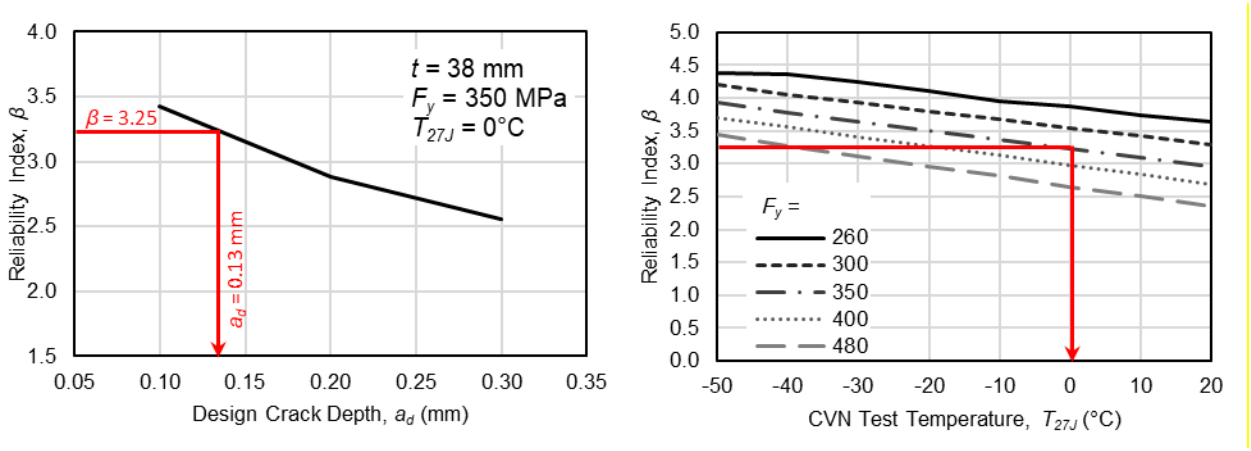


Figure 3-12 Calibration of a_d (left) and β vs. T_{27J} curves (right)

3.5.5 Time-Independent Reliability Analysis and T_{27J} Calibration

The time-independent MATLAB code using MCS followed the primary steps:

1. Statistical parameters and deterministic parameters are input into the code.
2. Parameters that need to be treated probabilistically are sampled.
3. The historical temperature database consisting of yearly minima is read, and a minimum temperature is sampled for the trial year assuming the historical database to follow a normal distribution.
4. K_{mat} is then calculated using that temperature.
5. The live load for the time step is sampled from the Gumbel distribution for yearly extreme live load obtained from the real traffic database. K^*_{appld} is then calculated using that live load.
6. A ductile fracture check is performed, to determine if the applied stress is sufficient to yield the cross section. If yielding occurs, a failure by ductile fracture is recorded.
7. Failure by brittle fracture is assumed if $g(x) < 0$.
8. If failure has occurred, it is recorded, and the next bridge year is simulated (go to Step 2).
9. This process repeats until the required number of bridge years (or "trials") has been simulated.
10. Probability of failure (P_f) for each mode is calculated by dividing the failures by total number of trials. β for both ductile and brittle fracture are subsequently calculated.

A flow chart illustrating the time-independent model is shown in Figure 3-13.

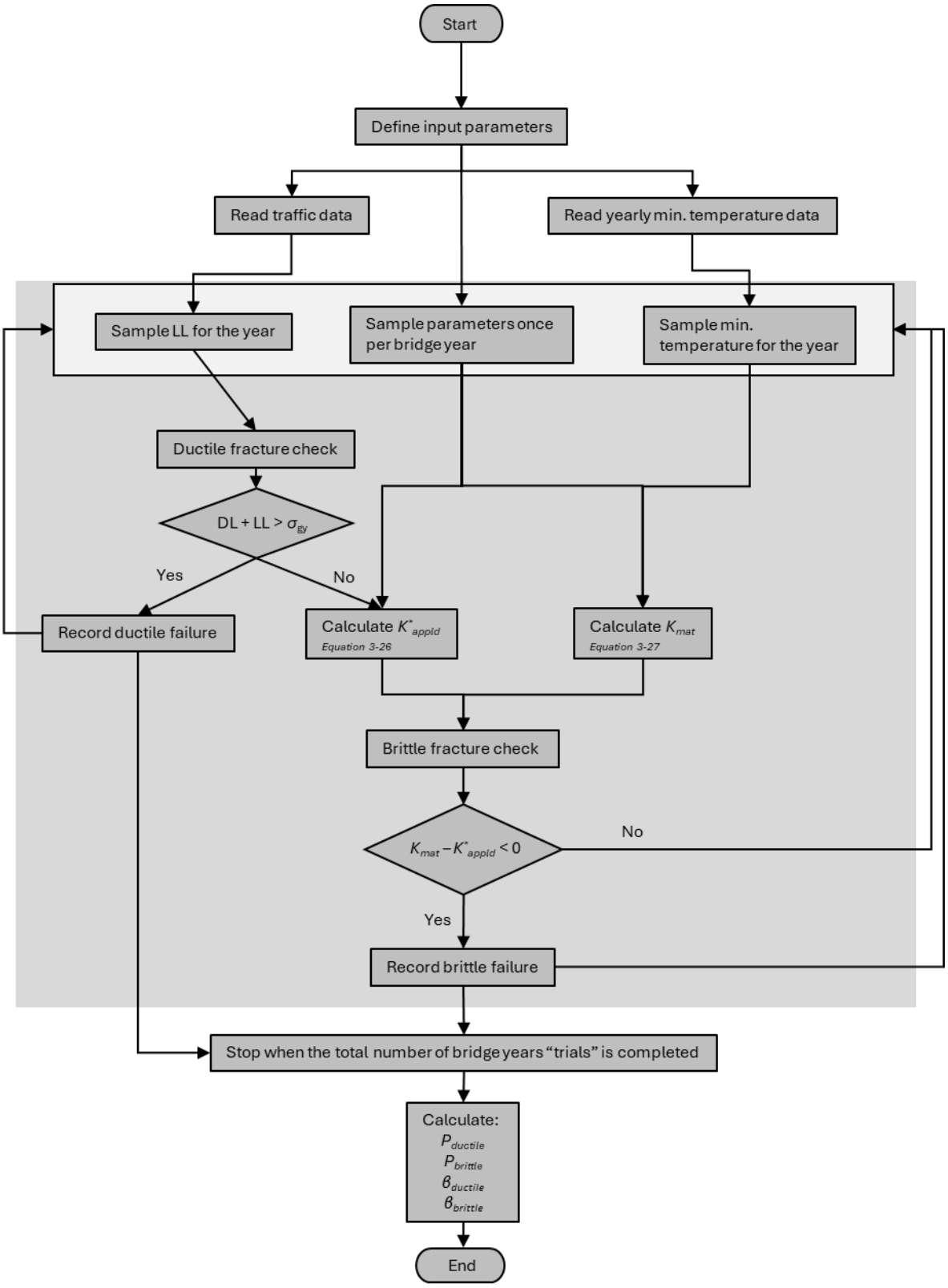


Figure 3-13 Flow chart of time-independent model

This was repeated for different T_{27J}, varying between -50 °C and 20 °C (at 10 ° C increments), and different yield strengths presented in CSA S6. Curves of T_{27J} vs β were generated for each steel grade. A line of best fit was generated, and the recommended T_{27J} was calibrated to the target β.

The process was then repeated for different demand-to-capacity ratios (DCR), ranging between 0.5 to 1 at increments of 0.125. The DCR affects the scaling of the dead and live stresses, such that $1.1D + 1.7L = DCR * 0.9F_y$. This may be useful for posting load limits on a bridge to ensure the target reliability is met. Contour plots of F_y vs. T_{27J} vs. DCR were then generated using MATLAB. Values of T_{27J} above 20 °C were capped, as CVN tests are generally not conducted above room temperature.

The results of the studies and new design tools are presented in Chapter 7.

4 Comparison of Design Provisions for a Typical Bridge

As a first study to assess the level of consistency in codes around the world, a comparison between the Eurocode, CSA S6, and AASHTO LRFD Part 6 was made. Figure 4-1 to Figure 4-6 were produced to show the variation in the required CVN test temperature corresponding to the required steel grade/sub-grade in the three design codes for varying plate thickness. Figure 4-7 shows the changes in the steel toughness requirement along the bridge span due to changes in the girder plate thickness and applied stresses at each point, using the EN 1993-1-10 provisions.

4.1 Part 1 – Single Point Analysis

The toughness requirements in CSA S6 are independent of plate thickness, as represented by the orange horizontal line in Figure 4-1 to Figure 4-6, and are more conservative than EN 1993-1-10 for thinner plates, resulting in a lower CVN test temperature requirement for 27 J notch toughness. Both codes have the same toughness requirement in the middle range of plate thicknesses, and EN 1993-1-10 is more conservative for thicker plates. The AASHTO toughness requirement also varies with thickness, however, it still follows a similar trend in being more conservative than the Eurocode for thinner plates and less conservative for thicker plates when the CVN test requirements from the AASHTO Table C6.6.2.1-1 are converted from Imperial to Metric units. This is illustrated as the grey line in Figure 4-1 to Figure 4-6. Solid lines for both the CSA and AASHTO curves represent the non-fracture-critical member in the case of the case study bridge used, but the dashed orange and grey lines show the results for what would be fracture critical members, had there been any on the bridge. It is noteworthy that the Eurocode makes no such distinction between regular and fracture critical members, as is done in North America.

Figure 4-1 to Figure 4-6 also show that the EN 1993-1-10 fracture mechanics method follows the same trend as the simplified method, with the simplified method being slightly more conservative. The yellow curve represents the results from the standard defect size calculated using Equation 3-7, while the dark blue and green curves represent the results when the defect size, a_d, is varied by +/-20%. The dashed lines of the fracture mechanics curves exceeding the 20 °C CVN test temperature indicate the theoretical upward trend of these curves, while realistically, CVN tests would not generally be conducted at those higher temperatures. Figure 4-1a shows the results using the code-specified temperature for analysis, and Figure 4-1b shows the results at a common ambient temperature (before applying any code-specified temperature shifts). It is observed that for the common temperature scenario, the Eurocode curves are shifted to the right, extending the range of thin plates for which the Eurocode is less conservative than the North American counterparts for this example.

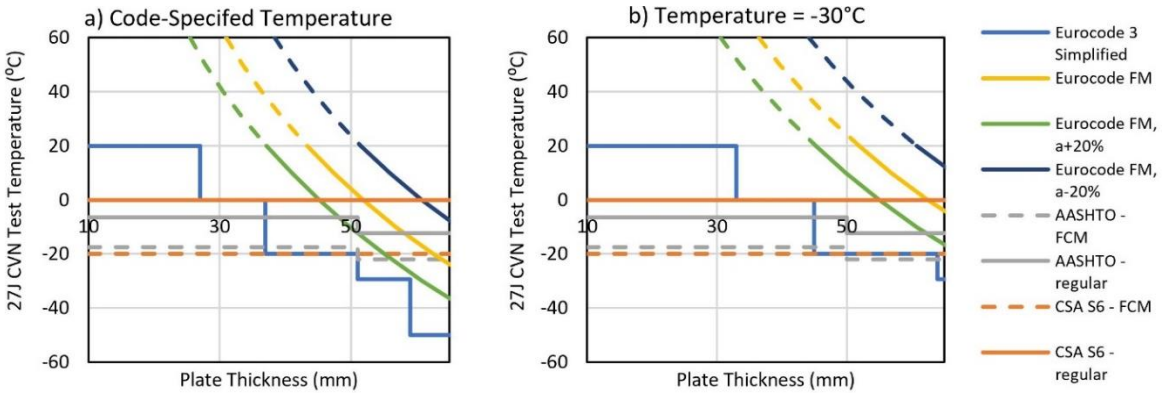


Figure 4-1 Required CVN test temperature for Waterloo (σ_{ed} / $f_y(t)$ = 0.46)

Similar trends were observed for Vancouver, shown in Figure 4-2, and Fort McMurray, shown in Figure 4-3. Although this analysis is specific to a particular loading scenario for the CISC design example bridge and the climatic data for the three cities of interest, the step function trend from the simplified method is similar for other European steel grades, such that toughness requirements for thicker plates are more rigorous.

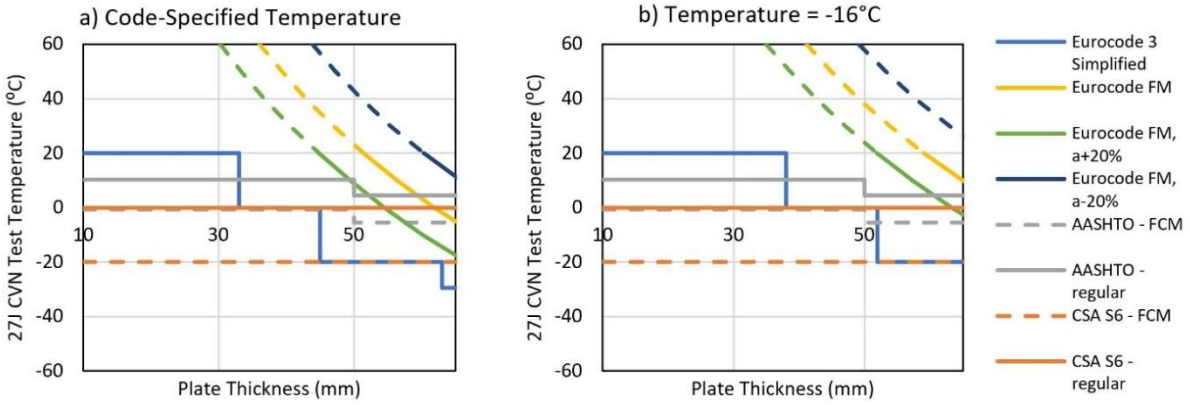


Figure 4-2 Required CVN test temperature for Vancouver (σ_{ed} / $f_y(t)$ = 0.46)

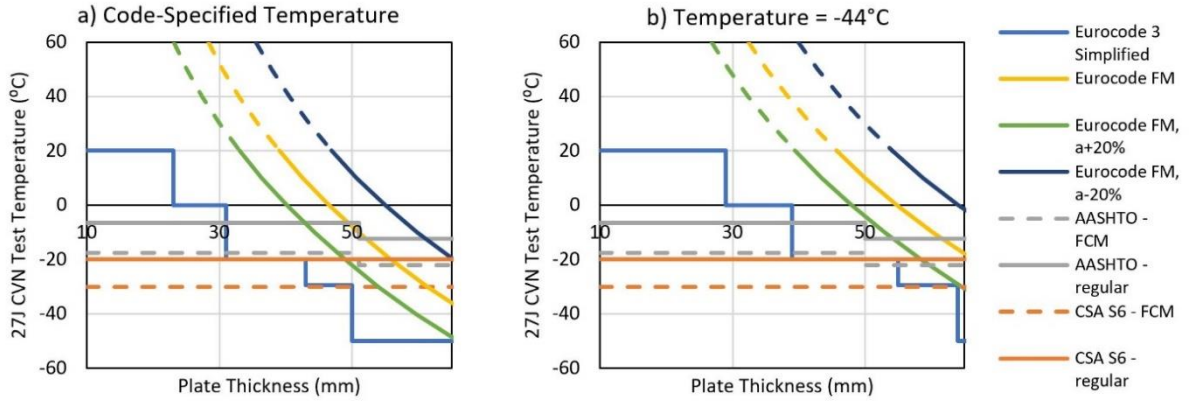


Figure 4-3 Required CVN test temperature for Fort McMurray (σ_{ed} / $f_y(t)$ = 0.46)

Figure 4-4 to Figure 4-6 illustrate the effects of the changes in stress level on the toughness requirement. (Note: code-specified design temperatures are assumed in this comparison.). It can be seen that when a plate is subjected to lower stress levels ($0.25f_y(t)$), the CSA and AASHTO requirements are consistently more conservative for the range of plate thicknesses considered. At the higher stress levels of 0.46 $f_y(t)$ and 0.75 $f_y(t)$, the EN 1993-1-10 curves for both the simplified and fracture mechanics methods shift to the left, becoming more conservative for thicker plates, while the CSA and AASHTO still remain conservative for thinner plates at these stresses. The red dashed line on the graphs at 0.75 $f_y(t)$ for Waterloo and Fort McMurray represents the limit on maximum plate thickness from the Eurocode 3 simplified method, meaning that any plate exceeding the limit would not be permissible for those stress and climate conditions.

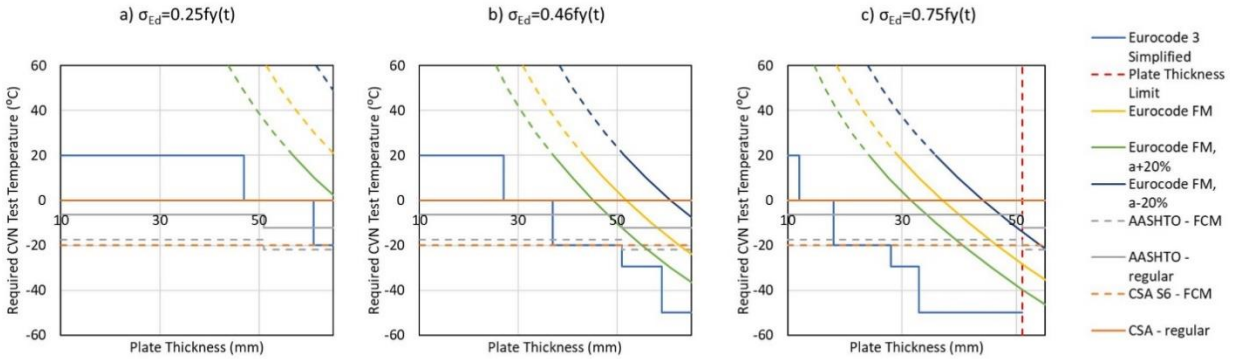


Figure 4-4 Required CVN test temperature for different stress levels for Waterloo

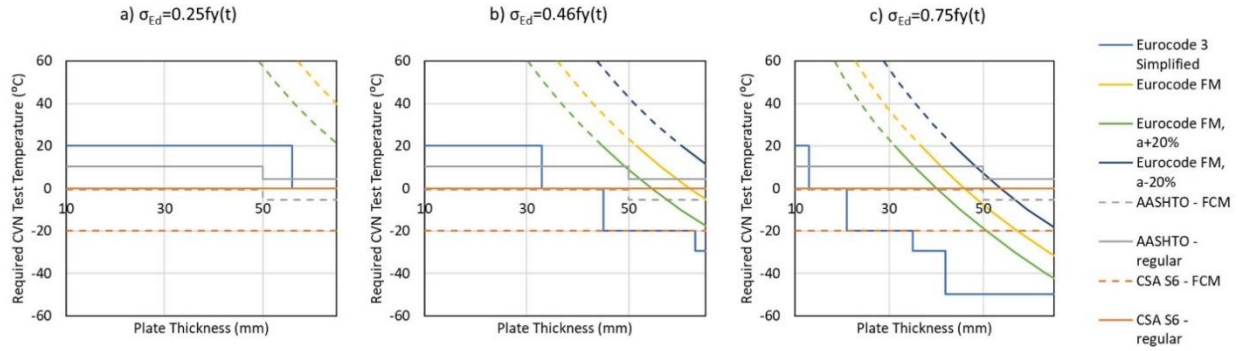


Figure 4-5 Required CVN test temperature for different stress levels for Vancouver

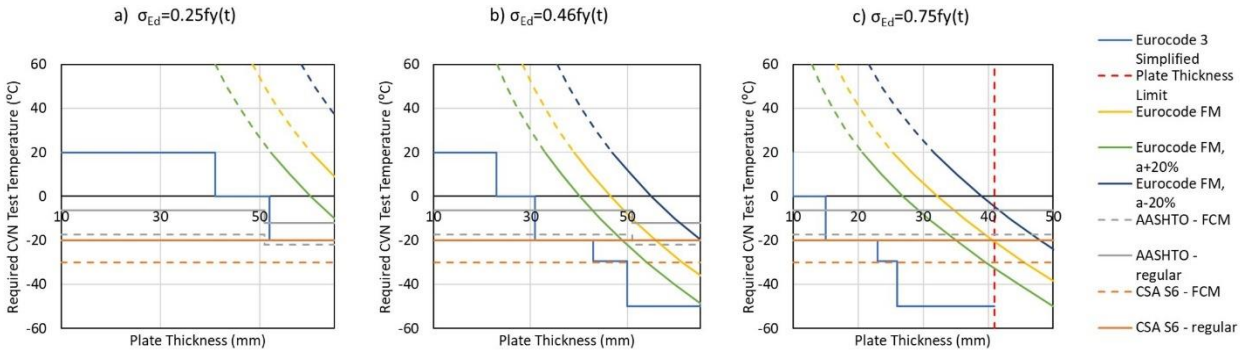


Figure 4-6 Required CVN test temperature for different stress levels for Fort McMurray

4.2 Part 2 – Entire Girder Analysis

Depending on the stresses and plate thickness, the toughness requirement along the length of the bridge can vary significantly, based on EN 1993-1-10. This is shown in Figure 4-7. As expected, a mild climate such as Vancouver may utilize a smaller range of steels with lower toughness requirements using the simplified method – between JR to K2, M, N – while the climatic conditions of Waterloo would require the full range of sub-grades for the European S355 steel grade. In the severe climate, Fort McMurray, a steel sub-grade could not be specified for Span Reference 11 (in the vicinity of the intermediate bridge pier), where the maximum negative moment occurs, as indicated by the dotted red lines in Figure 4-7c). This discontinuity occurs because the plate thickness exceeds the maximum allowable plate thickness – even for the toughest available sub-grade of S355 – for the particular stress condition and reference temperature using the simplified method. In this case, a different steel grade would need to replace the S355 for the plate thickness at this location to fall within allowable limits.

It is also observed that the fracture mechanics curve follows the same trend as the simplified method, similar to the single point analysis. In general, the toughness requirement from the simplified method remains more conservative than the fracture mechanics method, with few exceptions near the 5 to 10 m distance from the abutment. This could be due to the use of the "round up" method when applying the *Table 2.1* of EN 1993-1-10 to generate Figure 4-7, where stress level and reference temperature were rounded up on the table instead of interpolated. It is also noted that since the fracture mechanics method is generally less conservative than the simplified method, there is no discontinuity at Span Reference 11, and the steel grade of S355 would be permissible.

This type of graph could help designers determine the toughness requirement to properly specify steel grade for the design of new bridges. Although the toughness requirement varies along the length, it is generally preferable to use the same grade along the entire bridge for ease of construction. In this example case study, the pier is the location of maximum negative stress and governs the fracture toughness requirement for the

entire bridge. It is observed that the locations of lower toughness requirement (i.e. JR subgrade) are generally near the inflection points. One possible use for this type of output might be to permit a lower toughness level at positions along the span other than the critical one for assessment purposes, such as assessing a point along the bridge span where a fatigue crack has been detected or the structure has been damaged – e.g. by vehicle impact – or has a fatigue prone detail present.

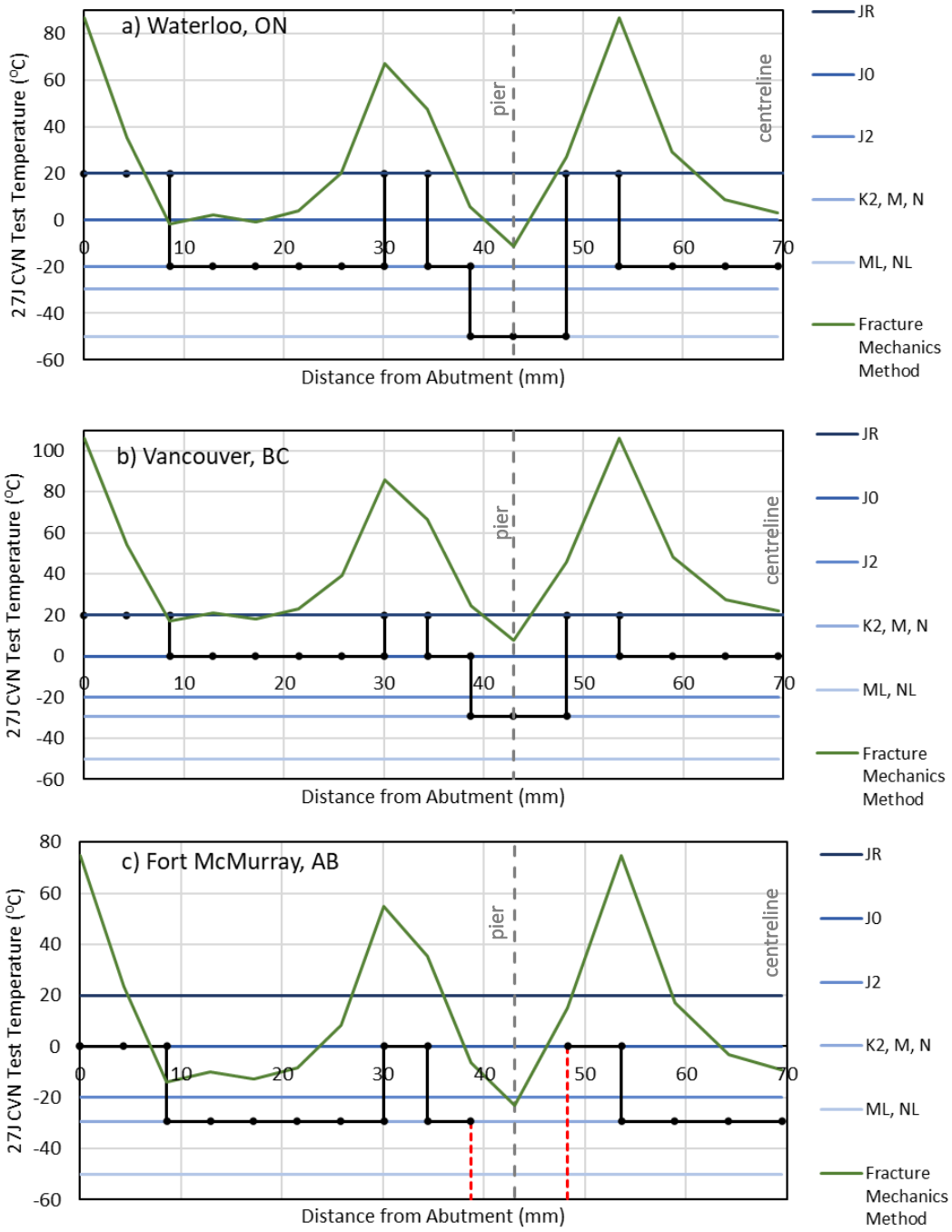


Figure 4-7 Comparison of Eurocode simplified and fracture mechanics models for three locations

5 Probabilistic Fracture Mechanics Analysis

In this chapter, the results are presented for the preliminary comparison of codes, which led to the study of implementing the Eurocode fracture mechanics in a probabilistic framework with Excel's Visual Basic to compare the sensitivity of changes in each of the input parameters of the Eurocode fracture mechanics method to the probability of failure, P_f. These are presented in Sections 5.1 through 5.5.Each of these demonstrates the impact of each parameter on the brittle fracture risk and the gaps that the current CSA S6 design tables may have.

In Section 5.6, the initial results, and limitations (including the computational demand), of the initial time-dependent probabilistic MATLAB code are presented and discussed.

5.1 Results: Base Case Analysis

First, a base case analysis was performed, which assumed the bridge was located in Ft. McMurray, AB, and fabricated with steel having notch toughness, T_{27J} = -30 °C. Figure 5-1 shows sample output using MCS with 10,000 trials, for the histograms of K_{mat} and K^*_{appld}, where failure is indicated by the areas where the histograms overlap. On this basis of this simulation, an annual probability of failure of P_f = 0.0054 is calculated (β = 2.55). It is noted that this annual reliability index is low and would not satisfy fracture-critical requirements. However, these results are to illustrate a "proof of concept" analysis to build upon later on, and so no further effort is made at this stage to calibrate the model or otherwise address this issue. The following should be noted:

- The basis for this probability of failure calculation is a 50-year service period, which is used to calculate the extreme live load and the extreme cold temperature. It is then very conservatively assumed that these two events occur at exactly the same time.
- It should not be surprising that such a low probability of failure is obtained with such a highly conservative assumption implicitly made in the analysis. Clearly, in order to estimate the probability of failure more reasonably, a time-dependent reliability framework is needed, where the live load and temperature are allowed to fluctuate realistically over time, or the effect of this realistic fluctuation is captured using an appropriate approximation.
- For the purpose of assessing the implications of the assumed analysis period, in the sensitivity studies presented in the following sections, two service periods are considered: the 50-year service period employed in the base case analysis and a 1-year service period, the latter yielding "annual probability of failure" results, which still employ the overly conservative assumption that the extreme live load and temperature occur at the same time within the service period. In order to do this, the statistical approaches in Agarwal et al. (2007) were employed with the raw traffic statistical data for the province of Ontario for midspan moment of a simply supported 40 m girder. (In future

analyses, more recent raw data for Ontario, BC, and Alberta could be used where appropriate. However, for this study, the bridge "location" only affected the extreme temperature statistics.)

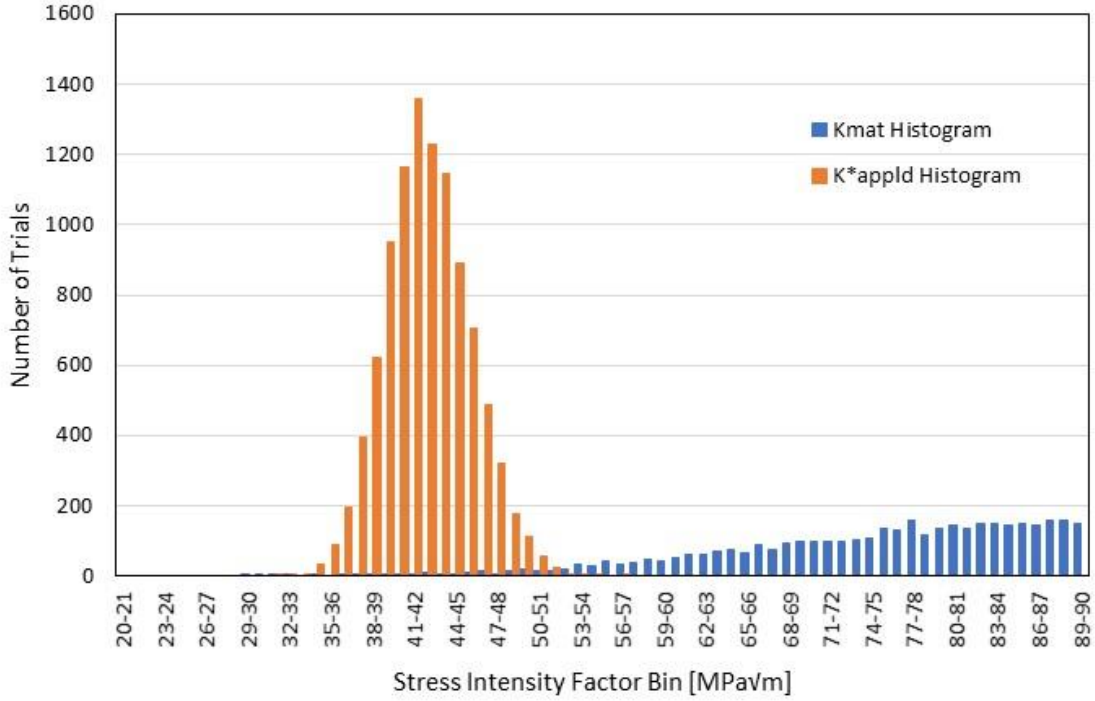


Figure 5-1 Sample output for base case (Ft. McMurray, 50-year service period, T_{27J} = -30°C)

5.2 Variation of Crack Size

As CSA S6 currently does not consider crack size in the design against brittle fracture, a parametric study for this factor was of interest, due to the impact that a_d has in the equation for K^*_{appld} (recall Equation 2-10 and Equation 2-11).

A semi-elliptical crack shape was assumed, with "size" referring to the crack depth. The mean crack size was varied between 2 mm and 20 mm, and as expected, the probability of failure increases with increasing crack size. The results are presented in Figure 5-2, highlighting the impact that crack size has on brittle fracture and reinforcing the need for this parameter to be considered in codes. Looking at this figure, it can be seen that the annual probability of failure curves are – as expected – lower than the 50-year service period curves, as the opportunity of an extreme temperature event and high truck load occurring together are more likely in a longer service period.

Note that in order to present curves with only two variables changing at a time (location, which affects extreme temperature nominal and bias factor values, and mean crack size), the fracture toughness of the steel was held fixed at T_{27J} = -20 °C, even though CSA S6-19 would require a lower value of -30 °C for the coldest (Ft. McMurray) location. Looking at these curves, it can be seen that as the climate becomes more

severe, the probability of failure curve shifts upwards, as expected. Figure 5-3 presents the corresponding set of reliability index vs. mean crack size curves, based on Equation 3-19.

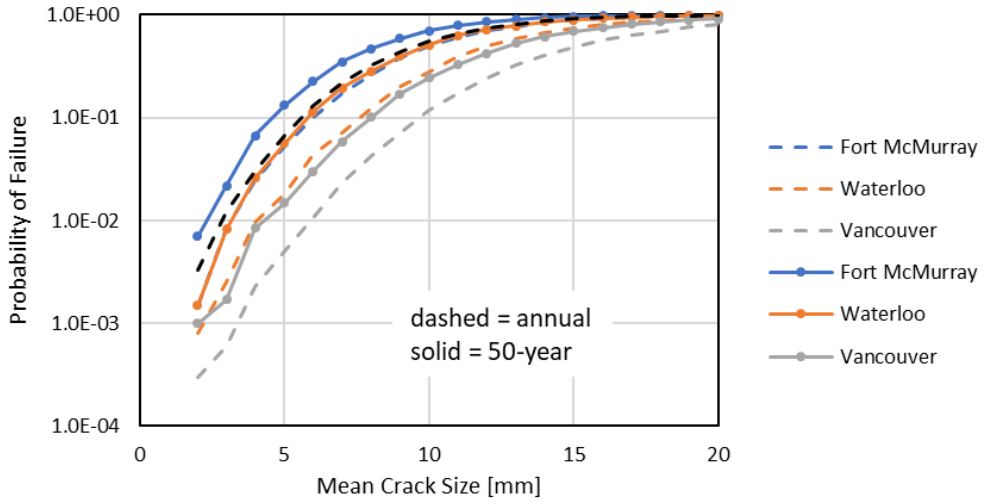


Figure 5-2 P_f vs. Crack Size (T_{27J} = -20°C)

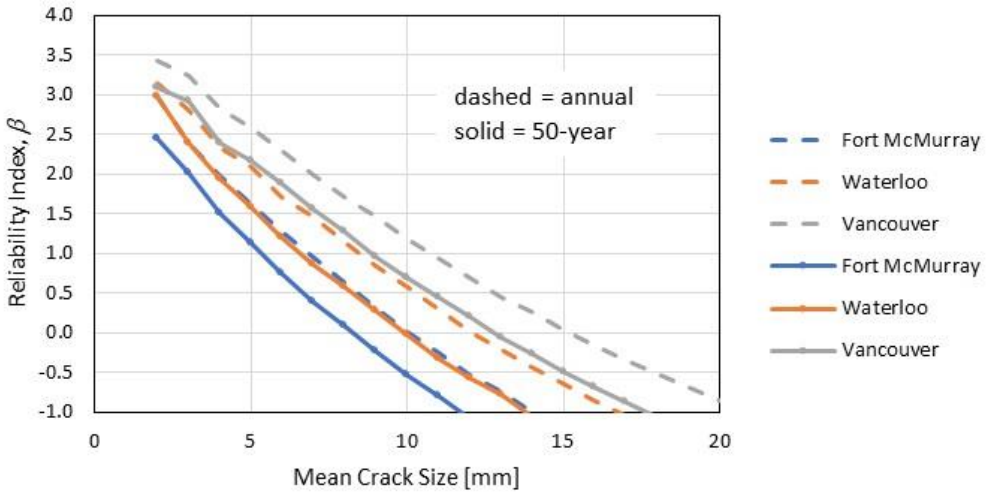


Figure 5-3: β vs. Crack Size (T_{27J} = -20°C)

5.3 Variation of Load

In the next sensitivity study, the maximum nominal applied stress at the detail was varied to investigate the effect of this parameter. The dead-to-live load ratio was maintained all analyses. As can be seen in Figure 5-4, the results show an expected increase in the probability of failure with an increase in the maximum nominal applied stress, which was expected, due to the direct correlation between σ_{Ed} and K^*_{appld} in Equation 2-10 and Equation 2-11. It should be noted that the higher stress levels in this analysis exceed the nominal yield strength of the steel. This raises broader questions regarding the competing ductile and brittle

fracture failure modes, warranting further study, which was incorporated later in the probabilistic studies in Chapters 6 and 7.

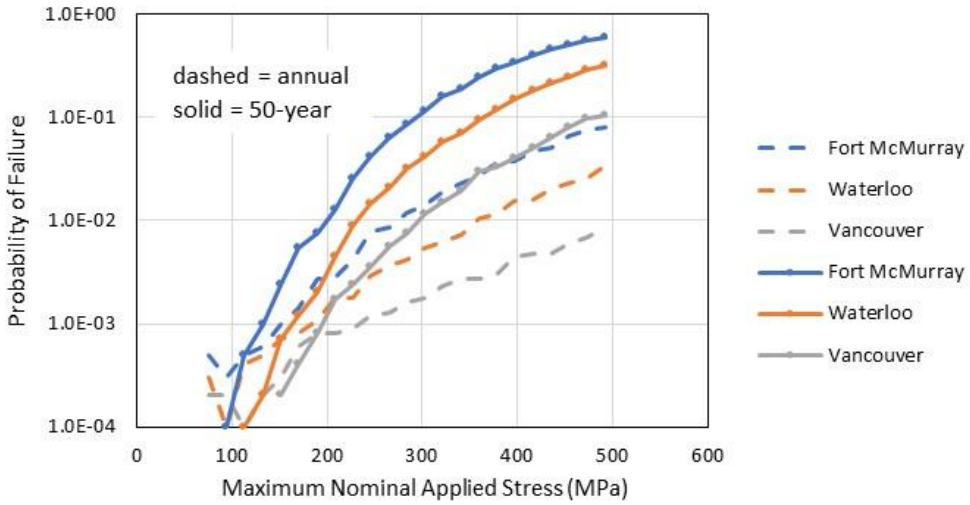


Figure 5-4: P_f vs. Maximum Nominal Applied Stress (T_{27J} = -20°C)

5.4 Variation of Weld Size

The fillet weld height and width affect the calculation of the M_k parameter for semi-elliptical surface cracks, shown in Figure 2-9. As shown in Figure 5-5, the failure probability showed little change with variation in the fillet weld size (in this case, height and width which are assumed to be equal). While the figure shows the results for an 8 mm crack, the process was repeated for two other crack sizes, 10 mm and 12 mm, and the results were all consistently flat.

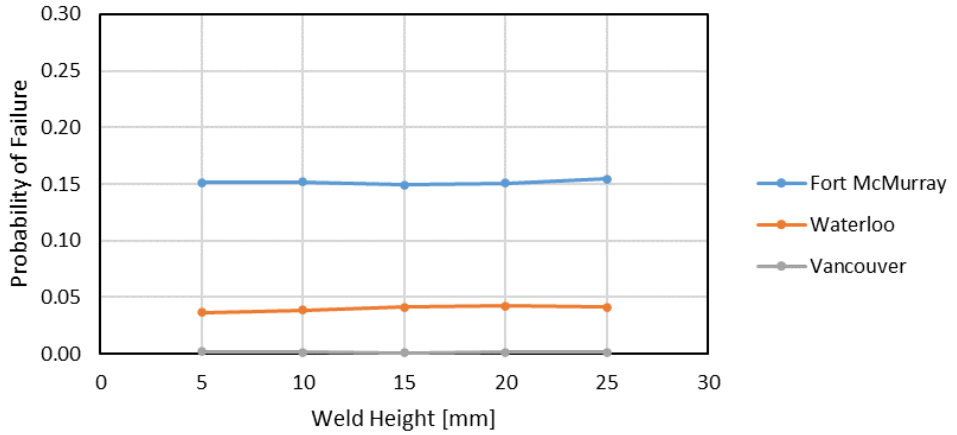


Figure 5-5 P_f vs. Weld Size (8 mm crack case)

5.5 Variation of Plate Thickness

The plate thickness affects several parameters of the fracture mechanics model, including the calculation of the crack shape correction factor, Y, correction factor for semi-elliptical cracks, M_k, the critical crack front length, b_{eff} (for certain crack shapes), and the through-thickness adjustment, ΔT_t. This means that in the Eurocode, t affects parameters on both action and resistance sides, K^*_{appld}, and K_{mat}, of Equation 2-9, and its impact on the probability of failure was not as clear as crack size and load.

The simulation results from a flange plate thickness variation study interestingly showed a local minimum point in the P_f vs. flange plate thickness output, in contrast with the monotonically increasing curves obtained in the first two studies. Initially, the failure probability is high, as the crack takes up a significantly large proportion of the overall plate depth, making it a point of weakness as there is an insufficient amount of uncracked flange area to prevent failure. In the first portion of the graph, P_f decreases when the thickness increases, as gradually the crack is taking up less of the cross section. At a point near 50 mm thickness, the local minimum is reached. Beyond the optimum point, the P_f increases again as the increased thickness causes a reduction in ductility. The graph for the 8 mm crack is shown in Figure 5-6.

Plate thickness variation was simulated for four different mean initial crack sizes ranging from 6 to 12 mm. The results for the 12 mm crack are shown in Figure 5-7. In general, the trends were seen to be similar. However, as the mean crack size increases, the flange plate thickness for which the probability of failure by brittle fracture is a minimum also increases. Also, as expected, the probabilities of failure increase for all cases with an increase in the mean initial crack size or severity of the local climate.

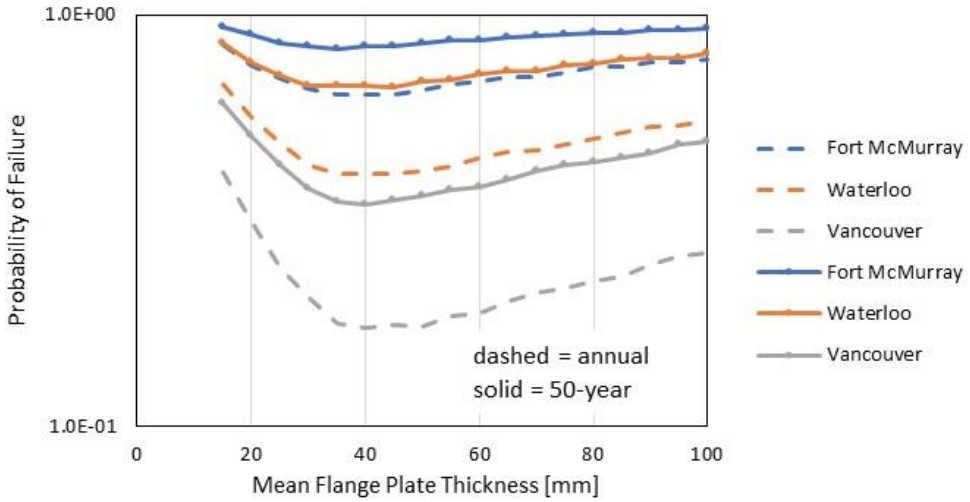


Figure 5-6: P_f vs. plate thickness (8 mm mean initial crack size, T_{27J} = -20°C)

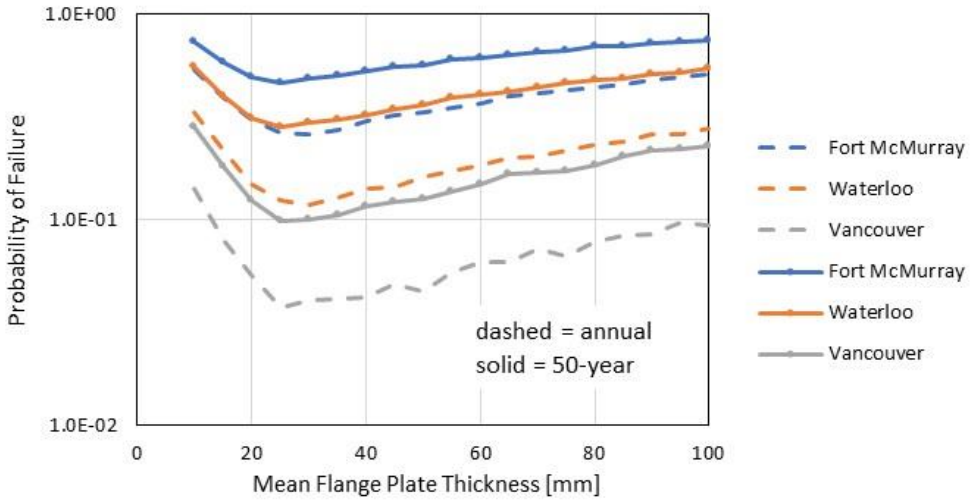


Figure 5-7: P_f vs. plate thickness (12 mm mean initial crack size, T_{27J} = -20°C)

5.6 Preliminary Time-Dependent Probabilistic Model

As it was noted in the base case analysis that the assumption of minimum temperature and maximum load is conservative, a time-dependent probabilistic model better reflects the realistic hourly fluctuations in temperature and load, which is described in Section 3.3.

PDFs and CDFs generated for K_{mat}, which capture uncertainty in the toughness of the material (Step 1 in the procedure described in Section 3.3.1 of this thesis), are shown in Figure 5-8. The CDFs are used to for the interpolation of a value of K_{mat} based on the hourly temperature (Step 4a).

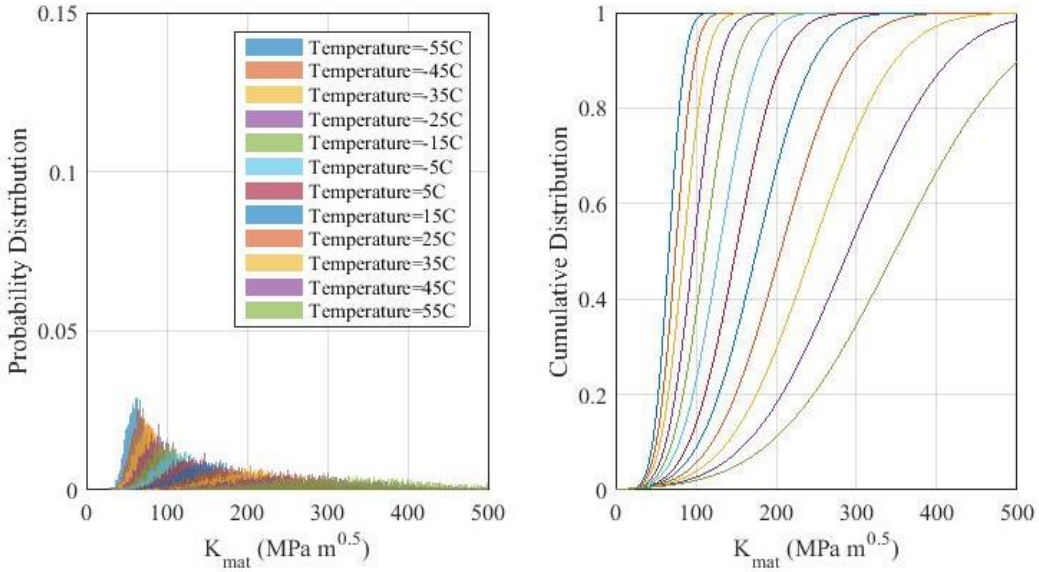


Figure 5-8 Probability and cumulative distributions for K_{mat}

The PDFs and CDFs for K^*_{appld}, which capture uncertainty in the stress intensity factor due to applied loads (Step 2 in the procedure described in Section 3.3.1 of this thesis), are shown in Figure 5-9. The CDFs are used for the interpolation of K^*_{appld} based on the maximum hourly live load (Step 4b).

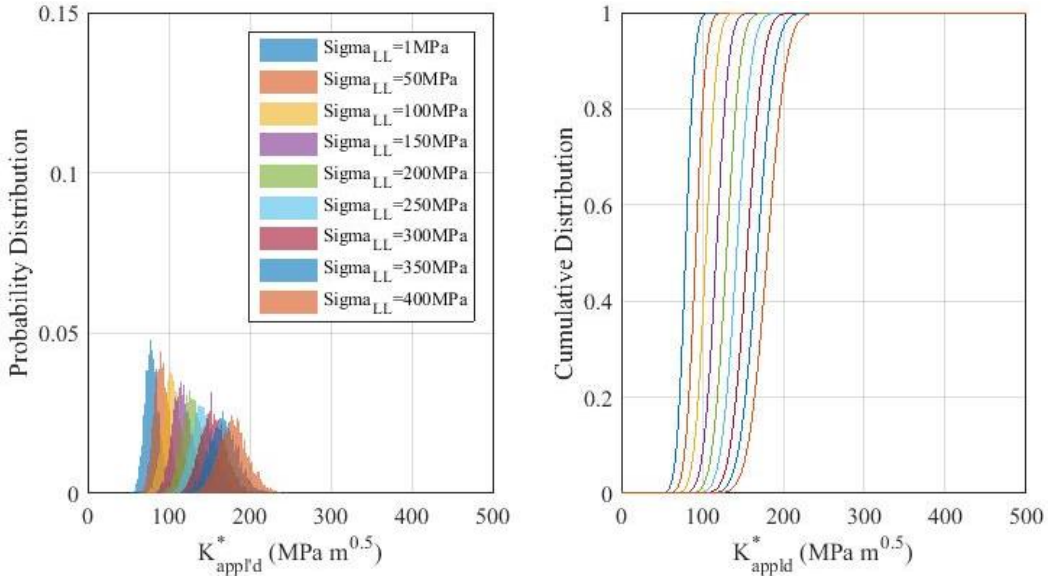


Figure 5-9 Probability and cumulative distributions for K^*_{appld}

Figure 5-10 illustrates examples of the fluctuation of the minimum hourly temperature (left) and maximum live stress (right) for each time step, in one-hour increments, over the course of one year (8760 hours). The input hourly temperature was calculated by random sampling from a normal distribution of recorded temperatures at each hour between 2003 and 2021. Furthermore, the live load was sampled at each hour using the Gumbel distribution method discussed in Agarwal et al. (2007).

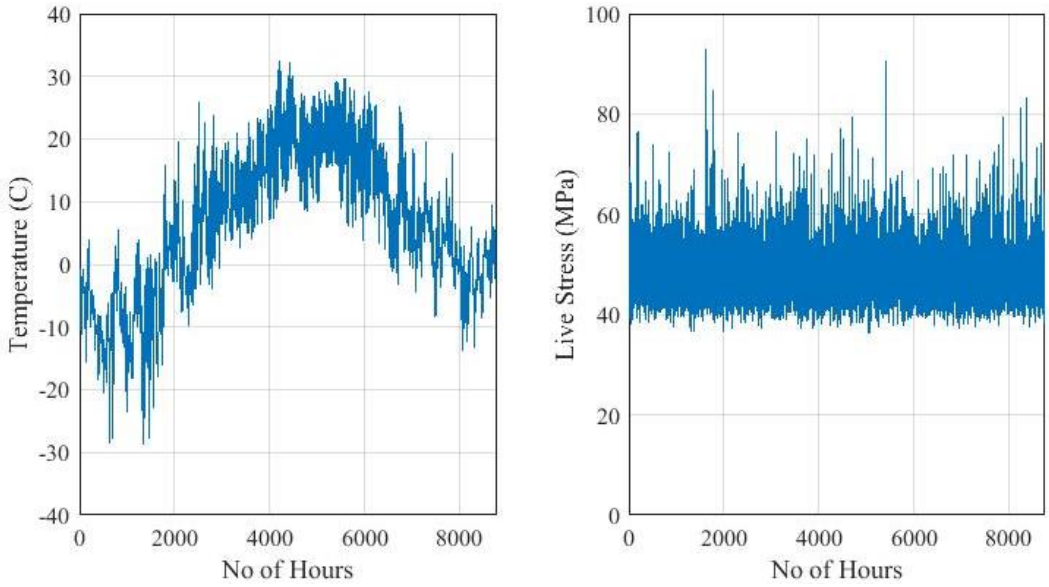


Figure 5-10 Sample temperature and live load stress fluctuations over one year

Figure 5-11 shows the results of a set of MCS trials simulating 100 years of service, for an assumed crack size of 14 mm. In each 1-hour time step, temperature and load are randomly sampled, which is then repeated for 8760 hours (time steps) per year. This process is then repeated for 100 service years in this simulation. It is observed that the annual probability of failure in this analysis is converging on approximately 0.5 after the first few years. Although this probability of failure is quite high, it should be noted that this only shows a preliminary result of an example scenario with a high failure probability associated with a fairly large crack size of 14 mm.

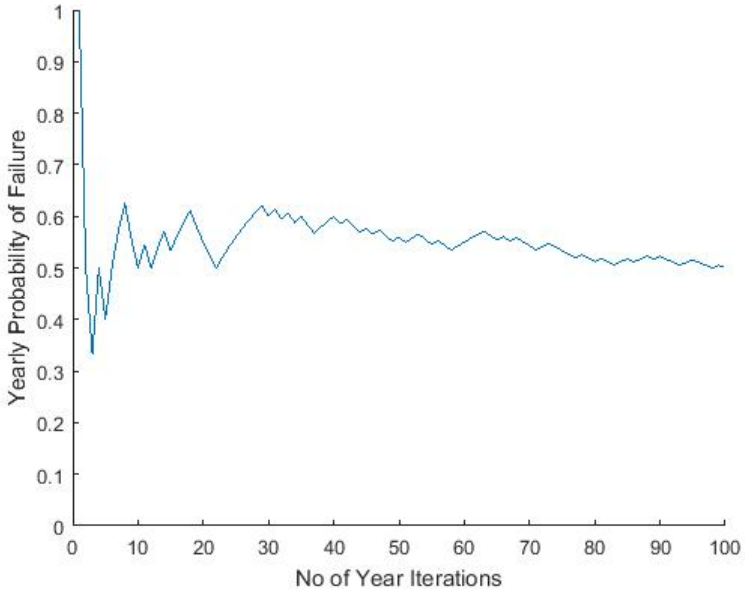


Figure 5-11 Annual probability of failure over number of iterations (100 years)

It was initially hypothesized that generating CDFs at the first step, and using interpolation between the CDFs at each time step would save computational energy. However, this was proven to be false as the code took approximately 22 hours for a 10,000-year analysis. For-loops were designed to break and jump to the next year if a failure occurred within the year, thus for larger crack sizes (or scenarios where a larger probability of failure is expected to occur), the code took a shorter time to run compared to the smaller crack sizes. However, running the model for longer analysis periods was especially crucial for the smaller failure probability scenarios, which was of higher practical interest. Ultimately, this version of the code was abandoned due to the high demand in computational time, though it is still shown in the thesis as a possible methodology of generating CDFs for interpolation.

6 Time-Dependent Probabilistic Assessment of Current CSA S6 Design Tables

In this chapter, the refined MATLAB model described in Section 3.4 are used to assess the extent to which the Canadian provisions provide uniform and adequate levels of reliability against brittle fracture over a range of steel grades, plate thicknesses, and climates. Several additional sensitivity studies are also presented for the δ_2 parameter (which characterizes uncertainty in the conversion from impact toughness to fracture toughness), strain rate, live-to-dead load (L/D) ratio, and design crack size.

Before presenting results of the time-dependent reliability analysis, it is perhaps worthwhile to explain what is happening in the analysis during a typical 1-year hour-by-hour simulation. Figure 6-1 illustrates an example of the first 1500 hours of a year with SIFs fluctuating over time, where a failure by brittle fracture is counted when K_{mat} drops below K^*_{appld} or $g(\boldsymbol{x}) < 0$. Worth noting in this figure is the relatively large fluctuation in K_{mat}, which are driven by the daily and seasonal temperature fluctuations, are dominant over the relatively minor fluctuations in K^*_{appld}, which look like they could almost be ignored, with minimal impact on the probability of failure prediction. Larger fluctuations in K^*_{appld} may be seen if a more sophisticated traffic simulation were performed, including truck platooning and natural daily fluctuations in the volume or nature of the truck traffic. However, since a primary objective of the current work is to verify existing CVN test requirements for consistency from a reliability perspective, the employed approach is thought to be reasonable for the intended purpose, and no further effort is made to explore situations that might result in larger hourly fluctuations in the K^*_{appld} parameter for a specific site.

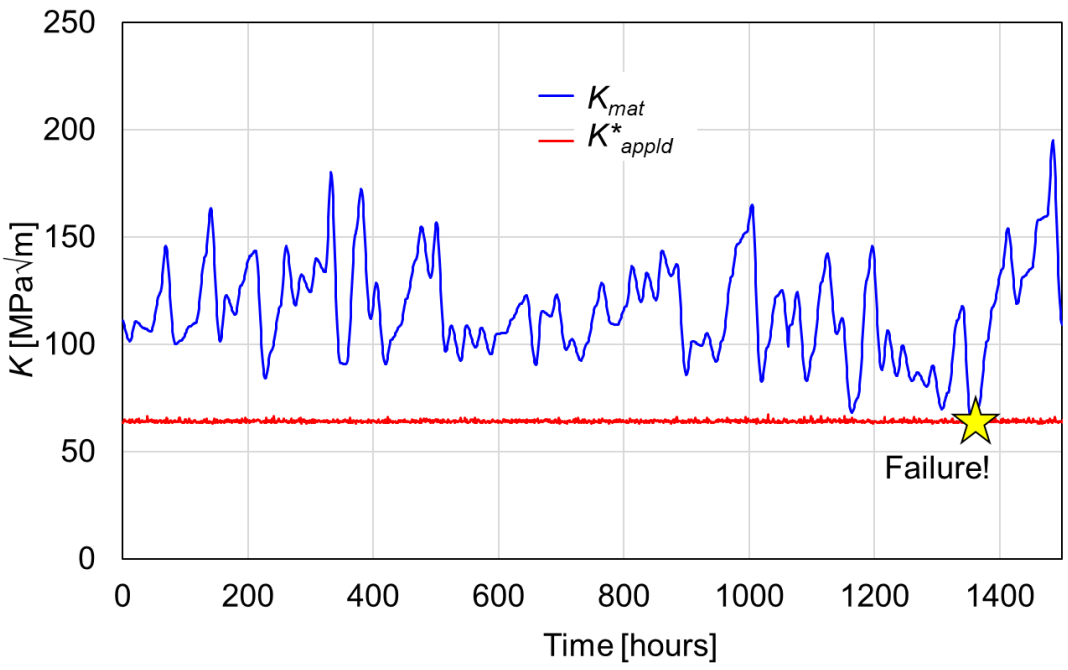


Figure 6-1 Typical K_{mat} and K^*_{appld} fluctuation over time

6.1 Reliability Index Provided by CSA S6-19 for Various Cases

6.1.1 Effect of Steel Strength

With a_d calibrated to a value of 0.53 mm using the process described earlier in Section 3.4.5, reliability vs. design T_{27J} curves can be generated for various steel strengths, F_y, as shown in Figure 3-9 (right). Alternatively, reliability analyses can be performed with the T_{27J} set to the value specified in the design tables in CSA S6, and the reliability level provided by the design T_{27J} can then be calculated. The results of such an analysis are shown in Figure 6-2, again for the case of t = 38 mm and again with a_d = 0.53 mm for the locations in both climate zones. In this figure, the black squares indicate results for base metal (BM) and the white diamonds indicate weld metal (WM).

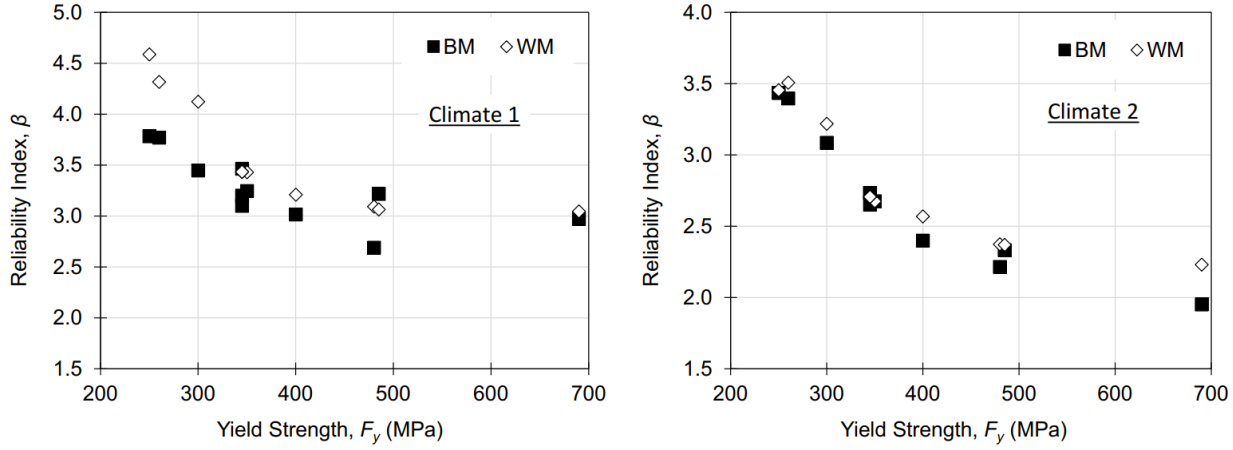


Figure 6-2 Annual reliability index for t = 38 mm, a = 0.53 mm

From Figure 6-2, several conclusions can be drawn. First, it is observed that many of the current CVN requirements do not meet the target annual reliability index of β =3.25, particularly for higher strength steels. This is more significant in the colder Climate 2. On the other hand, the target annual reliability index is exceeded for the lower strength steels. The choice of steel strength used for the calibration has a significant influence. However, regardless of this choice, it is apparent there is a lack of consistency in the provided safety levels across the various steel strengths according to this analysis. For a given steel strength, variations in the provided safety levels are also seen, as different T_{27J} requirements are specified by the code for some steel alloys having essentially the same strength. In general, the weld metal T_{27J} requirements provide slightly higher safety levels, which can be explained presumably by the code writers being more concerned about the prospects of brittle fracture happening in the weld metal and addressing this concern by specifying slightly higher toughness requirements for the weld metal.

6.1.2 Effect of Plate Thickness

Figure 6-3 to Figure 6-6 show similar analysis results covering a range of plate thicknesses, with the two assumptions concerning a_d (i.e., that a_d is either independent of or linearly proportional to plate thickness). Looking at these figures, similar trends are seen for the relationship between safety (reliability) level and yield strength, across a range of plate thicknesses. In general, the reliability levels are seen to decrease with an increase in plate thickness, as the plate thickness varies from 25 to 75 mm. This trend occurs regardless of the assumption made regarding a_d, but is more pronounced when a_d is varied with plate thickness, t. It is also noteworthy that some of the milder steels, which previously met the target annual reliability index for the base case analysis (t = 38 mm, Climate 1), no longer meet it, particularly in the colder Climate 2.

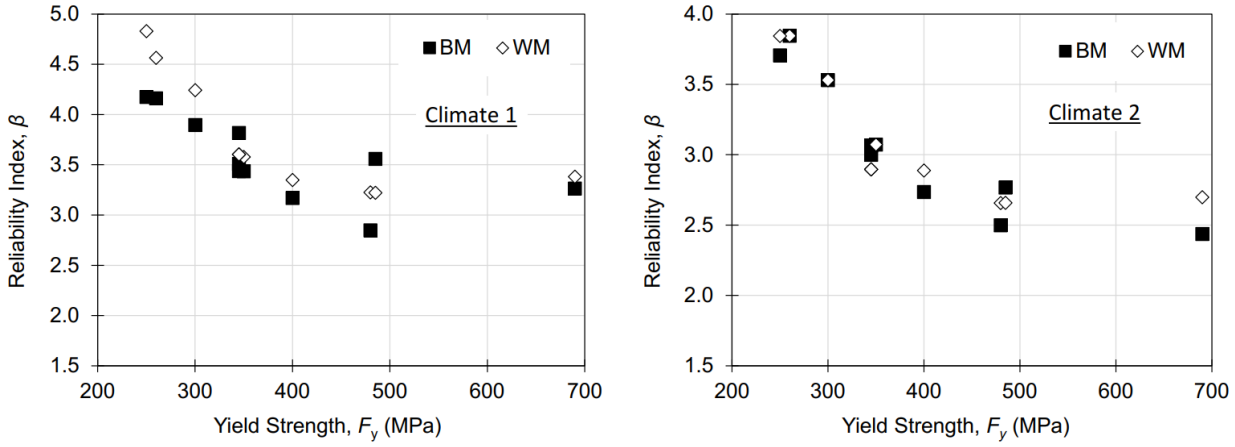


Figure 6-3 Annual reliability index for t = 25 mm, a = 0.53 mm

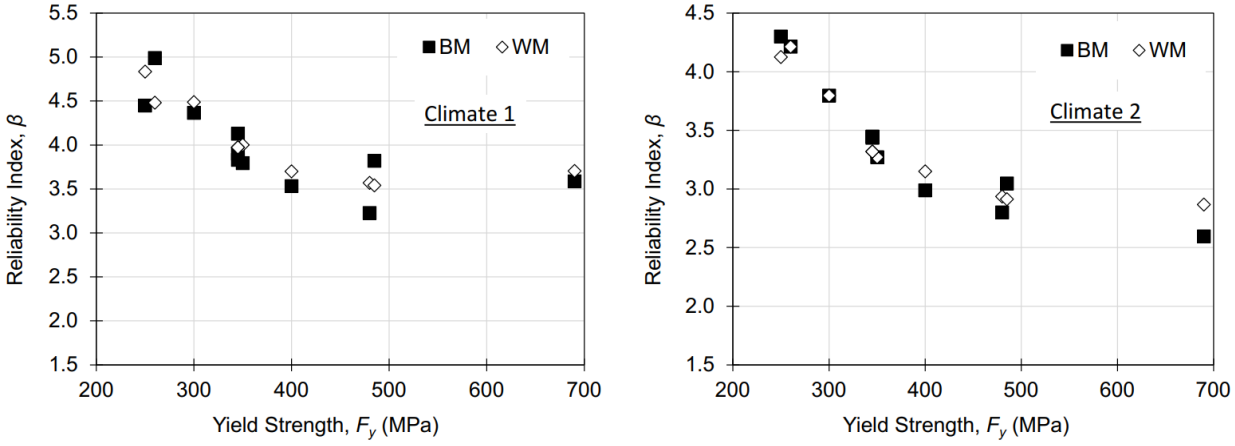


Figure 6-4 Annual reliability index for t = 25 mm, a = 0.35 mm

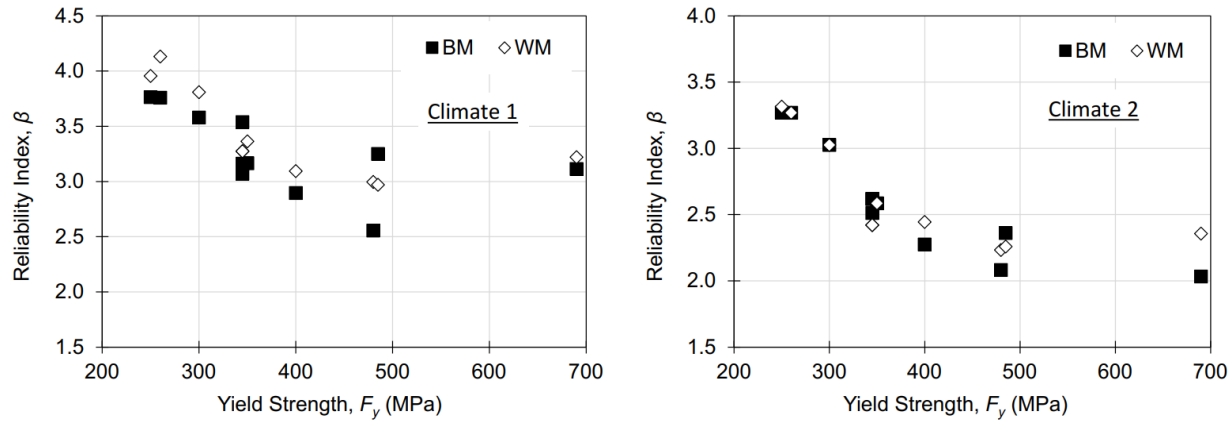


Figure 6-5 Annual reliability index for t = 75 mm, a = 0.53 mm

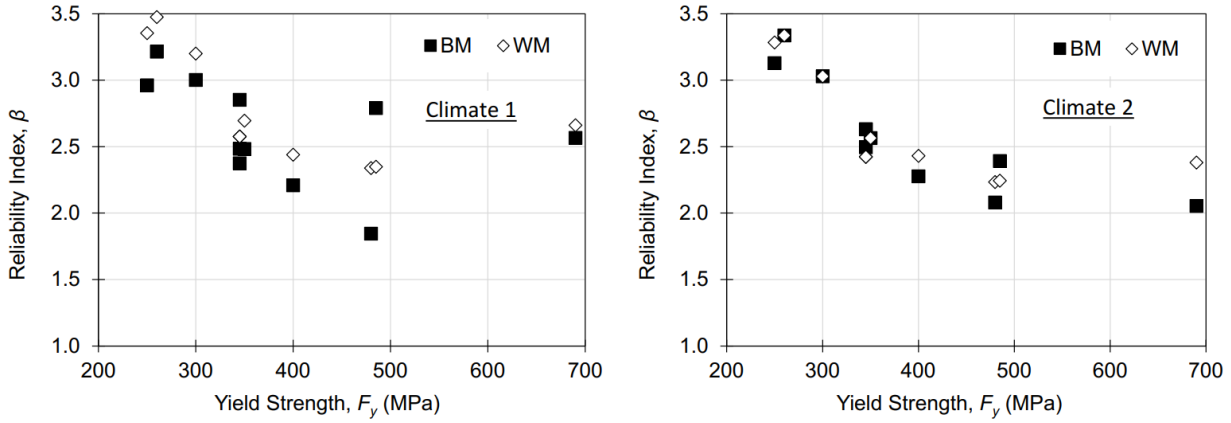


Figure 6-6 Annual reliability index for t = 75 mm, a = 1.06 mm

6.2 T_{27J} Required to Achieve Consistent Reliability Level

By varying the T_{27J} for each steel strength and generating curves like those shown in Figure 3-9 (right), appropriate T_{27J} values can be established, which will result in a consistent reliability level.

From the parametric study, graphs of β vs. T_{27J} were plotted and the resulting slope and intercept values were obtained, to interpolate or extrapolate the desired T_{27J} for the target annual reliability index. A sample graph is shown in Figure 6-7 and Figure 6-8 for t = 38 mm and a_d = 0.53 mm in Climate 1, for CSA G40.21 Grades and ASTM A709M Grades, respectively. Similar graphs were produced for all other cases.

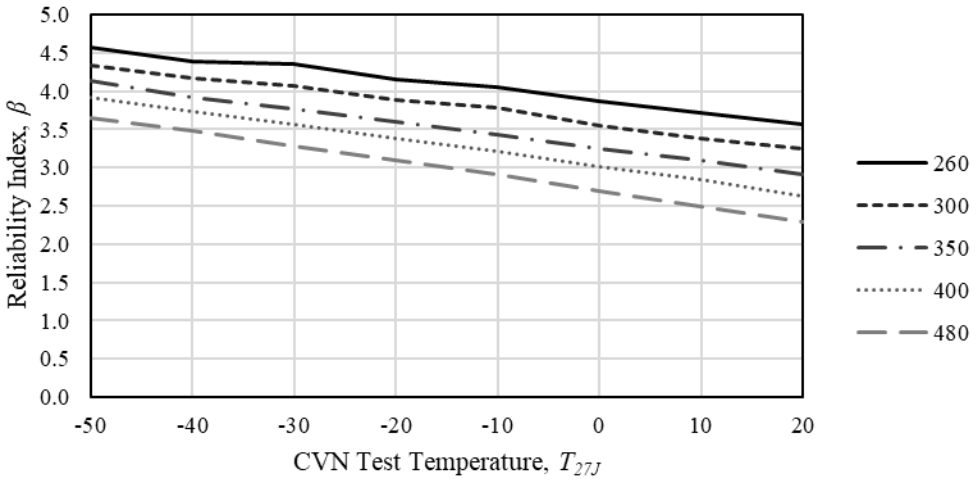


Figure 6-7 β vs. T_{27J} for t = 38 mm, a = 0.53 mm, CSA Grades, Climate 1

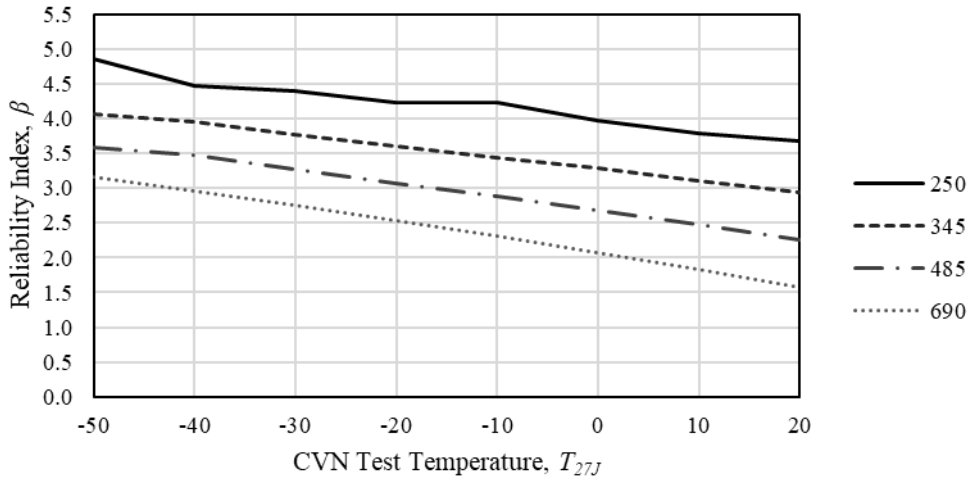


Figure 6-8 β vs. T_{27J} for t = 38 mm, a = 0.53 mm, ASTM Grades, Climate 1

6.2.1 Effect of Steel Strength

By drawing a horizontal line at the target reliability index level on a graph such as one of the ones in Figure 6-7 or Figure 6-8 and noting where this line intersects the reliability vs. T_{27J} curve for a given steel yield strength, curve can be generated of required T_{27J} vs. yield strength, which can then be compared directly with the T_{27J} requirements in the existing CSA S6-19 design tables.

To illustrate, Figure 6-9 shows the old and newly recommended T_{27J} for the base case of t = 38 mm and a_d = 0.53 mm, where the old toughness values are the data points obtained from the CSA S6-19 design tables and the proposed or "new" toughness values have been obtained using the method described in the previous paragraph. It is worth noting that in CSA S6-19, not all the CVN test temperatures are defined at a 27J

notch toughness. In order to facilitate the graphical comparison, Equation 2-33 developed by Kühn (2005) was used to convert values in the table to equivalent test temperatures for T_{27J} in Chapter 2.

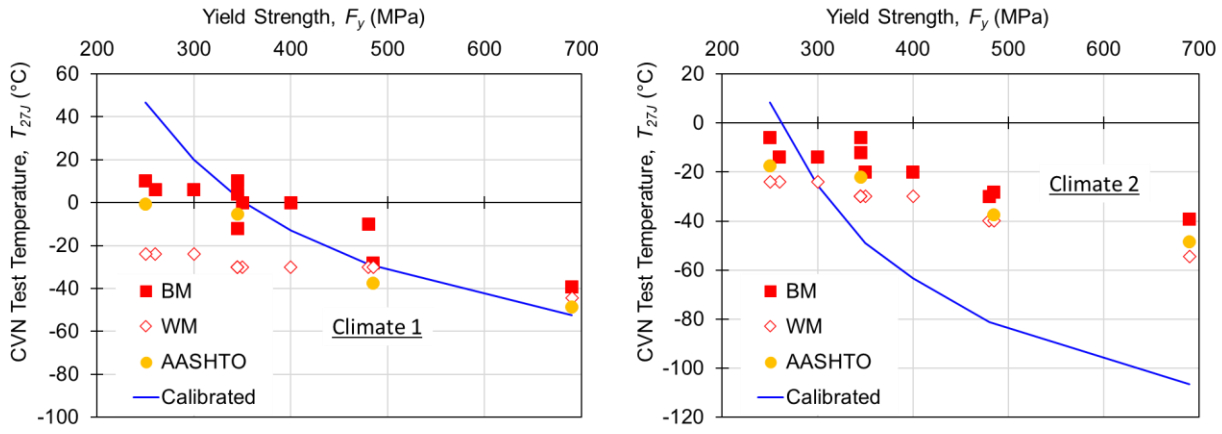


Figure 6-9 T_{27J} before and after calibration for t = 38 mm, a = 0.53 mm

Looking at Figure 6-9 (left), is observed that for the case of F_y = 350 MPa, the calibrated T_{27J} value for Climate 1 falls in the middle of the range of currently specified T_{27J} requirements at 0°C, which is expected, as this was the calibration point for establishing a_d. As the yield strength increases or decreases, a difference between the specified T_{27J} and the calibrated T_{27J} can be seen, which corresponds with the shift in the T_{27J} requirement that one might recommend, based on the current analysis. For Climate 2, it can be seen that this shift is generally more pronounced. In Figure 6-9, for comparison purposes, the AASHTO CVN test requirements for steel alloys permitted by both the Canadian and US standards are also indicated (in orange). In essence, the AASHTO and CSA S6-19 CVN test requirements for these alloys are seen to be identical, suggesting that the findings of this analysis may also hold relevance with respect to the AASHTO CVN test requirements, although repetition of these analyses with US truck GVW data and representative climate data is recommended to confirm this.

6.2.2 Effect of Plate Thickness

Figure 6-10 to Figure 6-13 again show similar analysis results covering a range of plate thicknesses (t = 25 to 75 mm), again with the two assumptions concerning the design crack depth, a_d.

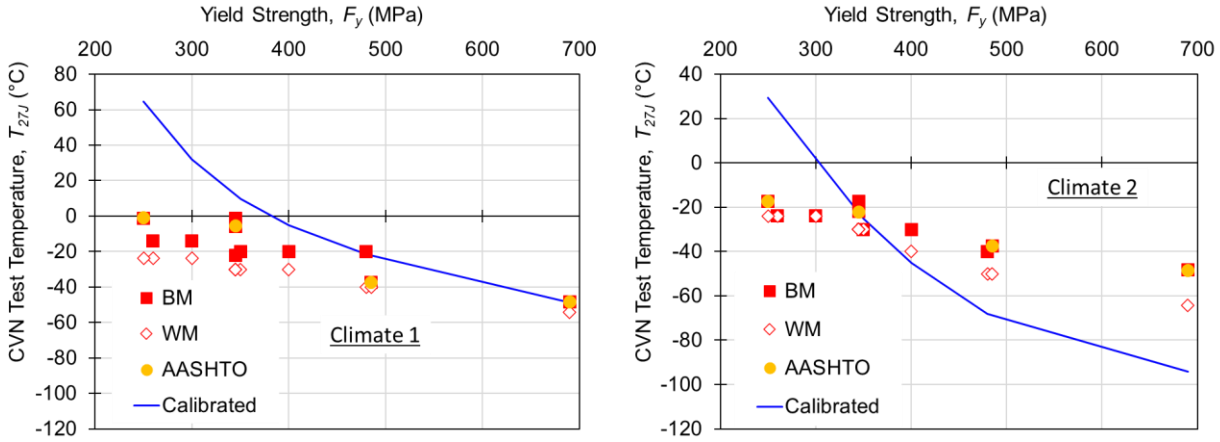


Figure 6-10 T_{27J} before and after calibration for t = 25 mm, a = 0.53 mm

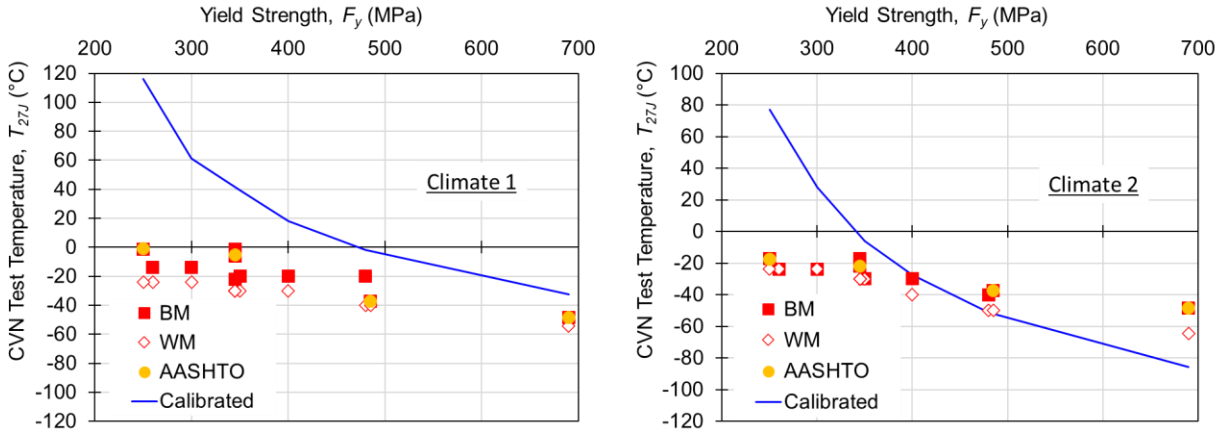


Figure 6-11 T_{27J} before and after calibration for t = 25 mm, a = 0.35 mm

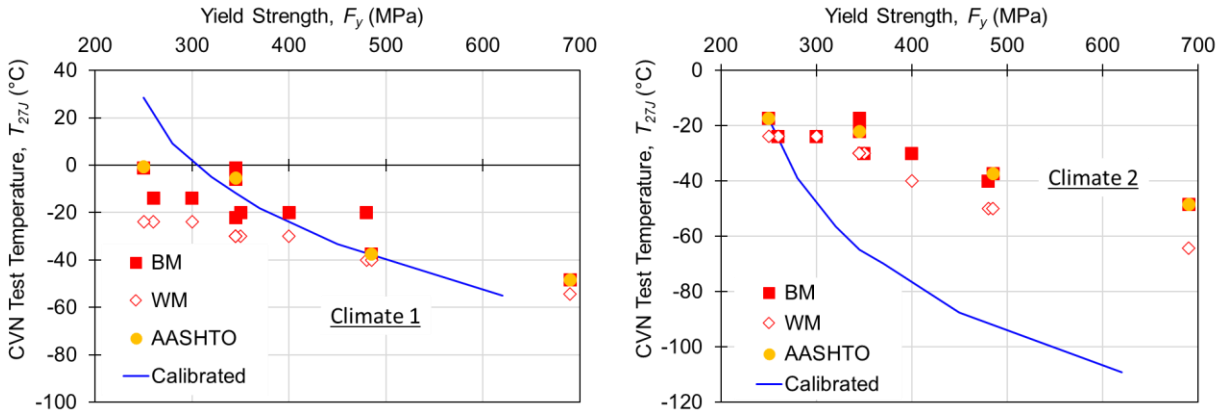


Figure 6-12 T_{27J} before and after calibration for t = 75 mm, a = 0.53 mm

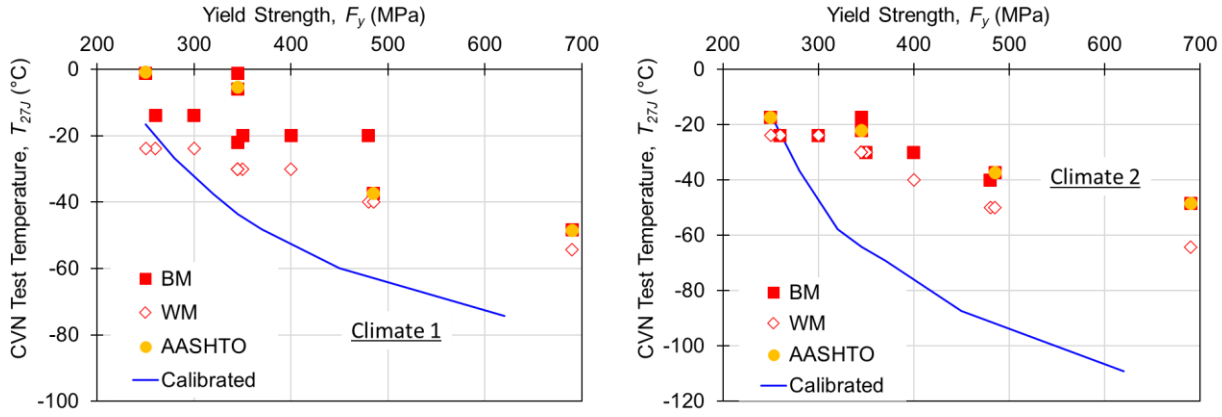


Figure 6-13 T_{27J} before and after calibration for t = 75 mm, a = 1.06 mm

Looking at these figures, it is seen that the change in the required T_{27J} before and after calibration increases significantly as plate thickness increases and climate becomes more severe. On the other hand, this analysis suggests that the design CVN test requirements could be reduced for thinner plates and milder steels.

6.3 Sensitivity Studies

6.3.1 COV of *Z17* (δ_2) Parameter

From a review of Collins et al. (2016), it was realized that the COV of the CVN to fracture toughness conversion may be much larger than the one suggested in Sedlacek et al. (2008) and used in the current study (13 °C). Using a larger COV of 34.2 °C based on Collins et al. (2016), a new design crack size for the base case scenario (Climate 1, t = 38 mm) was calibrated and found to be equal to 0.37 mm. Using this new COV and calibrated design crack size, a new T_{27J} vs. yield strength curve was generated, using the procedure described earlier. The result was a minor change (increase) in the slope of this curve. This is illustrated in Figure 6-14.

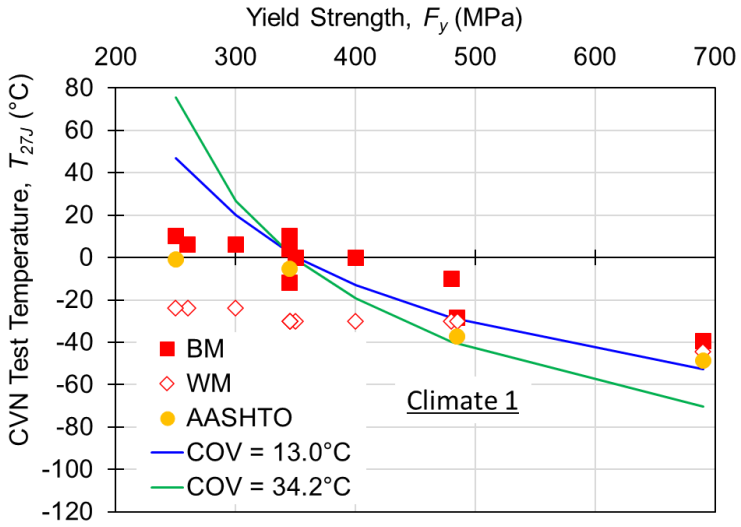


Figure 6-14 T_{27J} for CVN to Fracture Toughness Conversion COVs of 13 and 34.2 for t = 38 mm

6.3.2 Strain Rate

A key assumption in the model presented previously is that there is no strain rate adjustment, based on Sedlacek et al. (2008). A literature review revealed that a large range of strain rates may be observed on a bridge. Kühn (2005) states that vehicle crossings are in the quasi-static stress range, between 10^{-4} to 10^{-1} s^{-1}. In this reference, it is also noted that the assumption of a "static" or low strain rate is appropriate, because the peak strain rate typically does not coincide with the point in time when the load effect is greatest as a truck passes across a bridge. Sedlacek et al. (2008) shows a design example where the strain rate is 0.005 s^{-1}, Barsom (1975) states that the typical strain rate encountered on actual bridges is closer to slow loading than impact loading, and is around 10^{-3} s^{-1}. Based on this, an additional study was conducted using a strain rate of 10^{-3}, into Equation 6-1, where ε_0 =10^{-4} s^{-1}, from Sedlacek et al. (2008).

$$\Delta T_\varepsilon = \frac{1440 - f_y(t)}{550}\left(\ln\frac{\varepsilon}{\varepsilon_0}\right)^{1.5} \qquad \text{Equation 6-1}$$

ΔT_ε was calculated to be -6.93 °C, a temperature adjustment that was then used to adjust the value of T_{Ed} in Equation 3-27., which was then used to recalibrate the design crack size (a_d = 0.5 mm) and the required T_{27J}. Figure 6-15 illustrates that the curves are near identical.

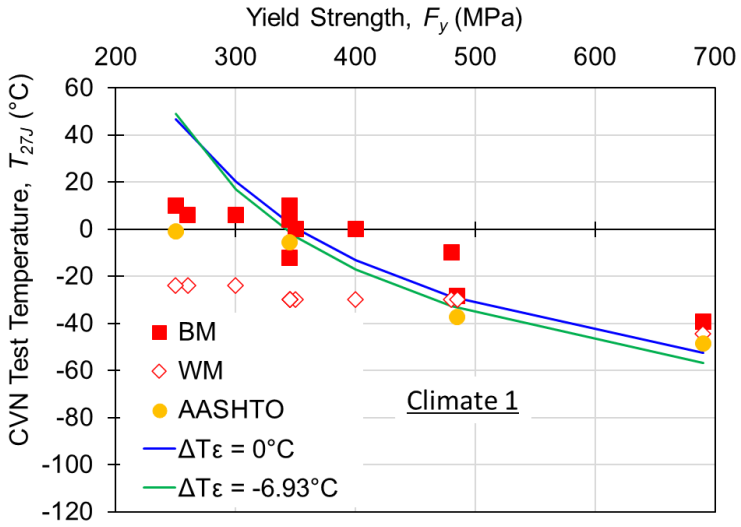


Figure 6-15 T_{27J} for different strain rate adjustments

6.3.3 *L/D* Ratio

It was previously noted that an *L/D* ratio of 0.5 is very low, in particular highway bridges with longer spans. A sensitivity study was thus performed with different *L/D* ratios to determine the effect of this parameter on the analysis results. Design examples tend to have *L/D* closer to 1.0 (Canadian Institute of Steel Construction, 2002). Using the previously described procedure, this value, plus an even larger value of *L/D* = 4.0 were used to assess the influence of this parameter on the calibrated T_{27J} vs. steel strength curve. Figure 6-16 illustrates the effects of all three *L/D* ratios for Climate 1, t = 38 mm.

Looking at this figure, it is observed that all three curves are nearly identical.

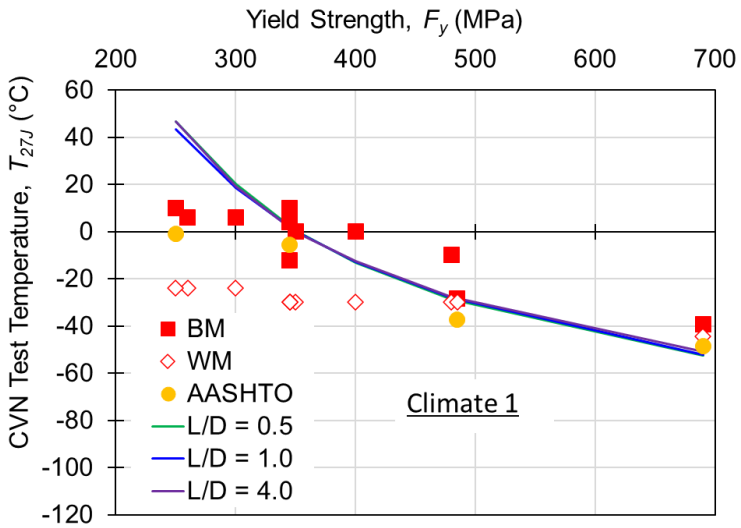


Figure 6-16 T_{27J} for *L/D* of 0.5, 1.0, and 4.0

6.3.4 Design Crack Size

It must be acknowledged that the calibrated design crack size for a target annual reliability index of β = 3.25 is very small and undetectable through visual inspection. On this basis, it was decided to perform an additional calibration with a larger design crack. For this study, the crack size was assumed to be ¼ of the thickness of a 38 mm plate, or a_d = 9.5 mm. With this design crack size, a new target reliability could be back-calculated for the 350 MPa grade case at T_{27J} = 0 °C. Doing this resulted in a target reliability index of β = - 0.064. The new target β and larger crack size were then used to recalibrate the CVN test requirements for the other steel strengths. Figure 6-17 shows the result. As expected, the curves for the two design crack sizes cross near the calibration point (350 MPa, T_{27J} = 0 °C). The result shows that the main observations from the previous analysis are relatively insensitive to the design crack size.

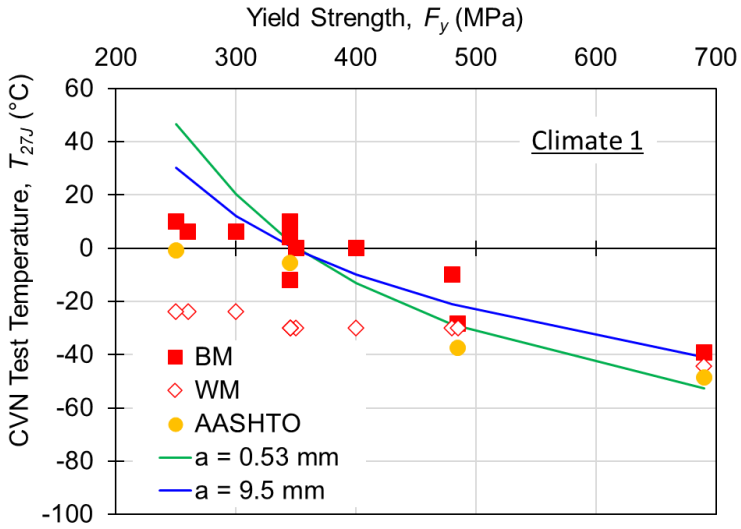


Figure 6-17 T_{27J} for crack sizes of 0.53 and 9.5 mm

6.3.5 Fracture Critical / Non-Redundant Tension Members

A target annual reliability index of β = 3.25 based on CSA S6-19 was appropriate for a primary tension member, whereas a higher target reliability index could be more appropriate for a fracture-critical (or "non-redundant tension") member. Figure 6-18 illustrates the curves for different reliability indexes, up to 4.0, for the same design crack size of a_d = 0.53 mm for a 38 mm thick plate. On the same graph, the increased CVN test requirements currently specified in CSA S6-19 for fracture-critical members are superimposed. Looking at this figure, it can be seen that the increased toughness requirements in the standard correspond with a relatively small increase in the target annual reliability index. Further study is needed to fully assess the implications of this result considering a broader range of factors. Thus, further conclusions cannot be drawn. However, the result shows how this type of analysis may be a useful tool for code writers to determine the CVN test requirements for different levels of reliability desired.

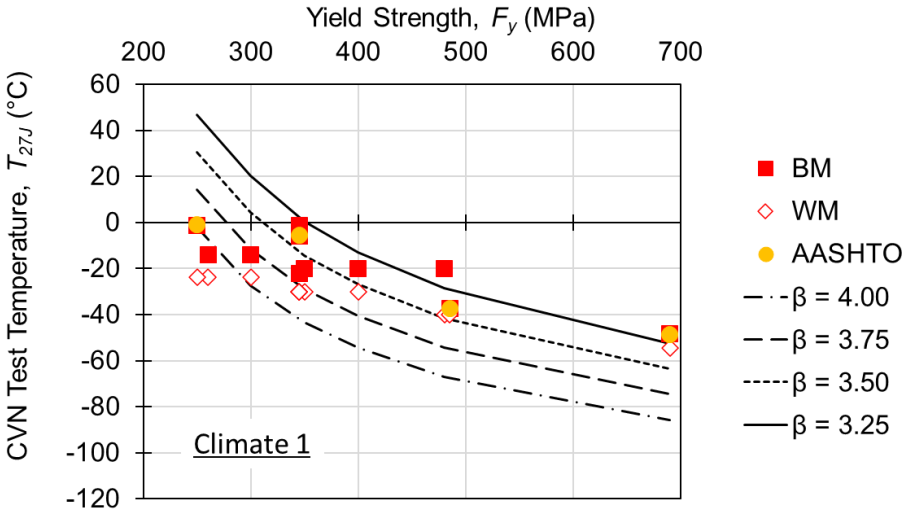


Figure 6-18 T_{27J} for β = 3.25, 3.5, 3.75, and 4.0 in Climate 1

7 Sensitivity Studies and Design Tool Development

In this chapter, results obtained using time-dependent and -independent versions of the reliability analysis are compared, sensitivity studies are performed. Following this, work performed to develop a new tool for design against brittle fracture is presented, which allow toughness requirements to be defined in terms of steel grade, plate thickness, demand-to-capacity ratio, traffic volume, and fracture-criticality.

7.1 Comparison of Time-Dependent and -Independent Analysis Results

In Chapter 6, a time-dependent model was used to assess reliability against brittle fracture, where traffic and temperature were simulated hourly, taking into account the fluctuations occurring throughout the year. While more realistic, the simulations required for this analysis were time-consuming and resource intensive. One important question was to address whether the computational time/cost of time-dependent analyses was necessary, or whether faster time-independent analyses where each parameter is sampled only once per bridge-year could yield sufficiently accurate results for practical purposes.

To answer this question, a comparison was made between analysis results obtained using the time-dependent and -independent models. To perform this comparison, a necessary first step was calibrating the design crack size to the time-independent model in a similar manner to what was done previously for the time-dependent model. As a reminder, the procedure for the calibration is defined in Section 3.5.4 and essentially consists of establishing the crack size that achieves a desired annual reliability index for a typical case seen in practice where there is a historical record of good brittle fracture performance.

Following the same procedure as used previously for the time dependent code, a calibrated design crack depth of a_d = 0.13 mm was obtained for the time-independent code, which is smaller than the calibrated crack depth of a_d = 0.53 mm obtained previously for the time-dependent code. This was expected and can be explained by the conservative assumption made in the time-independent analysis that the maximum load and minimum temperature during the analysis period (one year) occur at the same time.

Following the calibration step, a comparison was made of required toughness vs. yield strength curves generated using the two models. An example result is shown in Figure 7-1. The results in this figure are for a primary tension member in Climate Zone 1 (Waterloo). In this figure, the curves generated using the two models are near identical. This suggests that employing the time-independent model with a smaller design crack (a_d = 0.13 mm) is a reasonable approach for running the quantities of analyses required to perform sensitivity studies and develop practical tools for design. On this basis, the calibrated time-independent code has been used to generate the remainder of the results presented in this chapter.

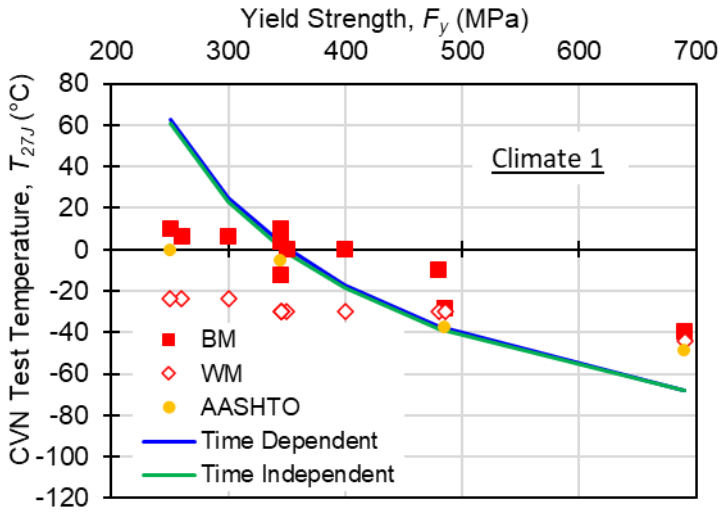


Figure 7-1 Comparison of time-dependent and -independent models

7.2 Sensitivity Studies

Using the time-independent model, studies were performed to assess the sensitivity of the results to variations in the following parameters: climate, bridge span and influence line, traffic volume, and consideration of multiple vehicle presence. In the following sections, the results are presented.

7.2.1 Climate Study

CSA S6 presents CVN requirements for design against brittle fracture in tables separated into two climate zones: a moderate zone with a minimum mean daily temperature of > -30°C, and a severe zone for -30°C to -52°C. Notably, each zone encompasses a large temperature range. Cities and towns dispersed across Canada may have very different climate histories despite falling within the same temperature zone. In the previous work, only one town in each climate zone was chosen to demonstrate implementation of the analysis methods. In this section, results are compared for several locations located in each climate zone to assess the sensitivity of the analysis to location. This was an important area of investigation as temperature, T_{Ed}, directly affects the K_{mat} parameter representing material toughness (recall Equation 3-27).

For this sensitivity study, three locations distributed across Canada were selected within each climate zone, to represent both coastal and inland regions where temperature cycles may vary appreciably over the course of a year. Waterloo, Halifax, and Kamloops were the locations selected for Climate Zone 1. Similarly, Whitehorse, Fort McMurray, and Winnipeg were the locations selected for Climate Zone 2, based on Figure A3.1.2 in CSA S6 (Canadian Standards Association, 2019).

Figure 7-2 presents the required fracture toughness vs. yield strength curves obtained for each of these locations. In short, this figure shows that the location within each climate zone has minimal impact on the

CVN test requirements, with the toughness requirement for a given steel yield strength not varying by more than 3-4 °C. On this basis, the locations used previously to represent each climate zone were retained in subsequent analyses. In other words, Climate 1 is represented using climate data for the City of Waterloo, and Climate 2 is similarly represented by the City of Whitehorse.

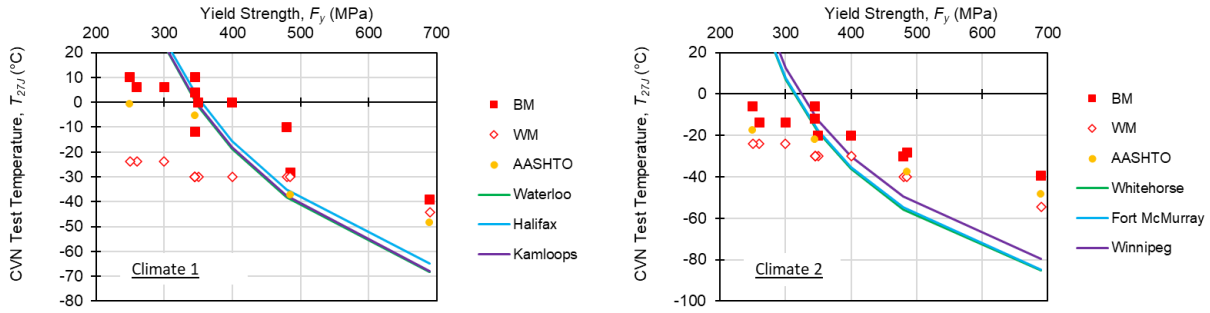


Figure 7-2 Effects of Location within each Climate Zone

7.2.2 Bridge Span and Influence Line Study

In the next sensitivity study, the influence of bridge span and influence line were investigated, as these parameters can significantly influence the stress histogram, which is used to obtain σ_{Ed} in the K_{appld} equation. As a reminder, in the previous work, the gross vehicle weight (GVW) histogram was assumed to be representative of the live load stress histogram, which would essentially be true if one were assessing bending stresses in a very long span, simply-supported bridge girder. In order to assess the sensitivity of the results to this assumption, in this study, girder spans of 10 m, 40 m, and 100 m were selected to represent short, medium, and long span bridges, and influence lines for two locations were considered – namely, the support reaction (ps_r) and the midspan moment (ps_m) for a simply-supported girder.

Results of the bridge span and influence line sensitivity study are presented in Figure 7-3. In this figure it can be seen that the girder span and influence line have negligible effects on the CVN test requirements. One point worth noting is that the same strain rate was assumed for all of these analyses. This is believed to be reasonable, for reasons discussed earlier. However, it is conceivable that for a very short influence line, such as the one that might be relevant for an expansion joint, it is likely that the strain rate is much more closely influenced by the impact of each axle hitting the joint, in which case a higher strain rate might be appropriate to represent this situation. That said, the results of this analysis show that the features of the stress histogram that vary with bridge span and influence line, on their own, are not sufficiently different to cause a meaningful shift in the required toughness vs. yield strength curve.

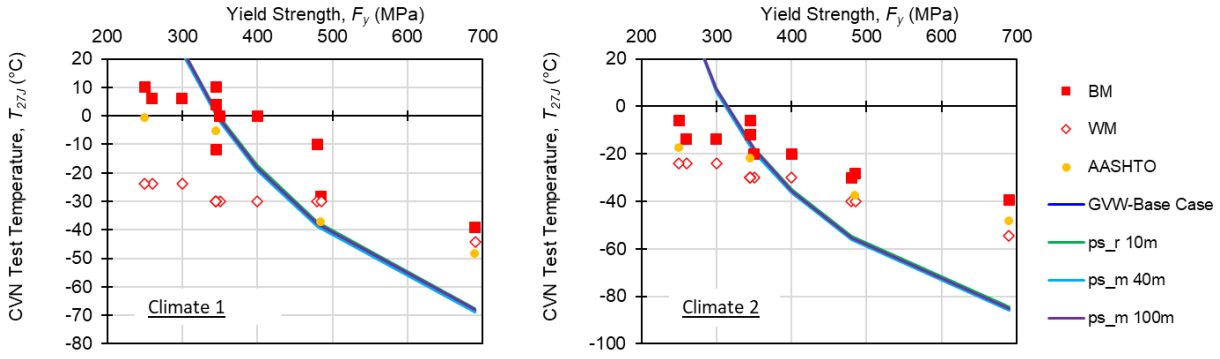


Figure 7-3 Effect of Bridge Span and Influence Line

7.2.3 Traffic Volume Study

CSA S6 (Canadian Standards Association, 2019) defines four different highway classes based on Average Daily Truck Traffic (ADTT) counts of 4000, 1000, 250, and 50. In this study, each of these highway classes was assessed. The influence of the traffic volume manifests itself in the definition of the live load stress distribution (σ_{LL}, the *Z13* parameter in Table 3-5), which is defined for each case based on extreme value statistics. Figure 7-4 show analysis results for four different traffic volumes.

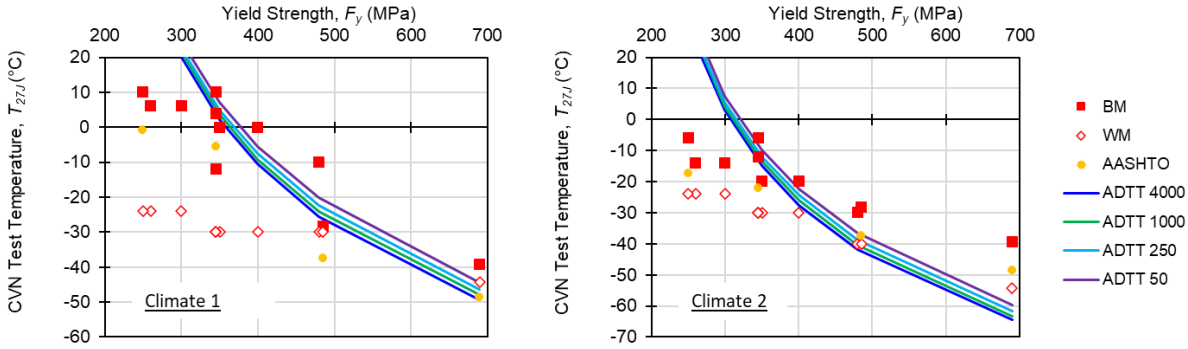


Figure 7-4 Required T_{27J} for various highway classes in Climate 1 and Climate 2

As expected, as the traffic volume increases, the result is a slightly more rigorous CVN test requirement (i.e., decrease in T_{27J}). This can be explained by the increased probability of an extremely heavy truck crossing the bridge during an extreme low temperature event as the traffic volume increases. Overall, the shifts in the curves are small – less than 5-6 °C over the full range of yield strengths – and the influence of traffic volume was found to be less significant than expected.

That said, the possibility of having different toughness requirements for bridges supporting low and high-volume roads could be worth considering to reduce the material cost for fabrication of bridges, e.g., in remote or rural regions. To show how this could be done, the traffic volume parameter has been retained as a variable in the development of a practical design tool presented later in this chapter.

7.2.4 Multiple Vehicle Crossing Study

In real traffic with heavy truck volumes and multiple lanes, occurrences of two trucks side-by-side or one behind the other passing over a bridge can be important – in particular for longer bridge spans. For this study, the required toughness vs. yield strength curve for "ps_m_100m" represents the base case for trucks crossing one-by-one over the influence line for the midspan moment of a 100 m span simply-supported bridge girder. Using a traffic simulation approach developed previously to study multiple presence effects on fatigue damage, two other analysis cases were developed to model two different kinds of multiple presence effects (Chehrazi et al., 2022). Specifically, a "ps_m_100m uni-dir" was developed with a stress histogram representative of a case where there are two lanes with trucks passing the bridge in the same direction. The multiple presence effects in this case could come from trucks in adjacent lanes or trucks following each other closely. In addition, a "ps_m_100m bi-dir" was developed with a stress range histogram representative of a case where there are two lanes supported by a bridge with trucks passing in opposite directions. In this case, the multiple presence effects could come from trucks passing each other in opposite directions on the bridge or trucks in one direction following each other closely. Details on the traffic simulation process can be found in Chehrazi et al. (2022). In short, a Poisson process model representing steady (as opposed to "stop-start") traffic flow developed by Bailey (1996) is used to determine the arrival time of each truck at the bridge. Trucks are then randomly sampled from the same GVW histogram used in the "one-by-one" analysis. For this study, a steady state flow rate of 0.2 veh/s was assumed. This flow rate is at the higher end of the range of flow rates studied in Chehrazi et al. (2022). It is likely representative of a worst case – e.g., during a rush hour – for a busy highway, which would not likely be sustained for a full day.

In Figure 7-5, the results of this sensitivity study are presented, it is observed that simultaneous truck crossings over a bridge have a significant influence on the required T_{27J}. The difference in the toughness requirements is on the order of 10°C for the higher yield strengths. The uni-directional simultaneous crossing case is the most critical of the three investigated.

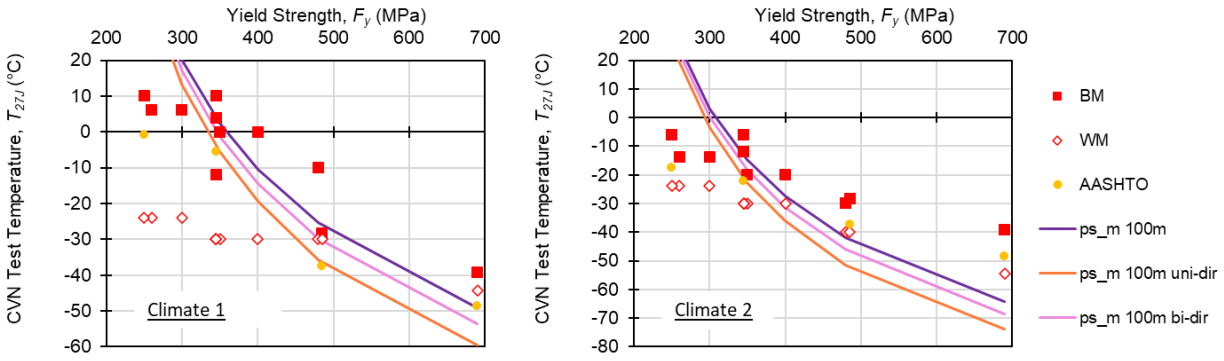


Figure 7-5 Simultaneous crossing effects on required T_{27J} in Climate 1 and Climate 2

7.3 Design Tool Development

As stated in the first chapter of this thesis, the third objective of this research project was to develop an improved practical tool for establishing toughness requirements for steel bridges. As also stated in the first chapter of this thesis, major shortcomings of the current design tables include: 1) the lack of an established relationship between the current toughness requirements and the reliability level against failure by brittle fracture, which they provide, and 2) the lack of sophistication of the tables in terms of their ability to treat factors that can have a significant impact on the toughness requirement, such as plate thickness and load level. At the same time, it is recognized that there would likely be a lack of uptake by practicing engineers in North America on a procedure that involved a complex series of calculations, such as those required by any of the Eurocode methods, and while offering a clear understanding of the brittle fracture risk, the use of a probabilistic fracture mechanics approach such as the one employed in the current project would clearly not be of interest for practitioners engaged in routine bridge designs.

Against this background, it was decided to use one of the probabilistic fracture mechanics models developed for the current project to run a series of simulations to establish toughness requirements for a broad range of practical situations and to then use the results to develop contour plots, which would allow the required toughness to be established as a function of two varying parameters. After considering various alternatives, the two parameters chosen were the yield strength of the steel and the "demand-to-capacity ratio" or the ratio of the maximum stress to the maximum allowable stress level after the various load and resistance factors in the ultimate limit strength limit state function are applied, shown in Equation **7-1**. Recall that the dead load factor, 1.1, is for factory-produced components, live load factor, 1.7, is for ULS Combination 1, and the resistance factor for steel yielding is 0.9 (Canadian Standards Association, 2019).

$$(1.1D + 1.7L = DCR \cdot 0.9F_y) \qquad \text{Equation 7-1}$$

It was then decided that additional contour plots could be created in order to consider additional parameters, such as climate zone, plate thickness, traffic volume, and fracture criticality.

7.3.1 Primary Tension Members

Figure 7-6 shows an example of a single contour plot generated in this manner for the base case of a 38 mm thick plate in a primary tension member, in Climate 1, and subjected to a traffic volume of 4000 trucks per day. In this figure, the contours represent minimum toughness requirement as the temperature associated with a fractur toughness of 27 J (T_{27J}). The demand-to-capacity (DCR) ratio is varied from 0.5 to 1.0 and the yield strength of the steel is varied between 250 and 700 MPa. Looking at this figure, it can be seen that higher toughness requirements (characterized by a lower value of T_{27J}) occur in the top left corner, where both the DCR and material yield strength are high. As one moves towards the origin in either direction, the toughness requirements are relaxed. For practical purposes, T_{27J} values higher than 20°C are not considered, as impact testing is rarely done above room temperature. It should be noted that the target annual reliability index used to generate this plot is β = 3.25. As mentioned previously, this target value is based on an assumption of system behaviour S2, element behaviour E2, and inspection possibility INSP2, from Table 14.5 in CSA S6-19 (Canadian Standards Association, 2019).

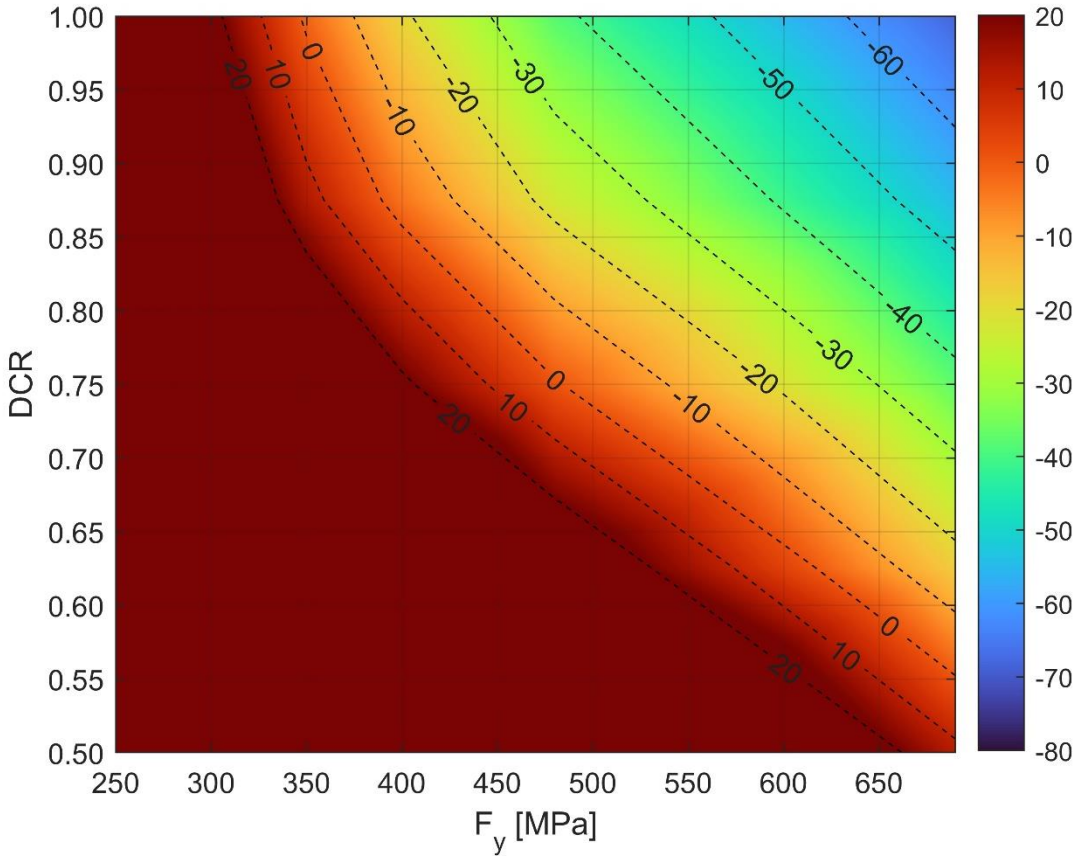


Figure 7-6 Contour plot for *t* = 38 mm, Climate 1, ADTT = 4000, primary tension member

Using the same procedure, similar contour plots were generated for a wide range of cases for primary tension members. These are shown in Figure 7-7 and Figure 7-8. For illustrative purposes, results are shown for two extreme traffic volumes (ADTT = 50 and 4000) and three plate thicknesses (t = 25, 38, and 75 mm). The two figures show these plots separated also into those for Climates 1 and 2.

As expected, looking at these figures it can be seen that the toughness requirements become more severe as plate thickness and/or traffic volume are increased. They are also more severe for Climate 2 vs. Climate 1. To use contour plots like these, a designer needs to know the DCR, yield strength, plate thickness, traffic volume, and climate. Given this information, they can select the appropriate contour plot and then use it to determine the design toughness requirement (T_{27J}). If they are evaluating a steel for which the toughness is defined by a temperature associated with an impact toughness other than 27 J, a conversion formula such as the one defined in Equation 2-33 can be employed.

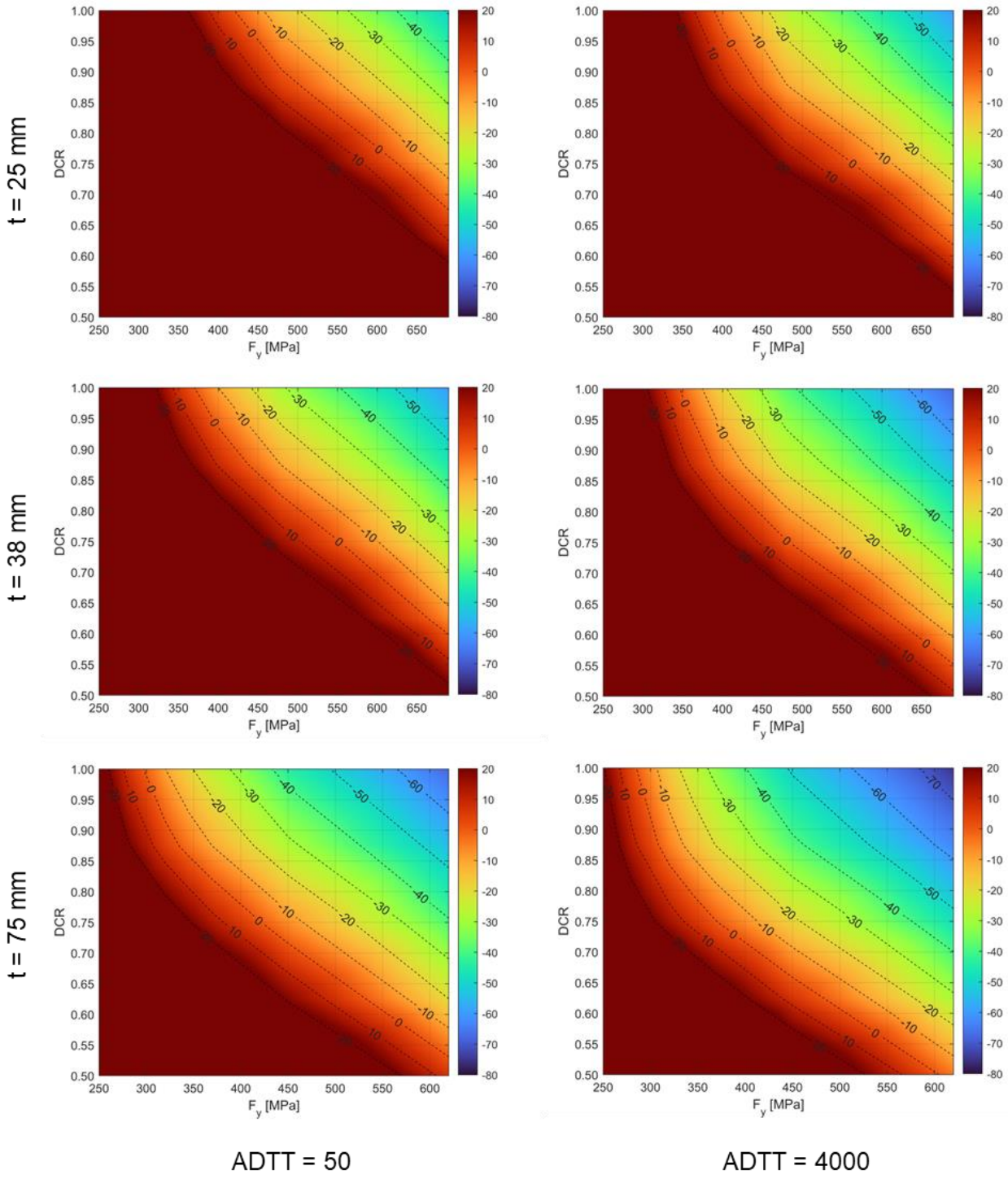


Figure 7-7 T_{27J} Contours for Primary Tension Members in Climate 1

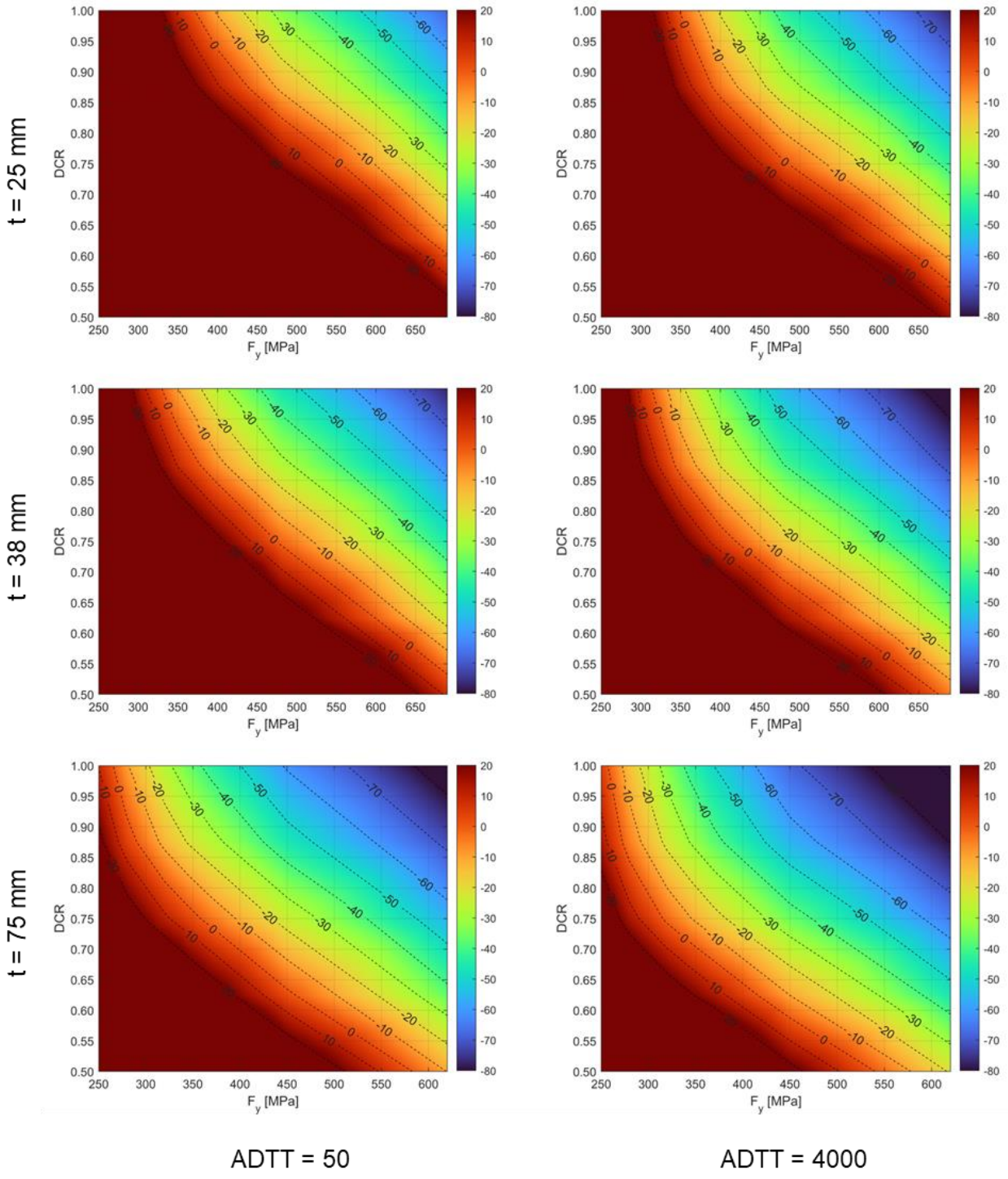


Figure 7-8 T_{27J} Contours for Primary Tension Members in Climate 2

7.3.2 Fracture Critical Members

In order to generate a similar set of contour plots for fracture critical members, a reasonable approach would be to reflect the fracture criticality with a higher target annual reliability index. This is consistent with the risk-based approach used in CSA S6 for assessment of structures, which basically says that as the consequence of failure increases, the probability of failure should decrease (recognizing that a simple definition for risk is failure cost × probability of failure). The design crack, a_d, should arguably be kept the same, to recognize that the defect profile likely does not vary appreciably between primary tension and fracture critical members. While the inspection requirements are slightly more rigorous for fracture critical members, they are generally made using similar welding technologies and welder skill levels.

To demonstrate how this can be done, a target annual reliability index for fracture critical members of β = 3.75 was assumed. This is the appropriate target index in CSA S6 for system behaviour S1 (low system-level redundancy), element level E1 (brittle failure), and inspection level INSP2 (inspection possible).

Based on these assumptions, the suggested T_{27J} requirements for fracture critical members are shown in Figure 7-9 and Figure 7-10 for Climate 1 and 2 respectively. Comparing these contour plots to the previous ones for primary tension members, it can be seen that – as expected – the result of increasing the target annual reliability index is an increase in the severity of the toughness requirement, all else being equal.

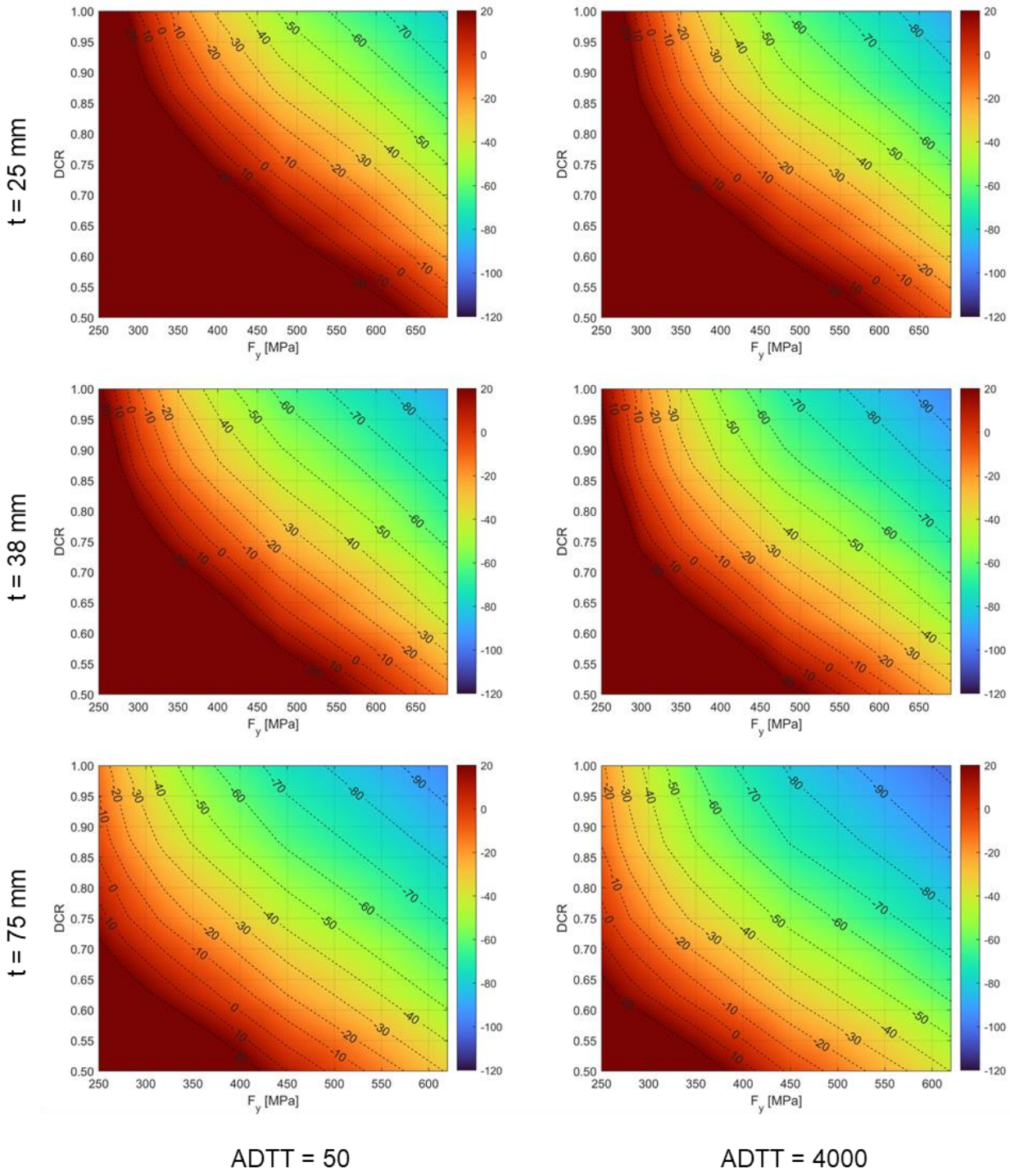


Figure 7-9 T_{27J} Contours for Fracture Critical Members in Climate 1

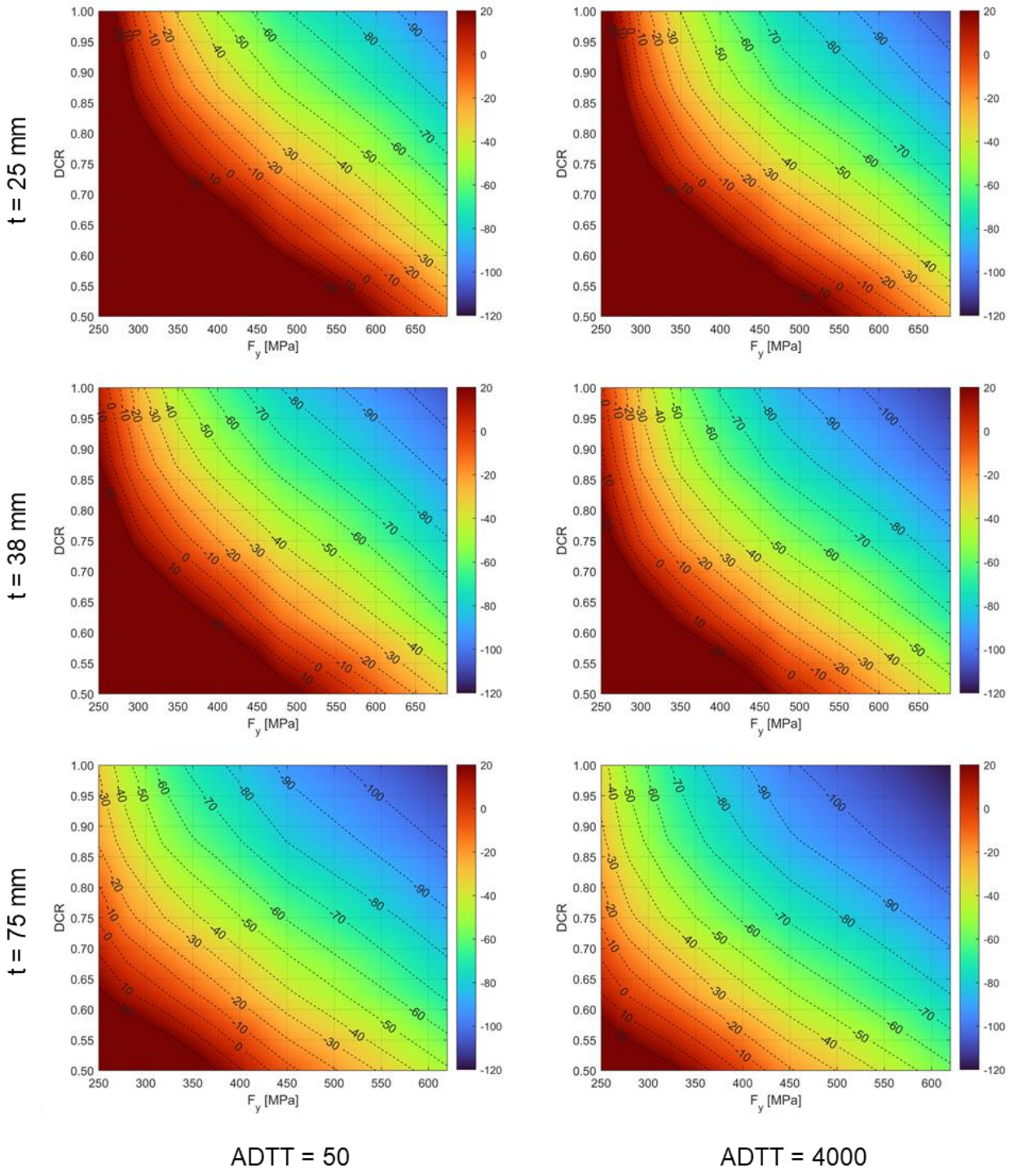


Figure 7-10 T_{27J} Contours for Fracture Critical Members in Climate 2

7.3.3 Consideration of Other Parameters and Situations

The contour plots presented in this chapter are intended to demonstrate the feasibility of the proposed design tool and to show how the toughness requirements vary with respect to the various considered parameters. In order to transform these plots into a "code ready" design tool, it is recommended that further consultation with practitioners take place to verify that the presented toughness requirements are achievable. In future efforts, the presented plots could be modified to consider other factors such as probability of detection of cracks through routine inspection by various means. The implications of structural redundancy could also be considered in a more sophisticated way, which may lead to a reduction in the target annual reliability index and a corresponding increase in the depth of the design crack, a_d. Future efforts could similarly be applied to consider other cases, such as impact damaged elements (where cold work effects might come into play), other structure types such as pedestrian bridges (where loading and strain rate will be different), and even other materials, such as aluminum. These possibilities are elaborated upon further in the next Chapter of this thesis. Lastly, it is noteworthy that – similarly to what was done in the calibration of the Eurocode methods – all of the work in this thesis is based on the assumption of a particularly poor weld detail from the point of view of the associated stress concentration (a welded longitudinal stiffener, e.g., in a loaded girder flange). Future efforts to generate detail-specific contour plots for less severe welded and non-welded connection details may be another potentially fruitful area of future study.

8 Conclusions and Recommendations for Future Work

This thesis project highlights the need for a more nuanced approach to setting CVN test requirements that considers the varying factors influencing reliability for design of steel bridges against brittle fracture. This chapter summarizes the key findings and conclusions from the previous studies and discusses how the project contributes to greater knowledge on brittle fracture for Canadian code writers and practitioners. Lastly, the limitations of this project are recognized, and areas of future work are suggested.

8.1 Conclusions

8.1.1 Ch. 4 – Comparison of Design Provisions for a Typical Bridge

In this chapter, a comparison of the design provisions in the Eurocode, CSA S6, and AASHTO LRFD Part 6 for a typical bridge reveals significant variations in the CVN test temperature requirements across different steel grades and plate thicknesses. The following key points are highlighted:

- Toughness Requirements Consistency: CSA S6 exhibits a uniform toughness requirement across all plate thicknesses, making it more conservative than the Eurocode for thinner plates but less conservative for thicker plates. AASHTO's requirements also vary to some degree with thickness but generally follow a similar trend. The Eurocode's fracture mechanics method shows a similar trend to its simplified method, with the latter being slightly more conservative.
- Impact of Stress Level: The analysis shows that at higher stress levels, the Eurocode becomes more conservative for thicker plates, while CSA and AASHTO remain conservative for thinner plates. This highlights the need for careful consideration of stress levels in bridge design.
- Geographical and Climatic Influence: Climatic conditions significantly influence the toughness requirements. Mild climates, like Vancouver, require lower toughness grades, whereas severe climates, like Fort McMurray, demand higher toughness grades or even different steel strengths when the thickness exceeds permissible limits.
- Practical Implications for Bridge Design: It is generally desired to specify a consistent steel strength and toughness along the entire bridge span for ease of construction, despite varying toughness requirements along the span. The location of maximum stress, such as near bridge piers, often dictates the toughness requirement for the whole structure. However, improved design tools could be used to permit a lower toughness requirement if the stress level is lower, e.g., in an area that has been damaged, or where a crack has been detected and can be monitored through routine inspection.

8.1.2 Ch. 5 –Probabilistic Fracture Mechanics Analysis

The application of the Eurocode fracture mechanics method in a probabilistic framework, implemented using Excel Visual Basic, offers insights on the sensitivity of the probability of failure of a typical bridge to variations in the various input parameters. In general, it was found that:

- The probability of failure generally increases with increasing crack size, a higher applied stress, or harsher climate conditions, which is to be expected.
- Variation in fillet weld size showed minimal impact on the probability of failure, indicating that weld size is a less critical parameter compared to crack size and applied stress.
- The plate thickness variation analysis revealed a local minimum point in the probability of failure versus flange plate thickness curve. Initially, P_f decreases with increasing plate thickness until an optimal point is reached, beyond which P_f increases again due to reduced ductility. The trends were consistent across crack sizes, with larger cracks shifting the optimal thickness point.
- This analysis also underscores the need to consider both ductile and brittle fracture modes, especially when stress levels exceed the steel's nominal yield strength.

From a subsequent effort to cast the problem in a time dependent framework, the following was found:

- PDFs and CDFs for material toughness (K_{mat}) and applied load stress intensity (K^*_{appld}) effectively capture the uncertainties inherent in these parameters. These functions can be used to facilitate the interpolation of values based on hourly fluctuations in temperature and live load.
- A model that simulates hourly temperature and live load fluctuations over the course of a year using historical data and statistical sampling provides a more realistic representation of the environmental conditions and loading a bridge might experience over the course of a year.
- However, this model brings with it associated computational challenges, particularly for smaller crack sizes, which require longer simulation periods to achieve convergence. The interpolation methodology of generating CDFs first, while theoretically promising, proved computationally intensive. The model took approximately 22 hours to run a 10,000-year analysis, indicating that more efficient computational approaches are needed for practical application.

8.1.3 Ch. 6 – Time-Dependent Probabilistic Assessment of Current CSA S6 Design Tables

For this chapter, a major redevelopment of the time-dependent probabilistic MATLAB code was undertaken, which involved discarding the for-loop method for each time step (or in other words the interpolation methodology described in Chapter 5) and instead calculating matrices of K_{mat} and K^*_{appld} values for all time steps. This resulted in significantly reduced analysis times. A comprehensive time-dependent probabilistic assessment was then done of the reliability levels against brittle fracture provided

by the existing CSA S6-19 tables across various steel grades, plate thicknesses, and climatic conditions. The presented analysis methodology offers a rational means for establishing CVN test requirements for design codes, based on a structural reliability analysis similar to those done to establish safety levels for design with respect to other limit states. From this work, the following was found:

- Steel Strength and Reliability: The analysis showed that the current CVN requirements for higher strength steels generally fail to meet the target annual reliability index of β = 3.25, especially in colder climates. Lower strength steels, on the other hand, often exceed this target. This inconsistency suggests that the current CSA S6-19 provisions do not uniformly ensure safety across different steel grades.
- Plate Thickness and Reliability: Reliability indices decrease with increasing plate thickness. This trend is more pronounced when the design crack size (a_d) is assumed to vary with plate thickness. The current CVN test requirements may be insufficient for thicker plates, particularly in colder climates.
- Design Crack Depth: The result of the small design crack depth (a_d = 0.53 mm) is surprising. This crack size generally cannot be detected through visual inspection. This is possibly due to some degree of conservatism in the Eurocode's fracture mechanics model used in this study.

Sensitivity studies on various input parameters indicated that:

- Higher COVs of the *Z17* parameter (δ_2, modelling the scatter in test data correlating T_{100} to the Charpy test temperature) slightly increased the slope of the T_{27J} vs. yield strength curve. It is likely that increasing the COVs for other parameters would have similar effects.
- Different strain rates and *L/D* ratios had minimal impact on the calibrated curves.
- Larger design crack sizes significantly reduced the target annual reliability index (as to be expected), yet the general trends remained consistent (regardless of the value of a_d assumed) regarding the CVN test requirements being conservative for mild steels and unconservative for high strength steels.
- Higher target reliability indices, greater than 3.25, are required for fracture-critical members, as specified in CSA S6-19, and correspond with an increase in the required T_{27J}.
- The calibrated values differ from the current CSA S6-19 requirements, indicating a need for revision to ensure uniform reliability levels. New T_{27J} values would potentially provide increased economy and flexibility for thinner plate structures and increased safety for thicker plate structures.
- Whether these shifts are appropriate or not depend on information that would ideally be established by code-writers, including industry stakeholders and bridge owners, such as: 1) the actual characteristics of the defects present in fabricated structures as well as structures that have been in

service and subjected to cyclic loading for some time, 2) the actual T_{27J} levels achievable in the various steel alloys, and 3) the appropriate target annual reliability index for design against brittle fracture.

- It is believed that the presented analysis never-the-less has value in demonstrating a practical methodology for performing such a calibration, based on accepted principles of brittle fracture and structural reliability analysis. It also makes the important contribution of flagging potential lack of consistency in the safety levels provided by the current requirements.

8.1.4 Ch. 7 – Sensitivity Studies and Design Tool Development

In this chapter, the comparison between time-dependent and time-independent models reveals that while the time-dependent approach is more realistic, the time-independent code with conservative assumptions (i.e. a smaller calibrated design crack size) yields comparable results with significantly reduced computational resources. This suggests that for practical applications and further development of improved design tools, the time-independent method may be more efficient without sacrificing accuracy.

In addition, the following conclusions are drawn from the work presented in this chapter:

- Sensitivity studies conducted on various parameters, including climate, bridge span, traffic volume, and consideration of multiple vehicle presence, highlight the robustness of the proposed methodology. While certain factors exhibit minimal impact on the CVN test requirements, others, such as traffic volume and consideration of multiple vehicle presence, significantly influence the results.
- The information from the previous studies can be tied together to perform analyses with the goal of creating useful design tools for specifying CVN test requirements for design.
- These design tools may be useful in helping designers answer questions of whether rigorous toughness requirements are really needed, e.g., for a low volume road, thin plates, or bridges with lower demand-to-capacity ratios. Such design tools also provide options for designers to explore different design solutions (e.g., achieving design requirements by reducing the demand-to-capacity ratio by increasing plate thickness, rather than paying for an expensive or hard-to-find high toughness steel).
- Overall, this work can contribute to advancing design standards to prevent brittle fractures, thereby improving the overall safety and economy of steel highway bridge structures.

8.2 Recommendations for Future Work

In this section, limitations of the current project and areas of further research are identified, ensuring the continuous advancement and refinement of knowledge in the area of brittle fracture. The development of

user-friendly design tools, such as contour plots for determining CVN test requirements, should be continued and expanded to cover a wider range of design scenarios and structural elements. By addressing these recommendations, future research can build upon the findings of this study, leading to improved steel bridge design standards, enhanced structural reliability, and more efficient maintenance practices.

8.2.1 European Code Verification

Expanding the study to include diverse geographic locations with varying climatic conditions can provide a more comprehensive understanding of the global applicability of design provisions. Climate data from different countries and traffic information (which would require working with various European transportation ministries) could be used to verify the Eurocode, as a probabilistic assessment of these requirements has not yet been done. Applying the methods presented in this thesis to European climate and traffic data will help assess and validate the reliability levels provided in EN 1993-1-10.

8.2.2 Rapid Assessment Tools for Bridge Inspection

The current work mainly focuses on the design of new bridges, but it would be advantageous to develop rapid assessment tools for evaluating existing bridge structures, which can significantly improve routine bridge inspections. Despite bridges being designed for toughness at the beginning of their service life, routine inspections are essential to assess damage, locate fatigue cracks, and address other potential issues that may impact safety. Rapid assessment tools allow engineers to quickly determine whether a defect is critical and make informed decisions about closing bridges to traffic until repairs are completed. Future work should focus on creating and validating new contour plots or tables for various bridge types and conditions, ensuring their practical applicability during field inspections.

8.2.3 Plastically Deformed Structures

Further studies may involve varying the degree of cold forming to investigate the effect of this parameter on required toughness. This may especially be useful for developing tools for existing bridges that have experienced vehicle impact damage where the steel has plastically deformed (even of the original steel in construction was not cold formed). Transforming the level of impact damage to an equivalent degree of cold forming is an area where further literature review and study will be needed.

8.2.4 Pedestrian Bridges

Sensitivity studies involving variations in strain rates should be conducted to simulate lower loading rates specific to pedestrian bridges. The recently developed tables for the CSA S7 Pedestrian, Cycling, and Multiuse Bridge Design Guideline (Canadian Standards Association, 2023) would benefit from verification using the probabilistic model from this thesis to ensure internal consistency and adequate safety levels.

Future research should validate and refine these tables to enhance the safety and economy of pedestrian bridge designs.

8.2.5 Aluminum Structures

The current CSA S6 Section 17 offers limited guidance for designing aluminum structures against brittle fracture. It is stated that fracture critical members need to be identified and should be considered in the material selection and design, but no further information is given, leaving the rest to engineering judgement and experience. To address this gap, future work should apply the developed model to simulate aluminum material properties and identify maximum tolerable defect sizes. This research can provide recommendations for preventing brittle fracture in aluminum structures and confirm whether brittle fracture (e.g., in the presence of a large crack) is a significant concern for this material or not.

8.2.6 Design Crack Depth Definition

Further efforts by researchers and industry stakeholders (fabricators, bridge owners) are recommended to establish rational values for the design crack depth, a_d, as the calibrated design crack depths were 0.53 and 0.13 mm for the time-dependent and time-independent models, respectively. As previously mentioned, a crack this small would not be detectable through visual methods. In practice, a_d is affected by quality control procedures, which are independent of steel strength and loading, and fatigue damage, which is dependent on loading. Further work in this area would include gathering data on fabrication defects and probability of crack detection, along with more work on fracture mechanics-based fatigue modelling.

8.2.7 Effects of Routine Inspection

Incorporating routine inspection protocols into fracture-critical member design criteria can enhance safety and reliability, warranting further research into the optimal inspection intervals. Economically, incorporating life-cycle cost analysis on the maintenance requirements and how this affects the probability of failure could assist in making informed and cost-effective design decisions.

8.2.8 Continued Refinement

Consideration for HAZ-specific toughness requirements could be developed to address gaps in the current code. Ongoing research and refinement of these approaches are essential for keeping up with urbanization, climate change, the evolving traffic patterns. Future work should incorporate more recent traffic data than 2012, which would provide a more accurate basis for establishing the live load statistical parameters. This may include diverse traffic data from different provinces (e.g. Ontario, BC, Alberta), which may use different code trucks (e.g. CL-800 in Alberta). This would be useful in refining the analysis and improve the generalizability of the findings and applicability of the results across Canada or may lead to province-specific design requirements. Considering the effects of emerging traffic patterns, such as truck platooning

and fluctuating daily traffic volumes, on the stress intensity factors could lead to more robust and realistic reliability assessments. Additionally, the new design tools should be updated using future climate data, as temperature trends are expected to change. These approaches will provide a more accurate basis for establishing live load statistical parameters and enhance the resilience of our bridges.

References

AASHTO. (2017). AASHTO LRFD Bridge Design Specifications. Washington D.C.

AASHTO. (2020). AASHTO LRFD Bridge Design Specifications.

Agarwal, A., Au, A., Becker, D., Foschi, R., Gagnon, D., Hong, H., . . . Nowak, A. (2007). Calibration Report for CAN/CSA-S6-06 Canadian Highway Bridge Design Code.

Altstadt, S., Wright, W., & Connor, R. (2014). Proposed Revisions to the Current Charpy V-Notch Requirements for Structural Steel Used in U.S. Bridges. *Journal of Bridge Engineering, 19*(1), 131-140.

American Welding Society. (2000). AWS D1.1: Structural Welding Code - Steel.

Ang, A. H.-S., & Tang, W. H. (2006). *Probability Concepts in Engineering: Emphasis on Applications to Civil and Environmental Engineering, 2nd Edition.* Wiley.

Artmont, F. A., & Murphy, T. P. (2018). Influence of Material Toughness on Fracture Reliability in Steel Bridges. *Transportation Research Record*.

Artmont, F. A., Murphy, T. P., Sause, R., Bocchini, P., & Mertz, D. (2018). *Influence of Material Toughness on Fracture Reliability in Steel Bridges.* U.S. Department of Transportation Federal Highway Administration (FHWA).

ASTM International. (2013). E23 - 12c. *Standard Test Methods for Notched Bar Impact Testing of Metallic Materials*. West Conshohocken, PA.

ASTM International. (2020). E1820 - 20a. *Standard Test Method for Measurement of Fracture Toughness*. West Conshohocken, PA.

ASTM International. (2020). E399 − 20. *Standard Test Method for Linear-Elastic Plane-Strain Fracture Toughness of Metallic Materials*. West Conshohocken, PA.

Bailey, S. (1996). Basic principles and load models for the structural safety evaluation of existing road bridges. Doctoral thesis. École Polytechnique Fédérale de Lausanne, Lausanne, Switzerland.

Barsom, J. M. (1975). Development of the AASHTO Fracture-Toughness Requirements for Bridge Steels. *Engineering Fracture Mechanics, 7*, 605-618.

Barsom, J. M., & Rolfe, S. T. (1970). Correlations Between KIc and Charpy V-Notch Test Results in the Transition-Temperature Range. *Impact Testing of Metals, ASTM STP 466*, 281-302. American Society of Testing Materials.

Campbell, L. E., Snyder, L. R., Whitehead, J. M., Connor, R. J., & Lloyd, J. B. (2019). *Probability of Detection Study for Visual Inspection of Steel Bridges: Volume 2—Full Project Report (Joint Transportation Research Program Publication No. FHWA/IN/JTRP-2019/22).* Purdue University, West Lafayette, IN. Retrieved from https://doi.org/10.5703/1288284317104

Canadian Institute of Steel Construction. (2002). *Straight Plate Girder Bridge Design Example 1.*

Canadian Institute of Steel Construction. (2021). Handbook of Steel Construction – 12th Edition.

Canadian Standards Association. (2018, May). Welded steel construction. W59-18.

Canadian Standards Association. (2019). Canadian highway bridge design code. CAN/CSA-S6-19.

Canadian Standards Association. (2019). Commentary on CSA S6-19, Canadian Highway Bridge Design Code. CSA-S6.1-19.

Canadian Standards Association. (2019). CSA S16-19. *Design of Steel Structures*. Standards Council of Canada.

Canadian Standards Association. (2023). Pedestrian, Cycling, and Multiuse Bridge Design Guideline. CSA - S7-23.

Chehrazi, A., Chien, M. Y., & Walbridge, S. (2022). A review of the fatigue limit for steel bridges under Ontario highway traffic loading. *Canadian Journal of Civil Engineering, 49*(12), 1796–1806.

Chien, M. Y., Chehrazi, A., Tolou Kian, M. J., & Walbridge, S. (2024). Effects of climate, traffic, and bridge configuration on brittle fracture risk in highway bridges. *CSCE Annual Meeting.* Niagara Falls.

Chien, M. Y., Tolou Kian, M. J., & Walbridge, S. (2022). Time-Dependent Probabilistic Analysis on Steel Bridge Brittle Fracture. *Proceedings of the Canadian Society of Civil Engineering Annual Conference 2022.* Springer.

Chien, M. Y., Tolou Kian, M. J., Chehrazi, A., & Walbridge, S. (2024). A Time-Dependant Reliability-Based Methodology for Assessing Fracture Toughness Requirements for Highway Bridges. *Journal of Bridge Engineering*.

Chien, M. Y., Walbridge, S., & Kühn, B. (2021). Comparison of International Brittle Fracture Design Code Provisions for Steel Bridges. *Transportation Research Record*, 676–687.

Chien, M. Y., Walbridge, S., & Kühn, B. (2021). Probabilistic Analysis of Brittle Fracture Design Code Provisions for Steel Bridges. *CSCE 2021 Annual Conference.* Virtual: Springer Nature.

Chow, D., & Levermore, G. J. (2007). New algorithm for generating hourly temperature values using daily maximum, minimum and average values from climate models. *Building Services Engineering Research and Technology, 28*(3), 237–248.

Collins, W., Sherman, R., Leon, R., & Connor, R. (2016). State-of-the-Art Fracture Characterization. II: Correlations between Charpy V-Notch and the Master Curve Reference Temperature. *Journal of Bridge Engineering, 21*(12).

Committee on Fatigue and Fracture Reliability of the Committee on Structural Safety and Reliability of the Structural Division, American Society of Civil Engineers. (1982). Fatigue Reliability: Introduction. *Journal of the Structural Division, 108*(1).

Connor, R. J., Dexter, R., & Mahmoud, H. (2005). Inspection and Management of Bridges with Fracture-Critical Details. *NCHRP Synthesis 354*.

Connor, R. J., Kaufmann, E. J., Fisher, J. W., & Wright, W. J. (2007, March/April). Prevention and Mitigation Strategies to Address Recent Brittle Fractures in Steel Bridges. *Journal of Bridge Engineering*, 164-173.

Environment Canada. (2022). *Historical Data*. Retrieved from Government of Canada: https://climate.weather.gc.ca/historical_data/search_historic_data_e.html

European Commission. (2006). Eurocode 3: Design of steel structures. EN 1993.

European Standard. (2004, December). EN 10163-3 Delivery requirements for surface condition of hot-rolled steel plates, wide flats and sections - Part 3: Sections. CEN.

Fan, M. Y., Walbridge, S., & Kühn, B. (2020). Comparison of Canadian and European Brittle Fracture Design Code Provisions for Steel Bridges. *Canadian Society for Civil Engineering.* Saskatoon.

Fan, M. Y., Walbridge, S., & Kühn, B. (2021). Comparison of International Brittle Fracture Design Code Provisions for Steel Bridges. *Transportation Research Board Annual Meeting.* Virtual.

Federal Highway Administration. (2019, September). Bridge Welding Reference Manual. U.S. Department of Transportation.

Feldmann, M., Eichler, B., Kühn, B., Stranghöner, N., Dahl, W., Langenberg, P., . . . Packer, J. (2012). *Choice of Steel Material to Avoid Brittle Fracture for Hollow Section Structures: Background documents in support to the implementation, harmonization and further development of the Eurocodes.* Joint Research Centre (JRC).

Ghosn, M., Moses, F., & Wang, J. (2003). *Design of Highway Bridges for Extreme Events. NCHRP Report 489.* Washington D.C.: Transportation Research Board.

Gordon, J. R. (1993). A Review of Fracture Assessment Procedures and Their Applicability to Welded Structures. *Canadian Metallurgical Quarterly, 32*, 195-203.

Graybeal, B., Walther, R., & Washer, G. (2000, November). Ultrasonic Inspection of Bridge Hanger Pins. *Transportation Research Record, 1697*, 19-23. doi:10.3141/1697-04

Harrison, R. L. (2010). Introduction To Monte Carlo Simulation. *AIP Conference Proceedings* (pp. 17-21). American Institute of Physics.

Hopwood, T., & Deen, R. C. (1984). *Periodic Nondestructive Evaluation of In-Service Metal Bridges.* Lexington, Kentucky: University of Kentucky.

Jarosz, J., & Sorgenfrei, D. (2005). Deterioration of Pin-Connected Bridge Trusses. *American Railway Engineering and Maintenance-of-Way Association (AREMA) 2005 Annual Conference.* Chicago, IL.

Joint Committee on Structural Safety. (2008). *Risk Assessment in Engineering: Principles, System Representation & Risk Criteria.*

Kala, Z., Melcher, J., & Puklický, L. (2009). Material and Geometrical Characteristics of Structural Steels Based on Statistical Analysis of Metallurgical Products. *Journal of Civil Engineering and Management, 15*(3), 299–307.

Kennedy, D., & Baker, K. (1984). Resistance factors for steel highway bridges. *Canadian Journal of Civil Engineering, 11*, 324-334.

Kennedy, D., & Gad Aly, M. (1980). Limit states design of steel structures - performance factors. *Canadian Journal of Civil Engineering, 7*, 45-77.

Kline, E. S. (2008, May). Steel Bridges: Corrosion Protection for 100 Years. *Journal of Protective Coatings & Linings*, 20-24,27-28,31.

Kühn, B. (2005). Beitrag zur Vereinheitlichung der europäischen Regelungen zur Vermeidung von Sprödbruch (Contribution to the standardization of the European regulations to avoid brittle fracture), PhD Dissertation. TU Aachen, Germany.

Langford, W. J. (1980). Selection and Interpretation of Fracture Test Methods for Fracture Control. *Canadian Metallurgical Quarterly, 19*, 13-22.

Lassen, T. (1991). Markov modelling of the fatigue damage in welded structures under in-service inspection. *International Journal of Fatigue, 13*(5), 417-422.

Linvill, D. E. (1990, January). Calculating Chilling Hours and Chill Units from Daily Maximum and Minimum Temperature Observations. *HortScience, 25*(1), 14-16.

MacGregor, J. G. (1976). Safety and limit states design for reinforced concrete. *Canadian Journal of Civil Engineering, 3*(4), 484-513.

Naess, A., & Røyset, J. Ø. (2000). Extensions of Turkstra's rule and their application to combination of dependent load effects. *Structural Safety*, 129-143.

National Academies of Sciences, Engineering, and Medicine. (2023). *Toughness Requirements for Heat-Affected Zones of Welded Structural Steels for Highway Bridges.* Washington DC: The National Academies Press. doi:https://doi.org/10.17226/27250

NDT Education Resource Center. (2020). *Impact Toughness*. Retrieved from NDT Education Resource Center: https://www.nde-ed.org/EducationResources/CommunityCollege/Materials/Mechanical/ImpactToughness.htm

North Dakota Department of Transportation Bridge Division. (2000, June). Bridge Inspector's Guide for Fracture Critical Bridges and Bridges with Special Features. Bismarck, North Dakota.

Nowak, A. (1999). *Calibration of LRFD Bridge Design Code. NCHRP Report 386.* Washington, D.C.: National Academy Press.

Nowak, A., & Lind, N. (1979). Practical bridge code calibration. *Journal of the structural division, 105*(12), 2497-2510.

Nussbaumer, A., Borges, L., & Davaine, L. (2011). *Fatigue Design of Steel and Composite Structures.* ECCS – European Convention for Constructional Steelwork.

Pandey, M., & Jyrkama, M. (2019). Course Notes: CIVE 601 Engineering Risk and Reliability. Department of Civil and Environmental Engineering, University of Waterloo.

Rahbarimanesh, S., & Tousignant, K. (2024). Monte Carlo simulation study on the reliability of concrete-filled HSS beam-column design provisions. *Canadian Journal of Civil Engineering*. doi:https://doi.org/10.1139/cjce-2023-0199

Schmidt, B., & Bartlett, F. (2002). Review of resistance factor for steel: data collection. *Canadian Journal of Civil Engineering, 29*, 98-108.

Sedlacek, G., Feldmann, M., Kühn, B., Tschickardt, D., Höhler, S., Müller, C., . . . Bijlaard, F. (2008). *EUR 23510 EN: Commentary and Worked Examples to EN 1993-1-10 "Material toughness and through thickness properties" and other toughness oriented rules in EN 1993.* European Commission Joint Research Centre. Luxembourg: European Communities.

Sjaarda, M., West, J. S., & Walbridge, S. (2021). Reliability analysis of welded stud shear connectors on simply-supported bridge girders. *Canadian Journal of Civil Engineering, 48*(6), 604-615.

Soriano, M., Casas, J. R., & Ghosn, M. (2017). Simplified probabilistic model for maximum traffic load from weigh-in-motion data. *Structure and Infrastructure Engineering*, 454-467.

Sun, D., Wang, X., & Sun, B. (2014). A Methodology for Multihazards Load Combinations of Earthquake and Heavy Trucks for Bridges. *The Scientific World Journal*.

Viehrig, H.-W., Zurbuchen, C., Schindler, H.-J., & Kalkhof, D. (2010). *Application of the Master Curve Approach to Fracture Mechanics Characterisation of Reactor Pressure Vessel Steel.* Wissenschaftlich-Technische Berichte.

Vojdani, A., Farrahia, G., Mehmanparast, A., & Wang, B. (2018). Probabilistic assessment of creep-fatigue crack propagation in austenitic stainless steel cracked plates. *Engineering Fracture Mechanics, 200*, 50–63.

Walbridge, S. (2005). A Probabilistic Study of Fatigue in Post-Weld Treated Tubular Bridge Structures. Lausanne: EPFL.

Walbridge, S., & Nussbaumer, A. (2007). A probabilistic model for determining the effect of post-weld treatment on the fatigue performance of tubular bridge joints. *International Journal of Fatigue, 29*(3), 516-532.

Wallin, K. (1992). Guidelines for Deriving Fracture Toughness Estimates from Normal and Miniature Size Charpy-V Specimen Data. *Rakenteiden Mekaniikka (Journal of Structural Mechanics), 25*, 24-40.

Wallin, K. (1998). *Master curve analysis of ductile to brittle transition region fracture toughness round robin data: The "EURO" fracture toughness curve.* Technical Research Centre of Finland (VTT).

Wallin, K. (2002). Master curve analysis of the "Euro" fracture toughness dataset. *Engineering Fracture Mechanics, 69*(4), 451-481.

Wright, W. (2002). Fracture toughness requirements for highway bridges: Past and future trends. *Progress in Structural Engineering and Materials, 4*(1), 96-104.

Wright, W. J. (2002). Fracture toughness requirements for highway bridges: Past and future trends. *Progress in Structural Engineering and Materials*, 4(1), 96-104.

Zamiri, F., Al-Emrani, M., & Kliger, R. (2018). *Advanced Assessment of Welded Bridges for Fatigue and Brittle Fracture: Final Report - Trafikverket project number 2014-007.* Chalmers University of Technology, Department of Architecture and Civil Engineering, Gothenburg, Sweden.

Zhao, Z., Haldar, A., & & Breen Jr, F. L. (1994). Fatigue-reliability evaluation of steel bridges. *Journal of structural engineering*, *120*(5), 1608-1623.

Appendix A – Time-Dependent MATLAB Code

This code is included to enable verification / reproducibility of the presented research. The code is based on an analytical approach developed by the author with direction from their thesis supervisor. The MATLAB coding itself would not have been possible without significant help from Dr. Chehrazi and Dr. Tolou Kian, who are gratefully acknowledged.

Call.m

```
clc;
clear;

% Inputs

p=1;
tempfile='2003_2021_Graphs.csv'; %the hourly temperature data
cracktype = 'Semi-elliptical Surface Crack'; %crack type
weldtoetype ='Type 2';  %weld type
ntrials=1000000;
t_cover = 25;%'cover plate thickness


%%%%%% Live load bias factor parameters from traffic simulation/GVW histogram%%%%%
%%% ONT-2012 database for hourly simulation
Alpha=14.53976566;
U=1.101351913;

%%%%%% Load Combination: DF*Dead stress+LF*Live stress*DAF = FF*fy %%%%%
DF=1.1;
LF=1.7;
FF=0.9;
RLD=1;  %Ratio of Live load to dead load
DAF=1.25;

DCR=1; %demand to capacity ratio


%%%%%% paramteric study %%%%%
Np=2;          %how many parameters to change simultaneously(0: one analysis; 1: one
vector; 2:one table)
FirstP="fy";  %the first parameter you want to vary
RangeFirstP=[260,300,350,400,480,250,345,485,690] %the range of the first parameter,
e.g, [20,30,60,70] or [10:10:100]

SecondP="T27J";  %the second parameter you want to vary
RangeSecondP=[-50,-40,-30,-20,-10,0,10,20]%; %the range of the second parameter, e.g,
[20,30,60,70] or [10:10:100]
%%%%%%%%%%%

Variables=["fy","lognormal";
                "t","lognormal";
```

```
                "B","deterministic";
                "Tmd","nan";
                "DTr","deterministic";
                "DTsigma","deterministic";
                "DTR","deterministic";
                "DTep","deterministic";
                "DTecf","deterministic";
                "T27J","deterministic";
                "a","deterministic";
                "SigmaDLbc","lognormal";
                "SigmaDLac","nan";
                "SigmaLL","nan";
                "H","lognormal";
                "W","lognormal";
                "delta 1","normal";
                "delta 2","normal";
                "sigma_s","lognormal";
                "sigma_Ed","lognormal";
                "ac ratio","lognormal";
                "Mk","lognormal";
                "SCF","lognormal";
                "DAF","normal"];

Data=[  350     1.101     0.0915 nan
        38      1.02      0.0120 nan
        375     nan     nan     nan
        nan     nan     nan     nan
        -5      nan     nan     nan
        0       nan     nan     nan
        0       nan     nan     nan
        0       nan     nan     nan
        0       nan     nan     nan
        0       nan     nan     nan
        0.00053  nan     nan     nan   %DETERMINISTIC crack
        nan     1.03      0.0800 nan
        nan     nan     nan     nan
        nan     nan     nan     nan
        10      1       0.1600   nan
        10      1       0.1600   nan
        1       1       0.2500   nan
        0       1       nan     34.2
        100     1       0.25     nan
        1       0.93      0.12   nan
        0.4     1       0.32     nan
        1       1       0.05     nan
        1       1       0.04     nan
        1        1.15    0.104    nan]; % please dont change the values for DLA (the
last row).


%%%%%%%%%%processing of input parameters%%%%%%%%%%%%%%%%
csvfile = dir(tempfile); %obtain csv file with hourly climate data
file = csvfile;
Recorded_Temps=xlsread(file.name,'2003_2021_Graphs','C3:U8762');
```

```
for j=1:2021-2003+1 %filling in void spaces in the temperature data
    for i=1:8762-3+1 %for every hour
        if isnan(Recorded_Temps(i,j))==true %test if the cell is empty
            Recorded_Temps(i,j)=Recorded_Temps(i-1,j); %if empty, fill the cell with
first available temperature on the list
        end
    end
end
EData=zeros(length(Data),2);
Data(12,1)=DCR*FF*Data(1,1)/(DF+LF*RLD*DAF);
LL=Data(12,1)*RLD;
Liveload=[LL,Alpha,U];

for i=1:length(Data)
    if Variables(i,2)=="normal"
        EData(i,1)=Data(i,1)*Data(i,2);
        EData(i,2)=EData(i,1)*Data(i,3);
        if Variables(i,1)=="delta 2"
            EData(i,1)=Data(i,1);
            EData(i,2)=Data(i,4);
        end
    elseif Variables(i,2)=="lognormal"
        AVE=Data(i,1)*Data(i,2);
        STD=Data(i,1)*Data(i,2)*Data(i,3);
        EData(i,2)=sqrt(log(1+STD^2/AVE^2));
        EData(i,1)=log(AVE)-0.5*EData(i,2)^2;
    elseif Variables(i,2)=="deterministic"
        EData(i,1)=Data(i,1);
    elseif Variables(i,2)=="nan"
        Check=1;
    else
        disp ("Please check the spelling of variables distribution in Variables 2
matrix");
    end
end

if Np==0
    disp ("analysis started");
    PP=TDA(Recorded_Temps,cracktype,weldtoetype,EData,Liveload,ntrials,t_cover);
    p=PP(1)
    p2=PP(2)
elseif Np==1
    disp ("analysis started");
    p=5*ones(1, length(RangeFirstP));
    for i=1:length(RangeFirstP)
        if FirstP=="fy"
            NN=RangeFirstP(i);
            Data(12,1)=DCR*FF*NN/(DF+LF*RLD*DAF);
            EData=inputupdate(EData,Data,Variables,"SigmaDLbc",Data(12,1));
            LL=Data(12,1)*RLD;
            Liveload=[LL,Alpha,U];
        end
        EData=inputupdate(EData,Data,Variables,FirstP,RangeFirstP(i));
        PP=TDA(Recorded_Temps,cracktype,weldtoetype,EData,Liveload,ntrials,t_cover);
        p(i)=PP(1);
```

```
        p2(i)=PP(2);
        disp   (string(i)+"   out   of   "+string(length(RangeFirstP))+"   analyses   is
performed.");
    end
    FirstM=["This    paramteric    study    varied    variable    "+FirstP+"    using
"+string(ntrials)+" trials or years. The restuls of Probability of failure (pf),
relibaility    index    (beta),    and    the    required    ntrials    are    as
follows:","","","","","","","","","","","","","","","","","","","","","","","","","",
"","","","","","","","","","","","","","","","","","","","","","","","","","","","","
","","","","","","","","","",""];

    beta=-norminv(p,0,1);
    reqntrials=floor(100.0./p);
    beta2=-norminv(p2,0,1);
    reqntrials2=floor(100.0./p2);


report=[FirstM(1:length(RangeFirstP)+1);FirstM(2:length(RangeFirstP)+2);FirstM(2:leng
th(RangeFirstP)+2);
        [FirstP,string(RangeFirstP)];["pf-
brittle",string(p)];FirstM(2:length(RangeFirstP)+2);

[FirstP,string(RangeFirstP)];["beta",string(beta)];FirstM(2:length(RangeFirstP)+2);
        [FirstP,string(RangeFirstP)];["required trials",string(reqntrials)];
        [FirstP,string(RangeFirstP)];["pf-
ductile",string(p2)];FirstM(2:length(RangeFirstP)+2);
        [FirstP,string(RangeFirstP)];["beta-
ductile",string(beta2)];FirstM(2:length(RangeFirstP)+2);
        [FirstP,string(RangeFirstP)];["required trials-ductile",string(reqntrials2)]];

    writematrix(report,'M_tab.csv','Delimiter','comma')

elseif Np==2
    disp ("analysis started");
    p=5*ones(length(RangeSecondP),length(RangeFirstP));
    for i=1:length(RangeFirstP)
        for j=1:length(RangeSecondP)
            if FirstP=="fy"
                NN=RangeFirstP(i);
                Data(12,1)=DCR*FF*NN/(DF+LF*RLD*DAF);
                EData=inputupdate(EData,Data,Variables,"SigmaDLbc",Data(12,1));
                LL=Data(12,1)*RLD;
                Liveload=[LL,Alpha,U];
            elseif SecondP=="fy"
                NN=RangeSecondP(j);
                Data(12,1)=DCR*FF*NN/(DF+LF*RLD*DAF);
                EData=inputupdate(EData,Data,Variables,"SigmaDLbc",Data(12,1));
                LL=Data(12,1)*RLD;
                Liveload=[LL,Alpha,U];
            end
            EData=inputupdate(EData,Data,Variables,FirstP,RangeFirstP(i));
            EData=inputupdate(EData,Data,Variables,SecondP,RangeSecondP(j));

PP=TDA(Recorded_Temps,cracktype,weldtoetype,EData,Liveload,ntrials,t_cover);
            p(j,i)=PP(1);
```

```
            p2(j,i)=PP(2);
            disp        (string((i-1)*length(RangeSecondP)+j)+"        out        of
"+string(length(RangeFirstP)*length(RangeSecondP))+" analyses is performed.");
        end
    end
    FirstM=["This paramteric study varied variables "+FirstP+"and "+SecondP+" using
"+string(ntrials)+" trials or years. The restuls of Probability of failure (pf),
relibaility    index    (beta),    and    the    required    ntrials    are    as
follows:","","","","","","","","","","","","","","","","","","","","","","","","","",
"","","","","","","","","","","","","","","","","","","","","","","","","","","","","
","","","","","","","","",""];

    beta=-norminv(p,0,1);
    reqntrials=floor(100.0./p);
    beta2=-norminv(p2,0,1);
    reqntrials2=floor(100.0./p2);

    report=[FirstM(1:length(RangeFirstP)+2);
            FirstM(2:length(RangeFirstP)+3);
            FirstM(2:length(RangeFirstP)+3);
            ["","",FirstP,FirstM(2:length(RangeFirstP))];
            ["","pf-brittle",string(RangeFirstP)];
            [[SecondP,FirstM(3:length(RangeSecondP)+1)]',[string(RangeSecondP')
string(p)]];
            FirstM(2:length(RangeFirstP)+3);
            FirstM(2:length(RangeFirstP)+3);
            ["","",FirstP,FirstM(2:length(RangeFirstP))];
            ["","beta",string(RangeFirstP)];
            [[SecondP,FirstM(3:length(RangeSecondP)+1)]',[string(RangeSecondP')
string(beta)]];
            FirstM(2:length(RangeFirstP)+3);
            FirstM(2:length(RangeFirstP)+3);
            ["","",FirstP,FirstM(2:length(RangeFirstP))];
            ["","required trials",string(RangeFirstP)];
            [[SecondP,FirstM(3:length(RangeSecondP)+1)]',[string(RangeSecondP')
string(reqntrials)]];
            FirstM(2:length(RangeFirstP)+3);
            FirstM(2:length(RangeFirstP)+3);
            ["","",FirstP,FirstM(2:length(RangeFirstP))];
            ["","pf-ductile",string(RangeFirstP)];
            [[SecondP,FirstM(3:length(RangeSecondP)+1)]',[string(RangeSecondP')
string(p2)]];
            FirstM(2:length(RangeFirstP)+3);
            FirstM(2:length(RangeFirstP)+3);
            ["","",FirstP,FirstM(2:length(RangeFirstP))];
            ["","beta-ductile",string(RangeFirstP)];
            [[SecondP,FirstM(3:length(RangeSecondP)+1)]',[string(RangeSecondP')
string(beta2)]];
            FirstM(2:length(RangeFirstP)+3);
            FirstM(2:length(RangeFirstP)+3);
            ["","",FirstP,FirstM(2:length(RangeFirstP))];
            ["","required trials-ductile",string(RangeFirstP)];
            [[SecondP,FirstM(3:length(RangeSecondP)+1)]',[string(RangeSecondP')
string(reqntrials2)]]];
    writematrix(report,'M_tab.csv','Delimiter','comma')
```

```
end
p
p2
```

inputupdate.m

```
function E=inputupdate(EData,Data,variables,variable,nominal)
    jj=0;
    for i=1:length(variables)
        if variable==variables(i)
            jj=i;
            break
        end
    end

    Data(jj,1)=nominal;
    i=jj;
    if variables(i,2)=="normal"
        EData(i,1)=Data(i,1)*Data(i,2);
        EData(i,2)=EData(i,1)*Data(i,3);
        if variables(i,1)=="delta 2"
            EData(i,1)=Data(i,1);
            EData(i,2)=Data(i,4);
        end
    elseif variables(i,2)=="lognormal"
        AVE=Data(i,1)*Data(i,2);
        STD=Data(i,1)*Data(i,2)*Data(i,3);
        EData(i,2)=sqrt(log(1+STD^2/AVE^2));
        EData(i,1)=log(AVE)-0.5*EData(i,2)^2;
    elseif variables(i,2)=="deterministic"
        EData(i,1)=Data(i,1);
    end
    E=EData;
end
```

TDA.m

```
function f=TDA(Recorded_Temps,cracktype,weldtoetype,Data,Liveload,ntrials,t_cover)


    %%%%%%%%%%Temperature Reading from CSV file%%%%%%%%%%%%%%%%%%%%%%%%%%%%%%%%%%%%

    %the following for-loop determine the maximum and minimum temps in days of
    %the recorded database

    for j=1:2021-2003+1
        for i=1:365
            Daily_Max_Temps(i,j)=max(Recorded_Temps((i-1)*24+1:i*24,j));%find     max
temps within each 24 hour period
            Daily_Min_Temps(i,j)=min(Recorded_Temps((i-1)*24+1:i*24,j));%find     min
temps within each 24 hour period
        end
    end
    Daily_Max_Temps=[Daily_Max_Temps(365,:);Daily_Max_Temps;Daily_Max_Temps(1,:)];
    Daily_Min_Temps=[Daily_Min_Temps(365,:);Daily_Min_Temps;Daily_Min_Temps(1,:)];

    Daily_Range_Temps=Daily_Max_Temps-Daily_Min_Temps;

    Daily_min_Temps_Mean=mean(Daily_Min_Temps')'; %Mean of daily min temperature
    Daily_min_Temps_Std=std(Daily_Min_Temps')';%Std of daily min temperature

    Daily_Range_Mean=mean(Daily_Range_Temps')'; %mean of daily range
    Daily_Range_Std=std(Daily_Range_Temps')';%stdev of daily range


    %writing data to Zbars and Stds%%%%%%%%%%%%%%%%%%%%%%%%%%%%

    z1bar = Data(1,1);%ActiveSheet.Range("G2")  fy - lognormal
    z2bar = Data(2,1);%ActiveSheet.Range("G3")  t-lognormal
    z3bar = Data(3,1);%ActiveSheet.Range("G4")  B-lognormal

    z5bar = Data(5,1);%ActiveSheet.Range("D6")  deltaTr-Deterministic -5
    z6bar = Data(6,1);%ActiveSheet.Range("D7")  deltaT_sigma-Deterministic zero
    z7bar = Data(7,1);%ActiveSheet.Range("D8")  deltaTR-Deterministic zero
    z8bar = Data(8,1);%ActiveSheet.Range("D9")  deltaTepsilon-Deterministic zero
    z9bar = Data(9,1);%ActiveSheet.Range("D10") deltaTepsilon-Deterministic zero
    z10bar = Data(10,1);%ActiveSheet.Range("D11")   T27J-Deterministic -20 in original
excel file
    z11bar = Data(11,1);%ActiveSheet.Range("G12")   a-lognormal
    z12bar = Data(12,1);%ActiveSheet.Range("G13")   SigmaDLbc-lognormal
    z13bar = Data(13,1);%ActiveSheet.Range("G14")   SigmaDLac-lognormal

    z15bar = Data(15,1);%ActiveSheet.Range("G16")   H-Lognormal
    z16bar = Data(16,1);%ActiveSheet.Range("G17")   W-lognormal
    z17bar = Data(17,1);%ActiveSheet.Range("D18")   Delta1-Normal
    z18bar = Data(18,1);%ActiveSheet.Range("D19")   Delta2-Normal
    z19bar = Data(19,1);%ActiveSheet.Range("G20")   Sigma_s-lognormal
    z20bar = Data(20,1);%ActiveSheet.Range("G21")   Sigma_ED-lognormal
    z21bar = Data(21,1);%ActiveSheet.Range("G22")   a/c ratio-lognormal
    z22bar = Data(22,1);%ActiveSheet.Range("G23")   Mk-lognormal
```

```
    z23bar = Data(23,1);%ActiveSheet.Range("G24")   SCF-lognormal
    z24bar = Data(24,1);%ActiveSheet.Range("D25")   DAF


    %standard deviations:

    z1std = Data(1,2);%ActiveSheet.Range("H2")
    z2std = Data(2,2);%ActiveSheet.Range("H3")
    z3std = Data(3,2);%ActiveSheet.Range("H4")

    z5std = Data(5,2);%ActiveSheet.Range("F6")
    z6std = Data(6,2);%ActiveSheet.Range("F7")
    z7std = Data(7,2);%ActiveSheet.Range("F8")
    z8std = Data(8,2);%ActiveSheet.Range("F9")
    z9std = Data(9,2);%ActiveSheet.Range("F10")
    z10std = Data(10,2);%ActiveSheet.Range("F11")
    z11std = Data(11,2);%ActiveSheet.Range("H12")
    z12std = Data(12,2);%ActiveSheet.Range("H13")
    z13std = Data(13,2);%ActiveSheet.Range("H14")

    z15std = Data(15,2);%ActiveSheet.Range("H16")
    z16std = Data(16,2);%ActiveSheet.Range("H17")
    z17std = Data(17,2);%ActiveSheet.Range("F18")
    z18std = Data(18,2);%ActiveSheet.Range("F19")
    z19std = Data(19,2);%ActiveSheet.Range("H20")
    z20std = Data(20,2);%ActiveSheet.Range("H21")
    z21std = Data(21,2);%ActiveSheet.Range("H22")
    z22std = Data(22,2);%ActiveSheet.Range("H23")
    z23std = Data(23,2);%ActiveSheet.Range("H24")
    z24std = Data(24,2);%ActiveSheet.Range("F25")


    No_Years_Batch=10; %should not be more than 1000 for RAM issues. Also, large
numbers decrease the speed.
    F=floor(ntrials/No_Years_Batch);  %the  above  No_Years_Batch  increases  by  this
factor; the actual number of years is equal to F*No_Years_Batch
    Failure_Year_Block=0;
    Failure_Year=zeros(No_Years_Batch*F,1);

    Failure_Year_Block2=0;
    Failure_Year2=zeros(No_Years_Batch*F,1);

    temp1index=ones(8760,No_Years_Batch);
    temp2index=ones(8760,No_Years_Batch);
    temp3index=ones(8760,No_Years_Batch);

    for i=1:8760
       temp1index(i,:)=i;
    end

    temp2index(1:5,:)=-10;
    temp3index(1:5,:)=5;

    for i=1:364
        temp2index((i-1)*24+6:(i-1)*24+14,:)=(i-1)*24+5;
```

```
        temp3index((i-1)*24+6:(i-1)*24+14,:)=(i-1)*24+14;

        temp2index((i-1)*24+15:(i-1)*24+29,:)=(i-1)*24+14;
        temp3index((i-1)*24+15:(i-1)*24+29,:)=(i-1)*24+29;
    end

    for i=365:365
        temp2index((i-1)*24+6:(i-1)*24+14,:)=(i-1)*24+5;
        temp3index((i-1)*24+6:(i-1)*24+14,:)=(i-1)*24+14;

        temp2index((i-1)*24+15:(i-1)*24+24,:)=(i-1)*24+14;
        temp3index((i-1)*24+15:(i-1)*24+24,:)=(i-1)*24+29;
    end
    tic
    for O=1:F
    clear arr
    arr=rand(No_Years_Batch,24);
    arr(:, 25) = logninv(arr(:, 1), z1bar, z1std);  %fy
    arr(:, 26) = logninv(arr(:, 2), z2bar, z2std);  %t
    arr(:, 27) = Data(3,1);%logninv(arr(:, 3), z3bar, z3std);  %B
    arr(:, 29) = Data(5,1);%ActiveSheet.Range("D6")     %-5
    arr(:, 30) = Data(6,1);%ActiveSheet.Range("D7")     %0
    arr(:, 31) = Data(7,1);%ActiveSheet.Range("D8")     %0
    arr(:, 32) = Data(8,1);%ActiveSheet.Range("D9")     %0
    arr(:, 33) = Data(9,1);%ActiveSheet.Range("D10")    %0
    arr(:, 34) = Data(10,1);%ActiveSheet.Range("D11")    %-20 in the original excel
sheet
    arr(:, 35) = Data(11,1);   %a
    arr(:, 36) = logninv(arr(:, 12), z12bar, z12std);   %sigmaDbc
    arr(:, 37) = 0;%logninv(arr(:, 13), z13bar, z13std);   %sigmaDac

    arr(:, 39) = logninv(arr(:, 15), z15bar, z15std);   %H
    arr(:, 40) = logninv(arr(:, 16), z16bar, z16std);   %W
    arr(:, 41) = norminv(arr(:, 17), z17bar, z17std);   %Delta 1
    arr(:, 42) = norminv(arr(:, 18), z18bar, z18std);   %Delta 2
    arr(:, 43) = logninv(arr(:, 19), z19bar, z19std);   %Sigma_s
    arr(:, 44) = logninv(arr(:, 20), z20bar, z20std);   %Sigma_ed
    arr(:, 45) = logninv(arr(:, 21), z21bar, z21std);   %a/c ratio
    arr(:, 46) = logninv(arr(:, 22), z22bar, z22std);   %Mk
    arr(:, 47) = logninv(arr(:, 23), z23bar, z23std);   %SCF
    arr(:, 48) = norminv(arr(:, 24), z24bar, z24std);%ActiveSheet.Range("D25")   % DAF

    fy = arr(:, 25)';%'yield strength of steel
    t = arr(:, 26)';%
    B = arr(:, 27)';%
    fyt = fy; %- 0.25 * t;%

    delta_Tr = arr(:, 29)';%     'radiation losses
    delta_Tsigma = arr(:, 30)';% 'adjustment for stress & yield strength, zero
    delta_T_R = arr(:, 31)';%    'adjustment for safety allowance, zero?
    delta_Te = arr(:, 32)';%     'adjustment for strain rate, zero
    delta_Tecf = arr(:, 33)';%   'adjustment for cold forming, zero

    T27J = arr(:, 34)';%         '27J test temp
    a = arr(:, 35)';%            'crack size in m
```

```
    Masterpf = arr(:, 17)';
    delta2 = arr(:, 42)';

    k=8760;
    Temp_Stepr=rand(k,No_Years_Batch);
    DTemp_Stepr=rand(367,No_Years_Batch);
    DTemp_Stepr2=rand(367,No_Years_Batch);

    DTemp_Step_min=norminv(DTemp_Stepr,Daily_min_Temps_Mean,Daily_min_Temps_Std);
    DTemp_Step_Range=norminv(DTemp_Stepr2,Daily_Range_Mean,Daily_Range_Std);
    DTemp_Step_max=DTemp_Step_min+DTemp_Step_Range;

    DTemp(1,:)=DTemp_Step_max(1,:);
    DTemp(732,:)=DTemp_Step_min(367,:);

    for i=1:365
        DTemp(2*i,:)=DTemp_Step_min(i+1,:);
        DTemp(2*i+1,:)=DTemp_Step_max(i+1,:);
    end

    D1Temp(1:5,:)=repmat(DTemp(1,:),5,1);
    D2Temp(1:5,:)=repmat(DTemp(2,:),5,1);

    for i=1:364
        D1Temp((i-1)*24+6:(i-1)*24+14,:)=repmat(DTemp(2*i,:),9,1);
        D2Temp((i-1)*24+6:(i-1)*24+14,:)=repmat(DTemp(2*i+1,:),9,1);

        D1Temp((i-1)*24+15:(i-1)*24+29,:)=repmat(DTemp(2*i+1,:),15,1);
        D2Temp((i-1)*24+15:(i-1)*24+29,:)=repmat(DTemp(2*i+2,:),15,1);
    end

    for i=365:365
        D1Temp((i-1)*24+6:(i-1)*24+14,:)=repmat(DTemp(2*i,:),9,1);
        D2Temp((i-1)*24+6:(i-1)*24+14,:)=repmat(DTemp(2*i+1,:),9,1);

        D1Temp((i-1)*24+15:(i-1)*24+24,:)=repmat(DTemp(2*i+1,:),10,1);
        D2Temp((i-1)*24+15:(i-1)*24+24,:)=repmat(DTemp(2*i+2,:),10,1);
    end


    Temp_Step=(D2Temp+D1Temp)./2-(D2Temp-D1Temp)./2.*cos(pi().*(temp1index-
temp2index)./(temp3index-temp2index));


    Tmd=Temp_Step;
    T_Ed = Tmd + delta_Tr + delta_Tsigma + delta_T_R + delta_Te + delta_Tecf;

    if strcmp(cracktype,'Semi-elliptical Surface Crack')
        b_eff = 5 * a * 1000;

        %'b_eff calculation for double edge crack
    elseif strcmp(cracktype,'Double Edge Crack')
        b_eff = 2 * t;
```

```
        %'b_eff calculation for through-thickness central crack
    elseif strcmp(cracktype,'Through-thickness Central Crack')
        b_eff = 2 * t;

        %'b_eff calculation for single edge crack
    elseif strcmp(cracktype,'Single Edge Crack')
        b_eff = t;
    end

    Kmat = 20 +  (77 * exp((T_Ed - T27J + 18 + delta2 + delta_T_R-13.*(0.5-Masterpf))
/ 52) + 11) .* ((25 ./ b_eff) .^ 0.25).*(log(1./(1-Masterpf))).^0.25;


    %%%%%%%%%%%%%%%%%%%%%%%%%%%%%%%%%%%%%%%%%%%%%%%%%%%%%%%%%%%%%%%%%%%%%%%
    %'-----Action Side-----(dependent on crack shape and orientation)
    LL=Liveload(1);
       Alpha=Liveload(2);
    U=Liveload(3);

    LiveStress_r1=rand(k,No_Years_Batch);
    LiveStress_Bias=-log(-log(LiveStress_r1))/Alpha+U;
    Hourly_Live_Stress=LL*LiveStress_Bias;
    sigma_LL=Hourly_Live_Stress;

    DAF=arr(:, 48)';
    sigma_DLbc = arr(:, 36)';%    'MPa, stress caused by dead loads before composite
action
    sigma_DLac = 0;%arr(:, 37)';%   'MPa, stress caused by dead loads after composite
action
    % sigma_LL = Stress_i;%arr(i, 38);%     'MPa, stress caused by live loads
    bias_liveloadanalysis = arr(:, 44)';
    sigma_p = sigma_DLbc + sigma_DLac + sigma_LL.* bias_liveloadanalysis.*DAF;% 'MPa,
total stress caused by external loads
    sigma_s = arr(:, 43)'; %      'MPa, residual stresses
    sigma_Ed = sigma_p + sigma_s ;%  'total stress plus 100MPa to account for residual
stresses due to welding
    a_mm = a * 1000;%           'crack size in mm
    ac_ratio = arr(:, 45)';
    c = a_mm ./ ac_ratio;%            'crack width in mm
    H = arr(:, 39)';%            'fillet weld height in mm
    W = arr(:, 40)';%            'fillet weld width in mm

    bias_Mk = arr(:, 46)';
    bias_SCF = arr(:, 47)';

    %'Calculation of Y, stress intensity correction factor, is dependent on the crack
type (shape)
    %    'Y calculation for semi elliptical crack
    if strcmp(cracktype,'Semi-elliptical Surface Crack')
        %CCC=2 * c ./ B > 0.5;
        %c = 0.5 ./ 2 * B;
        M1 = 1.13 - 0.09 * a_mm ./ c;
        M2 = -0.54 + 0.89 ./ (0.2 + a_mm ./ c);
        M3 = 0.5 - 1 ./ (0.65 + a_mm ./ c) + 14 * (1 - a_mm ./ c) .^ 24;
        phi = pi / 2;
```

```
        g = 1 + (0.1 + 0.35 * (a_mm ./ t) .^ 2) * (1 - sin(phi)) .^ 2;
        f_phi = ((a_mm ./ c) .^ 2 * (cos(phi)) .^ 2 + (sin(phi)) .^ 2) .^ 0.25;
        f_w = (1 ./ cos(phi * (c ./ B) .* sqrt(a_mm ./ t))) .^ 0.5;
        F_s = (M1 + M2 .* (a_mm ./ t) .^ 2 + M3 .* (a_mm ./ t) .^ 4) .* g .* f_phi .*
f_w;
        Q = 1 + 1.464 .* (a_mm ./ c) .^ 1.65;
        Y = F_s ./ sqrt(Q);
    %'Y calculation for double edge crack
    elseif strcmp(cracktype ,'Double Edge Crack')
        alpha = 2 .* a_mm ./ B;
        Y = 1.122 - 0.154 .* alpha + 0.807 .*alpha .^ 2 - 1.894 .* alpha.^ 3 + 2.494 .*
alpha.^ 4;

    %'Y calculation for through-thickness central crack
    elseif strcmp(cracktype,'Through-thickness Central Crack')
        alpha = 2 .* a_mm ./ B;
        Y = 1 - 0.025 .* alpha .^ 2 + 0.06 * (alpha .^ 4) .* sqrt(1 / cos(alpha * pi
/ 2));

    %'Y calculation for single edge crack
    elseif strcmp(cracktype,'Single Edge Crack')
        alpha = a_mm ./ B;
        Y = 1.12 - 0.231 * alpha + 10.55 * alpha .^ 2 - 21.72 * alpha .^ 3 + 30.39 *
alpha .^ 4;
    end

    %'Mk is an adjustment for semi-elliptical cracks at a weld toe only and is dependent
on the crack orientation. =1 if not semi-elliptical.

    %'Mk calculation for Type 1 - crack transverse to web
    if and(strcmp(cracktype,'Semi-elliptical Surface Crack'),strcmp(weldtoetype,'Type
1'))
        CC = 0.8068 - 0.1554 * (H ./ t) + 0.0429 * (H ./ t) .^ 2 + 0.0794 * (W ./ t);
        K = -0.1993 - 0.1839 * (H ./ t) + 0.0495 * (H ./ t) .^ 2 + 0.0815 * (W ./ t);
        Mk = max(CC .* (a_mm ./ t) .^ K, 1).*bias_Mk;

    %'Mk calculation for Type 2 - crack longitudinal to web
    elseif               and(strcmp(cracktype,'Semi-elliptical               Surface
Crack'),strcmp(weldtoetype,'Type 2'))
        CC = 0.8068 - 0.1554 * (H ./ t) + 0.0429 * (H ./ t) .^ 2 + 0.0794 * (W ./ t);
        K = -0.1993 - 0.1839 * (H ./ t) + 0.0495 * (H ./ t) .^ 2 + 0.0815 * (W ./ t);
        Mk = max(CC .* (a_mm ./ t) .^ K, 1).*bias_Mk;

    %'Mk calculation for Type 3 - cover plate
    elseif               and(strcmp(cracktype,'Semi-elliptical               Surface
Crack'),srtcmp(weldtoetype,'Type 3'))
        SCF = (-3.539 * (log(H ./ t) / log(10)) + 1.981 * (log(t_cover ./ t) / log(10))
+ 5.798)*bias_SCF;
        Mk = max(SCF ./ (1 + (1 / 0.1473) * (a_mm ./ t) ^ 0.4348), 1).*bias_Mk;

    else
        Mk = 1*bias_Mk;
    end
```

```
    %'Calculation of sigma_gy is dependent on the crack type (stress applied to the
gross section to obtain net section yielding)
    %    'for semi-elliptical surface crack
    if strcmp(cracktype,'Semi-elliptical Surface Crack')
        sigma_gy = fyt .* (1 - pi * 2.5 .* (a_mm) .^ 2 ./ (2 * t .* (5 .* (a_mm) +
t)));

    %    'for double edge crack
    elseif strcmp(cracktype,'Double Edge Crack')
        sigma_gy = fyt .* (1 - 2 * a_mm ./ W) .* (1 + 0.3 * 2 * a_mm ./ W);

    %'for through-thickness central crack
    elseif strcmp(cracktype,'Through-thickness Central Crack')
        sigma_gy = fyt .* (1 - 2 * a_mm ./ W);

    %'for single edge crack
    elseif strcmp(cracktype,'Single Edge Crack')
        sigma_gy = fyt .* (1 - a_mm ./ W);
    end

    sigma_Ed2=min(sigma_Ed,sigma_gy);
    Lr = sigma_Ed2 ./ sigma_gy;
    kR6 = max(1 ./ sqrt(1 + 0.5 * Lr .^ 2), 0.816);
    psi = sigma_s .* Lr ./ sigma_p;

    rho1=zeros(k,No_Years_Batch);
    tt=psi > 0 & psi <= 5.2;
    rho1(tt)=0.1 * psi(tt) .^ 0.714 - 0.007 * psi(tt) .^ 2 + 0.00003 * psi(tt) .^ 5;
    tt=psi>5.2;
    rho1(tt)=0.25;

    rho=zeros(k,No_Years_Batch);
    tt=Lr<=0.8;
    rho(tt)=rho1(tt);
    tt=Lr > 0.8 & Lr <= 1.05;
    rho(tt)=4 * rho1(tt) .* (1.05 - Lr(tt));

    Kappld = sigma_Ed2 .* sqrt(pi * a) .* Y .* Mk;
    K_appld = Kappld ./ (kR6 - rho);
    K_matA=K_appld;
    K_matT=Kmat;

    Failures=K_matA>K_matT;
    Failure_Year_Block=floor(double(sum(Failures)>0 | a_mm>t));

    Failures2=sigma_Ed>sigma_gy+sigma_s;
    Failure_Year_Block2=floor(double(sum(Failures2)>0 ));

    Failure_Year_Block3=Failure_Year_Block+Failure_Year_Block2;

    for oi=1:No_Years_Batch
        if Failure_Year_Block3(oi)>1
            rrr=randi([1,8760],1);
            FailuresR=[Failures(rrr:8760,oi);Failures(1:rrr,oi)];
            FailuresR2=[Failures2(rrr:8760,oi);Failures2(1:rrr,oi)];
```

```
            if find(FailuresR>0,1)>find(FailuresR2>0,1)
                Failure_Year_Block(oi)=0;
            else
                Failure_Year_Block2(oi)=0;
            end
        end
    end

    Failure_Year(No_Years_Batch*(O-1)+1:O*No_Years_Batch)=Failure_Year_Block';
    Failure_Year2(No_Years_Batch*(O-1)+1:O*No_Years_Batch)=Failure_Year_Block2';
    f=sum(Failure_Year)/No_Years_Batch/F;
    f2=sum(Failure_Year2)/No_Years_Batch/F;
    f=[f,f2];
end
```

Appendix B – Time-Independent MATLAB Code

This code is included to enable verification / reproducibility of the presented research. The code is based on an analytical approach developed by the author with direction from their thesis supervisor. The MATLAB coding itself would not have been possible without significant help from Dr. Tolou Kian and Dr. Chehrazi, who are gratefully acknowledged.

headcode.m

```
clear
clc
close all
DesignCrackType=0;

CMat={'C1','C2'};
AMat={'CC','VC'};

Climate=2
DesignCrack=1
pause


tsMat=[38]; %plate thickness, mm

if DesignCrackType==0
    asMat=0.13+0*tsMat;
elseif DesignCrackType==1
    asMat=0.4/38*tsMat;
end

for jjjavad=1:size(tsMat,2)

    t_step=tsMat(jjjavad)
    a_step=asMat(jjjavad);

    MCS_condensed_bias_v2_ParametricMine_MATRIXfORM9_CopyMichelle3;
    mkdir(num2str(jjjavad))
    cd(num2str(jjjavad))

    save(['matlab',CMat{Climate},AMat{DesignCrack+1}])
    cd('N:\Probabilistic Analysis\Time_Independent_Code20231020')

end
```

MCS_condensed_bias_v2_ParametricMine_MATRIXfORM9_CopyMichelle3.m

```
tic
clc

mode1No=1;
mode1_mat={'design','retrofit'}
mode1=mode1_mat(mode1No)
Analysis_Case='Parametric';

TrailNOver1000=1000;

deterministic=0;
Analysis_TypeNo=1;
ElementTypeNo=2;

%Definition%%%%%%%%%%%%%%%%%%%%%%%%%%%%%%%%%%%%%%%%%%%%%%%%%%%%%%%%%%%%%%%%%%%
Analysis_Types={'Deterministic','Probabilistic'};
Analysis_Type=Analysis_Types{Analysis_TypeNo}

Crack_Types={'Semi-elliptical Surface Crack','Double Edge Crack','Through-thickness
Central Crack','Single Edge Crack'};
Weld_Types ={'Type 0','Type 1','Type 2','Type 3'};

Element_Types={'Pin','Plate'};
ElementType=Element_Types{ElementTypeNo}

% ElementType='Pin'

LocationLoadMat={'Ontario','Quebec','Alberta','British'}
LocationTempMat={'Toronto';'Montreal';'Edmonton';'Vancouver'}

if strcmp(ElementType,'Pin')
    aOVERc=0.6;
    diameter=15*25.4;

    Ymat=[0.938,0.984,1.035;...
       0.836,0.901,0.987;...
       0.749,0.830,0.985;...
       0.683,0.795,1.041;
       0.629,0.782,1.056];
end

WeldTypeNo=2;
if WeldTypeNo==1+1
    L=1
    T=1
    teta=45
elseif WeldTypeNo==2+1
    %H and W
elseif WeldTypeNo==3+1
    % H
    T=1
end
```

```
%Defining Parameters%%%%%%%%%%%%%%%%%%%%%%%%%%%%%%%%%%%%%%%%%%%%%%%%%%%%%%
ParConst=[2,5:9];
ParProba=[1,2,4,12,13,14,15,16:23];
ParDetrm=[10,11];

if deterministic==1
    ParProba=[];
    ParDetrm=[1:4,10:23];
end

%Constant

B=100;
delta_Tr=-5;
delta_Tsigma=0;
delta_T_R=0;
delta_Te=0;
delta_Tecf=0;
bias_Mk=1;
t=25;


%Defining Parameters of Interest
POI=[1,2,11,24,25,10];

POI_Range10 =[260,300,350,400,480,250,345,485,690]; %fy for thin to med plates
POI_Range11= [250,280,320,370,450,250,345,450,620]; %fy for thick plates

if t_step<=65
    POI_Range1=POI_Range10;
elseif t_step>65
    POI_Range1=POI_Range11;
end

POI_Range2=[t_step];%[5:10:65];
POI_Range3=[a_step]/1000;

if strcmp(mode1,'design')
    POI_Range4=[1];%DCR
    POI_Range5=[1];%L/D
elseif strcmp(mode1,'retrofit')
    POI_Range4=[0.01,0.1:0.1:0.5];%D/Fy
    POI_Range5=[1];%L/D
end
POI_Range6=[20:-10:-50];%T27J

Maximus=0;CaseNo=1;
for POICounter=1:size(POI,2)
    aa=['Maximus=max(size(POI_Range',num2str(POICounter),',2),Maximus)']
    eval(aa)

   aa=['CaseNo=CaseNo*size(POI_Range',num2str(POICounter),',2);']
   eval(aa)
end
```

```
POI_Range=zeros(size(POI,2),max(Maximus));
for POICounter=1:size(POI,2)

aa=['POI_Range(',num2str(POICounter),',1:size(POI_Range',num2str(POICounter),',2))=PO
I_Range',num2str(POICounter),';']
    eval(aa)
end

Data_Parameters={
    'fy',                    '1',"lognormal";
    't',                     '2',"lognormal";
    'B',                     '3',"deterministic";
    'Tmd',                   '4',"extreme";
    'delta_Tr',              '5',"deterministic";
    'delta_Tsigma',          '6',"deterministic";
    'delta_T_R',             '7',"deterministic";
    'delta_Te',              '8',"deterministic";
    'delta_Tecf',            '9',"deterministic";
    'T27J',                  '10',"deterministic";
    'a',                     '11',"lognormal";
    'sigma_DLbc',            '12',"lognormal";
    'DAF',                   '13',"lognormal";
    'sigma_LL',              '14',"extreme";
    'H',                     '15',"lognormal";
    'W',                     '16',"lognormal";
    'Masterpf',              '17',"uniform";
    'delta2',                '18',"normal";
    'sigma_s',               '19',"lognormal";
    'bias_liveloadanalysis','20',"lognormal";
    'ac_ratio',              '21',"lognormal";
    'bias_Mk',               '22',"lognormal";
    'bias_SCF',              '23',"lognormal";
    'DoverFy',               '24',"deterministic";
    'LoverD',                '25',"deterministic";
    'Kv',                    '26',"deterministic";
};


POINames=Data_Parameters(POI)
Data=[
    350     0.0915  0   0   0   1.101   1;
    26      0.0120  0   0   0   1.020   2;
    375     0.0099  0   0   0   1.000   3;
    1       0.0000  0   0   0   1.000   4;
    -5      0.0000  0   0   0   1.000   5;
    0.0     0.0000  0   0   0   1.000   6;
    0.0     0.0000  0   0   0   1.000   7;
    0.0     0.0000  0   0   0   1.000   8;
    0.0     0.0000  0   0   0   1.000   9;
    %-20.0   0.0000  0   0   0   1.000   10;
    0  0.0000  0   0   0   1.000   10;
    0.0220   0.2000  0   0   0   1.000   11;
    106.08   0.0800  0   0   0   1.030   12;
    1.15    0.104   0   0   0   1.000   13;
```

```
    %1.25    0.104   0   0   0   1.000   13;
    150.00   0.0304  0   0   0   1.5228  14;
    10       0.1600  0   0   0   1.000   15;
    10      0.1600  0   0   0   1.000   16;
    1       0.2500  0   0   0   1.000   17;
    0       34.2      0   0   0   0.000   18;
    100      0.25    0   0   0   1.000   19;
    1       0.12    0   0   0   0.930   20;
    0.4     0.32    0   0   0   1.000   21;
    1        0.05    0   0   0   1.000   22;
    1       0.04    0   0   0   1.000   23;
    1        0       0   0   0   1.000   24;
    1       0       0   0   0   1.000   25;
    1       0       0   0   0   1.000   26;
];


%CSA S6 TABLE 10.4%
SelectedTable=14;
Weld=0;
Ts=-50;
SteelGrade=260;
Table1014=xlsread('BackGroundFiles\Table1014','Sheet1','D44:J49');
Table1015=xlsread('BackGroundFiles\Table1014','Sheet1','Q44:W48');


if SteelGrade==260
    row=1;
elseif SteelGrade==300
    row=2;
elseif SteelGrade==350
    row=3;
elseif SteelGrade==400
    row=4;
elseif SteelGrade==480
    row=5;
elseif SteelGrade==700
    row=6;
end
row;


if SelectedTable==14
    if Weld==0
        Table=Table1014(:,1:4);
        if Ts>=-30
            Table(:,4)=[];
        elseif and (Ts>-52,Ts<-30)
            Table(:,3)=[];
        end
    else
        Table=[Table1014(:,1),Table1014(:,5:7)];
        if Ts>=-40
            Table(:,4)=[];
        elseif and (Ts>-52,Ts<-40)
```

```
            Table(:,3)=[];
        end
    end

elseif SelectedTable == 15
    if Weld==0
        Table=Table1015(:,1:4);
        if Ts>=-30
            Table(:,4)=[];
        elseif and (Ts>-52,Ts<-30)
            Table(:,3)=[];
        end
    else
        Table=[Table1015(:,1),Table1015(:,5:7)];
        if Ts>=-40
            Table(:,4)=[];
        elseif and (Ts>-52,Ts<-40)
            Table(:,3)=[];
        end
    end
end
Table;

STEEL_FY=Table(row,1);%Table1014(:,1);Table1014(:,1)];
TKV=Table(row,3);%Table1014(:,4);Table1014(:,4)];
KV=Table(row,2);%


%Analysis%
for LLCounter=2%:3

    LocLoD=LocationLoadMat{LLCounter};
    LocLoD=LocationTempMat{LLCounter};

%Waterloo 2003-2021 (moderate)
Climate1=[-28.7     -27.3  -29.7  -17    -25.3  -22.3  -29    -21    -24    -16.7  -22.6
       -30.1  -32.7  -25.8  -27.5  -26.4  -25.7  -26.1  -21.1  -11.72]
%Whitehorse 1953-2021 (severe)
Climate2=[-44.4     -41.7  -44.4  -42.2  -41.7  -38.3  -42.8  -35.6  -44.4  -42.8  -43.9
       -43.9  -46.1  -46.7  -40    -51.1  -45.6  -44.4  -46.7  -44.4  -40.6  -47.2  -48.9
       -43.9  -45.9  -43.7  -45    -44.6  -42.8  -43.9  -45    -44.2  -41.4  -33.9  -38
       -37    -42.9  -43.7  -44.9  -45.1  -39.9  -40.2  -42.1  -47    -45.7  -41.4  -42
       -40.7  -36.5  -36.6  -39    -45.5  -46.1  -40.8  -37.9  -44.3  -40.6  -35.8  -40.2
       -39    -38.3  -35.9  -36.1  -35.4  -37.2  -38.2  -37.1  -40.5]

    if Climate==1
        MInTem_Arrange=Climate1;
    elseif Climate==2
        MInTem_Arrange=Climate2;
    end

    Temp_Extreme;
    Data(4,1)=1;Data(4,6)=1;
    AlphaMat(4,1)=-alpha1;UMat(4,1)=-Mu1;
```

```
%     LiveLoad_Extreme;
    % Ontario 1995 database for yearly simulation
    Alpha=51.77870836;
    U=1.241396554;


    AlphaMat(14,1)=Alpha;UMat(14,1)=U;

    for CrackTypeNo=1%:4

        cracktype = Crack_Types(CrackTypeNo);

        if CrackTypeNo==1
        else
            WeldTypeNo=1;
        end
        weldtoetype = Weld_Types(WeldTypeNo);

        if WeldTypeNo==3
            t_cover = 25;%'cover plate thickness;%??????????
        end


%Variable Inputs%%%%%%%%%%%%%%%%%%%%%%%%%%%%%%%%%%%%%%%%%%%%%%%%%%%%%%%%%%%%%%%%

%*********Completing Data Matrix******************
        zbar=zeros(24,1);zstd=zeros(24,1);zbar_Col1=zeros(27,1);
        for No_Parameters=1:24
            No_Parameters;

            if and(No_Parameters>=1,No_Parameters<=3)
                Data_Show(No_Parameters,1)=Data(No_Parameters,1);
                Data(No_Parameters,1)=Data(No_Parameters,1)*Data(No_Parameters,6);

Data(No_Parameters,3)=abs(Data(No_Parameters,1)*Data(No_Parameters,2));

Data(No_Parameters,5)=sqrt(log(1+Data(No_Parameters,3)^2/Data(No_Parameters,1)^2));
                Data(No_Parameters,4)=log(Data(No_Parameters,1))-
0.5*Data(No_Parameters,5)^2 ;

                zbar(No_Parameters,1) = Data(No_Parameters,4);
                zstd(No_Parameters,1) = Data(No_Parameters,5);


            elseif and(No_Parameters>=4,No_Parameters<=10)
                Data_Show(No_Parameters,1)=Data(No_Parameters,1);
                Data(No_Parameters,1)=Data(No_Parameters,1)*Data(No_Parameters,6);

Data(No_Parameters,3)=abs(Data(No_Parameters,1)*Data(No_Parameters,2));

                zbar(No_Parameters,1) = Data(No_Parameters,1);
                zstd(No_Parameters,1) = Data(No_Parameters,3);

                if No_Parameters==10
```

```
                    Data_Show(1,1)=STEEL_FY;
                    Data(1,1)=STEEL_FY*Data(1,6);
                    Data(1,3)=abs(Data(1,1)*Data(1,2));
                    Data(1,5)=sqrt(log(1+Data(1,3)^2/Data(1,1)^2));
                    Data(1,4)=log(Data(1,1))-0.5*Data(1,5)^2;

                    zbar(1,1) = Data(1,4);
                    zstd(1,1) = Data(1,5);

                    Data(10,1)=-20;

                    zbar(10,1) = Data(10,4);
                    zstd(10,1) = Data(10,5);

                end
            elseif and(No_Parameters>=11,No_Parameters<=16)
                Data_Show(No_Parameters,1)=Data(No_Parameters,1);
                Data(No_Parameters,1)=Data(No_Parameters,1)*Data(No_Parameters,6);

Data(No_Parameters,3)=abs(Data(No_Parameters,1)*Data(No_Parameters,2));

Data(No_Parameters,5)=sqrt(log(1+Data(No_Parameters,3)^2/Data(No_Parameters,1)^2));
                Data(No_Parameters,4)=log(Data(No_Parameters,1))-
0.5*Data(No_Parameters,5)^2;

                zbar(No_Parameters,1) = Data(No_Parameters,4);
                zstd(No_Parameters,1) = Data(No_Parameters,5);
            if No_Parameters==13
                    Data_Show(No_Parameters,1)=Data(No_Parameters,1);
                    Data(No_Parameters,1)=Data(No_Parameters,1)*Data(No_Parameters,6);

Data(No_Parameters,3)=abs(Data(No_Parameters,1)*Data(No_Parameters,2));
            end
            elseif and(No_Parameters>=17,No_Parameters<=18)
                Data_Show(No_Parameters,1)=Data(No_Parameters,1);
                Data(No_Parameters,1)=Data(No_Parameters,1)*Data(No_Parameters,6);

Data(No_Parameters,3)=abs(Data(No_Parameters,1)*Data(No_Parameters,2));
                if No_Parameters==18
                    Data(No_Parameters,3)=34.2;
                end
                zbar(No_Parameters,1) = Data(No_Parameters,1);
                zstd(No_Parameters,1) = Data(No_Parameters,3);

            elseif and (No_Parameters>=19, No_Parameters<=23)
                Data_Show(No_Parameters,1)=Data(No_Parameters,1);
                Data(No_Parameters,1)=Data(No_Parameters,1)*Data(No_Parameters,6);

Data(No_Parameters,3)=abs(Data(No_Parameters,1)*Data(No_Parameters,2));

Data(No_Parameters,5)=sqrt(log(1+Data(No_Parameters,3)^2/Data(No_Parameters,1)^2));
                Data(No_Parameters,4)=log(Data(No_Parameters,1))-
0.5*Data(No_Parameters,5)^2;

                zbar(No_Parameters,1) = Data(No_Parameters,4);
```

```
                zstd(No_Parameters,1) = Data(No_Parameters,5);

            elseif No_Parameters==24
                  Sd=1/1.1*Data(1,1)*(0.9-1.7* 0.2);
                  Sl=Data(1,1)*0.2;

                Stress_d=Sd*Data(12,6);
                Stress_Std_id=sqrt(log(1+(abs(Stress_d*Data(12,2)))^2/(Stress_d)^2));
                Stress_Bar_id=log((Stress_d))-0.5*Stress_Std_id^2;

                zstd(12,1)=Stress_Std_id;
                zbar(12,1)=Stress_Bar_id;

                Stress_l=Sl*Data(14,6);
                Stress_Std_il=sqrt(log(1+(abs(Stress_l*Data(14,2)))^2/(Stress_l)^2));
                Stress_Bar_il=log((Stress_l))-0.5*Stress_Std_il^2;

                zstd(14,1)=Stress_Std_il;
                zbar(14,1)=Stress_Bar_il;


                Data_Show(12,1)=Sd;
                Data(12,1)=Stress_d;

                Data_Show(14,1)=Sl;
                Data(14,1)=Stress_l;

            end
            zbar_Col1(No_Parameters,1)=Data(No_Parameters,1);
        end
        % Data_Show=Data;

%*********Only Overwriting Parameters of Interest (POI)******************
        n=1;zbars=zeros(24,CaseNo);zstds=zeros(24,CaseNo);zbars_Col1=zeros(24,CaseNo);

        for POICounter6=1:size(POI_Range6,2)
            for POICounter5=1:size(POI_Range5,2)
                for POICounter4=1:size(POI_Range4,2)
                    for POICounter3=1:size(POI_Range3,2)
                        for POICounter2=1:size(POI_Range2,2)
                            for POICounter1=1:size(POI_Range1,2)


POICounter=[POICounter1,POICounter2,POICounter3,POICounter4,POICounter5,POICounter6];

                                Data_Show(1,1)=STEEL_FY;
                                Data(1,1)=STEEL_FY*Data(1,6);
                                Data(1,3)=abs(Data(1,1)*Data(1,2));
                                Data(1,5)=sqrt(log(1+Data(1,3)^2/Data(1,1)^2));
                                Data(1,4)=log( Data(1,1))-0.5*Data(1,5)^2;

                                zbar(1,1) = Data(1,4);
                                zstd(1,1) = Data(1,5);
```

```
                                for No_Parameters=1:size(POI,2)

                                    No_Parameters;
                                    POI(No_Parameters);

POI_Range(No_Parameters,POICounter(No_Parameters));
                                    if
and(POI(No_Parameters)>=1,POI(No_Parameters)<=3)

Data_Show(POI(No_Parameters),1)=POI_Range(No_Parameters,POICounter(No_Parameters));

Data(POI(No_Parameters),1)=POI_Range(No_Parameters,POICounter(No_Parameters))*Data(PO
I(No_Parameters),6);

Data(POI(No_Parameters),3)=abs(Data(POI(No_Parameters),1)*Data(POI(No_Parameters),2));

Data(POI(No_Parameters),5)=sqrt(log(1+Data(POI(No_Parameters),3)^2/Data(POI(No_Parame
ters),1)^2));

Data(POI(No_Parameters),4)=log(Data(POI(No_Parameters),1))-
0.5*Data(POI(No_Parameters),5)^2 ;

                                        zbar(POI(No_Parameters),1)                  =
Data(POI(No_Parameters),4);
                                        zstd(POI(No_Parameters),1)                  =
Data(POI(No_Parameters),5);

                                    elseif and(POI(No_Parameters)==4,2>1)

Data_Show(POI(No_Parameters),1)=POI_Range(No_Parameters,POICounter(No_Parameters));

Data(POI(No_Parameters),1)=POI_Range(No_Parameters,POICounter(No_Parameters))*Data(PO
I(No_Parameters),6);

Data(POI(No_Parameters),3)=abs(Data(POI(No_Parameters),1)*Data(POI(No_Parameters),2));

                                        zbar(POI(No_Parameters),1) = Data(4,1);
                                        zstd(POI(No_Parameters),1) = Data(4,3);


                                    elseif
and(POI(No_Parameters)>=5,POI(No_Parameters)<=10)

Data_Show(POI(No_Parameters),1)=POI_Range(No_Parameters,POICounter(No_Parameters));
                                        zbar(POI(No_Parameters),1)                  =
Data(POI(No_Parameters),1);
                                        zstd(POI(No_Parameters),1) = 0;

                                    elseif
and(POI(No_Parameters)>=11,POI(No_Parameters)<=16)

Data_Show(POI(No_Parameters),1)=POI_Range(No_Parameters,POICounter(No_Parameters));

Data(POI(No_Parameters),1)=POI_Range(No_Parameters,POICounter(No_Parameters))*Data(PO
I(No_Parameters),6);
```

```
Data(POI(No_Parameters),3)=abs(Data(POI(No_Parameters),1)*Data(POI(No_Parameters),2));

Data(POI(No_Parameters),5)=sqrt(log(1+Data(POI(No_Parameters),3)^2/Data(POI(No_Parame
ters),1)^2));

Data(POI(No_Parameters),4)=log(Data(POI(No_Parameters),1))-
0.5*Data(POI(No_Parameters),5)^2;

                                    zbar(POI(No_Parameters),1)                =
Data(POI(No_Parameters),4);
                                    zstd(POI(No_Parameters),1)                =
Data(POI(No_Parameters),5);

                                elseif
and(POI(No_Parameters)>=17,POI(No_Parameters)<=18)

Data_Show(POI(No_Parameters),1)=POI_Range(No_Parameters,POICounter(No_Parameters));

Data(POI(No_Parameters),1)=POI_Range(No_Parameters,POICounter(No_Parameters))*Data(PO
I(No_Parameters),6);

Data(POI(No_Parameters),3)=abs(Data(POI(No_Parameters),1)*Data(POI(No_Parameters),2));

                                    if POI(No_Parameters)==18
                                        Data(POI(No_Parameters),3)=34.2;
                                    end

                                    zbar(POI(No_Parameters),1)                =
Data(POI(No_Parameters),1);
                                    zstd(POI(No_Parameters),1)                =
Data(POI(No_Parameters),3);

                                elseif              and(POI(No_Parameters)>=19,
POI(No_Parameters)<=23)

Data_Show(POI(No_Parameters),1)=POI_Range(No_Parameters,POICounter(No_Parameters));

Data(POI(No_Parameters),1)=POI_Range(No_Parameters,POICounter(No_Parameters))*Data(PO
I(No_Parameters),6);

Data(POI(No_Parameters),3)=abs(Data(POI(No_Parameters),1)*Data(POI(No_Parameters),2));

Data(POI(No_Parameters),5)=sqrt(log(1+Data(POI(No_Parameters),3)^2/Data(POI(No_Parame
ters),1)^2));

Data(POI(No_Parameters),4)=log(Data(POI(No_Parameters),1))-
0.5*Data(POI(No_Parameters),5)^2;

                                    zbar(POI(No_Parameters),1)                =
Data(POI(No_Parameters),4);
                                    zstd(POI(No_Parameters),1)                =
Data(POI(No_Parameters),5);
```

```
                                    elseif
or(POI(No_Parameters)==24,POI(No_Parameters)==25)

                                        Data_Show(24,1)=POI_Range4(POICounter4);

                                        if strcmp(mode1,'design')

Sd=POI_Range4(POICounter4)*0.9*Data_Show(1,1)/(1.1+1.7*POI_Range5(POICounter5));
                                        elseif strcmp(mode1,'retrofit')
                                            Sd=Data_Show(1,1)*POI_Range4(POICounter4);
                                        end

                                        Stress_d=Sd*Data(12,6);

Stress_Std_id=sqrt(log(1+(abs(Stress_d*Data(12,2)))^2/(Stress_d)^2));
                                        Stress_Bar_id=log((Stress_d))-
0.5*Stress_Std_id^2;

                                        Data_Show(12,1)=Sd;
                                        Data(12,1)=Stress_d;
                                        zstd(12,1)=Stress_Std_id;
                                        zbar(12,1)=Stress_Bar_id;

                                        Data_Show(25,1)=POI_Range5(POICounter5);

                                        if strcmp(mode1,'design')

Sl=POI_Range5(POICounter5)*POI_Range4(POICounter4)*0.9*Data_Show(1,1)/(1.1+1.7*POI_Ra
nge5(POICounter5));
                                        elseif strcmp(mode1,'retrofit')
                                            Sl=Sd*POI_Range5(POICounter5);
                                        end

                                        Data_Show(14,1)=Sl;
                                        Data(14,1)=Sl;

                                        zstd(14,1)=0;
                                        zbar(14,1)=Sl;


Data_Show(27,1)=(1.1*Data_Show(12,1)+1.7*Data_Show(14,1))/(0.9*Data_Show(1,1));

                                    elseif POI(No_Parameters)==25

                                    elseif POI(No_Parameters)==26

                                        Data_Show(26,1)=POI_Range6(POICounter6);

                                        Data_Show(10,1)=TKV   +   41.33   -   8.16   *
(POI_Range6(POICounter6) - 1.373).^0.5;
                                        Data(10,1)=          TKV  +  41.33  -  8.16  *
(POI_Range6(POICounter6) - 1.373).^0.5;
                                        zbar(10,1) = Data(10,1);
                                        zstd(10,1) = 0;
                                    end
```

```
                                end
                                zbars(1:24,n)=zbar;
                                zstds(1:24,n)=zstd;

                                zbar_Col1(:,1)=Data_Show(:,1);
                                zbars_Col1(1:27,n)=zbar_Col1;

                                n=n+1;
                            end
                        end
                    end
                end
            end
        end
        zbars_Col1_Ref=zbars_Col1;


%Analysis%

        Results=zeros(5,size(zbars_Col1_Ref,2));

        NoNegativeF=zeros(1,CaseNo);
        NoNegative_GeneralYield=zeros(1,CaseNo);
        NoNegative_LocalYield=zeros(1,CaseNo);
        ntrials=10000;
        NoNegatives=zeros(1,CaseNo);
        NoNegativesy=zeros(1,CaseNo);
        Pf=zeros(1,size(NoNegatives,2));
        Ns=zeros(1,size(NoNegatives,2));

        N=0;CaseNo_Aug=size(NoNegatives,2);
        while and(N<TrailNOver1000 , CaseNo_Aug>0)
        %  for N=1:10
             Case_Aug=find(Ns==N);
             CaseNo_Aug=size(Case_Aug,2);

            Rand_mat=rand(size(ParProba,2)*ntrials,CaseNo_Aug);
            [N,Ns(1)];
            if mod(N,100)==0
            N
            end
            N;

            clear arr
            for i=1:size(ParProba,2)%24
                iii=ParProba(i);

                if strcmp(Data_Parameters{iii,3},'normal')
                    arr((i-1)*ntrials+1:i*ntrials,1:CaseNo_Aug)                    =
norminv(Rand_mat((i-1)*ntrials+1:i*ntrials,:),                  zbars(iii,Case_Aug),
zstds(iii,Case_Aug));

                elseif strcmp(Data_Parameters{iii,3},'lognormal')
```

```
                    arr((i-1)*ntrials+1:i*ntrials,1:CaseNo_Aug)                    =
logninv(Rand_mat((i-1)*ntrials+1:i*ntrials,:),                    zbars(iii,Case_Aug),
zstds(iii,Case_Aug));

                elseif strcmp(Data_Parameters{iii,3},'extreme')
                    arr((i-1)*ntrials+1:i*ntrials,1:CaseNo_Aug)                    =
zbars(iii,Case_Aug).*(-log(-log(Rand_mat((i-
1)*ntrials+1:i*ntrials,:))))/AlphaMat(iii,1)+UMat(iii,1));

                elseif strcmp(Data_Parameters{iii,3},'uniform')
                    arr((i-1)*ntrials+1:i*ntrials,1:CaseNo_Aug)    =    Rand_mat((i-
1)*ntrials+1:i*ntrials,:);

                end
            end

            for i=1:size(ParDetrm,2)%24
                iii=ParDetrm(i);
                arr1(i,1:CaseNo_Aug)=zbars_Col1(iii,Case_Aug);
            end


%             Kmat_Kapp=zeros(2,CaseNo_Aug);
             N=N+1;

            for j=1:CaseNo_Aug
                jj=Case_Aug(j);

                if Ns(1,jj)*ntrials<100/Pf(1,jj)

                    N;
                    Ns(1,jj)=Ns(1,jj)+1;

                    Negatives=0;
                    n = 0;%'number of failures, starting at zero

                    if N==1
                        gg=1;gg1=1;clear aaaa aaaa1


                        for i=1:size(ParProba,2)
                            iii=ParProba(i);
                            aaaa{gg}=[Data_Parameters{iii},'=arr((i-
1)*ntrials+1:i*ntrials, j);'];
                            gg=gg+1;
                        end


                        for i=1:size(ParDetrm,2)
                            iii=ParDetrm(i);
                            aaaa1{gg1}=[Data_Parameters{iii},'=arr1(i, j);'];
                            gg1=gg1+1;
                        end
                    end
```

```
                    if size(ParProba,2)>=1
                        for i=1:size(aaaa,2)
                            eval(aaaa{i});
                        end
                    end

                    for i=1:size(aaaa1,2)
                        eval(aaaa1{i});
                    end


                    fyt = fy ;%- 0*0.25 * t;%
                    T_Ed = Tmd + delta_Tr + delta_Tsigma + delta_T_R + delta_Te +
delta_Tecf;

                    sigma_p = sigma_DLbc   + sigma_LL.* bias_liveloadanalysis.*DAF;%
'MPa, total stress caused by external loads
        %               sigma_s=0*sigma_s;
                   sigma_Ed = (sigma_p + sigma_s);%   'total stress plus 100MPa to
account for residual stresses due to welding
                    a_mm = a * 1000;%           'crack size in mm

                    %'b_eff is dependent on crack type
                    %    'b_eff calculation for semi-elliptical surface crack
                    if strcmp(cracktype,'Semi-elliptical Surface Crack')
                        b_eff = 5 * a * 1000;

                        %'b_eff calculation for double edge crack
                    elseif strcmp(cracktype,'Double Edge Crack')
                        b_eff = 2 * t;

                        %'b_eff calculation for through-thickness central crack
                    elseif strcmp(cracktype,'Through-thickness Central Crack')
                        b_eff = 2 * t;

                        %'b_eff calculation for single edge crack
                    elseif strcmp(cracktype,'Single Edge Crack')
                        b_eff = t;
                    end

%                       Kmat = 20 + delta1 .* (70 * exp((T_Ed - T27J + 18 + delta2 +
delta_T_R) / 52) + 10) .* ((25 ./ b_eff) .^ 0.25);
        %             pastearr(i, 1) = Kmat;
                    Kmat = 20 +  (77 * exp((T_Ed - T27J + 18 + delta2 + delta_T_R-
13.*(0.5-Masterpf))  /  52)  +  11)  .*  ((25  ./  b_eff)  .^  0.25).*(log(1./(1-
Masterpf))).^0.25;


%'-----Action Side-----(dependent on crack shape and orientation)%%%%%%%%%%

                         %'Calculation of Y, stress intensity correction factor, is
dependent on the crack type (shape)
                             %    'Y calculation for semi elliptical crack
                    if strcmp(ElementType,'Plate')
```

```
                    if strcmp(cracktype,'Semi-elliptical Surface Crack')
                        c = a_mm ./ ac_ratio;%            'crack width in mm

                        if 2 * c ./ B > 0.5
                            stop
%                             c = 0.5 / 2 * B;
                        elseif 2 * c ./ B <= 0.5
                            c = c;
                        end
                        M1 = 1.13 - 0.09 * a_mm ./ c;
                        M2 = -0.54 + 0.89 ./ (0.2 + a_mm ./ c);
                        M3 = 0.5 - 1 ./ (0.65 + a_mm ./ c) + 14 * (1 - a_mm ./
c) .^ 24;
                        phi = pi / 2;
                        g = 1 + (0.1 + 0.35 * (a_mm ./ t) .^ 2) * (1 - sin(phi))
^ 2;
                        f_phi = ((a_mm ./ c) .^ 2 * (cos(phi)) ^ 2 + (sin(phi)) ^
2) .^ 0.25;
                        f_w = (1 ./ cos(phi * (c ./ B) .* sqrt(a_mm ./ t))) .^ 0.5;
                        F_s = (M1 + M2 .* (a_mm ./ t) .^ 2 + M3 .* (a_mm ./ t) .^
4) .* g .* f_phi .* f_w;
                        Q = 1 + 1.464 * (a_mm ./ c) .^ 1.65;
                        Y = F_s ./ sqrt(Q);

                    %'Y calculation for double edge crack
                    elseif strcmp(cracktype ,'Double Edge Crack')
                        alphaJ = 2 * a_mm ./ B;
                        Y = 1.122 - 0.154 * alphaJ + 0.807 * alphaJ .^ 2 - 1.894
* alphaJ .^ 3 + 2.494 * alphaJ .^ 4;

                    %'Y calculation for through-thickness central crack
                    elseif strcmp(cracktype,'Through-thickness Central Crack')
                        alphaJ = 2 * a_mm ./ B;
                        Y = 1 - 0.025 * alphaJ .^ 2 + 0.06 * (alphaJ .^ 4) .*
sqrt(1 ./ cos(alphaJ * pi / 2));

                    %'Y calculation for single edge crack
                    elseif strcmp(cracktype,'Single Edge Crack')
                        alphaJ = a_mm ./ B;
                        Y = 1.12 - 0.231 * alphaJ + 10.55 * alphaJ .^ 2 - 21.72 *
alphaJ .^ 3 + 30.39 * alphaJ .^ 4;
                    end
                elseif strcmp(ElementType,'Pin')

                    aOVERc;
                    aOVERd=a_mm/diameter;
                    aOVERdMat=[0.05;0.125;0.2;0.275;0.35];

                    FirstY_NO=0;
                    for Ycounter=1:size(aOVERdMat,1)
                        if a_mm>=aOVERdMat(Ycounter,1)*diameter
                            FirstY_NO=Ycounter;
                        end
                    end
                    if FirstY_NO==0
```

```
Y=interp1([aOVERdMat(1),aOVERdMat(2)],[Ymat(1,3),Ymat(2,3)],aOVERd,          'linear',
'extrap');

                        elseif FirstY_NO==size(aOVERdMat,1)

Y=interp1([aOVERdMat(FirstY_NO),aOVERdMat(FirstY_NO+1)],[Ymat(FirstY_NO,3),Ymat(First
Y_NO+1,3)],aOVERd);

                        elseif and(FirstY_NO>0,FirstY_NO<size(aOVERdMat,1))
                            Y=interp1([aOVERdMat(Ycounter),aOVERdMat(Ycounter-
1)],[Ymat(Ycounter,3),Ymat(Ycounter-1,3)],aOVERd, 'linear', 'extrap');
                        end
                    end


                    if strcmp(ElementType,'Plate')

                        if strcmp(weldtoetype,'Type 0')
                            Mk=1;
                        else
                        %'Mk is an adjustment for semi-elliptical cracks at a weld toe
only and is dependent on the crack orientation. =1 if not semi-elliptical.

                        %    'Mk calculation for Type 1 - crack transverse to web
                            if     and(strcmp(cracktype,'Semi-elliptical     Surface
Crack'),strcmp(weldtoetype,'Type 1'))
                                CC = 0.9089 - 0.2357 * (T ./ t) + 0.0249 * (L ./ t) -
0.00038 * (L ./ t) .^ 2 + 0.0186 * B./t -0.1414 * teta/45;
                                K = -0.02285 + 0.0167 * (T ./ t) - 0.3863 * teta/45 +
0.1230 * (teta/45).^2;
                                Mk = max(CC .* (a_mm ./ t) .^ K, 1).*bias_Mk;

                            %'Mk calculation for Type 2 - crack longitudinal to web
                            elseif    and(strcmp(cracktype,'Semi-elliptical    Surface
Crack'),strcmp(weldtoetype,'Type 2'))
                                CC = 0.8068 - 0.1554 * (H ./ t) + 0.0429 * (H ./ t) .^
2 + 0.0794 * (W ./ t);
                                K = -0.1993 - 0.1839 * (H ./ t) + 0.0495 * (H ./ t) .^
2 + 0.0815 * (W ./ t);
                                Mk = max(CC .* (a_mm ./ t) .^ K, 1).*bias_Mk;

                            %'Mk calculation for Type 3 - cover plate
                            elseif    and(strcmp(cracktype,'Semi-elliptical    Surface
Crack'),strcmp(weldtoetype,'Type 3'))
                                SCF = (-3.539 * (log(H ./ t) / log(10)) + 1.981 *
(log(t_cover ./ t) / log(10)) + 5.798).*bias_SCF;
                                Mk = max(SCF / (1 + (1 / 0.1473) * (a_mm ./ t) .^
0.4348), 1).*bias_Mk;

                            else
                                Mk = 1*bias_Mk;
                            end
                        end
                    elseif strcmp(ElementType,'Pin')
```

```
                    Mk = 1;
                end


                 %'Calculation of sigma_gy is dependent on the crack type (stress
applied to the gross section to obtain net section yielding)
                 %'for semi-elliptical surface crack
                 WW=B;
                 if strcmp(cracktype,'Semi-elliptical Surface Crack')
                    sigma_gy = fyt .* (1 - pi * 2.5 * (a_mm) .^ 2 ./ (2 * t .* (5
* (a_mm) + t)) );

              %    'for double edge crack
                 elseif strcmp(cracktype,'Double Edge Crack')
                    sigma_gy = fyt .* (1 - 2 * a_mm ./ WW) .* (1 + 0.3 * 2 *
a_mm ./ WW);

                 %'for through-thickness central crack
                 elseif strcmp(cracktype,'Through-thickness Central Crack')
                    sigma_gy = fyt .* (1 - 2 * a_mm ./ WW);

                 %'for single edge crack
                 elseif strcmp(cracktype,'Single Edge Crack')
                    sigma_gy = fyt .* (1 - a_mm ./ WW);
                 end


                 sigma_Ed2=min(sigma_Ed,sigma_gy);
                 Lr = sigma_Ed2 ./ sigma_gy;
                 kR6 = max(1 ./ sqrt(1 + 0.5 * Lr .^ 2), 0.816);
                 psi = sigma_s .* Lr ./ sigma_p;

                 rho1=zeros(size(psi,1),size(psi,2));
                 tt=psi > 0 & psi <= 5.2;
                 rho1(tt)=0.1 * psi(tt) .^ 0.714 - 0.007 * psi(tt) .^ 2 + 0.00003
* psi(tt) .^ 5;
                 tt=psi>5.2;
                 rho1(tt)=0.25;

                 rho=zeros(size(psi,1),size(psi,2));
                 tt=Lr<=0.8;
                 rho(tt)=rho1(tt);
                 tt=Lr > 0.8 & Lr <= 1.05;
                 rho(tt)=4 * rho1(tt) .* (1.05 - Lr(tt));

                 Kappl_d = sigma_Ed .* sqrt(pi * a) .* Y .* Mk;
                 Kappld = Kappl_d ./ (kR6 - rho);
%

                 sigma_Ed3=sigma_gy;
                 Lrgy = 1;
                 kR6gy = 0.816;
                 psigy = sigma_s.*Lrgy ./ sigma_p;

                 rho1gy=zeros(size(psigy,1),size(psigy,2));
```

```
                    tt=psigy > 0 & psigy <= 5.2;
                    rho1gy(tt)=0.1 * psigy(tt) .^ 0.714 - 0.007 * psigy(tt) .^ 2 +
0.00003 * psigy(tt) .^ 5;
                    tt=psigy>5.2;
                    rho1gy(tt)=0.25;

                    rhogy=zeros(size(psigy,1),size(psigy,2));
                    rhogy=4 * rho1gy .* (1.05 - 1);

                    Kappl_dgy = sigma_gy .* sqrt(pi * a) .* Y .* Mk;
                    Kappldgy =Kappl_dgy ./ (0.816 - rhogy);


                    if deterministic==1

Results(1:12,j)=[Mk,Y,kR6,rho,psi,Lr,Kappld,Kmat,sigma_Ed,sigma_gy,fyt,b_eff];
                    end

Result_Para_Name={'Mk','Y','kR6','rho','psi','Lr','Kappld','Kmat','sigma_Ed','sigma_g
y','fyt','b_eff'};

                    sigma_Ed_LESS_sigma_gy = find(sigma_Ed <= sigma_gy);

                    FNY=find(Kmat(sigma_Ed_LESS_sigma_gy)-
Kappl_d(sigma_Ed_LESS_sigma_gy)<=0);
                    NFNY=find(Kmat(sigma_Ed_LESS_sigma_gy)-
Kappl_d(sigma_Ed_LESS_sigma_gy)>0);


                    sigma_Ed_sigma_gy100_sigma_gy = find(and(sigma_Ed > sigma_gy ,
sigma_Ed < sigma_gy + sigma_s));

                    Kappld = Kappldgy;
                    NFLY=find(Kmat(sigma_Ed_sigma_gy100_sigma_gy)-
Kappld(sigma_Ed_sigma_gy100_sigma_gy)>0);
                    FNLY=find(Kmat(sigma_Ed_sigma_gy100_sigma_gy)-
Kappld(sigma_Ed_sigma_gy100_sigma_gy)<=0);


                    sigma_Ed_100_sigma_gy = find(sigma_Ed > sigma_gy + sigma_s);

                    Kappld = Kappldgy;
                    NFGY=find(Kmat(sigma_Ed_100_sigma_gy)-
Kappld(sigma_Ed_100_sigma_gy)>0);
                    FNGY=find(Kmat(sigma_Ed_100_sigma_gy)-
Kappld(sigma_Ed_100_sigma_gy)<=0);


NoNegativeF(1,j)=NoNegativeF(1,j)+size(FNY,1)+size(FNLY,1)+size(FNGY,1);

NoNegative_LocalYield(1,j)=NoNegative_LocalYield(1,j)+size(NFLY,1);

NoNegative_GeneralYield(1,j)=NoNegative_GeneralYield(1,j)+size(NFGY,1);

                end
```

```
            end
        end
        if deterministic==1
            ntrials=1;
        end
        toc


        K1=2;
        k2=1;
        Pf_Ref=(NoNegativeF)./Ns/ntrials;
        Py_Ref=NoNegative_GeneralYield./Ns/ntrials;

    end
end

%Results

%Probability
Py_Ref
%Input Data for Different Cases
zbars_Col1_Ref
```

Temp_Extreme.m

```
N=1;%No of Years
MInTem_Arrange=MInTem_Arrange(find(MInTem_Arrange<0));
 figure('Name', 'pdf as is')

histogram(MInTem_Arrange,'Normalization','pdf','BinWidth',5)
paramEstsMaxima = evfit(MInTem_Arrange)

x = -50:0.1:10;
y = evpdf(x, paramEstsMaxima(1), paramEstsMaxima(2));
yc = evcdf(x, paramEstsMaxima(1), paramEstsMaxima(2));

hold on
plot(x, y)

figure
plot(1*x,yc)


VN = paramEstsMaxima(1);
SN = paramEstsMaxima(2);
CovN=SN/VN;
%
BiasFactor=min(MInTem_Arrange)/VN;

TemData=-(MInTem_Arrange);
Vn = mean(TemData);
sigma =      std(TemData);

alpha1 = 1.282/sigma;
Mu1 = Vn-0.577/alpha1;

alphaN = alpha1;
MuN = Mu1+log(N^(1/alpha1));

VN = MuN+0.577/alphaN;
SN = 1.282/alphaN;
CovN=SN/VN;

BiasFactor=max(TemData)/VN;

pp=0:0.01:1;
xx=0:-1:-60;
CDF=exp(-exp(-alphaN*(abs(xx)-MuN)));
PDF=alphaN*exp(-alphaN*(abs(xx)-MuN)).*exp(-exp(-alphaN*(abs(xx)-MuN)));

InvCDF=MuN-log(-log(pp))/alphaN;
%

figure
subplot(1,3,3)
hold on
plot(pp,-InvCDF)
xlabel('p')
```

```
ylabel('Minimum Daily Mean Temp (C)')
box on
set(gca,'FontSize',12,'FontName','Times New Roman','tickLength',[0,0])
grid on
ylim([-60 0])

subplot(1,3,2)
hold on
plot(CDF,xx)
xlabel('CDF')
ylabel('Minimum Daily Mean Temp (C)')
box on
set(gca,'FontSize',12,'FontName','Times New Roman','tickLength',[0,0])
grid on


subplot(1,3,1)
hold on
plot(PDF,xx)

ylims=ylim;
xlims=xlim;

plot([0,xlims(1,2)],[-MuN,-MuN])
text(0.4*xlims(1,2),-MuN+2,['\mu=',num2str(-MuN,3)],'rotation',0)

plot([0,xlims(1,2)],[-VN,-VN])
text(0.4*xlims(1,2),-VN-2,['\lambda_L=',num2str(-VN,3)],'rotation',0)

xlabel('PDF')
ylabel('Minimum Daily Mean Temp (C)')
box on
grid on
set(gca,'FontSize',12,'FontName','Times New Roman','tickLength',[0,0])
```